DEFINITION AND INTERROGATION OF THE GENE REGULATORY NETWORK OF *CEBPA* DOUBLE-MUTATED AML

by

Assunta Adamo

A Thesis submitted to the University of Birmingham for the Degree of

DOCTOR OF PHILOSOPHY

Institute of Cancer and Genomic Sciences

College of Medical and Dental Sciences

University of Birmingham

April 2022

Abstract

Mutations in C/EBPα and RUNX1 transcription factors are oncogenic drivers in acute myeloid leukaemia (AML). The *CEBPA* gene is usually hit by two different biallelic mutations. This genetic change results in the expression of two distinct proteins: one shows impaired DNA binding or dimerization abilities, the other lacks a transactivation domain. To this day the molecular mechanisms that promote leukaemogenesis in affected patients, referred to as *CEBPA* double-mutated (*CEBPA*$^{N/C}$), are still not completely understood. The RUNX1 gene is frequently affected by the t(8;21) translocation, generating the fusion product RUNX1-ETO. Previous work from our lab has demonstrated that *CEBPA*$^{N/C}$ and t(8;21) AMLs are epigenetically related, and that a similar gene regulatory network is corrupted in both forms of leukaemia. In the study presented here we confirmed this observation with a larger dataset, including 10 *CEBPA*$^{N/C}$ and 7 t(8;21) AML samples.

To address the question of the molecular mechanisms governing the maintenance of *CEBPA* double-mutated leukaemia, we employed multi-omics approaches to comprehensively characterize *CEBPA*$^{N/C}$ AMLs using purified primary patient-derived cells and a *CEBPA*$^{N/C}$ AML cell line. We studied the gene expression at both the bulk and single cell level in blasts and leukaemic stem cells, determined open chromatin regions, mapped mutant C/EBPα binding sites using chromatin immunoprecipitation assays followed by sequencing (ChIP-Seq) and linked these regions to their rightful genes using promoter capture HiC. We used ChIP-Seq to show that a large number of C/EBPα binding sites overlap with RUNX1 and c-FOS binding sites. We found that C/EBP binding is associated with a composite C/EBP:AP-1 binding motif capable to bind a heterodimer of both proteins, a feature specific for

CEBPA$^{N/C}$ AML. Based on this data, we determined the core gene regulatory network (GRN) of *CEBPA*$^{N/C}$ AML and compared it to normal cells. Finally, we interrogated this GRN and identified AP-1 and the C/EBP family itself as important factors maintaining *CEBPA*$^{N/C}$ AML. Our work has enhanced our insight into *CEBPA*$^{N/C}$ AML pathogenesis and represents an important resource for identifying novel targets for therapeutic intervention.

Acknowledgements

Foremost, I thank my supervisors Conny Bonifer and Peter Cockerill for their constant support and all the precious advice. Their immense knowledge, enthusiasm and passion for science are a source of inspiration for me.

I can never thank enough all the past and present members of the Bonifer-Cockerill lab for making me feel welcome from day one, and for all the help and the encouragement. I wish to express my particular thanks to Peter Keane for all his “bioinformatics for dummies” lessons and the support with data analyses.

I am grateful to Jen for putting up with me and being an extraordinary friend. The last four years would have not been the same without her.

I cannot thank my parents enough for always supporting me, even if far away. If I arrived here, it is also thanks to them. Grazie ma’, grazie pa’.

Last but not least, I thank Maurizio, my life partner, for his infinite patience, for all his back-up and for always having my back, through good times and bad.

Contributions

Salam Assi and Peter Keane performed part of the computational analyses presented in this work.

Paulynn Chin performed part of the ChIP-seq experiments.

CHi-C experiment has been performed alongside with Anetta Ptasinska.

Sandeep Potluri generated the doxycycline-inducible dnFOS vector

Mary Clarke and Adriana Flores-Langarica performed all the FACS sorting.

All the next generation sequencing libraries were sequenced by Genomics Birmingham, University of Birmingham.

Contributions are also described in the figure legend.

Table of Contents

List of illustration

List of tables

List of abbreviations

3C - chromosome conformation capture

3D - three-dimensional

5hmC - 5-hydroxymethylcytosine

5mC - 5-methylcytosine

AD - activation domain

AETFC - AML1–ETO-containing transcription factor complex

AGM - aorta-gonad-mesonephros

Alpha MEM - Minimum Essential Medium Eagle -Alpha modification

AML - Acute Myeloid Leukaemia

AP-1 – activator protein 1

ATAC - Assay for Transposase-Accessible Chromatin

ATL - adult T-cell leukaemia

bHLH - basic helix-loop-helix

bp - base pair

BSA - Bovine Serum Albumin

bZIP - basic region-leucine zipper

C/EBP - CCAAT/ Enhancer Binding Protein

CBFβ - Core Binding Factor Betha

CCND2 - Cyclin D2

CENP-A - centromere protein A

CGI - CpG island

ChIP - Chromatin Immunoprecipitation

CHIP - clonal hematopoiesis of indeterminate potential

CLP - common lymphoid progenitors

CML - chronic myeloid leukaemia

CMP - common myeloid progenitor

CRE - cAMP responsive elements

CSF-1R - colony stimulating factor 1 receptor

CSF-3R - colony stimulating factor 3 receptor

CTCF - CCCTC-binding factor

CTD - carboxyterminal domain

DBD - DNA-binding domain

DGF - digital genomic footprinting

DHS - DNase I Hypersensitive Site

DMEM - Dulbecco Modified Eagle Media

DMSO - Dimethyl Sulfoxide

DMSZ - Deutsche Sammlung von Mikroorganismen und Zellkulturen

dnC/EBP – dominant negative C/EBP

dnFOS – dominant negative FOS

DSG - Disuccinimidyl glutarate

EDTA - Ethylenediaminetetraacetic Acid

EHT - endothelial-to-haematopoietic transition

ETO - eight-twenty-one

ETS - E-twenty-six

FCS - fetal calf serum

FLT3L - FMS-like tyrosine kinase 3 ligand

FPKM - fragment per kilobase of transcript per million fragments

GFP - Green Fluorescent Protein

GMP - granulocyte-monocyte progenitor

GRN – gene regulatory network

GTF - general transcription factors

HAT - histone acetyltransferase

HDAC - histone deacetylase

HEK - Human Embryonic Kidney

hGM-CSF - human granulocyte/macrophage colony stimulating factor

HMT - histone methyltransferase

HSC - Haematopoietic Stem Cell

IL3 - Interleukin 3

IP - Immuno Precipitation

iPSC – induced pluripotent stem cell

IRES-GFP - Internal Ribosome Entry Site-Green Fluorescent Protein

JAK - Janus kinase

JCRB - Japanese Collection of Research Bioresources Cell Bank

KEGG – Kyoto Encyclopaedia of Genes and Genomes

LB – Luria-Bertani

L-Glu - L-Glutamine

LSC – leukaemia stem cell

LSK - Lineage-negative, Sca1-positive, Kit-positive

LZ – leucine-zip

MDS - myelodysplastic syndrome

MLL - mixed lineage leukaemia

MMP - multipotent progenitor

NHR - Nervy Homology Region

nt - nucleotide

ORF – Open Reading Frame

PBS – Phosphate Buffered Saline

PBSC – Peripheral Blood Stem Cell

Pen-Strep - Penicillin-Streptomycin

PIC - pre-initiation complex

PIC - Protein Inhibitor Cocktail

Pol II - Polymerase II

PTMs - posttranslational modifications

qPCR - quantitative Polymerase Chain Reaction

RHD – Runt-homology domain

RIN - RNA Integrity Number

RPMI - Roswell Park Memorial Institute

RT - room temperature

RUNX - Runt-related transcription factor

SCF - Stem Cell Factor

SCID - severe combined immune-deficient

scRNA-seq - single cell RNA-seq

SFEM II - StemSpanTM Serum-Free Expansion Medium II

SRI - Stem Regenin 1

STAT - signal transducers and activators of transcription

TAD - Topologically associated domains

TAD1 – transactivation domain 1

TAF - TBP-associated factor

TAL1 - T-cell acute lymphocytic leukaemia protein 1

TBP - TATA-box binding protein

TET2 - ten-eleven translocation 2

TF - Transcription Factor

TPA - 12-O-tetradecanoylphorbol-13-acetate

TPO - thrombopoietin

T-ALL - T-cell Acute Lymphoid Leukaemia

TRE - TPA responsive element

TSS - transcription starting site

VAF - variant allele frequency

WHO - World Health Organization

ZF - zinc finger

Chapter 1 - Introduction

1.1 Genome organization

The human genome is made up of 3.2 billion DNA base pairs spanning about 2 meters and densely packed within a 10 μm nucleus. This incredible compaction is achieved through an extensive folding of chromatin, a DNA-protein complex, in highly organized hierarchical structures.

1.1.1 Chromatin structure

The basic unit of chromatin is made of nucleosomes and is formed by ~147 base pairs (bp) of double helix DNA tightly wrapped around an octamer of proteins called histones (Kornberg, 1977) (Fig. 1.1 A). The repeating of this basic unit, interspaced by a 20-50 bp DNA linker, gives the chromatin the characteristic appearance of “beads on a string”. At this stage, chromatin fibres have a diameter of about 10 nm and the length of the genome is shortened by about 5-fold. A further level of condensation is obtained with the addition of the H1 histone (Thoma et al., 1979). This protein contacts both the DNA and the nucleosome histone core, forcing the chromatin into a 30 nm fibre which structure is still controversial. One model proposes that, upon bending of the linker DNA, consecutive nucleosomes interact with each other forming a solenoid (Robinson et al., 2006) (Fig. 1.1 B). Another model suggests that the DNA linker is straight and alternate nucleosomes interact with each other forming a zig-zag structure (Schalch et al., 2005) (Fig. 1.1 B).

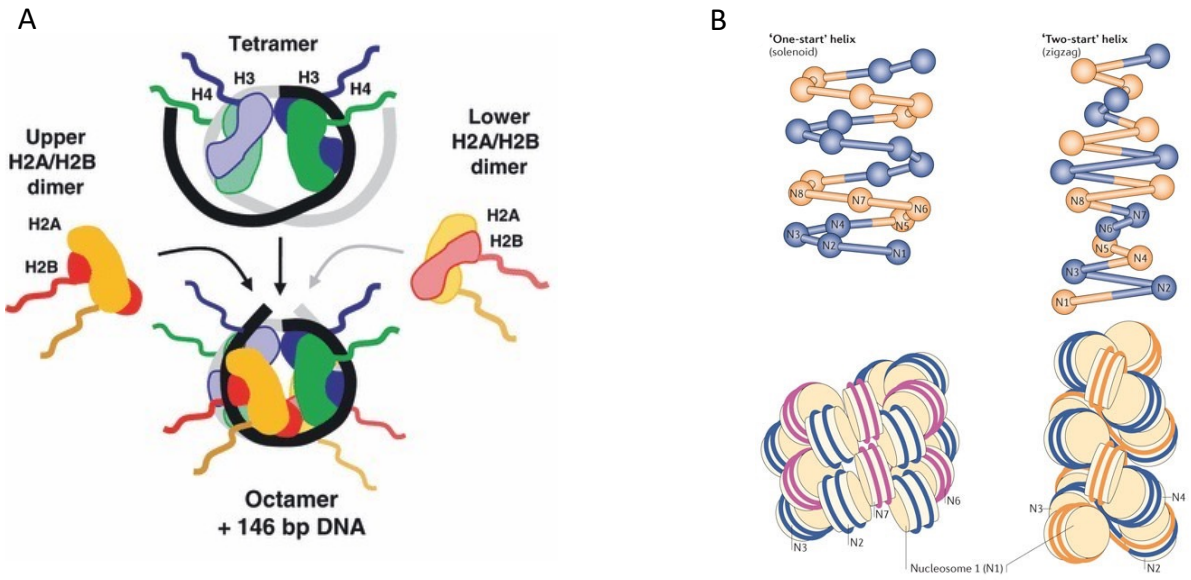

Figure 1.1*:* The structure of chromatin

(A) Schematic representation of a nucleosome, formed by ~147 bp of DNA wrapped around a core histone octamer. Figure from (Cockerill, 2011). (B) Two models for the 30 nm fibre structure. In the solenoid model (left) contiguous chromosome interact with each other; in the zig-zag model (right) interactions occur between alternate nucleosomes. Figure from (Luger et al., 2012).

1.1.2 Histones and histone variants

Histones are a class of basic proteins rich in arginine and lysine subdivided into 5 families: histone H1/H5 (linker histones), H2A, H2B, H3 and H4 (core histones). Core histones form the protein heart of the nucleosome, made up by two H2A-H2B dimers and a H3-H4 tetramers (Luger et al., 1997). Protein-protein interactions between the core constituents and hydrogen bonds and electrostatic interactions between histones and DNA stabilize the nucleosome structure, while histone amino acid tails protrude from the core to interact with the nearby nucleosome (Dorigo et al., 2003; Villasenor and Baubec, 2021). In addition to canonical histones, that are incorporated into the nucleosomes during DNA replication and are mostly expressed during the S-phase of the cell cycle (Sauer et al., 2018), a plethora of variants exists. Histone variants

participate in nucleosome formation in a DNA replication-independent manner, are expressed throughout the cell cycle and are involved in several processes, including transcription control, DNA repair and meiotic segregation (Talbert and Henikoff, 2010). For example, H3.3 and H2A.Z histones are associated with active regulatory elements, including enhancer and promoters (Jin et al., 2009), while the H3 variant centromere protein A (CENP-A) epigenetically marks centromere regions on chromosomes (McKinley and Cheeseman, 2016).

1.1.3 Histone modifications

Histone tails and globular domains are subject to several posttranslational modifications (PTMs) that influence chromatin compaction and cellular processes such as gene regulation, DNA repair and mitosis. The most common PTMs include acetylation, methylation, phosphorylation, ubiquitination, SUMOylation, citrullination and ADP-ribosylation (Villasenor and Baubec, 2021) (Fig. 1.2).

Acetylation is controlled by two group of enzymes, histone acetyltransferases (HATs) and histone deacetylases (HDACs). Acetylation of lysine residues neutralizes histones' positive charge and weakens the electrostatic interactions with the DNA backbone. Highly acetylated histones are usually associated with more accessible chromatin and active transcription (Wade et al., 1997). For example, acetylation of the lysine at position 27 of H3 (H3K27ac) is found at active enhancers and promoters (Creyghton et al., 2010; Gao et al., 2020). Phosphorylation of serine, threonine and tyrosine residues creates a repulsive force that destabilize the histone-DNA interaction and is associated with transcriptional activation in response to environmental stimuli (Li et al.,

2021). The variant histone H2AX is phosphorylated on serine 139 (γH2AX) following DNA damage and recruits the repair factors at the break point (Fink et al., 2007).

Histone methylation occurs on lysine and arginine residues and, unlike acetylation and phosphorylation, does not impact on histone charge but promotes the recruitment of factors such as chromatin remodellers. Methylation is regulated by histone methyltransferase (HMTs) and histone demethylase and can be associated with either transcriptional activation or repression. Trimethylation of lysine 4 on H3 (H3K4me3) occurs at the promoters of active genes (Liang et al., 2004), while trimethylation of lysine 27 on the same histone (H3K27me3) is associated with heterochromatin formation and transcriptional repression (Ferrari et al., 2014).

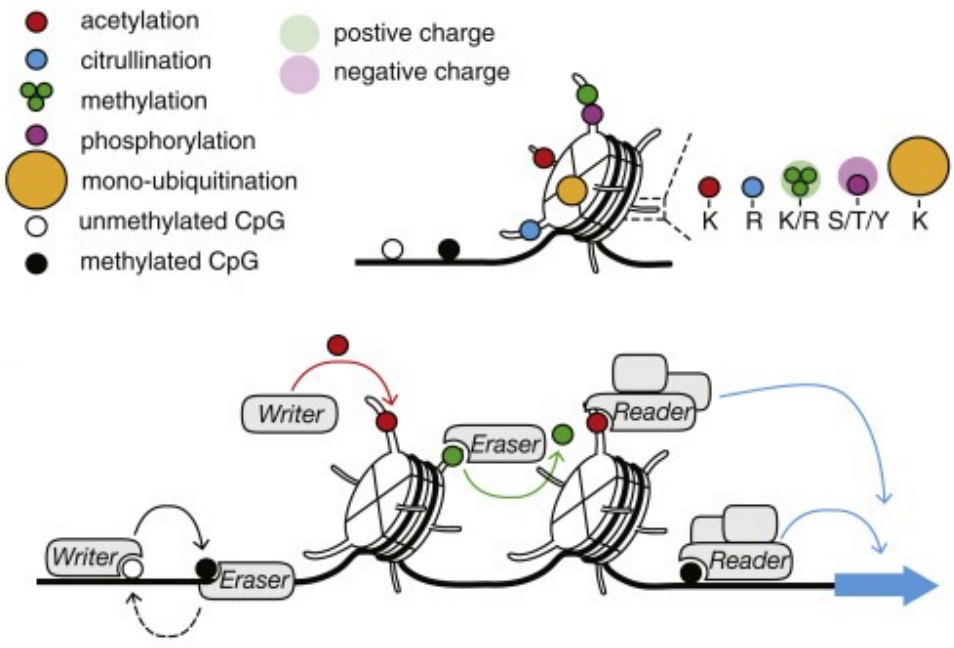

Figure 1.2: Histone posttranslational modifications

Histones tails and globular domains are enzymatically modified to regulate chromatin compaction. The addition, deletion and recognition of these modifications is controlled by specialized proteins collectively called writers, erasers and readers. Figure from (Villasenor and Baubec, 2021).

1.2 Gene expression regulation

1.2.1 The transcriptional machinery

Eukaryotic transcription progresses through three sequential stages: initiation, elongation and termination.

Initiation of transcription starts at gene core promoters, where general transcription factors (GTFs) and the RNA polymerase II (Pol II) are recruited to form the pre-initiation complex (PIC) (Geiger et al., 1996) (Fig. 1.3). PIC assembly usually begins with the binding of transcription factor IID (TFIID), a complex composed by TATA-box binding proteins (TBPs) and subunits called TBP-associated factors (TAFs) (Louder et al., 2016; Patikoglou et al., 1999), followed by TFIIA and TFIIB, the pol II-TFIIF complex, TFIIE and TFIIH (Sainsbury et al., 2015; Thomas and Chiang, 2006). Following PIC assembly, the DNA duplex at the core promoter is melted forming the transcription bubble, and Pol II can start RNA polymerization in absence of a primer (Fig. 1.3). At this stage Pol II remains bound to the promoter and synthetizes and releases several truncated mRNA. Many cycles of this so-called abortive initiation take place. Productive elongation starts after the carboxyterminal domain (CTD) of Pol II is phosphorylated by TFIIH on Ser5 and Ser7 and the enzyme dissociates from the transcription starting site (TSS) binding GEFs (Hahn, 2004)(Fig. 1.3).

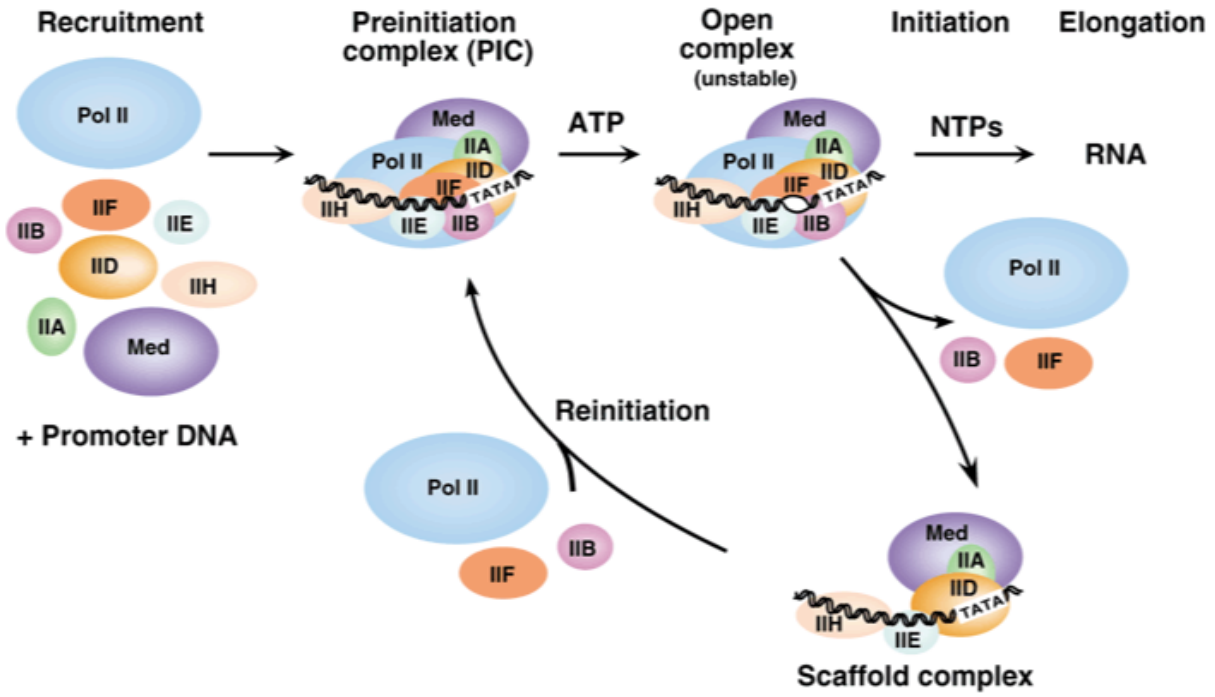

Figure 1.3 Schematic of eukaryotic transcription

Pol II and general transcription factors (GTFs) are recruited at gene promoter to form the pre-initiation complex (PIC). After the DNA surrounding the transcription start site (TSS) is melted to form the open complex, Pol II begins to synthesize and release short mRNAs. Several cycles of this so-called abortive initiation may take place before Pol II is released from the TSS to start the elongation stage. Figure from (Hahn, 2004).

1.2.2 Promoters

Promoters are specialized DNA sequences required for DNA polymerase binding and transcription initiation. About 70% of human promoters are associated with CpG island (CGI) (Saxonov et al., 2006). These structures tend to impair nucleosome assembly and promote polymerase access (Deaton and Bird, 2011). This type of promoter is often found at ubiquitously expressed or housekeeping genes (Zhu et al., 2008). In contrast, expression of developmental or cell-type specific genes is often under the control of TATA-containing promoters (Sandelin et al., 2007). Promoter activation

requires the activity of TFs, that recruit chromatin modifiers and the components of transcriptional machinery at the TSS of their target genes .

1.2.3 Enhancers

Enhancers are the major determinant of cell specific gene expression. These small DNA sequences, typically few hundreds bp, are able to markedly increase the expression of target genes (Banerji et al., 1981) regardless of their orientation or position. Indeed, these elements can be located near the promoter they regulate, upstream, downstream or within the gene body, and sometimes megabases away (Schoenfelder and Fraser, 2019). Enhancers are typically found in region of open chromatin sensitive to DNase I and are flanked by nucleosomes carrying H3K4me1/ H3K4me2 and H3K27ac (Zentner et al., 2011) and contain clusters of different transcription factor binding sites. Despite hundreds of thousands of enhancers having been identified in humans (Consortium, 2012) they are not all active at the same time. For example, in human peripheral blood T cells the GM-CSF enhancer is activated upon induction of NFAT and AP-1 (Johnson et al., 2004). Enhancers have been traditionally identified by using transcriptional reporter gene assays in cultured cells or developing embryos (Barakat et al., 2018; Kvon et al., 2014). However, these techniques fail to link enhancers to their target genes or assess their function in native chromatin. Recent studies have suggested the existence of an enhancer chromatin “signature”, consisting of H3K4Me1/Me2, H3K27ac and the absence of H3K4Me3, that is instead enriched at promoters (Consortium et al., 2007; Heintzman et al., 2007). Genome-wide studies of histone modifications are widely used for enhancer prediction and have increased our understanding in transcriptional regulation. That is the case of

bivalent chromatin, consisting of large regions of H3K27 methylation harbouring smaller regions of H3K4 methylation at poised enhancers (Bernstein et al., 2006). Nonetheless, none of the histone modifications alone or in combination shows a perfect correlation with enhancer activity and many active enhancers do not present characteristic marks (Barakat et al., 2018). To date, combinatorial analysis of multiple TFs occupancy across the genome is the most accurate method to predict enhancer activity (Dogan et al., 2015).

1.2.4 Silencers

Silencers exert a negative effect on gene transcription (Ptashne, 1967) and have been found to be enriched in binding sites for repressors (Doni Jayavelu et al., 2020). Similar to enhancers, silencers can affect nearby genes or act at long distance and repress multiple enhancers and promoters (Brand et al., 1985; Zinn et al., 1983). Several models have been proposed to explain silencer function. Some repressors seem to inhibit PIC assembly and transcription activation (Chen and Widom, 2005), while others recruits histone-modifiers (Li and Arnosti, 2011).

The distinction between silencers and enhancers is not sharp and studies have demonstrated a dual activity of silencers switching to enhancers and vice versa depending on the context. For example, during hematopoietic differentiation GATA-1 replaces GATA-2 at a cis-regulatory element upstream of the *Gata2* promoter, abrogating the transcription of the latter (Grass et al., 2003).

1.2.5 Insulators

The eukaryotic genome is divided into discrete domains of transcriptional regulation by the presence of boundary elements called insulators. Based on their function, insulators are classified as enhancer-blocking insulators, which hinder promoter-enhancer physical interaction, and barrier-insulators, that prevent heterochromatin-mediated gene silencing (Sun and Elgin, 1999). The first and most well-characterized vertebrate insulator was the chicken β-globin insulator cHS4, which combines both enhancer-blocking and barrier activities (Chung et al., 1993; Pikaart et al., 1998). CTCF is the only known insulator-binding protein in vertebrates (Bell et al., 1999). It acts as both enhancer-blocker when located between an enhancer and a promoter (Phillips and Corces, 2009) and chromatin barrier between active and repressive domains (Cuddapah et al., 2009).

1.2.6 Transcription factors

The rate of transcription is ultimately controlled by transcription factors (TFs). Upon binding the DNA in a sequence specific fashion, these proteins control a plethora of biological processes, including development, differentiation and cell cycle progression (Dynlacht, 1997; Pearson et al., 2005; Shivdasani and Orkin, 1996) (Fig. 1.4). A TF can occupy different sets of cis-regulatory elements depending on developmental stage and conditions (Pilon et al., 2011), and the same TF can regulate different genes in different cell types (Mullen et al., 2011).

Usually TFs consist of a DNA-binding domain (DBD), a dimerization domain and an activation domain (AD) (Keegan et al., 1986) (Fig. 1.4). The DBD is responsible for the recognition and binding of small 6-12 bp-long DNA sequences and is used to classify

TFs to families (Jolma et al., 2013; Stormo and Zhao, 2010). The sequences preferentially bound by families are modelled as motifs, which are in turn graphically represented as sequence logos (Schneider and Stephens, 1990). The AD lies at the heart of TFs effector functions. This domain can recruit PIC components and co-activators to gene promoters (Horikoshi et al., 1988), mediate the interactions with other TFs allowing cooperative binding (Huber et al., 1993), or recall histone and chromatin modifier at target genes. This last case is exemplified by C/EBPα, KLF4, and TFCP2l1, which drive Tet2-mediated enhancer demethylation and activation during B-cell reprogramming into induced pluripotent stem cells (iPSCs) (Sardina et al., 2018). The human genome encodes for ~1600 TFs (Lambert et al., 2018) and gene loci encoding for these proteins are among the most conserved genomic elements (Bejerano et al., 2004).

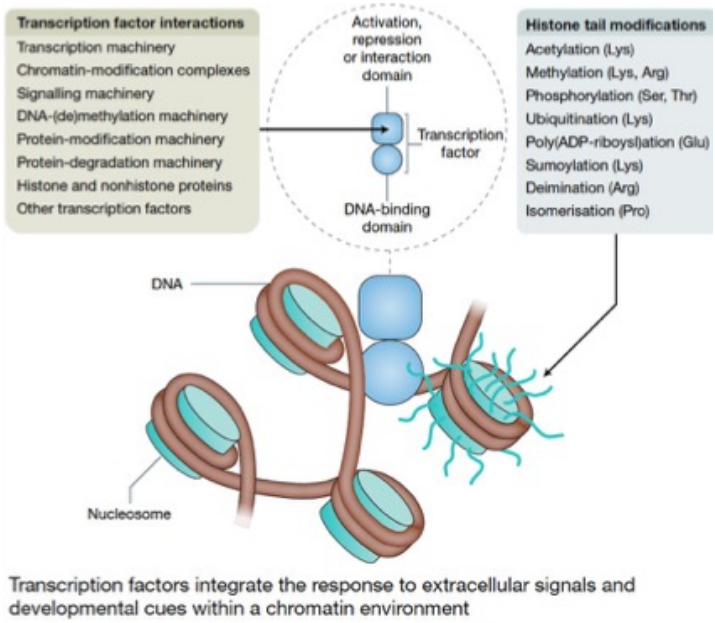

Figure 1.4: Transcription factors control a plethora of biological processes

Transcription factors bind to chromatin through their DNA binding domain. The activation domain mediates interactions with different molecules, including other transcription factors, to regulate the cellular response to extracellular signals. Figure from (Bonifer and Bowen, 2010).

1.2.7 Chromatin remodelling and pioneer factors

Nucleosomes form a strong barrier for transcription factor access to DNA (Blomquist et al., 1996). In order to remove nucleosomes, TFs recruit chromatin remodellers which use ATP to either slide or expel nucleosomes from their binding sites and thus facilitate subsequent TF binding (Hargreaves and Crabtree, 2011).

“Pioneer factors” are a class of TFs able to recognize and bind their target sites within nucleosomal DNA without the requirement of chromatin remodellers, triggering chromatin remodelling and providing accessibility to non-pioneer TFs. Such factors of the FOX class of TFs tend to have a "winged-helix" domain which mimics the one found in Histone H1 (Zaret and Carroll, 2011). This is exemplified by FOXA1 which allows GATA-4 to bind to the liver *Alb-1* enhancer in highly compacted chromatin and increase DNA accessibility in absence of ATP-dependent enzymes (Cirillo et al., 2002). Pioneer factors play a key role in development and cell fate specification, establishing competence for gene expression program (Zaret, 2020). C/EBPα has been thought to act as pioneer factor in pre-B cells where its induction establishes a myeloid expression program by activating de-novo enhancers (van Oevelen et al., 2015). However, it is not clear whether it is able to act completely on its own.

1.2.8 How to find a cis-regulatory element

A comprehensive genome-wide identification of the active cis-regulatory elements is paramount to understand how gene expression is precisely controlled. It has long been known that active chromatin harbouring regulatory regions is more accessible and thus more sensitive to cleavage by nucleases such as DNase I or transposases (Weintraub and Groudine, 1976). Therefore, the DNase-I hypersensitive sites sequencing (DNase-

seq) (Boyle et al., 2008) and the Assay for Transposase-Accessible Chromatin sequencing (ATAC-seq) (Buenrostro et al., 2013) are widely used for cis-regulatory elements identification. Both techniques have proved to be powerful tools to map the regulatory landscape of different cell types, developmental stages and conditions (Corces et al., 2018; Stergachis et al., 2013; Thurman et al., 2012).

Another way to identify and characterise cis-regulatory elements is by mapping the binding sites of TFs. One of the most widely used methods to assess TF binding *in vivo* is chromatin immunoprecipitation followed by deep sequencing (ChIP-seq) (Johnson et al., 2007). In this technique TFs are covalently cross-linked to their cognate binding sites on chromatin and immunoprecipitated by using TF-specific antibodies. The DNA fragment corresponding to the TF binding sites are then isolated, sequenced and computationally analysed. ChIP-seq enables the identification of thousands of putative cis-regulatory elements in a single experiment (Zinzen et al., 2009). However, the method can characterize the binding pattern of only one TF at a time, requires high-quality antibodies and a substantial amount of chromatin, and is not able to distinguish between direct and indirect DNA binding (Neph et al., 2012b). As a consequence, ChIP output does not always reflect sequence-specific TF occupancy or tissue-specific enhancer activity.

The presence of TF-DNA complexes within the DHSs and its contact to DNA prevents the digestion of small, ~6-20 nt long sequences by nucleases, highlighting stretches of nucleotides termed “footprints” (Galas and Schmitz, 1978) (Fig. 1.5). Advances in sequence technologies have enabled the digital genomic footprinting (DGF), allowing the determination of global TF occupancy in a single experiment (Hesselberth et al., 2009). The advent of DGF has not only allowed a better understanding of TF

occupancy patterns across differentiation but, when combined with databases containing TF recognition sequences, enables the construction and analysis of TF regulatory networks (Neph et al., 2012a). A recent advance in the field was the development of the 'Wellington" algorithm which uses chromatin features to highlight regions of transcription factor occupancy which significantly improved the identification of TF bound DNA sequences (Piper et al., 2013).

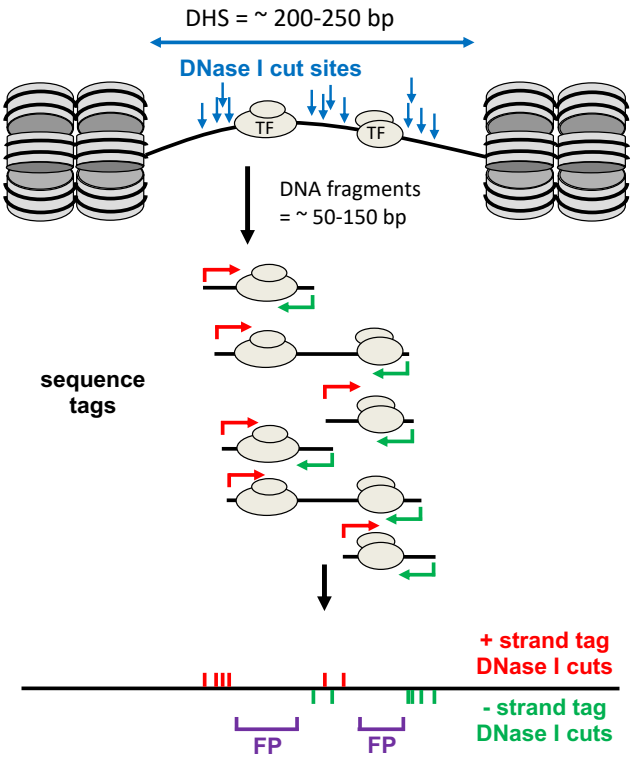

Figure 1.5: DNA footprinting principles

In this technique the genomic DNA is exposed to nucleases, such as DNase I. DNA bound by transcription factors is protected from enzymatic cleavage, resulting in the generation of short undigested fragments termed “footprints”. Courtesy of Prof Peter Cockerill, University of Birmingham.

1.2.9 Topologically associated domains

Eukaryotic chromosomes are not linear but are folded up in specific structures which compartmentalise them into active and inactive regions. Contiguous chromatin locally organizes into three-dimensional (3D) mega-base units called Topologically Associated Domains (TADs) (Fig. 1.6). TADs include highly interacting genomic regions that rarely contact loci belonging to other domains (Dixon et al., 2012). These structures are highly conserved between cell types and species (Dixon et al., 2012; Nora et al., 2012); however, their function is still not completely understood. It has been proposed that TADs are involved in gene expression control by restricting interactions of promoters with regulatory elements within the TADs. It was indeed found that the boundaries of TADs consist of sequences enriched in the architectural proteins CCCTC-binding factor (CTCF) and cohesin (Rao et al., 2014) which function as transcriptional insulators (Wendt et al., 2008). TAD disruption can lead to inappropriate cis-element pairings and cause several diseases including AML (Groschel et al., 2014; Lupianez et al., 2016) as a result of transcriptional dysregulation.

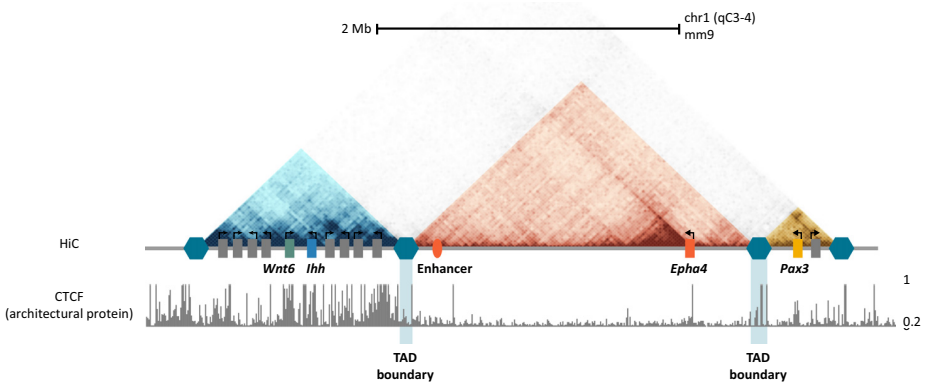

Figure 1.6: Representation of a topologically associated domains (TADs)

The interaction profile within each TAD is shown in a heatmap, where each dot represents an interaction pair. The boundaries at both sides of a TAD are enriched in CTCF and cohesin. Figure from (Lupianez et al., 2016).

1.2.10 Enhancer - promoter communication

Transcriptional regulation involves the physical interaction between regulatory elements and promoters that can be located at a large genomic distance. Distal regulatory elements do not always interact with the nearest promoter (Mumbach et al., 2019). As a consequence, DNA topology plays a paramount role in gene expression control. Different models have been proposed to explain the mechanism of these long-range interactions (Ptashne, 1986), but the most accredited is the DNA looping model which requires the intervening DNA to be looped out to bring regulatory elements and promoters into close proximity (Bulger and Groudine, 1999).

The looping model is widely supported by studies on chromatin architecture using the chromosome conformation capture (3C) technique (Dekker et al., 2002) which was later developed into a global methodology (Hi-C) (Lieberman-Aiden et al., 2009). These methods enable the quantification of the frequency of interaction between loci that are nearby in the folded chromatin but far away, even on different chromosomes, in the linear genome. In this assay intact nuclei are treated with formaldehyde to cross-link interacting DNA fragments that, after digestion with restriction enzymes, are intramolecularly ligated. Ligation products are reverse cross-linked and purified generating a collection of chimeric sequences formed by interacting loci which in the case of Hi-C are then analysed by next generation sequencing to identify pairs of interacting sequences. This methodology has been modified in different ways, with the most important one being the development of "promoter-capture-HiC" (Mifsud et al., 2015) (Fig. 1.7).

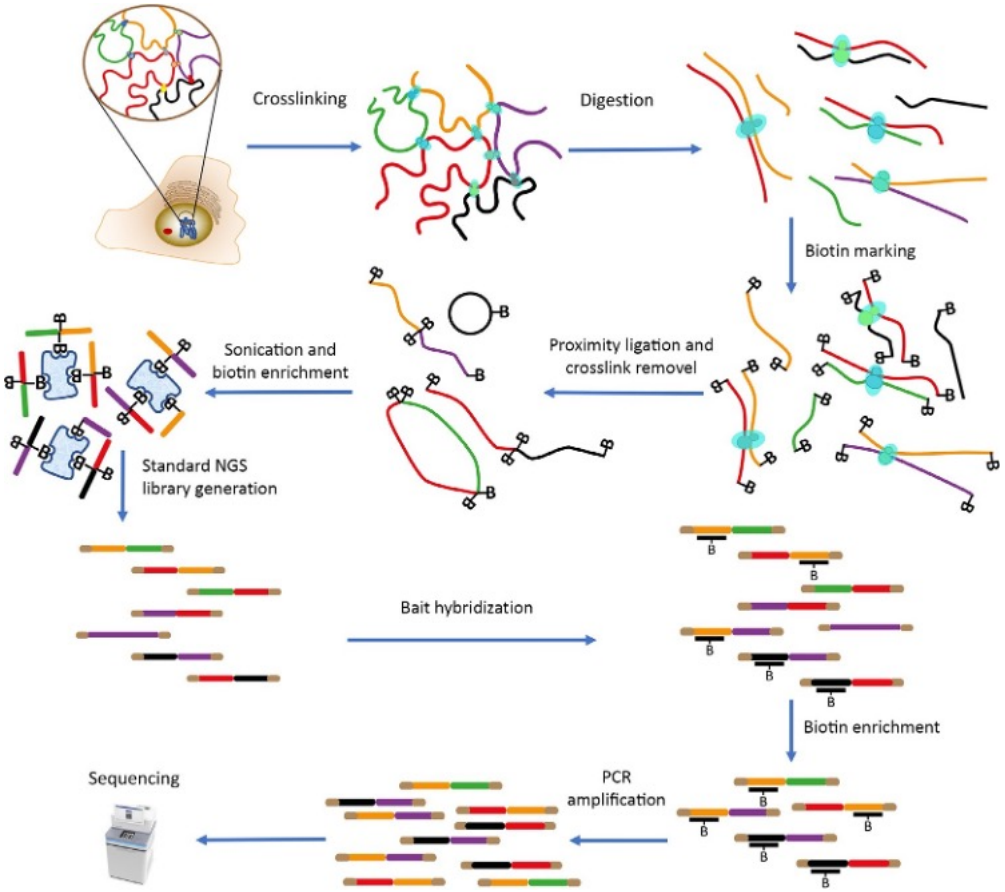

Figure 1.7: Capture Hi-C overview

Genomic DNA is crosslinked and digested with restriction enzymes. Restriction fragments are biotinylated, intramolecularly ligated and, after cross-linking removal, sonicated. Chimeric biotinylated products are then enriched by streptavidin pulldown and used to prepare a standard NGS library. Genomic region of interest (promoters in the case of promoter-CHi-C) are enriched with biotin-labelled baits, PCR amplified and sequenced. Figure from (Davis et al., 2020).

1.2.11 Gene regulatory networks

The regulatory interconnections between TFs are represented by gene regulatory networks (GRNs). GRNs are powerful ways to represent complex systems, such as the regulome driving embryonic endoderm specification (Peter and Davidson, 2011), and gain a mechanistical insight in the factors involved in their change or maintenance. GRNs inference has traditionally relied on gene expression perturbation studies where the relationship between two genes is deduced from the impact that the expression of

a gene has on another (Kucinski et al., 2020). However, to be able to obtain statistically significant results, a large number of perturbations have to be performed and indirect effects of a specific factor cannot be distinguished from direct effects. More recently connections between genes have been determined using ChIP assays and DGF, which allow to link a TF to its target genes (Assi et al., 2019b; Collombet et al., 2017; Neph et al., 2012a).

In a GRN each TF is represented as a node and the connections between TFs are represented as edges. Cell identity and biological functions are established through combinatorial cross-regulation of hundreds of TFs that regulate their own and the expression of other genes, so that multiple edges can go towards or emanating out from a node (Fig. 1.8). Highly interconnected nodes represent genes important for the maintenance of the network and are often under feed-forward or feed-back control, allowing fine gene expression control.

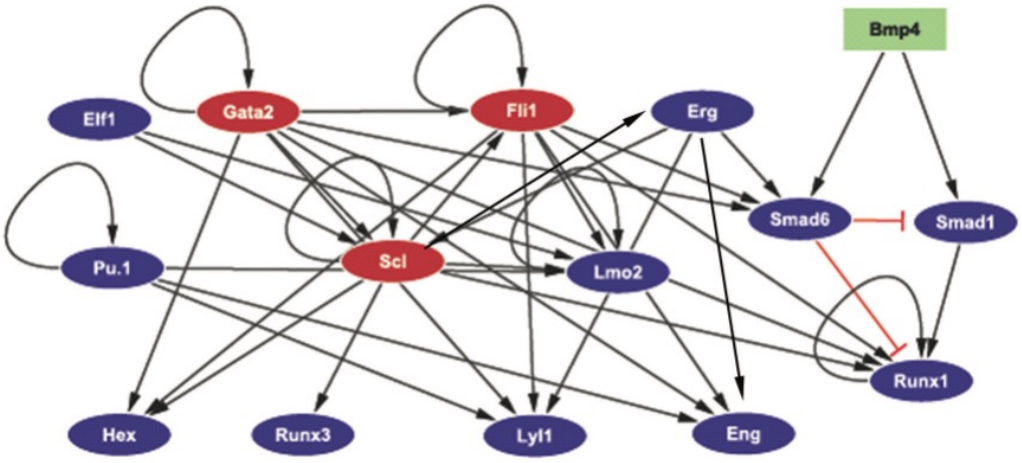

Figure 1.8: Schematic of the hematopoietic stem cell network

Figure from (Pimanda and Gottgens, 2010).

Disruption of the GRN governing cell identity can lead to oncogenic transformation (Wilkinson et al., 2017). In AML mutations in genes encoding for TFs, epigenetic regulators or signalling molecules reshape the network architecture, interfering with differentiation and promoting cell growth (Edginton-White and Bonifer, 2022).

It is interesting to note that different driver mutations seem to affect the same nodes (Assi et al., 2019b), suggesting that they impact on similar pathways and may dysregulate the same transcriptional network. As a consequence, modelling of the GRN on which specific cancer rely may enable identification of common vulnerabilities suitable for therapeutic intervention.

1.3 Haematopoiesis

Haematopoiesis is the complex and tightly regulated process through which mature blood cells are derived from a multipotent Haematopoietic Stem Cell (HSC), which in the adult mammalian organism resides in the bone marrow (Muller-Sieburg et al., 1986). Beside its ability to differentiate and sustain haematopoiesis, this rare cell type is characterized by the ability to self-renew and to generate new daughter stem cells.

1.3.1 The origin of HSCs

In mammals, the emergence of the haematopoietic system occurs early in the development in the yolk sac, an extraembryonic tissue. At this stage, called primitive haematopoiesis, progenitors with limited potency and renewal abilities appear (Moore and Metcalf, 1970). In mammals, the first definitive HSCs are generated in the aorta-gonad-mesonephros (AGM) region of the embryo from a specialized population of endothelial cells called haemogenic endothelium (Lancrin et al., 2009; Medvinsky et

al., 1993). During this process, termed endothelial-to-haematopoietic transition (EHT), selected endothelial cells become rounder and detach from the neighbouring endothelial cells, forming intra-aortic haematopoietic clusters (Boisset et al., 2010; Yvernogeau et al., 2016). Through the circulation these HSCs colonize the foetal liver, where they expand and mature before finally reaching the bone marrow to sustain haematopoiesis after birth.

1.3.2 HSC differentiation

Classically, haematopoiesis has been described as a multistep process, where HSCs progressively lose their self-renewal ability and potency to generate a multipotent progenitor (MPP), that shows a higher proliferative rate. MPPs give rise to the common myeloid progenitors (CMPs) and common lymphoid progenitors (CLPs), that generate myeloid and lymphoid lineages respectively (Akashi et al., 2000; Kondo et al., 1997) (Fig. 1.9 A). More recently, with the advances in next-generation techniques and the advent of single cell RNA-seq (scRNA-seq) that enable study of individual HSCs along the whole differentiative route, our picture of haematopoiesis is deeply changing. Terminally differentiated blood elements appear not to be generated passing through intermediate cell types, but through a continuum of transitory states of undifferentiated progenitors that gradually acquire lineage-specific characteristics (Macaulay et al., 2016; Velten et al., 2017) (Fig. 1.9 B).

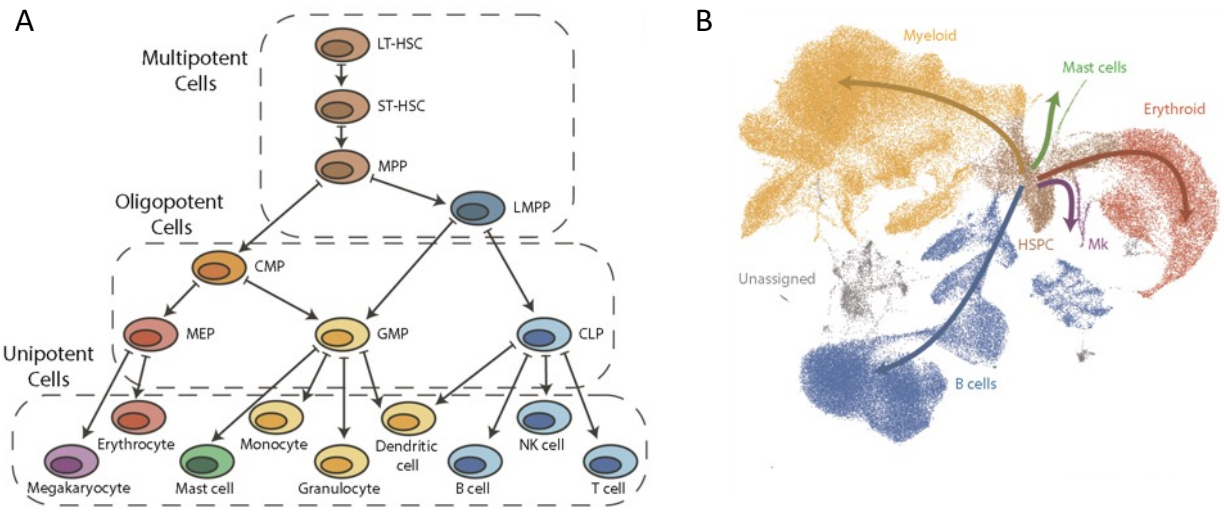

Figure 1.9: Haematopoiesis

(A) Classic hierarchical model of haematopoiesis. LT-HSC = Long Term Haematopoietic Stem Cell, ST-HSC = Short Term Haematopoietic Stem Cell, MPP = Multipotent Progenitor, LMPP = Lymphoid-primed Multipotent Progenitor, CMP = Common Myeloid Progenitor, MEP = Megakaryocyte-Erythroid Progenitor, GMP = Granulocyte-Monocyte Progenitor, CLP = Common Lymphoid Progenitor. (B) Uniform Manifold Approximation and Projection for Dimensional Reduction (UMAP) map of scRNA-seq data from bone marrow mononuclear cells, depicting haematopoiesis as a continuum of differentiation states. Figure from (Watcham et al., 2019).

1.4 Transcription factors in Haematopoiesis

The emergence of HSCs and progenitor differentiation are orchestrated by a fine-tuned gene expression program, whereby TFs are essential for the execution of the different cell fates (Obier and Bonifer, 2016) (Fig. 1.10). The experimental evidence for this notion comes from multiple gene targeting studies in mice which showed that the absence of specific factors leads to the absence of specific branches of the haematopoietic hierarchy. The next paragraphs will review some of the TF involved in hematopoiesis.

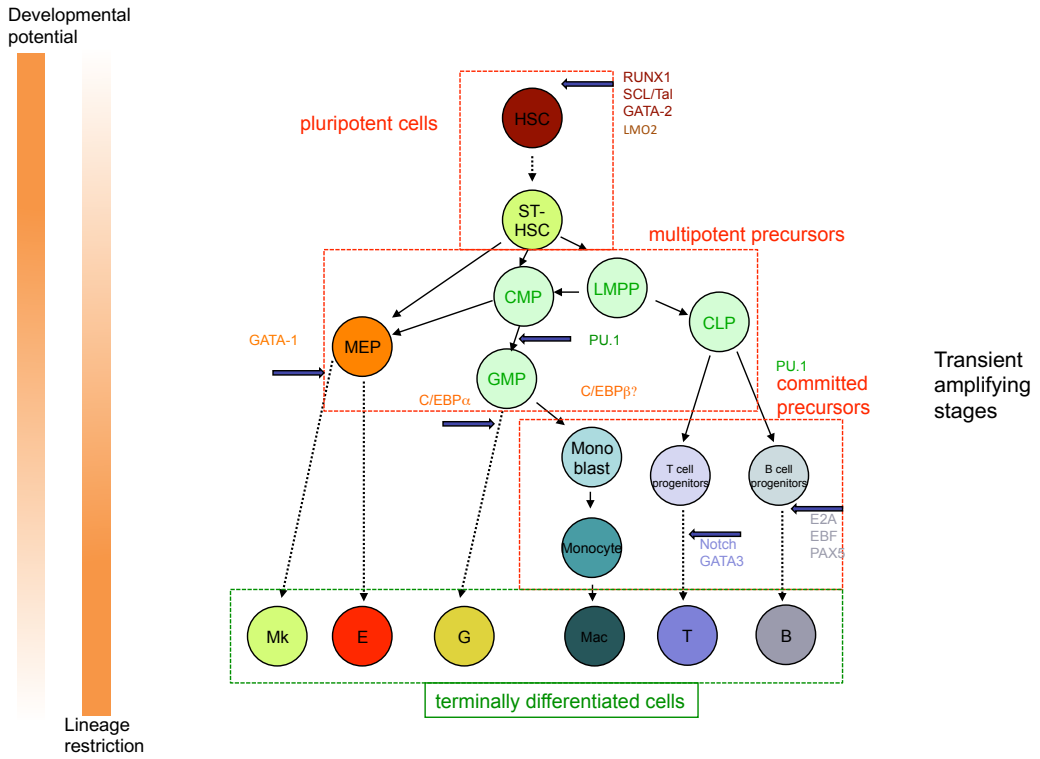

Figure 1.10: Cell fates are regulated by transcription factors

The expression of lineage specific transcription factors drives the differentiation of pluripotent precursors into terminally differentiated cells. Courtesy of Prof Constanze Bonifer, University of Birmingham.

1.4.1 RUNX1

Runt-related transcription factor 1 (RUNX1), together with RUNX2 and RUNX3, belongs to the core-binding factor-α (CBFα) TF family (Speck and Baltimore, 1987). All the members of the family share a conserved Runt-homology domain (RHD), responsible for the DNA binding at the consensus sequence TG(T/C)GGT (Meyers et al., 1993). The RHD also mediates the interaction with CBFβ. This factor does not associate directly with DNA but stabilizes RUNX1 factors binding to the runt-domain binding element (Wang et al., 1996b). The RUNX1 gene is located on the long arm of chromosome 21 and is transcribed in three major isoforms by using two different

promoters and alternative splicing (Fujita et al., 2001; Ghozi et al., 1996). The RUNX1a isoform lacks the C-terminal AD, that is instead retained in both RUNX1b and RUNX1c, and seems to act as dominant negative by competing with the long isoforms (Fig. 1.11). RUNX1 plays a key role in the emergence of embryonic haematopoiesis and is widely expressed throughout the whole haematopoietic system (North et al., 2004). It is required for the emergence of HSCs from the haemogenic endothelium within the dorsal aorta and RUNX1 deficiency in mice leads to defective angiogenesis and embryonic lethality (North et al., 1999; Okuda et al., 1996; Wang et al., 1996a; Yokomizo et al., 2001). However, loss of RUNX1 expression in adult mice does not lead to haematopoiesis failure but causes several abnormalities, such as the expansion of a Lineage-negative, Sca1-positive, Kit-positive (LSK) population and myeloid progenitors in the bone marrow and neutrophilia (Chen et al., 2009; Motoda et al., 2007). RUNX1 is also crucial for myelopoiesis, where it is required for the expression of lineage-specific TFs such as PU.1 and C/EBPα (Guo et al., 2012; Hoogenkamp et al., 2007; Imperato et al., 2015).

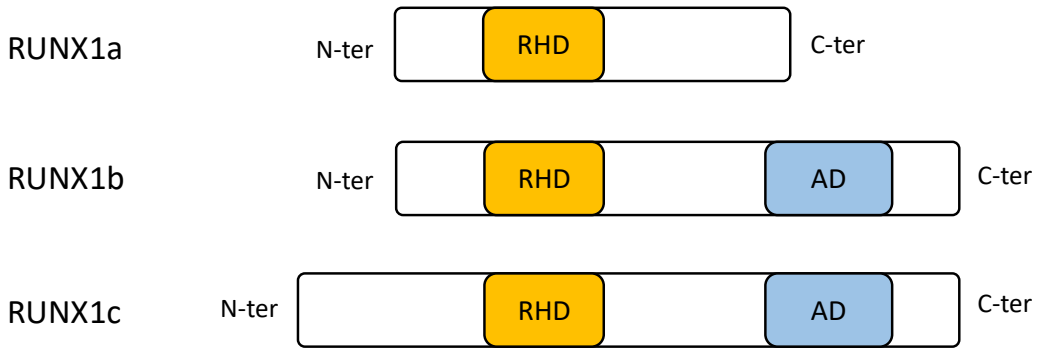

Figure 1.11: RUNX1 isoforms structure.

Runx1 is translated in three isoforms, all sharing a conserved RHD domain required for DNA binding. RUNX1a isoform lacks the C-terminal AD, that is instead retained in both RUNX1b and RUNX1c.

1.4.2 TAL1

T-cell acute lymphocytic leukaemia protein 1 (TAL1) is a member of the basic helix-loop-helix (bHLH) family of TFs (Cheng et al., 1993). It has been first identified because it was involved in a chromosomal translocation recurrent in T-cell acute leukaemia (T-ALL) (Begley et al., 1989). In hematopoietic cells, TAL1 regulates the expression of its target genes by forming complexes with other proteins such as GATA-1 and the LIM-only proteins LMO2 and LDB-1 (Wadman et al., 1997). It is essential for HSC specification during embryonic development (Robb et al., 1995) and for embryonic erythropoiesis (Shivdasani et al., 1995) but dispensable for adult HSCs function (Mikkola et al., 2003). TAL1 is highly expressed in adult HSCs, myeloid and erythroid progenitors, megakaryocytes and mast cell, but is expressed at a low level in early lymphoid progenitors and absent in differentiate B and T lymphocytes (Mouthon et al., 1993; Visvader et al., 1991). Overexpression of TAL1 is one of the causes of T-ALL (Ferrando et al., 2004).

1.4.3 PU.1

PU.1 is a member of the E-twenty-six (ETS) family of TFs (Klemsz et al., 1990), characterized by a highly conserved winged helix-turn-helix DNA binding domain, also known as ETS domain, and recognizes the purine-rich motif (G/C)(G/A)GGAAGT) (Kodandapani et al., 1996). The ETS domain also mediates the interactions with other TFs, such as RUNX1 (Hu et al., 2011), GATA-1 (Nerlov et al., 2000) and JUN (Behre et al., 1999). Additional sequences important for PU.1 function are the N-terminal activation domain, which contains three acidic subdomains and one glutamine-rich subdomain required for transactivation activity (Klemsz and Maki, 1996), and the PEST

domain, responsible for protein-protein interactions and transcriptional regulation (Pongubala et al., 1992; Pongubala et al., 1993).

The *Spi1* gene, encoding PU.1, is specifically expressed in hematopoietic tissues, predominantly in the B lymphoid and monocytic lineages (Nutt et al., 2005), and is required to drive differentiation in multiple haematopoietic lineages. Homozygous mutations in mice result in prenatal lethality due to severe anemia, while heterozygous mutant embryos show defects in the generation of B and T lymphocytes, monocytes and granulocytes (McKercher et al., 1996; Scott et al., 1994). Together with C/EBPα, PU.1 promotes myeloid differentiation by upregulating the expression of GM-CSF (Hohaus et al., 1995) and CSF-1R (colony stimulating factor receptor 1) (Aikawa et al., 2010). In addition, PU.1 is essential for the maintenance of the adult HSC compartment, were controls multiple cell-cycle regulators preventing stem cell exhaustion (Staber et al., 2013). Reduced PU.1 expression is associated with myeloid leukemia in mice (Rosenbauer et al., 2004) and heterozygous PU.1 mutations have been reported in AML patients (Mueller et al., 2002).

1.4.4 C/EBPα

CCAAT-enhancer binding protein alpha (C/EBPα) is the prototype of the C/EBP basic region-leucine zipper (bZIP) TF family, that also includes C/EBPβ, C/EBPδ, C/EBPε, C/EBPγ, and C/EBPζ (Williams et al., 1991). All the members of the family share similar leucine-zip (LZ) and basic DBD at their C-terminus. The LZ region is required to form homodimers or heterodimers with other TFs, including C/EBPs, while the DBD is responsible for direct binding to the consensus DNA sequence (A/G)TTGCG(C/T)AA(C/T) (Landschulz et al., 1988; Osada et al., 1996; Vinson et al.,

1989). *CEBPA* is an intronless gene located on chromosome 19 in humans. It is transcribed into a single mRNA that can be translated in two protein isoforms, p42 (42 KDa) and p30 (30 KDa), depending on usage of two alternative AUG start codons within the same open reading frame (ORF) (Lin et al., 1993). The short p30 isoform lacks the N-terminal activation domain 1 (AD1), that is instead present in the full-length p42 protein (Fig. 1.12).

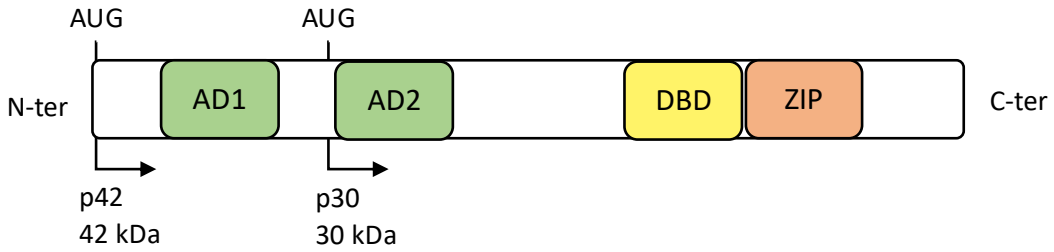

Figure 1.12: C/EBPα structure

C/EBPα is characterized by two N-terminal AD and a C-terminal bZIP region, required to dimerize with other TFs and bind the DNA. Depending on start codon usage, C/EBPα is translated into a full-length p42 isoform and a short p30 isoform, which retains only one of activation domains.

The isoform ratio has a deep impact on cell differentiation state. C/EBPα-p42 exerts antimitotic effects through E2F-mediated repression of c-myc and recruits TBP/TFIIB to lineage-specific promoters, inducing granulocytic differentiation, while C/EBPα-p30 is associated with an immature cell state (Koschmieder et al., 2007; Nerlov and Ziff, 1995; Porse et al., 2001). Moreover, the p30 isoform can form heterodimers with the full-length counterpart, thus inhibiting p42-mediated gene transactivation (Cleaves et al., 2004). Furthermore, both isoforms retain the activation domain 2 (AD2) that controls proliferation via interaction with Cdk2/Cdk4 and the chromatin remodelling complex SWI/SNF (Muller et al., 2004; Wang et al., 2001). C/EBPα is a major factor

for myeloid specification. It is essential for the generation of terminally differentiated and functional granulocytes, and its expression is required for the differentiation of CMPs to GMPs (Radomska et al., 1998; Zhang et al., 1997). In multipotent GM progenitors, *CEBPA* upregulation promotes the expression of myeloid lineage genes, such as *CSFR3*, *GF1* or *CEBPE*, as well as its own expression, while acting as repressor for non-myeloid genes (Friedman, 2007; Ma et al., 2014; Timchenko et al., 1995; Zhang et al., 1998). Previous work showed that enforced expression of C/EBPα is sufficient to reprogram B cell progenitors into macrophage-like cells (Bussmann et al., 2009). In addition, C/EBPα is indispensable to maintain adult HSCs in a quiescent state to avoid their exhaustion and assure hematopoietic system integrity (Hasemann et al., 2014; Ye et al., 2013).

1.5 Acute Myeloid Leukaemia

Acute myeloid leukaemia (AML) is a haematological malignancy characterized by a block of differentiation and abnormal proliferation of hematopoietic progenitors. Despite advances in the understanding of AML biology and treatments available, refractory diseases and relapse are common, and the overall outcome is still extremely poor (Dohner et al., 2015; Meyer and Levine, 2014).

1.5.1 AML mutation classification

Depending on their role in leukaemia pathogenesis, AML-causing genetic abnormalities can be classified into three classes (Papaemmanuil et al., 2016; Takahashi, 2011). Class I mutations constitutively activate signal transduction pathways, increasing proliferation and survival of malignant clones. This category of

mutations includes those that activate the tyrosine kinases FLT3, KIT and JAK2, or the GTPases NRAS and KRAS. Class II mutations affect TFs and transcriptional coactivators, interfering with self-renewal and differentiation of hematopoietic progenitors. Belonging to this category are mutations that involve *RUNX1* and its cofactor CBFβ, CEBPA, PU.1 (Frohling et al., 2005; Kelly and Gilliland, 2002). Finally, class III mutations alter genes encoding epigenetic regulators, such as the DNA methyltransferase DNMT3, IDH1/2 and the methylcytosine dioxygenase TET2 (Fathi and Abdel-Wahab, 2012).

AML is a multistep process which requires the acquisition of multiple driver mutations within the same clone over time (Welch et al., 2012). The two-hit model postulates that at least two mutations belonging to two different classes are needed to give rise to full blown AML (Gilliland and Griffin, 2002). This has been exemplified in mouse models expressing the AML1/ETO fusion protein, which do not develop leukaemia in absence of cooperative mutations (Schessl et al., 2005; Yuan et al., 2001). An exception is represented by mutations in the mixed lineage leukaemia (*MLL*) gene, encoding for the lysine-methyltransferase KMT2A and frequent target of chromosomal translocation in paediatric AMLs (Biondi et al., 2000). The sole expression of MLL fusion proteins in stem and progenitor mice cells is sufficient to induce leukemogenic transformation (Cozzio et al., 2003). However, the number of driver mutations differs between individual patients, with an average of 13 mutations per AML (Cancer Genome Atlas Research et al., 2013). “Early” lesions usually increase self-renewal and often impair differentiation thus causing the expansion of a clonal pre-leukemic population (Shlush et al., 2014), while “late” mutations activate signalling pathways which promote proliferation and fully block differentiation (Zheng and Small, 2005). Mutations

involving epigenetic regulators are the most common early hits (Corces-Zimmerman et al., 2014) and are the main drivers of a process called clonal haematopoiesis of indeterminate potential (CHIP), characterized by the clonal expansion of stem and progenitor cells harbouring cancer-associated mutations (Jaiswal and Ebert, 2019). CHIP is mainly associated with the elderly population and occurs also in healthy individuals (Busque et al., 2012). While not representing a malignancy itself, CHIP is associated to an increased risk to develop haematological cancers (Genovese et al., 2014; Jaiswal et al., 2014).

1.5.2 Leukaemic Stem Cells

Leukaemic stem cells (LSCs) have been first described as a rare population within the tumour bulk able to give rise to leukaemia when transplanted in severe combined immune-deficient (SCID) mice (Lapidot et al., 1994). Similar to HSCs, LSCs reside in the bone marrow and are able to self-renew, proliferate and incompletely differentiate into leukaemic blasts following a hierarchical organization (Bonnet and Dick, 1997). LSCs can originate from mutations in either HSCs or committed progenitors, which de-differentiate and acquire stem-cell like characteristics (Jordan et al., 2006) (Fig. 1.13).

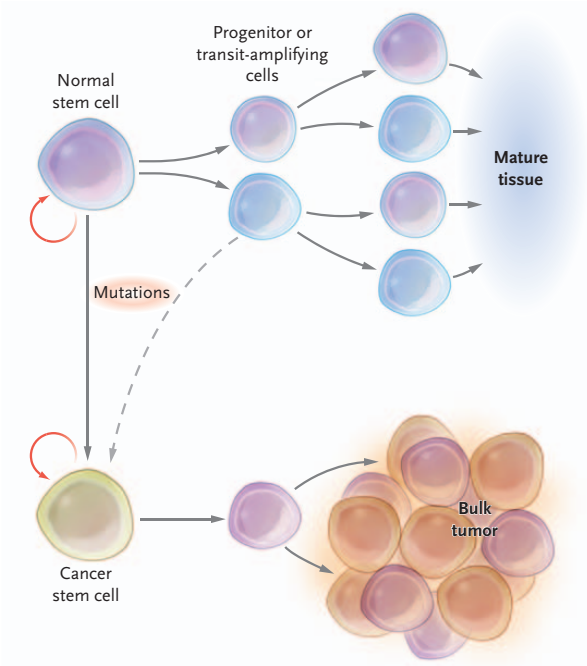

Figure 1.13: The origin of leukaemic stem cells

Mutations in HSCs or progenitors can give rise to LSCs which, similarly to normal stem cells, have the ability to self-renew and differentiate into leukaemic blasts. Figure from (Jordan et al., 2006).

LSCs are enriched within but not limited to the CD34+ CD38- CD90- compartment (Blair et al., 1997; Lapidot et al., 1994). It has been shown that two distinct LSC populations can coexist in most of AMLs: the more immature, CD38- population functionally mirrors LMPPs, while the more mature, CD38+ population resembles GMPs (Goardon et al., 2011). Several studies aimed at defining a LSC gene expression signature have shown that malignant stem cells rely on a chimeric transcriptional network that resemble both HSCs and progenitors (Barreyro et al., 2012; Gentles et al., 2010; Majeti et al., 2009), but is enriched for self-renewal gene expression (Sachs et al., 2020). Moreover, the expression of a LSC gene signature has been associated with worse clinical outcome in AML patients independent of their cytogenetic status (Gentles et al., 2010).

LSCs represent a reservoir of malignant blasts, driving disease maintenance and progression (Dick, 2008), and have been linked to disease relapse. The reason for this

feature is their low division rate which make them difficult to target with most conventional antiproliferative drugs (Guan et al., 2003). Thus, complete eradication of these cells is paramount to achieve a long-lasting remission and cure AML and there is a big effort to identify characteristics unique to LSCs and develop targeted therapies.

1.5.3 C/EBPα in AML

The *CEBPA* gene is mutated in ~15% of all AMLs (Pabst et al., 2001b). Most mutations are concentrated in two hotspots in the coding region, affecting either the N-terminal TAD1 or the C-terminal bZIP domain. N-terminal mutations are usually out-of-frame and cause the formation of a premature stop codon. In this case, re-initiation of translation from the internal start codon results in the exclusive expression of the C/EBPα-p30 isoform. On the other hand, C-terminal mutations are mainly in-frame insertions/deletions (indels) that alter the bZIP domain and disrupt C/EBPα DNA-binding and/or dimerization ability (Mueller and Pabst, 2006; Nerlov, 2004). C/EBPα C-terminal mutants in which the DNA binding domain is corrupted but the dimerization ability is preserved sequester C/EBPα partners and prevent their binding to DNA, functioning in a dominant-negative fashion (Asou et al., 2003). About 70% of *CEBPA* mutant AML cases exhibit biallelic mutations. In most, N-terminal and C-terminal lesions are combined (*CEBPA*$^{N/C}$), although very rare N-terminal/N-terminal or C-terminal/C-terminal combinations also occur (Wouters et al., 2009; Wouters et al., 2007). Previous work in mouse models showed that homozygous C-terminal mutations promote the expansion of pre-leukaemic HSCs but impair myeloid differentiation. In contrast, N-terminal mutations do not impact on proliferation and preserve myeloid commitment. As a consequence, the combination of both mutations accelerates

leukemogenesis and explains the *CEBPA*$^{N/C}$ prevalence (Bereshchenko et al., 2009). However, the sole expression of the p30 isoform links myeloid commitment with loss of proliferation control and is sufficient to develop AML with complete penetrance in mice (Kirstetter et al., 2008).

AMLs with biallelic but not monoallelic C/EBPα mutations or wild-type C/EBPα, are associated with a favourable prognosis (Dufour et al., 2010; Fasan et al., 2014; Wouters et al., 2009), and since 2016 have been recognized as a separate group in the World Health Organization (WHO) classification of myeloid neoplasms and acute leukaemia (Arber et al., 2016). However, recent studies suggest that in-frame mutations in the C/EBPα bZIP domain confer a better outcome compared to those affecting the AD, regardless of their occurrence as biallelic or single mutations (Tarlock et al., 2021; Taube et al., 2022; Wakita et al., 2022). These findings may challenge the actual WHO classification and patient management.

Germline heterozygous mutations in *CEBPA* predominantly cluster within the N-terminus of the protein and are associated with CEBPA-associated familiar AML (Tawana et al., 2017). These mutations are highly penetrant and cause an early onset leukaemia but have a more favourable outcome (Tawana et al., 2015). Affected patients usually acquire a second mutation targeting the C-terminus of C/EBPα (Pabst et al., 2008) and appear to have an increased risk of AML recurrence. However, the original diagnostic somatic mutations are absent at the relapse, suggesting that recurrence is driven by distinct independent clones (Tawana et al., 2015).

1.5.4 Mutations that co-occur with *CEBPA$^{N/C}$*

CEBPA$^{N/C}$ AMLs are often associated with mutations in genes encoding for other TFs, epigenetic regulators and signalling molecules. Interestingly, *CEBPA* and *CEBPA$^{N/C}$* mutations seem to be mutually exclusive with cytogenetic abnormalities, included the t(8;21) translocation (Papaemmanuil et al., 2016). *GATA2* is frequently co-mutated with *CEBPA*. *GATA2* mutations are reported in 15-35% of *CEBPA$^{N/C}$* cases and confer a better prognosis compared to the presence of wild-type *GATA2* (Wilhelmson and Porse, 2020). Mutations in the zinc finger (ZF) 1 domain of GATA2 reduce C/EBPα-p30 dependent transcriptional activation while enhancing the expression of C/EBPα target genes, such as *JUNB*, *FOS* and *CEBPB* (Greif et al., 2012a). Interestingly, in most of *CEBPA$^{N/C}$* - *GATA2$^{-/+}$* AMLs the mutated GATA2 allele is preferentially expressed (Mulet-Lazaro et al., 2021). Mutations in the *CSF3R* (colony stimulating factor 3 receptor) gene have been frequently described together with *CEBPA$^{N/C}$* and are associated with an unfavourable prognosis (Su et al., 2019). CSF3R signals predominantly through the Janus kinase (JAK) – signal transducers and activators of transcription (STAT) pathway (Maxson et al., 2013), and *CEBPA$^{N/C}$* – *CSF3R* mutated AMLs have been reported to be sensitive to JAK inhibitors (Lavallee et al., 2016). The ten-eleven translocation 2 (TET2) is a methylcytosine dioxygenase that catalyses the conversion of 5-methylcytosine(5mC) to 5-hydroxymethylcytosine (5hmC) (Nonaka et al., 2014). This enzyme plays a key role in DNA demethylation, regulating transcriptional activation. *TET2* is co-mutated with *CEBPA* in 40% of cases, conferring a poor prognosis (Grossmann et al., 2013; Konstandin et al., 2018). In addition, the tumour suppressor Wilms tumor 1 (WT1), a zinc-finger TF is frequently mutated in *CEBPA$^{N/C}$* AML (Wilhelmson and Porse, 2020).

Of note, RUNX1 mutations co-occur very rarely with *CEBPA* and *CEBPA*$^{N/C}$ mutations (Greif et al., 2012b; Schnittger et al., 2011).

1.5.5 RUNX1 in AML

The RUNX1 gene is frequently mutated in AML (Papaemmanuil et al., 2016). The most recurrent aberration is the translocation t(8;21), that leads to the juxtaposition of the RUNX1 gene on chromosome 21 to almost the entire eight-twenty-one (ETO) gene located on chromosome 8 (Downing et al., 1993; Miyoshi et al., 1993). The resulting fusion protein RUNX1-ETO retains the RUNX1 RHD and thus the ability to interact with CBFβ and bind the DNA at canonical sites, while the transactivation domain is replaced by ETO. ETO contains four Nervy Homology Regions (NHRs) able to recruit transcriptional co-repressors, such NCoR/SMRT, mSin3 and HDACs (Amann et al., 2001), inhibiting the expression of RUNX1 targets.

Another relevant translocation, the inv(16), affects the RUNX1 binding partner CBFβ and generates the fusion gene *CBFB-MYH11* (Liu et al., 1993). The chimeric protein CBFβ-SMMHC is still able to heterodimerize with RUNX1 and interfere with its function thus acting as a transcriptional repressor by sequestering RUNX1 in the cytoplasm and leading to wide-spread disruption of RUNX1 binding in the genome (Adya et al., 1998; Kanno et al., 1998; Mandoli et al., 2014). CBFβ-SMMHC expression in mice blocks haematopoiesis at the stem-cell level, recapitulating the RUNX1 knock-out phenotype (Castilla et al., 1996), but is not sufficient for leukaemogenesis (Castilla et al., 1999; Castilla et al., 2004).

RUNX1 point mutations include deletions, frameshift, missense, nonsense and splicing mutations and are associated with a worse outcome (Gaidzik et al., 2016; Schnittger et al., 2011). Mutations that truncate the AD domain or impact on the DNA binding can produce an unstable or non-functional protein, leading to haploinsufficiency (Beri-Dexheimer et al., 2008). In some cases, the mutated RUNX1 acts as a dominant negative factor (Matheny et al., 2007). For example, the R201Q mutation in the DBD interferes with wild-type RUNX1, reducing its interaction with CBFβ and DNA binding (Kellaway et al., 2021). Mutations in RUNX1 are rarely early events in leukaemogenesis but are implicated in the onset of myelodysplastic syndrome (MDS), a clonal hematopoietic disorder characterized by ineffective haematopoiesis that frequently progresses to AML (Harada et al., 2004; Hirsch et al., 2016; Tefferi and Vardiman, 2009).

1.5.6 t(8;21) molecular pathogenesis

Classically, RUNX1-ETO mediated leukaemogenesis has been explained as a dominant inhibition of RUNX1 function. ETO recruits HDACs and methyltransferases to RUNX1 target gene promoters, primarily through the NHR2 and NHR4 domains, (Amann et al., 2001; Gelmetti et al., 1998; Lutterbach et al., 1998; Wang et al., 1998). The result of co-repressor recruitment is transcriptional repression of hematopoietic targets, including genes encoding myeloid transcription factors such as PU.1, GATA-1 and C/EBPα (Choi et al., 2006; Pabst et al., 2001a; Vangala et al., 2003). However, several studies have demonstrated that the binding of RUNX1-ETO can also be compatible with active transcription. The presence of the fusion protein leads to an up-regulation of AP-1 which drives *CCND2* (Cyclin D2) expression and promotes cell cycle

progression (Martinez-Soria et al., 2018) and of the transcription factor FOXO1 to enhance self-renewal and block differentiation (Lin et al., 2017). FOXO1 is consistently upregulated in t(8;21) AMLs and share most of its binding sites at crucial self-renewal genes with RUNX1-ETO. Accordingly, pharmacological inhibition of FOXO1 inhibits the stem cell molecular program (Lin et al., 2017). In addition, RUNX1-ETO inhibits apoptosis by promoting the transcription of BCL-2 (Klampfer et al., 1996).

RUNX1-ETO function is dependent on the formation of the so called AML1–ETO-containing transcription factor complex (AETFC), which includes CBF-β, FLI1/ERG, the E proteins HEB and E2A, LYL1, LMO2 and LDB1 (Mandoli et al., 2016; Sun et al., 2013). AETFC stability is fundamental for aberrant gene expression and leukaemogenesis and point mutations in or knock down of components of the complex lead to loss of RUNX1-ETO induced self-renewal (Mandoli et al., 2016; Sun et al., 2013). In addition to complex formation, the interaction of RUNX1-ETO with CBFβ is important to repress the expression of RUNX1 haematopoietic targets (Roudaia et al., 2009). The extent of this requirement has been the subject of intense debate (Park et al., 2009). Of note, the expression of the wild-type RUNX1 allele is essential for the survival of t(8;21) AML cells and RUNX1 knock down leads to cell-cycle arrest and apoptosis (Ben-Ami et al., 2013; Loke et al., 2017; Mandoli et al., 2016).

Genome-wide studies showed that RUNX1-ETO impacts on chromatin accessibility, TF binding and histone modifications primarily by competing with and displacing RUNX1 from its binding sites to set up an aberrant gene regulatory network (Kellaway et al., 2020). RUNX1-ETO expression in murine myeloid precursors leads to downregulation of myeloid genes governed by RUNX1, such as C/EBPα, while simultaneously increases the expression of stem cell genes, such as GATA2 and ERG

(Regha et al., 2015). RUNX1-ETO knock-down results in an increased RUNX1 binding at both sites previously occupied by the fusion protein and de novo targets (Ptasinska et al., 2012) and leads to a differentiation program mainly driven by the upregulation of C/EBPα (Ptasinska et al., 2014), This transcriptional rewiring is accompanied by a rearrangement of cis regulatory element-promoter interactions, demonstrating that RUNX1-ETO controls leukemogenesis also by shaping the 3D genome structure (Ptasinska et al., 2019). Recently a small core transcriptional network made up of ~60 RUNX1-ETO direct targets has been defined by combining rapid RUNX1-ETO degradation to nascent RNA measurement immediately after (Stengel et al., 2021). The network included important regulators of myeloid differentiation, such as C/EBPα, and almost all the target genes were upregulated upon RUNX1-ETO degradation, confirming its repressive role. This study confirmed that the transcriptional changes previously observed in knock-down experiments was determined by both direct and indirect effects of RUNX1-ETO depletion.

1.5.7 Mutations co-occurring with mutant RUNX1-ETO

The t(8;21) translocation is an early event in leukaemogenesis, as demonstrated by the presence of this lesion in the pre-leukaemic clones and during remission and relapse (Shima et al., 2014; Wiemels et al., 2002). However, RUNX1-ETO expression is not sufficient to cause AML and additional genetic alterations must occur for leukaemia development (Shima et al., 2014). Gain of function mutations of *FLT3*, *KIT*, *NRAS* and *KRAS* genes are the most frequent and promote malignant transformation by inducing a proliferative advantage in pre-leukaemic cells (Renneville et al., 2008). Activating c-KIT mutations enhance DNA repair, promote proliferation and reduce

apoptosis in RUNX1-ETO-expressing hematopoietic progenitors (Wichmann et al., 2015), while the expression of the G12D mutant NRAS in RUNX1-ETO-expressing $CD34^{+}$cord blood cells was shown to promote cytokine-independent growth, colony formation and cell survival (Chou et al., 2011).

In addition to growth factor receptor mutations, alteration of epigenetic regulators such as DNMT3, TET2, EZH2, ASXL1/2 and IDH2 are also frequently reported in t(8;21) AML (Christen et al., 2019). Mutations in DNA methyltransferase such as DNMT3 and TET2 show a high variant allele frequency (VAF) and seem to be early events in leukaemogenesis, in contrast to mutations in ASXL1/2 that appear to occur in later stage (Christen et al., 2019). Of note, the t(8;21) genomic lesion seems to be mutually exclusive with *CEBPA* mutations (Leroy et al., 2005).

1.6 AML as a disease of myeloid differentiation going side-ways

In the last years it became increasingly clear that AML is not one disease, but many, with different mutations leading to different disease phenotypes, clinical outcomes and morphology of leukaemic cells (Fig. 1.14). Depending on the mutation, cells also displayed different transcriptional programs (Valk et al., 2004). However, the reason behind these different gene expression profiles was unclear.

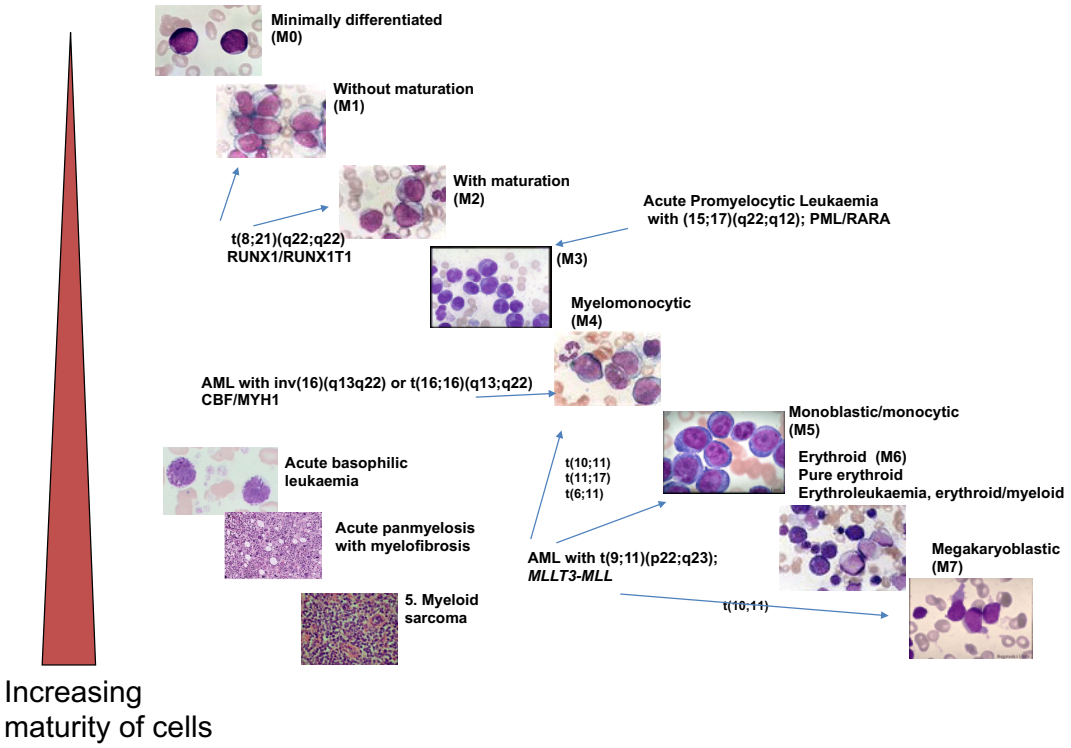

Figure 1.14: AML comprises a group of heterogeneous diseases

The French-American-British (FAB) classification system of haematological disease subdivide AMLs into 9 groups, based on the morphology of leukaemic blasts (Bennett et al., 1985). Genetically defined AMLs subtypes display a different phenotype and are classified accordingly to their maturation stage. Courtesy of Dr Manoj Raghavan, University of Birmingham.

To address this question, Assi et. al (2019b) defined the GRNs of different AML subtypes by collecting transcriptome, digital footprinting and chromatin conformation capture data of cells from AML patients with different and defined TF and signalling mutations (Assi et al., 2019b). In this study, CD34+ or CD117+ blasts were purified from peripheral blood or bone marrow of AML patients harbouring *t(8;21), Inv(16), FLT3-TKD, FLT3-ITD, NPM1, RUNX1*, $CEBPA^{N/C}$ and *CEBPA* single mutations. At least 3 sets of data from these patients were compared to those from CD34+ peripheral

blood stem cells PBSCs and CD34+ cord blood cells. Data were integrated as shown in Fig. 1.15.

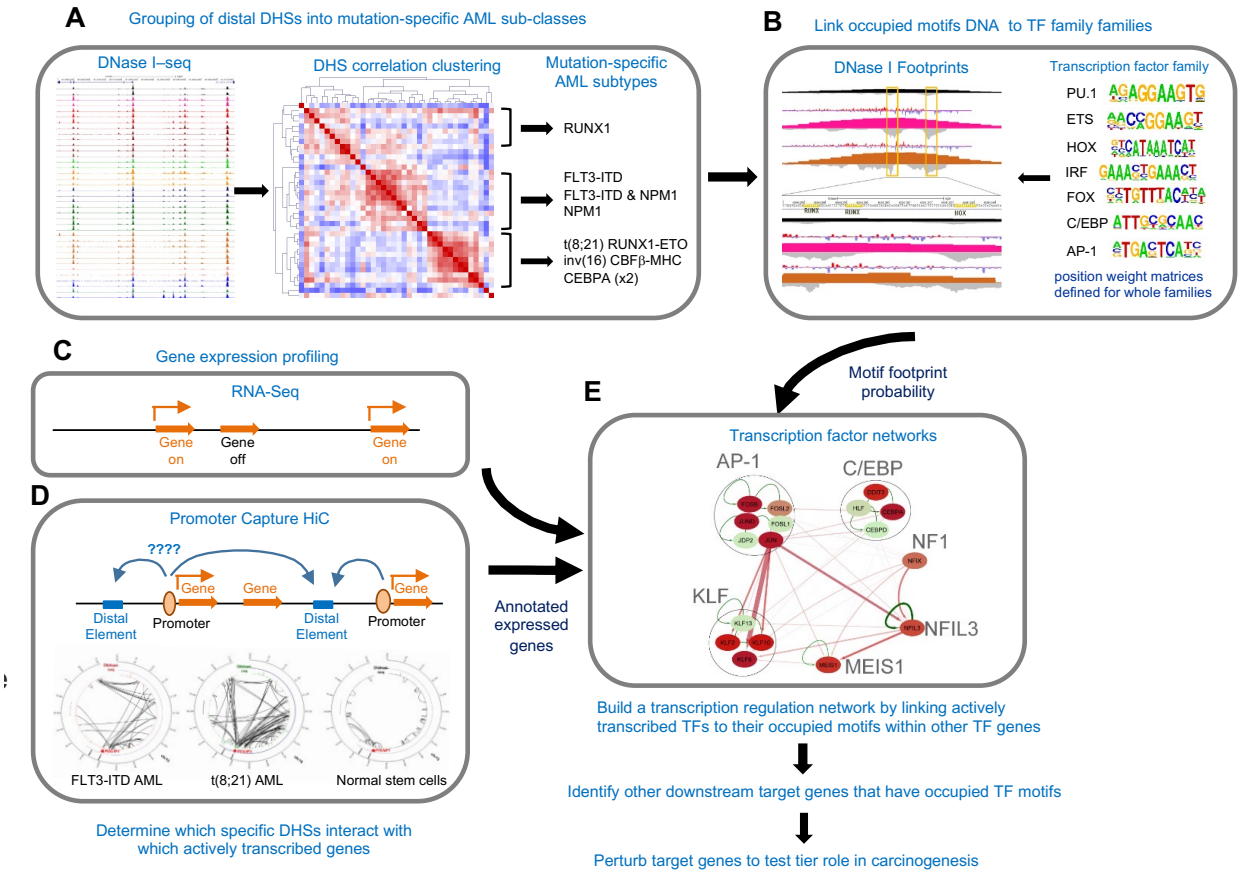

Figure 1.15: Using multi-omics analyses to identify the AML mutation-specific GRNs

After the identifications of AML subtype-specific open chromatin regions (A), TF occupancy is inferred by digital genomic footprinting (B) and genes specifically expressed in each subtype are identified by RNA-seq (C). Using Chi-C data to assign cis-regulatory regions to the right promoter (D), all data can be integrated to construct the AML subtype-specific GRN (E). Figure from (Assi et al., 2019a).

This comparative analysis showed that each AML-subtype is maintained by its own gene regulatory network which differs from that of normal myeloid progenitor cells. Differentiation is not blocked but has gone side-ways generating a new cell type. Importantly, despite being secondary mutations, also signalling mutations such as the

FLT3-ITD shape the genomic landscape of AML and impose a common chromatin pattern regardless of additional mutations.

1.6.1 AP-1 forms an important node in AML-specific GRNs

Another important finding was that the AP-1 family formed an important node in the GRN of every AML described in this study.

The activator 1 (AP-1) transcription factor is a dimeric complex formed by members of the JUN, FOS, ATF and MAF protein families (Fig. 1.16), characterized by the presence of a basic leucine zipper domain. Upon dimerization, AP-1 can bind the DNA at the 12-O-tetradecanoylphorbol-13-acetate (TPA) responsive elements (TRE) TGA(C/G)TCA or the cAMP responsive elements (CRE) TGACGTCA (Nakabeppu et al., 1988; Rauscher et al., 1988) (Fig. 1.16). Different dimers preferentially bind to one sequence or another and regulate different genes (Chinenov and Kerppola, 2001; Hai and Curran, 1991). JUN proteins can form both homodimers and heterodimers with FOS proteins whereas FOS proteins can only form heterodimers and JUN-FOS complexes have higher affinity for TRE (Hai and Curran, 1991).

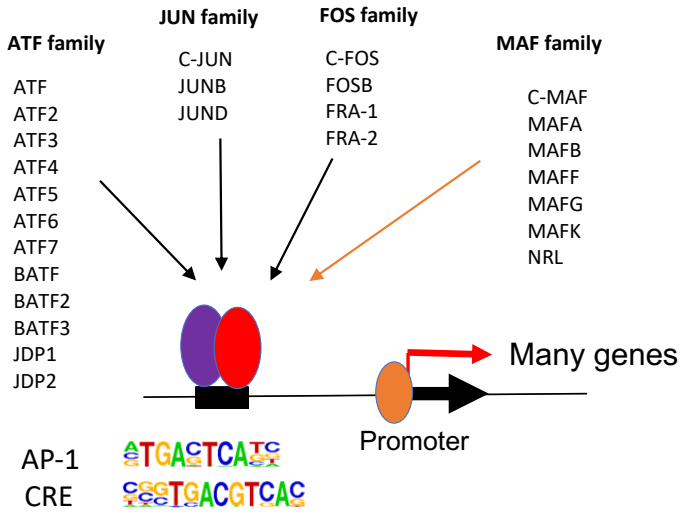

Figure 1.16: The AP-1 family of transcription factors

AP-1 is a heterodimer composed by members of the ATF, JUN, FOS and MAF family. Depending on the dimerization partners forming the complex, AP-1 can bind the DNA at the 12-O-tetradecanoylphorbol-13-acetate (TPA) responsive elements (TRE) TGA(C/G)TCA or the cAMP responsive elements (CRE) TGACGTCA. Figure courtesy of Prof Constanze Bonifer, University of Birmingham.

AP-1 family member genes are widely expressed and play essential roles in signalling responsiveness in multiple tissues. For example, AP-1 is an essential component of signalling responsiveness in macrophages (Heinz et al., 2010; Madrigal and Alasoo, 2018).

AP-1 activity is rapidly induced by intracellular and extracellular signaling, including growth factors, cytokines and oncoproteins, and controls cell proliferation, apoptosis and differentiation (Angel and Karin, 1991). AP-1 family members have a crucial role in normal and malignant haematopoiesis. *Fos* knock-out mice have altered haematopoiesis (Wang et al., 1992) while *JunB* inactivation causes embryonic lethality due to vascular defects (Schorpp-Kistner et al., 1999). Inhibition of AP-1 binding in ESCs by a dominant negative version of FOS that blocks all AP-1 activity (Olive et al., 1997) impairs the differentiation of vascular smooth muscle and mature myeloid cells

(Obier et al., 2016), consistent with previous studies demonstrating that JUN and FOS are positive regulators of myeloid differentiation (Lord et al., 1993) and highly expressed in human granulocytes (Mollinedo et al., 1991). Moreover, AP-1 is a potent inducer of monopoiesis. FOS and JUN members can heterodimerize with C/EBPα to bind the hybrid consensus site TGA(C/T)GCAA, enhance PU.1 expression and induce monocytic differentiation (Cai et al., 2008; Hong et al., 2011; Rangatia et al., 2002).

In haematopoietic cancers, AP-1 can act both as oncogene and tumour suppressor. In mice, loss of *JunB* leads to HSC expansion (Passegue et al., 2004; Santaguida et al., 2009), causing a myeloproliferative disorder which eventually progresses to myeloid leukaemia (Passegue et al., 2001). In contrast, deletion of *c-Fos* in a BCR-ABL mouse model of chronic myeloid leukaemia (CML) suppresses tumour growth (Kesarwani et al., 2017) while AP-1 is highly expressed and constitutively activated in adult T-cell leukaemia (ATL) patient derived cells (Mori et al., 2000).

To investigate the significance of the AP-1 proteins in t(8;21) and FLT3-ITD AMLs, Assi et al. (2019b) exploited a dominant negative FOS peptide (dnFOS), in which the basic region of the FOS bZIP domain is replaced by an acidic amphipathic sequence (Olive et al., 1997). dnFOS heterodimerizes with JUN proteins forming a complex which is unable to bind the DNA, resulting in global suppression of AP-1 activity (Olive et al., 1997). The expression of dnFOS in Kasumi-1 and MV411, a t(8;21) and a FLT3-ITD positive cell line respectively, inhibited proliferation *in vitro* and leukaemia propagation *in vivo.* The induction of dnFOS also impaired the colony formation of CD34+ FLT3-ITD positive patient derived cells but not CD34+ PBSCs (Assi et al., 2019b). These results demonstrated that AP-1 is crucial for the maintenance of the leukemic phenotype in both t(8;21) and a FLT3-ITD AML subtypes. This observation is

corroborated by another recent piece of work from Ptasinska et al. which showed that RUNX1-ETO depletion in Kasumi-1 cells leads to a rewiring of promoter-enhancer interactions associated with loss of AP-1 binding and the acquisition of C/EBPα binding (Ptasinska et al., 2019).

1.6.2 *CEBPA$^{N/C}$* and t(8;21) AMLs show similarities in their chromatin and transcriptome landscapes

Cluster analysis showed that t(8;21) and *CEBPA$^{N/C}$* AMLs share similar chromatin accessibility and gene expression patterns (Fig. 1.17). Moreover, the *POU4F1* gene was found specifically upregulated in these two AML subtypes and motif enrichment analysis revealed that POU4F1 motifs are significantly occupied in t(8;21) and *CEBPA$^{N/C}$* AMLs but not in others. It has been previously shown that RUNX1-ETO promotes POU4F1 expression and that the two TFs synergize to drive the B-lymphoid gene expression signature typically found in t(8;21) leukaemia (Dunne et al., 2010; Dunne et al., 2012). However POU4F1 has never been linked to *CEBPA$^{N/C}$* AMLs before. These findings indicate that both t(8;21) and *CEBPA$^{N/C}$* leukaemia subtypes may rely on similar regulatory circuits, despite the presence of different driver mutations. Indeed, RUNX1-ETO represses *CEBPA* transcription and strongly downregulates its expression (Pabst et al., 2001a; Ptasinska et al., 2012) while depletion of the fusion protein establish a differentiation-specific transcriptional network driven by C/EBPα (Ptasinska et al., 2014; Ptasinska et al., 2019). Moreover, C/EBPα overexpression in t(8;21) cells reverses the transcriptional landscape established by RUNX1-ETO, upregulating genes involved in differentiation and suppressing stem cell maintenance program (Loke et al., 2018).

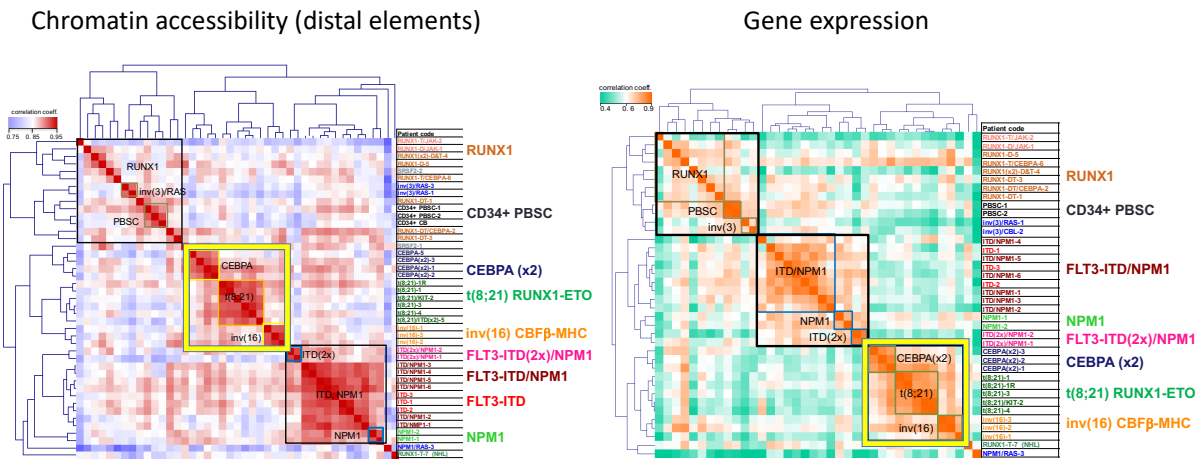

Figure 1.17: *CEBPA*$^{N/C}$ and t(8;21) AMLs are epigenetically related

Different AML subtypes adopt a unique transcriptome and chromatin landscape accordingly to their mutation status. *CEBPA*$^{N/C}$ and t(8;21) AML show similar gene expression and chromatin accessibility patterns and form a cluster together. Figure from (Assi et al., 2019b). Note that patient CEBPA-5 is likely to be a double mutant but was not originally classified as such based on the data from Birmingham Genetics.

1.7 Hypothesis

Using multi-omics approaches we will be able to identify pathways required for *CEBPA*$^{N/C}$ AML maintenance suitable for therapeutic intervention.

1.8 Aims of the project

1) Refine the core GRN specific for *CEBPA*$^{N/C}$ AMLs

The mechanisms through which *CEBPA* biallelic mutations drive tumorigenesis are not completely understood. *Assi et al. 2019* defined the GRN required for the maintenance of different AML subtypes, including *CEBPA*$^{N/C}$ leukaemia. However only distal regulatory elements were considered for the construction of the network, excluding promoters. Moreover, at the time of the study, our collection included only three unequivocally characterized *CEBPA*$^{N/C}$ patient samples and Promoter Capture Hi-C data for this AML subtype were not available. One aim of this project is therefore to collect gene expression and chromatin accessibility data for additional *CEBPA*$^{N/C}$ primary specimens and produce genome-wide interaction data for *CEBPA*$^{N/C}$ AML. These data then need to be integrated to refine the core transcriptional network on which *CEBPA*$^{N/C}$ AMLs rely.

2) Compare t(8;21) and *CEBPA*$^{N/C}$ AMLs

It has been clearly demonstrated that *CEBPA*$^{N/C}$ and t(8;21) AMLs are epigenetically related, and that similar regulatory mechanisms are corrupted in both leukaemia. A second aim of this project is therefore to compare the chromatin and expression

profiles of the two AML subtypes to identify common and subtype-specifically deregulated genes.

3.) Identify the binding pattern of C/EBPα and other transcription factors in *CEBPA*$^{N/C}$ AML

The binding pattern of C/EBPα and other cooperating transcription factors in *CEBPA*$^{N/C}$ primary cells and cell lines is unknown. In this study, we will use genome-wide chromatin immunoprecipitations assays, together with binding motif and gene expression analyses, to answer the question of (i) where mutated C/EBPα binds in *CEBPA*$^{N/C}$ AML, (ii) and to address the question of which other transcription factors it cooperates with.

4) Elucidate the role of C/EBP and AP-1 TF families in *CEBPA*$^{N/C}$ AMLs

Assi et al. showed that both C/EBP and AP-1 transcription factor families constitute major nodes of the t(8;21) and *CEBPA*$^{N/C}$ AMLs GRNs, suggesting an important role of these proteins in both leukaemia subtypes. An important aim of this project is therefore to directly test this hypothesis by expressing two inducible dominant negative peptides, dnC/EBP and dnFOS to abolish the binding of all C/EBP and AP-1 family members in two cell line models for *CEBPA*$^{N/C}$ and t(8;21) AMLs, respectively. After induction, we aim to assess changes in chromatin accessibility, gene expression and proliferation.

5) Identify the chromatin and gene expression pattern of *CEBPA*$^{N/C}$ AML leukaemic stem and blast cells

Leukaemic stem cells (LSCs) are a rare population within the tumour bulk able to give rise to leukaemia. These cells reside in the CD34+, CD38-, CD90- bone marrow population in contrast to blast cells which are CD34+, CD38+, CD90-. However, the differences in the chromatin landscape and the expression of specific genes in *CEBPA*$^{N/C}$ blasts and LSCs is unknown. Moreover, no data exist on the gene expression pattern of single *CEBPA*$^{N/C}$ LSC and blast cells. Here we aim to analyse and compare the two populations of cells at the bulk and single cell level to answer these questions.

6) The response of *CEBPA*$^{N/C}$ AML cells to drugs targeting RUNX1 and the MAP Kinase pathway

The final aim of this study is to use specific inhibitors to block the growth of *CEBPA*$^{N/C}$ AML cells *in vitro* as informed by the *CEBPA*$^{N/C}$ AML GRN.

Chapter 2 - Materials and Methods

2.1 Cell lines and cell line culture

Kasumi-1 and Human Embryonic Kidney (HEK) 293T cells were purchased from DMSZ (Deutsche Sammlung von Mikroorganismen und Zellkulturen), while KO52 were obtained from JCRB (Japanese Collection of Research Bioresources Cell Bank). Kasumi-1 were cultured in Roswell Park Memorial Institute (RPMI)-1640 (Sigma-Aldrich) supplemented with 10% (v/v) fetal calf serum (FCS) (Gibco), 5% (v/v) Penicillin-Streptomycin (Pen-Strep) (Sigma-Aldrich), 5% (v/v) L-Glutamine (L-Glu) (Sigma-Aldrich). HEK 293T cells were cultured in Dulbecco Modified Eagle Media (DMEM) supplemented with 10% (v/v) FCS (Gibco), 5% (v/v) Pen-Strep (Sigma-Aldrich), 5% (v/v) L-Glu (Sigma-Aldrich). KO52 were cultured in Minimum Essential Medium Eagle - Alpha Modification (Alpha MEM) (Lonza) supplemented with 10% (v/v) FCS (Gibco), 5% (v/v) Pen-Strep (Sigma-Aldrich), 5% (v/v) L-Glu (Sigma-Aldrich).

2.2 Primary patient samples

Patient samples (Table 2.1) were obtained from either the Haematological Malignancy Diagnostic Service (HMDS) in Leeds, the University Hospital Birmingham NHS trust and from the sample collection of the Erasmus MC Cancer Institute, Rotterdam.

Patient code	t(8;21)	CEBPA	Other mutations
PBSC-1			
PBSC-2			
CEBPA $^{N/C}$-1		*CEBPA* $^{N/C}$	
CEBPA $^{N/C}$-2		*CEBPA* $^{N/C}$	GATA2
CEBPA $^{N/C}$-3		*CEBPA* $^{N/C}$	GATA2, TET2
CEBPA $^{N/C}$-4		*CEBPA* $^{N/C}$	FLT3-ITD
CEBPA $^{N/C}$-5		*CEBPA* $^{N/C}$	GFI1_SNP
CEBPA $^{N/C}$-6		*CEBPA* $^{N/C}$	DNMT3A
CEBPA $^{N/C}$-7		*CEBPA* $^{N/C}$	
CEBPA $^{N/C}$-8		*CEBPA* $^{N/C}$	RUNX1, TET2, JAK2
CEBPA $^{N/C}$-9		*CEBPA* $^{N/C}$	del9q
CEBPA $^{N/C}$-10		*CEBPA* $^{N/C}$	DNMT3A, del(11)(q14 q25)
t(8;21)-1	t(8;21)		TET2
t(8;21)-2	t(8;21)		TET2, KIT
t(8;21)-3	t(8;21)		FLT3-TK
t(8;21)-4	t(8;21)		NOTCH1, KIT
t(8;21)-5	t(8;21)		
t(8;21)-6	t(8;21)		FLT3-ITD
t(8;21)-7	t(8;21)		
inv(16)-1			inv(16), KIT
inv(16)-2			inv(16)
inv(16)-3			inv(16), ASXL1
inv(3)/RAS-1			inv(3), GATA2, SF3B1, NRAS
inv(3)/CBL-2			inv(3), SF3B1, CBL
ITD-1			DNMT3A, TET2x2, BCOR, TP53, FLT3-ITD
ITD-2			DNMT3A, TET2, FLT3-ITD, tri(13)
ITD-3			DNMT3A, FLT3-ITD
ITD(2x)/NPM1-1			DNMT3A, IDH2, NPM1, FLT3-ITDx2
ITD(2x)/NPM1-2		CEBPA	IDH2, NPM1, FLT3-ITDx2
ITD/NPM1-1			WT1, DNMT3A, NPM1, FLT3-ITD
ITD/NPM1-2			NPM1, FLT3-ITD
ITD/NPM1-3			NPM1, FLT3-ITD
ITD/NPM1-4			GATA2, DNMT3A, NPM1, FLT3-ITD
ITD/NPM1-5			DNMT3A, BCOR, NPM1, FLT3-ITD
ITD/NPM1-6			WT1, DNMT3A, TET2, PHF6, NPM1, FLT3-ITD
NPM1-1			IDH1, NPM1
NPM1-2			DNMT3A, TET2x2, NPM1
NPM1/RAS-3			PTPN11, DNMT3A, IDH1, NPM1, NRAS
RUNX1-DT-1			CREBBP, DNMT3A, SF3B1, RUNX1, FLT3, tri(13)
RUNX1-DT/CEBPA-2		CEBPA	WT1x2, SF3B1, TP53, RUNX1, FLT3-ITD
RUNX1-DT-3			RUNX1
RUNX1(x2)-D&T-4			DNMT3A, IDH2, SRSF2, RUNX1x2
RUNX1-D-5			IDH1, BCORL1x2, SRSF2x2, RUNX1
RUNX1-T/CEBPA-6		CEBPA	EZH2, RUNX1, NRAS, tri(8)
RUNX1-T-7 (NHL)			TET2x2, PHF6, RUNX1, tri(21)

Table 2.1: Mutation status of primary patient samples used in this study.

2.3 Isolation of hematopoietic stem/progenitor cells (HSPCs)

Patient CD34+ or CD117+ hematopoietic progenitors were isolated with CD34 MicroBead Kit, human or CD117 MicroBead Kit, human (Miltenyi-Biotech). Up to 10^8 mononuclear cells were resuspended in 300 µL of MACS buffer (500 mL PBS, 0.5% (v/v) bovine serum albumin (BSA), 2 mM Ethylenediaminetetraacetic Acid (EDTA)) and incubated with 100 µL of FcR Blocking Reagent and 100 µL of CD34 or CD117 MicroBeads at 4°C for, respectively, 30 or 15 minutes. Cells were washed with MACS buffer, centrifuged at 300xg for 10 minutes and resuspended in 500 µL of MACS. The cellular suspension was then applied onto an LS Column (Miltenyi-Biotech) placed in a magnetic separator. After washing the column 3 times, the magnetic labelled progenitors were flushed out in 5 mL of MACS buffer by pushing the plunger into the column. To increase cell purity, the eluted fraction was applied onto a new LS column and the whole procedure repeated.

2.4 Primary cell culture

CEBPA$^{N/C}$-8 patient cells were cultured at the concentration of $1x10^6$ cell/mL in StemSpanTM Serum-Free Expansion Medium II (SFEM II) (STEMCELL Technologies) supplemented with 10% (v/v) StemSpanTM CD34+ Expansion Supplement (STEMCELL Technologies) and 175nM UM171 (STEMCELL Technologies). All other patient cells were grown in SFEM II supplemented with 100 ng/mL thrombopoietin (TPO) (Peprotech), 10 ng/mL FMS-like tyrosine kinase 3 ligand (FLT3L) (Peprotech), UM729 (STEMCELL Technologies), 750 nM Stem Regenin 1 (SRI) (Peprotech), 10 ng/mL Interleukin 3 (IL3) (Peprotech), 10 ng/mL human

granulocyte/macrophage colony stimulating factor (hGM-CSF) (Peprotech), 150 ng/mL Stem Cell Factor (SCF) (Peprotech).

2.5 Inducible dnC/EBP and dnFOS plasmid generation

The doxycycline inducible pCW57.1-dnC/EBP plasmid was generated using Gateway Gene Cloning (Thermo Fisher Scientific), according to manufacturer's instructions. Briefly, the first step of the Gateway Technology is the construction of an entry plasmid containing the insert of interest flanked by attL1 and attL2 recombination sites. The insert is then transferred into a destination vector containing the recombination sites attR1 and attR2. The recombination between attL and attR sequences is catalysed by the LR Clonase enzyme, leading to the generation of an expression vector containing the insert of interest and plasmid containing a toxic bioproduct.

The CMV500 A-C/EBP plasmid containing the dnC/EBP insert was a gift from Charles Vinson, National Cancer Institute, Bethesda, USA (Olive et al., 1996). dnC/EBP cDNA was PCR amplified (Table 2.2 and 2.3) with Phusion DNA polymerase (New England Biolabs) using primers containing SalII and NotI restriction enzymes overhangs (Table 2.4). The PCR product was resolved on a 1.6% (w/v) agarose and purified by using MinElute Gel Extraction Kit (QIAGEN). 1.5 µg of the amplified dnC/EBP cDNA were digested with 10 units of SalI-HF (NEB), 10 units of NotI-HF (NEB) in CutSmart Buffer 1x (NEB) and H_2O up to 50 µL at 37°C for 4 hour and purified with MinElute Reaction Cleanup Kit (QIAGEN).

The dnC/EBP open reading frame (ORF) was then inserted in pENTR-IRES-GFP (a modification of the Invitrogen pENTR plasmid constructed by Benjamin Edginton-White, University of Birmingham, UK) upstream of the IRES-GFP (Internal Ribosome

Entry Site-Green Fluorescent Protein). 6 µg of a pENTR-IRES-GFP were digested with 30 units of SalI-HF (New England Biolabs), 30 units of NotI-HF (New England Biolabs) in CutSmart Buffer 1x (New England Biolab) and H_2O up to 100 µL at 37°C for 1 hour. The digested plasmid was resolved on a 0.8% (w/v) agarose gel and gel extracted by using MinElute Gel Extraction Kit (QIAGEN). The pENTR-IRES-GFP backbone was ligated with the dnC/EBP insert in a 1:3 molar ratio using 400 units of T4 DNA Ligase (NEB), 1x T4 DNA Ligase Reaction Buffer (NEB) and H_2O up to 20 µL at RT for 2 hours. JM109 competent E.coli. were transformed with 10 ng of ligation product and let grow over night on Luria-Bertani (LB) agar (Sigma-Aldrich) plates containing 50 µg/mL kanamycin at 37°C. Single bacteria colonies were grown in 5 mL of LB broth (Sigma-Aldrich) supplemented with 50 µg/mL kanamycin over night at 37°C. The amplified plasmids were isolated from bacteria pellet by using the QIAprep Spin Miniprep Kit (QIAGEN) and screened by restriction enzyme digestion and Sanger sequencing.

The dnC/EBP insert was then transferred into the Tet-on pCW57.1 backbone (Addgene plasmid #41393) by using the Gateway Gene Cloning System. 150 ng of pENTR-IRES-GFP-dnC/EBP were mixed with 150 ng of pCW57.1, 1.5 µL of LR Clonase II (Thermo-Fisher) and TE buffer pH 8.0 up to 8 µL and incubated at 35°C for 1 hour. JM109 competent E.coli. were transformed with 10 ng of pCW57.1 containing the dnC/EBP insert, plated onto LB agar plates containing 100 µg/mL ampicillin and let grow and screened as previously. The bacterial colony with the desired plasmid was grown in 250 mL of LB broth containing 100 µg/mL ampicillin. The final doxycycline inducible dnC/EBP expression vector was isolated by using the EndoFree

Plasmid Maxi Kit and screened again by restriction enzyme digestion (Fig. 2.1) and Sanger sequencing. Below are reported:

(A) the sequence of the dnC/EBP insert amplified from the CMV500 A-C/EBP plasmid,

(B) the pCW57.1-dnC/EBP vector sequence expected after Gateway Cloning Recombination,

(C) and (D) the actual pCW57.1-dnC/EBP vector Sanger sequencing results.

The dnC/EBP coding sequence is highlighted in turquoise, the GFP coding sequence in green, the attR1 and attR2 sites in grey.

(A) dnC/EBP sequence

ATGGACTACAAGGACGACGATGACAAGCATATGGCTAGCATGACTGGTGGACAGCAAATGGG
TCGGGATCCTGACCTGGAACAACGTGCTGAGGAACTGGCCCGTGAAAACGAAGAGCTGGAAA
AAGAGGCCGAAGAGCTGGAGCAGGAAAACGCTGAACTCGAGCAGAAGGTGTTGGAGTTGACC
AGTGACAATGACCGCCTGCGCAAGCGGGTGGAACAGCTGAGCCGTGAACTGGACACGCTGCG
GGGTATCTTCCGCCAGCTGCCTGAGAGCTCCTTGGTCAAGGCCATGGGCAACTGCGCG

(B) pCW57.1-dnC/EBP sequence

ACAAGTTTGTACAAAAAAGCAGGCTGGCGCCGGAACCAATTCAGTCGACGCCACC**ATGGACTAC**
AAGGACGACGATGACAAGCATATGGCTAGCATGACTGGTGGACAGCAAATGGGTCGGGATCC
TGACCTGGAACAACGTGCTGAGGAACTGGCCCGTGAAAACGAAGAGCTGGAAAAAGAGGCCG
AAGAGCTGGAGCAGGAAAACGCTGAACTCGAGCAGAAGGTGTTGGAGTTGACCAGTGACAAT
GACCGCCTGCGCAAGCGGGTGGAACAGCTGAGCCGTGAACTGGACACGCTGCGGGGTATCTT
CCGCCAGCTGCCTGAGAGCTCCTTGGTCAAGGCCATGGGCAACTGCGCGTGAGGCGAATTCAA
GCTTCTAGAGGTAATTCGCGGCCGCACTCGAGATATCTAGACCCAGCTTTCTTGTACAAAGTGGT
GATTCCCCCGGGCTGCAGGAATTCCGCCCCCCCCCCCTAACGTTACTGGCCGAAGCCGCTTGG
AATAAGGCCGGTGTGCGTTTGTCTATATGTTATTTTCCACCATATTGCCGTCTTTTGGCAATGTGA
GGGCCCGGAAACCTGGCCCTGTCTTCTTGACGAGCATTCCTAGGGGTCTTTCCCCTCTCGCCAA
AGGAATGCAAGGTCTGTTGAATGTCGTGAAGGAAGCAGTTCCTCTGGAAGCTTCTTGAAGACAAA
CAACGTCTGTAGCGACCCTTTGCAGGCAGCGGAACCCCCCACCTGGCGACAGGTGCCTCTGCG
GCCAAAAGCCACGTGTATAAGATACACCTGCAAAGGCGGCACAACCCCAGTGCCACGTTGTGAG
TTGGATAGTTGTGGAAAGAGTCAAATGGCTCTCCTCAAGCGTATTCAACAAGGGGCTGAAGGATG
CCCAGAAGGTACCCCATTGTATGGGATCTGATCTGGGGCCTCGGTGCACATGCTTTACATGTGTT

TAGTCGAGGTTAAAAAAACGTCTAGGCCCCCCGAACCACGGGGACGTGGTTTTCCTTTGAAAAAC
ACGATGATAATATGGCCACAACCATGGTGAGCAAGGGCGAGGAGCTGTTCACCGGGGTGGTGC
CCATCCTGGTCGAGCTGGACGGCGACGTAAACGGCCACAAGTTCAGCGTGTCTGGCGAGGGCG
AGGGCGATGCCACCTACGGCAAGCTGACCCTGAAGTTCATCTGCACCACCGGCAAGCTGCCCGT
GCCCTGGCCCACCCTCGTGACCACCCTGACCTACGGCGTGCAGTGCTTCAGCCGCTACCCCGA
CCACATGAAGCAGCACGACTTCTTCAAGTCCGCCATGCCCGAAGGCTACGTCCAGGAGCGCACC
ATCTTCTTCAAGGACGACGGCAACTACAAGACCCGCGCCGAGGTGAAGTTCGAGGGCGACACCC
TGGTGAACCGCATCGAGCTGAAGGGCATCGACTTCAAGGAGGACGGCAACATCCTGGGGCACA
AGCTGGAGTACAACTACAACAGCCACAACGTCTATATCATGGCCGACAAGCAGAAGAACGGCAT
CAAGGCGAACTTCAAGATCCGCCACAACATCGAGGACGGCAGCGTGCAGCTCGCCGACCACTA
CCAGCAGAACACCCCCATCGGCGACGGCCCCGTGCTGCTGCCCGACAACCACTACCTGAGCAC
CCAGTCCGCCCTGAGCAAAGACCCCAACGAGAAGCGCGATCACATGGTCCTGCTGGAGTTCGTG
ACCGCCGCCGGGATCACTCTCGGCATGGACGAGCTGTACAAGTAATGAATTAATTAAGAATTATC
AAGCTTATCGATACCGTCGAGATATCTAGACCCAGCTTTCTTGTACAAAGTGGT

(C) Sanger sequencing validation with LNCX-F primer

GNNNNNNGCTAGCATCACAGTTTNTACNAAAAAGCAGGCTGGCGCCGGAACCAATTCAGTCGAC
GCCACC**ATGGACTACAAGGACGACGATGACAAGCATATGGCTAGCATGACTGGTGGACAGCA**
AATGGGTCGGGATCCTGACCTGGAACAACGTGCTGAGGAACTGGCCCGTGAAAACGAAGAGC
TGGAAAAAGAGGCCGAAGAGCTGGAGCAGGAAAACGCTGAACTCGAGCAGAAGGTGTTGGA
GTTGACCAGTGACAATGACCGCCTGCGCAAGCGGGTGGAACAGCTGAGCCGTGAACTGGACA
CGCTGCGGGGTATCTTCCGCCAGCTGCCTGAGAGCTCCTTGGTCAAGGCCATGGGCAACTGCG
CGTGAGGCGAATTCAAGCTTCTAGAGGTAATTCGCGGCCGCACTCGAGATATCTAGACCCAGCT
TTCTTGTACAAAGTGGTGATTCCCCCGGGCTGCAGGAATTCCGCCCCCCCCCCCTAACGTTACT
GGCCGAAGCCGCTTGGAATAAGGCCGGTGTGCGTTTGTCTATATGTTATTTTCCACCATATTGCC
GTCTTTTGGCAATGTGAGGGCCCGGAAACCTGGCCCTGTCTTCTTGACGAGCATTCCTAGGGGT
CTTTCCCCTCTCGCCAAAGGAATGCAAGGTCTGTTGAATGTCGTGAAGGAAGCAGTTCCTCTGGA
AGCTTCTTGAAGACAAACAACGTCTGTAGCGACCCTTTGCAGGCAGCGGAACCCCCCACCTGGC
GACAGGTGCCTCTGCGGCCAAAAGCCACGTGTATAAGATACACCTGCAAAGGCGGCACAACCCC
AGTGCCACGTTGTGAGTTGGATAGTTGTGGAAAGAGTCAAATGGCTCTCCTCAAGCGTATTCAAC
AAGGGGCTGAAGGATGCCCAGAAGGTACCCCATTGTATGGGATCTGATCTGGGGCCTCGGTGCA
CATGCTTTACATGTGTTTAGTCGAGGTTAAAAAAACGTCTAGGCCCCCCGAACCACGGGGANNN
GGTTTTCCTTTGAAAAANACGATGANNANNTGGCCACAACCATGGTGAGCAAGGGCAAGAACTGT
TCACCGGGGNGGTGCCCATCCTGGTCAANCTGGACGGCAACTAAACGGCCCAANTTCACCNNTC
TGGCAAGGGCAAGGGCAANCCCCCTACGGGAANNNGACCCTGAAATTNNNTNGCCCCCCGGAA
ANNCCCNNGCNGGCCCCCCNNNGAACCCCCTGNNCNNNAGGGGGGNNNGNTTTTCCCC

(D) Sanger sequencing validation with O.PGK1b-R primer

CCACCANNTTGCCGTTCNTTTGCNAANNNNNGGGCCCGGAAACCTGGGNCCNTTTTTTCTGANN
AGCATTCTTANGGGTTCTTTCCCCTCTTCNCCAAAGGAATGCAANGTCNTNTTGAANNTTNNNAA
GGAAGCAGTTCNTCTGGAAGTTTCTGAAGACAAACAACGTTTGTAGCGACCCTTTGCAGGCAGN
GGAACCCCCCCACCTGGNNACAGGTGCCTTCTGCGGCCAAAAGCCACGTGTATAAGATACACCT
GCAAAGGCGGCACAACCCCAGTGCCACGTTGTGAGTTGGATAGTTGTGGAAAGAGTCAAATGGC
TCTCCTCAAGCGTATTCAACAAGGGGCTGAAGGATGCCCAGAAGGTACCCCATTGTATGGGATCT
GATCTGGGGCCTCGGTGCACATGCTTTACATGTGTTTAGTCGAGGTTAAAAAAACGTCTAGGCCC
CCCGAACCACGGGGACGTGGTTTTCCTTTGAAAAACACGATGATAATATGGCCACAACCATGGTG
AGCAAGGGCGAGGAGCTGTTCACCGGGGTGGTGCCCATCCTGGTCGAGCTGGACGGCGACGTA
AACGGCCACAAGTTCAGCGTGTCTGGCGAGGGCGAGGGCGATGCCACCTACGGCAAGCTGACC
CTGAAGTTCATCTGCACCACCGGCAAGCTGCCCGTGCCCTGGCCCACCCTCGTGACCACCCTGA
CCTACGGCGTGCAGTGCTTCAGCCGCTACCCCGACCACATGAAGCAGCACGACTTCTTCAAGTC
CGCCATGCCCGAAGGCTACGTCCAGGAGCGCACCATCTTCTTCAAGGACGACGGCAACTACAAG
ACCCGCGCCGAGGTGAAGTTCGAGGGCGACACCCTGGTGAACCGCATCGAGCTGAAGGGCATC
GACTTCAAGGAGGACGGCAACATCCTGGGGCACAAGCTGGAGTACAACTACAACAGCCACAACG
TCTATATCATGGCCGACAAGCAGAAGAACGGCATCAAGGCGAACTTCAAGATCCGCCACAACATC
GAGGACGGCAGCGTGCAGCTCGCCGACCACTACCAGCAGAACACCCCCATCGGCGACGGCCCC
GTGCTGCTGCCCGACAACCACTACCTGAGCACCCAGTCCGCCCTGAGCAAAGACCCCAACGAGA
AGCGCGATCACATGGTCCTGCTGGAGTTCGTGACCGCCGCCGGGATCACTCTCGGCATGGACG
AGCTGTACAAGTAATGAATTAATTAAGAATTATCAAGCTTATCGATACCGTCGAGATATCTAGACC
CAGCTTTCTTGTACAAAGTGGTTTAGTAATGAACCGGTCCACCACCACCACCACTAAGGATC
CGGGGTTGGGGTTGCGCCTTTTCCAAGGCAGCCCTGGGTTTGCGCAGGGACGCGGCTGCTCTG
GGCGNGGTCCGNNNACGCNGNNNNNNNNN

Reagent	Volume (µL)
Buffer HF 5x	10
Forward primer 10 µM	2.5
Reverse primer 10 µM	2.5
dNTP 10 mM	1
Phusion polymerase	0.5
Plasmid	-
Sterile H_2O	-
Final volume	50

Table 2.2: PCR setup for the amplification of dnC/EBP cDNA

Temperature (°C)	Duration	Cycles
98	30 sec	1
98	10 sec	35
62	30 sec	
72	30 sec	
72	10 min	1
4	∞	

Table 2.3: PCR conditions for the amplification of dnC/EBP cDNA

Target	Primer sequence
dnC/EBP-SalI Forward	ATTGTCGACGCCACCATGGACTACAAGGACGACG
dnC/EBP-NotI Reverse	TAGGCGGCCGCGAATTATAGAAGCTTGCCTCAAGC

Table 2.4: Primers containing SalI and NotI restriction enzyme overhangs used for the amplification of dnC/EBP cDNA

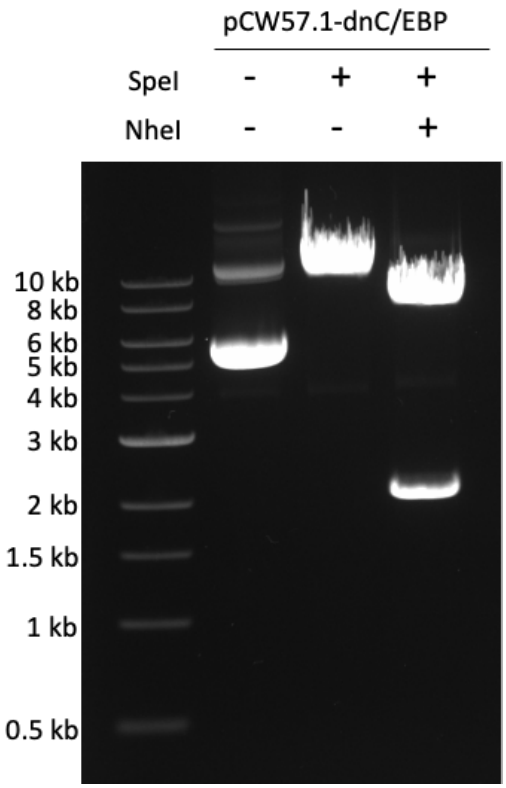

Figure 2.1: pCW57.1-dnC/EBP plasmid digestion.

The gel shows the pattern of bands observed after digestion of pCW57.1-dnC/EBP with SpeI alone or in combination with NheI. As expected SpeI digestion produces a 10 kb band, whereas SpeI and NheI combined digestion produces two bands of 8 and 2 kb respectively.

The pCW57.1 containing the dnFOS insert was generated by Dr Sandeep Potluri (University of Birmingham) following the same protocol (Martinez-Soria et al., 2018).

2.6 Lentiviral production and cell infection

Lentiviral particles containing pCW57.1-dnC/EBP / dnFOS or the empty vector were generated in HEK293T cells using calcium-phosphate transfection. Cells were cultured in DMEM supplemented with 10% (v/v) foetal calf serum (FCS), 5% (v/v) Penicillin-Streptomycin (Pen-Strep), 5% (v/v) L-Glutamine (L-Glu) and 5% (v/v) Sodium Pyruvate and seeded to achieve about 30-40% confluency at the time of transfection. 12 µg of pCW57.1-dnC/EBP or empty vector were transfected with 0.6 ug of REV, 0.6 ug of

GAG/POL, 1.2 ug of VSV-G and 0.6 ug of TAT packaging plasmids. Viral supernatant was harvested at 24, 36, 48, 60 and 72h and concentrated with Centricon Plus- 70 columns (Merk-Millipore) using manufacturer's instructions. Concentrated viral particles were filtered through 0.45 um filter and stored at -80°C or immediately used to infect recipient cells. To carry out the spin infection, 1 x 10^6 Kasumi-1 or KO52 cells were plated in 6-well plates with the viral supernatant and 8 ug/mL of polybrene, and centrifuged for 1h 30m at 1500 x g at 32°C. After infection cells were incubated at 37 °C for 12 hours and then resuspended in fresh media. Few days after infection, cells were cultured in medium supplemented with puromycin 1.5 ug/mL and 2ug/mL for 5 days, allowing the selection of cells positive for pCW57.1-dnC/EBP. Single clones were then isolated from the bulk Kasumi-1 population, expanded and tested for leakiness and induction of dnC/EBP measuring both GFP and FLAG expression through both FACS and RT-qPCR. Despite several attempts, it was not possible to expand KO52 single cell clones with either vector and the bulk population was used for downstream experiments. Dominant negative peptides expression was induced by adding 2 µg/mL of doxycycline to culture medium.

2.7 Proliferation assay in cell lines expressing dnC/EBP and dnFOS

$3x10^5$ cells/mL for each condition were seeded and treated with 2 µg/mL of doxycycline where appropriate. Cell viability was assessed by using Trypan Blue (Sigma-Aldrich) and $3x10^5$ cells/mL were re-seeded in media with or without doxycycline every two days up to ten days. KO52 cells were induced prior to the start of the time-course and GFP+ FACS sorted cells were used to set up the assay as described above.

2.8 Pharmacological inhibition of RUNX and MAPK in primary blasts

$3x10^5$ cells/mL were seeded as usual (see section 2.4) and treated with 5, 10, 20 and 40 μM of the CBFβ inhibitor (Illendula et al., 2016) or 6.25, 12.5, 25, 50, or 100 μM of the MEK inhibitor CH5126766 (Ishii et al., 2013). After 7 days, cell viability was assessed by using Trypan Blue (Sigma-Aldrich).

2.9 RNA extraction and Real-Time RT-qPCR

Total RNA was extracted with NucleoSpin RNA (Machery-Nagel) and 1 ug of nucleic acid was retrotranscribed using SuperScriptTM II Reverse Transcriptase kit (Thermo Fisher) and 0.5 μg of Oligo(dT) primers (Promega), according to the manufacturer's instruction. Target gene expression was calculated using target specific standard curve obtaining a sample cDNA in water at the serial dilution 1:10, 1:50, 1:250, 1:1250 and 1:6250. Sample cDNA was diluted 1:100 in water prior to quantification. Real time PCRs were performed using a 2x dilution of SYBR® Green PCR Mix (Applied Biosystems) and 100 nM forward and reverse primers. 2.5 uL of standard or sample diluted as specified above were added in a final volume of 10 uL. *GAPDH* was used as reference gene for relative gene expression calculation Analysis were performed on an ABI 7500 real-time PCR system using StepOneTM Plus software.

2.10 RNA-seq library preparation

The quality of the RNA starting material was assessed with the eukaryotic RNA 6000 Pico Kit (Agilent). RNA-seq library were prepared with the TruSeq Stranded Total RNA kit (Illumina) following manufacturer's instruction. Briefly, 100 ng of RNA were diluted in nuclease-free H_2O to a final volume of 10 μL, mixed with 5 μL of rRNA Binding

Buffer and 5 µL of rRNA Removal Mixture and incubated at 68°C for 5 minutes. To remove the rRNA, samples were incubated with 35 µL of rRNA Removal Beads for 1 minute at room temperature and placed on a magnet. The remaining RNA was purified by adding 2x RNAClean XP Beads (Beckman Coulter) to the supernatant. After 15 minutes at room temperature, beads were washed with 200 µL of 70% (v/v) EtOH, air-dried for 15 minutes and resuspended in 11 µL of Elution Buffer. To fragment the RNA, 8.5 µL of supernatant was mixed with 8.5 µL of Elute, Prime and Fragment (EPF) solution and incubated at 94°C for a length of time determined by the RNA Integrity Number (RIN).

The first strand cDNA was synthetized by adding 8 µL of a First Strand First Strand Synthesis Act D Mix (FSA) – SuperScript II mixture and incubating at 25°C for 10 minutes, 42°C for 15 minutes and 70°C for 15 minutes; the second strand was synthetized by adding 10 µL of Resuspension Buffer (RSB) and 20 µL of Second Strand Marking Master Mix (SMM) and incubating at 16°C for 1 hour. The cDNA was purified with 1.25x AMPure XP beads (Beckman Coulter) and eluted in 17.5 µL of RSB. The 3' ends of the blunt cDNA fragments were adenylated by adding 2.5 µL of RSB and 12.5 µL of A-Tailing Mix (ATL) and incubating at 37°C for 30 minutes and 70°C for 5 minutes. The desired index adapters were added by incubating the samples with 2.5 µL of RSB, 2.5 µL of Ligase (LIG) and 2.5 µL of a 1:4 adapter dilution at 30°C for 10 minutes. The reaction was stopped by adding 5 µL of Stop Ligation Buffer (SLB). Ligated fragments were purified with 0.85x and 1x AMPure XP beads sequentially and eluted in 22.5 µL of RSB. The DNA fragments that had adapters on both ends were selectively enriched in a 14 cycles PCR reaction (Table) after adding 25 µL of PCR

Master Mix (PMM) and 5 µL of PCR Primer Cocktail (PPC). The amplified library was finally purified with 1x AMPure XP Beads and eluted in 30 µL of nuclease-free H2O.

2.11 DNase I Hypersensitive Site mapping

2.11.1 DNase I digestion

DNase I digestion was performed using different concentrations of enzyme, ranging from 2 to 100 U/mL, to determine the optimal condition for the assay. For each digestion point, 2 x 10^6 cells were centrifuged 300xg, RT, 5 min, washed in PBS and resuspended in 150 µL of DNase I resuspension buffer (60mM KCl (Sigma-Aldrich), 10 mM Tris pH 7.4 (Sigma-Aldrich , 15 mM NaCl (Sigma-Aldrich), 5 mM MgCl2 (Sigma-Aldrich) and 300 mM sucrose (Sigma-Aldrich) in 1.5 mL Eppendorf tubes. Samples were equilibrated to 22°C in a water bath for 5 min. Following, 150 µL of a 2X DNase I dilution was added to each sample and incubated for exactly 3 min. Digestion reaction was stopped by adding 300 µL of DNase I cell lysis buffer (0.3 M Sodium Acetate (Sigma-Aldrich), 10 mM EDTA (Sigma-Aldrich) pH 7.4, 1% (w/v) SDS (Sigma-Aldrich), 1 mg/mL Proteinase K (Sigma-Aldrich)), and samples were incubated overnight at 45°C to ensure protein digestion. 100 µg/mL of RNase A (Sigma-Aldrich) were added to each sample and incubated at 37°C for 1 h, allowing RNA degradation. To check the quality of digestion, 6 µL of each sample (~130 ng of DNA) were loaded onto a 0.7% (w/v) agarose gel (1X TAE and 0.5 /mL ethidium bromide) and electrophoresis was performed at 20 V overnight. Sample digestion was evaluated on the base of gel image analysis (2.1).

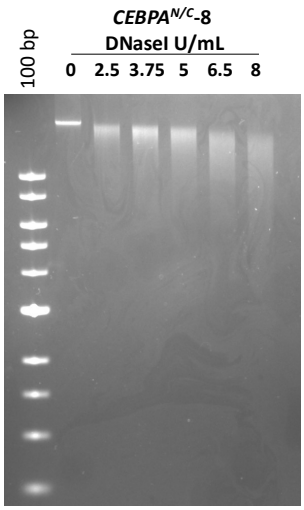

Figure 2.2: *CEBPA*$^{N/C}$-8 blasts DNase I digestion control.

2.11.2 DNA purification

Samples were treated one more time with 100 ug/mL RNase A and incubated at 37°C for 30 min. An equal volume of phenol (Sigma-Aldrich) was added, and the mixture was incubated for 1h at RT on the wheel. The samples were centrifuged at 16000xg 5 minutes at RT and the upper phase was transferred into new tubes. An equal volume of 1:1 phenol:chloroform (Sigma-Aldrich) solution was added, and samples were incubated for 30 min at RT on the wheel and centrifuged as previously. The upper phase was transferred into new tubes, an equal volume of chloroform was added, and samples were incubated and centrifuged as before. The purified DNA was then precipitated by adding two volumes of 100% Ethanol and incubating at -20°C for 30 min. Precipitated DNA was centrifuged 16000xg at 4°C for 5min. Pellet was washed with 70% (v/v) ethanol and air-dried for 15 min at RT. The pellet was then dissolved in 30 µL of 1X TE, leaving the sample at RT overnight.

2.11.3 Digestion quality control

Samples optimally digested and suitable for further analysis were identified by qPCR analysis using primers for specific regions in the TATA box Binding Protein (TBP) promoter (extremely sensitive to DNase I cleavage), the β-Actin gene body (lowly sensitive to DNase I cleavage) and a chromosome 18 (Chr18) gene desert (mainly insensitive to DNase I cleavage) (Fig. 2.2). Optimally digested samples gave a TBP/Chr18 signal ratio between ~0.4 to 0.7.

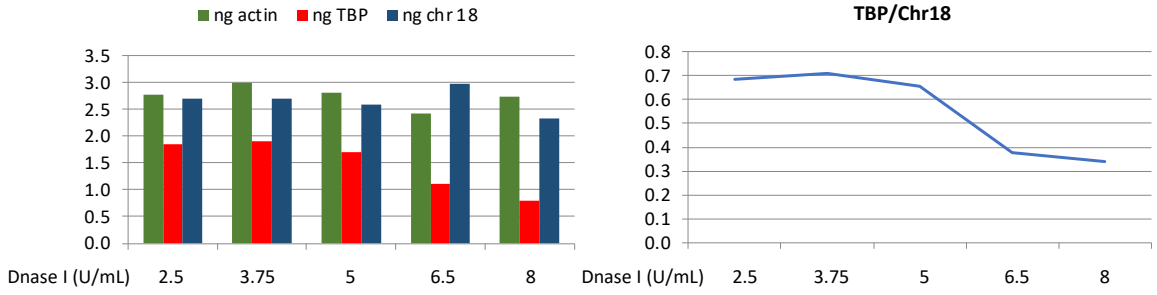

Figure 2.3: DNase I digestion quality control *CEBPA*$^{N/C}$-8 genomic DNA by TBP/Chr18 signal ratio measurement

2.11.4 DNA size selection and extraction from agarose gel

Chosen samples were loaded onto a 1.5% (w/v) agarose gel and separated by electrophoresis at 80 V for 2 h. DNA fragments between 50 and 250 bp were then excised from the gel and purified using a MinElute Gel Extraction kit (QIAGEN) (Fig. 2.3, upper panels). The gel slices were weighted and incubated with 3 volumes of QG buffer at RT on rotation until the gel was completely dissolved. 1 volume of isopropanol was added, and the mixture was loaded onto a MinElute spin column (QIAGEN) and centrifuged. The columns were then washed with 500 uL of QG buffer and 750 µL of PE buffer. After removing all residual ethanol from PE buffer, purified DNA was eluted

in 14 µL of 0.1X TE buffer. All centrifugations were carried out at 16000xg for 1 minute. Size-selected DNA fragments were validated again by qPCR, this time using shorter amplicon PCR primers for *TBP* and Chr18. Samples showing the highest *TBP/Chr18* ratio were selected for genome-wide sequencing (Fig. 2.3, lower panels).

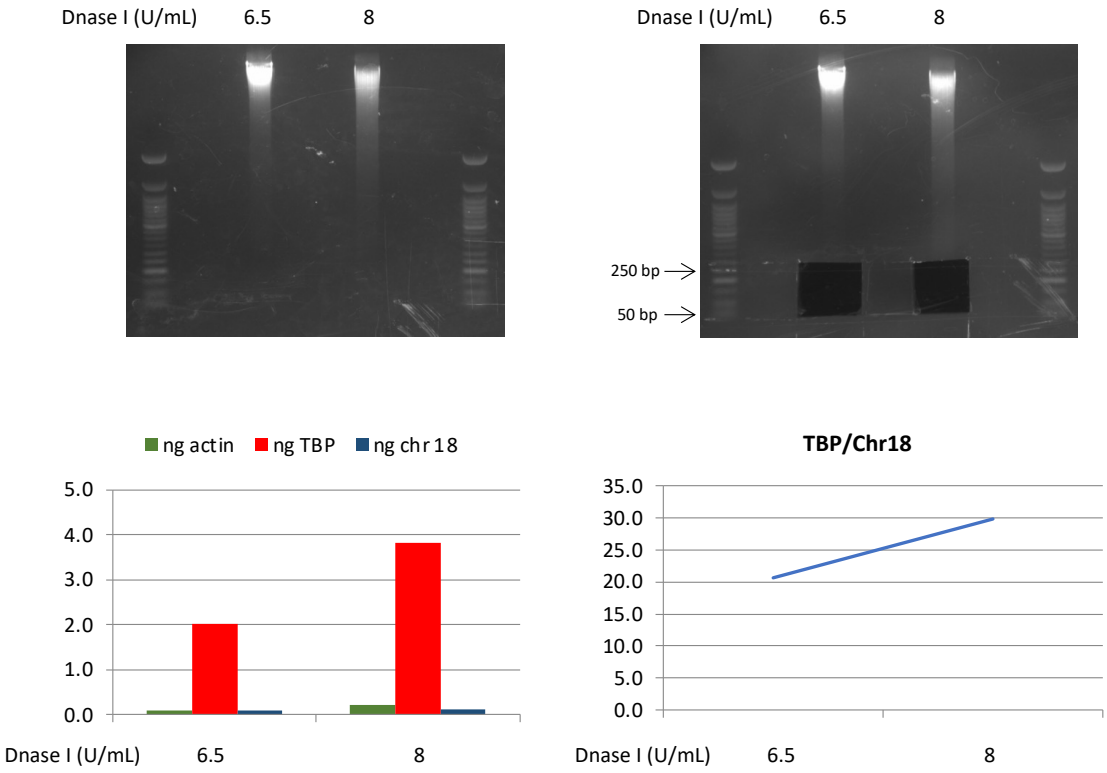

Figure 2.4: *CEBPA*$^{N/C}$-8 DNase I digested sample size selection and validation.

2.11.5 DNase I library preparation

DNase I library preparation was performed by using the KAPA Hyper Prep Kit (Roche) according to manufacturer's instructions. Briefly, fragmented double-stranded DNA was mixed with 7 µL of End Repair & A-Tailing Buffer, 3 µL of End Repair & A-Tailing Enzyme Mix and incubated at 20°C for 30 minutes and 65°C for 30 minutes. Adapter ligation reaction was set up by adding 5 µL of a 1:9 dilution of the chosen adapter, 5 µL of nuclease-free H_2O, 30 µL of Ligation Buffer and 10 µL of DNA Ligase. The reaction was incubated at 20°C for 15 minutes. Ligation products were purified with 0.8x AMPure XP Beads (Beckman Coulter) and eluted in 25 µL of nuclease-free H2O. The library was finally amplified by adding 25 µL of KAPA HiFi HotStart Ready Mix 2x 5 µL of KAPA Library Amplification Primer Mix 10x and incubating at 98°C for 45 seconds, followed by 12-15 cycles of 98°C for 15 seconds, 60°C for 30 seconds, 72°C for 30 seconds and 72°C for 1 minute. The amplified library was purified with 1x AMPure XP beads and eluted in 20 µL of nuclease-free H2O. For size selection, the library was mixed with 1X green gel loading buffer and separated by electrophoresis on a 1.5% (w/v) agarose gel with TAE/EtBr at 80 V for 2 h (Fig. 2.4, upper panels). Library fragments between 200 and 350 bp were purified using a MinElute Gel Extraction kit (QIAGEN) according to manufacturer's instructions and eluted in a final volume of 12 µl. The quality, yield and fragment size distribution of the purified libraries was assessed by the Bioanalyzer system (Fig. 2.4, lower panels).

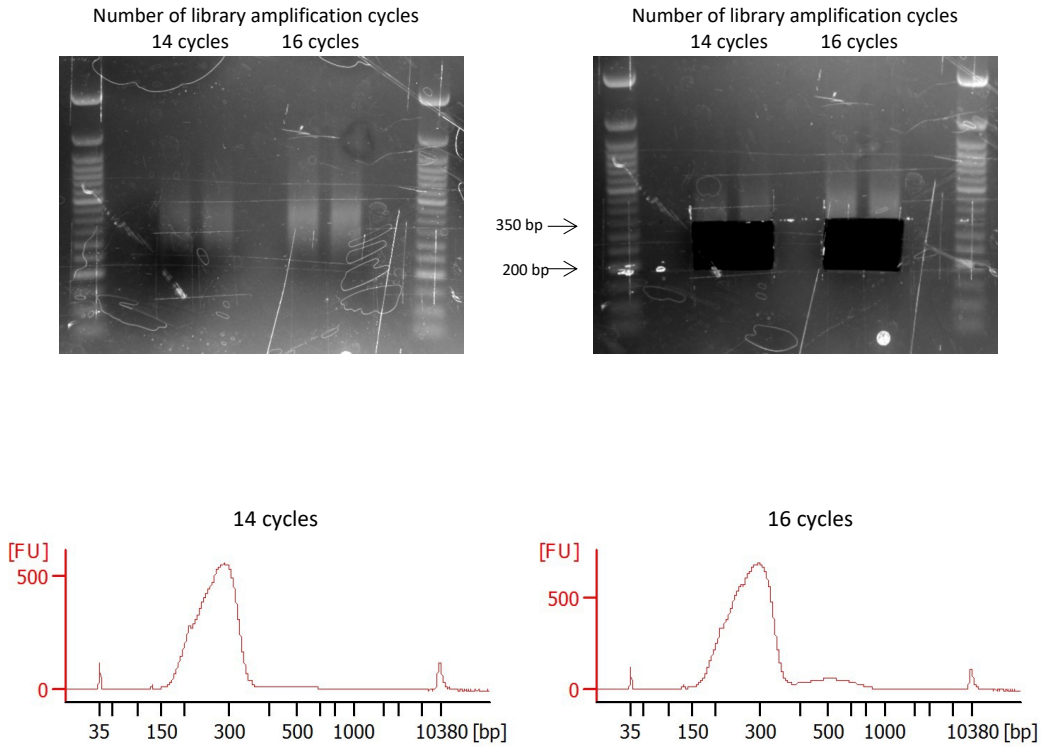

Figure 2.5: *CEBPA*$^{N/C}$-8 DNase I library size selection and quality control.

2.12 ATAC-seq and Data analysis

2.12.1 Fragment transposition

ATAC libraries were generated following the Omni-ATAC protocol from (Corces et al., 2017). $50x10^3$ viable cells were pelleted in a fixed angle centrifuge at 500xg at 4°C for 5 min, resuspended in 50 µL of cold ATAC-Resuspension Buffer (RSB) (1M Tris-HCl pH 7.4, 5M NaCl, 1M $MgCl_2$ in sterile H_2O) containing 0.1% (v/v) NP40 (Sigma-Roche), 0.1% (v/v) Tween-20 (Sigma-Roche), 0.01% Digitonin (v/v) (Promega) and incubated in ice for 3 min. Lysis was washed out by adding 1 mL of cold ATAC-RSB containing 0.1% (v/v) Tween-20 (Sigma/Roche) only. Nuclei were pelleted at 500xg at 4°C for 10 min and resuspended in 50 µL of transposition mix (25 µL of 2x TD buffer (Illumina), 2.5 µL of Tn5 Transposase enzyme (Illumina), 16.5 µL of PBS, 0.5 µL of 1% (w/v) Digitonin (Promega), 0.5 µL of 10% (v/v) Tween-20 (Sigma-Roche), 5 µL of H_2O). The mixture was then incubated at 37°C for 30 minutes in a heated block shaking at 1000 RPM. This reaction allowed the Tn5 transposase to simultaneously fragment and tag the chromatin with sequencing adapters.

2.12.2 Clean-up and pre-amplification of transposed fragments

Transposed fragments were purified by using the MinElute Reaction Cleanup Kit (QIAGEN) following manufacturer's instructions. Briefly, the transposition reaction was mixed with 300 µL of Buffer ERC and loaded onto a MinElute column. The column was centrifuged and washed with 750 µL of Buffer PE. Two sequential centrifugations were performed in order to remove any residual ethanol. Chromatin was eluted in 21 µL of H_2O. All centrifugation steps were performed at 17900 x g for 1 min. The whole eluted

product was amplified for 5 cycles (Table 2.5 and 2.6). Pre-amplified library was stored in ice.

Reagent	Volume (µL)
Primer Ad1 25 µM	2.5
Primer Ad2 25 µM	2.5
NEBNext Master Mix 2x (NEB)	25
Transposed Sample	20

Table 2.5: PCR reagents for the pre-amplification of transposed fragments

Temperature (°C)	Duration	Cycles
72	5 min	
98	30 sec	1
98	10 sec	
63	30 sec	5
72	1 min	
4	∞	

Table 2.6: PCR conditions for the pre-amplification of transposed fragments

2.12.3 RT-qPCR to determine additional cycles

To determine the number of additional cycles needed for an optimal library amplification, 5 µL of pre-amplified library were used to set up a RT-qPCR reaction (Table 2.7 and 2.8). Linear relative fluoresce values were plotted against cycles, and the number of additional cycles needed was defined as the cycle number corresponding to 1/3 of the maximum fluorescence intensity (Buenrostro et al., 2015).

Reagent	Volume (µL)
Sterile H_2O	3.76
Primer Ad1 25 µM	0.5
Primer Ad2 25 µM	0.5
SYBR Green 25x _(in DMSO)	0.24
NEBNext Master Mix 2x (NEB)	25
Transposed Sample	20

Table 2.7: Setup of the RT-qPCR to determine the number of additional cycles of ATAC library amplification

Temperature (°C)	Duration	Cycles
98	30 sec	1
98	10 sec	20
63	30 sec	
72	1 min	
4	∞	

Table 2.8: RT-qPCR conditions to determine the number of additional cycles of ATAC library amplification

2.12.4 Final amplification and clean-up

The remainder of pre-amplified library was amplified for the additional cycles required following the condition in table 2.8. The reaction was purified using the QIAquick PCR Purification Kit (QIAGEN) following manufacturer's instructions. Briefly, the sample was mixed with 5 volumes of Buffer PB and loaded onto a MinElute column (QUIAGEN). The column was centrifuged and washed with 750 µL of Buffer PE. Two sequential centrifugations were performed to remove any residual ethanol. All centrifugation steps were performed at 17900 x g for 1 min. Libraries were eluted in 20 µL of H_2O and, to avoid adapter contamination, further purified by adding 1.2x volumes of AMPure XP beads (Beckman Coulter) following manufacturer's instructions. The libraries were then eluted in 20 µL of H_2O.

2.13 Chromatin Immunoprecipitation followed by sequencing (ChIP-seq)

2.13.1 Cross-linking

Double step-step crosslink (protein-protein cross-linking followed by protein-DNA crosslinking) was used when immunoprecipitating chromatin with the c-Fos antibody, a single-step approach (protein-DNA cross-linking) in all other cases.

2.13.2 Protein-protein cross-linking

10^7 cells were washed 3 times in PBS and resuspended in 10 mL of PBS. To achieve protein-protein cross-linking, cells were incubated with 0.25M Di(N-succinimidyl) glutarate (DSG) (Sigma-Aldrich) for 45 min on rotation at RT. Cross-linked cells were pelleted and washed 3 times with 10 mL of PBS, spinning at 300xg for 5 min at 4°C between washes.

2.13.3 Protein-DNA cross-linking

The pellet was resuspended in 10 mL of PBS. Proteins were fixed to chromatin by adding 16% (w/v) formaldehyde (Pierce) to a final 1% (w/v) concentration and incubating on rotation for 10 min at RT. To quench the cross-linking reaction, cells were incubated on ice for 5 min with 0.4M glycine (Sigma-Aldrich). Cross-linked cells were pelleted and washed twice with 10 mL of ice-cold PBS, spinning at 300xg for 5 min at 4°C between washes.

2.13.4 Cell lysis

Cell pellet was resuspended in 10 mL of ice-cold lysis buffer A (10 mM HEPES pH 8.0, 10 mM EDTA pH 8.0, 0.5 mM EGTA pH 8.0, 0.25% (v/v) Triton-X 100) with the addition of 0.1x Protein Inhibitor Cocktail (PIC) (Sigma-Aldrich) and incubated on rotation for 10 min at 4°C. Residual nuclei were pelleted at 500xg for 10 min at 4°C, resuspended in 10 mL of ice-cold Buffer B (10 mM HEPES pH 8.0, 200 mM NaCl, 1 mM EDTA pH 8.0, 0.5 mM EGTA pH 8.0, 0.01% (v/v) Triton-X 100) with the addition of 0.1x PIC and incubated on rotation for 10 min at 4°C. Chromatin was pelleted at 500xg for 5 min at 4°C and resuspended to a final concentration of $5x10^6$ cells / 300 µL of ice-cold IP Buffer I (25 mM Tris-HCl, pH 8.0, 150 mM NaCl, 2 mM EDTA, pH 8.0, 1% (v/v) Triton-X 100, 0.25% (w/v) SDS) with the addition of 1x PIC.

2.13.5 Sonication

A maximum of 300 µL of chromatin suspension (i.e., $5x10^6$ cells) were aliquoted in Bioruptor tubes (Diagenode) and fragmented using a Bioruptor Pico Sonicator (Diagenode). Patient blasts and KO52 cells were sonicated for 10 cycles and 14 cycles respectively, in order to obtain chromatin fragments ranging between 200 and 1000 bp. Each cycle was 30 sec long with a 30 sec break. Sonicated chromatin was spun down at 16000xg for 15 min at 4°C and resuspended in 2 volumes of IP Buffer II (25 mM Tris-HCl, pH 8.0, 150 mM NaCl, 2 mM EDTA, pH 8.0, 1% (v/v) Triton-X 100, 7.5% (v/v) Glycerol) with the addition of 1x PIC. Separated reactions were pooled and 10% of the chromatin suspension was stored as input control.

2.13.6 Antibody-beads conjugation

The IP protocol was optimized for a maximum input of $5x10^6$ cells, therefore two IP reactions were set up for each experiment. For each IP performed using the C/EBPα G-10 antibody (sc-1662587, Santa Cruz), 20 µL of Dynabeads Protein G (Thermo Fisher) were washed once with 200 µL of 0.1M citrate phosphate pH 5.0 and twice with 200 µL of 100 mM NaH_2 pH 8.0 phosphate buffer, and 6 µg of antibody were added to 10 µL of 100 mM NaH_2 pH 8.0 phosphate buffer and 0.5% (w/v) BSA. In the other cases, 2 µg of C/EBPα 14AA (sc-61, Santa Cruz) or RUNX1 (Ab23980, Abcam) and 12.5 µL of c-Fos (MA5-15055, Invitrogen) antibodies, were added to 5 µL of 100 mM NaH_2 pH 8.0 phosphate buffer and 0.5% (w/v) BSA. Dynabeads Protein G - antibody mixtures were incubated on rotation for 2 hours at 4°C.

2.13.7 Immunoprecipitation and cross-link reversal

Chromatin was incubated with the antibody-beads mixture for 4 h (C/EBPα 14AA and RUNX-1 IPs) or overnight (C/EBPα G-10 and c-FOS IPs) on rotation at 4°C. Beads were washed once with Wash Buffer I (20 mM Tris-HCl, pH 8.0, 150 mM NaCl, 2mM EDTA pH 8.0, 1% (v/v) Triton-X 100, 0.1% (w/v) SDS), twice with Wash Buffer II (20 mM Tris-HCl, pH 8.0, 500 mM NaCl, 2mM EDTA pH 8.0, 1% (v/v) Triton-X 100, 0.1% (w/v) SDS), once with Lithium Chloride (LiCl) Buffer (10 mM Tris-HCl, pH 8.0, 250 mM LiCl, 1mM EDTA pH 8.0, 0.5% (v/v) NP-40, 0.5% (w/v) Na-Deoxycholate) and twice with TE/NaCl Buffer (10 mM Tris-HCl, pH 8.0, 50 mM NaCl, 1 mM EDTA pH 8.0). Chromatin was eluted from beads in 100 µL of freshly prepared Elution Buffer (EB) (100 mM $NaHCO_3$, 1% (w/v) SDS) incubating on a shaker for 30 minutes at RT. Samples, including the input control, were incubated overnight at 65°C in 500 mM NaCl

and 500 µg/ml proteinase K (Roche) to reverse crosslinks and digest proteins. After this step, multiple reactions were pooled together.

2.13.8 DNA isolation and quality control

Samples were incubated with 1.8x volumes of AMPure XP beads (Beckman Coulter) for 30 minutes at RT. After washing beads twice with 200 µL of ethanol, chromatin was eluted in 50 µL of 0.1x TE pH 8.0.

The quality of the ChIP was assessed by qPCR. The immunoprecipitated DNA and the input control were amplified using primers specific for both putative binding sites of the TF in exam as well as non-bounding sites (Table 2.8) and the enrichment of the target sequences was measured over the input.

Primer Target	Sequence
Chr18 Forward	ACTCCCCTTTCATGCTTCTG
Chr18 Reverse	AGGTCCCAGGACATATCCATT
IVL Forward	GCCGTGCTTTGGAGTTCTTA
IVL Reverse	CCTCTGCTGCTGCCACTT
PU.1 -14kb Enhancer Forward	AACAGGAAGCGCCCAGTCA
PU.1 -14kb Enhancer Reverse	TGTGCGGTGCCTGTGGTAAT
LAT2 Forward	AAACCCAGAACAACCCAGGC
LAT2 Reverse	ATGAGGAAGGATGTGTGTGCGG
IGFBP7 Forward	GTCAAGCACTAAAAGGACAAACCG
IGFBP7 Reverse	TGAATGCCACTGGGAG

Table 2.9: List of primers used to assess ChIP quality

2.13.9 ChIP-seq library preparation

ChIP library preparation was performed by using the KAPA Hyper Prep Kit (Roche) as described before in section 2.2.5, except for a 200-450 bp library size selection.

2.14 Promoter-capture Hi-C

The following protocol is a modification (Ptasinska et al., 2019) of a previously described method (Mifsud et al., 2015)

2.14.1 Cell fixation

$40x10^6$ CD34+ cells purified from patient *CEBPA*$^{N/C}$-9 were resuspended in DMEM + 10% (v/v) FBS and fixed in 2% (v/v) formaldehyde (37% (w/v) free from acid Merk) for 10 minutes at room temperature. The cross-linking was quenched by adding a glycine solution to a final concentration of 0.125M followed by 5 minutes of incubation at room temperature and 15 minutes on ice. Fixed cells were centrifuged at 400xg for 10 minutes at 4°C and washed in PBS. The cell pellet was then resuspended in 1mL of lysis buffer (10 mM Tris-HCl pH 8, 10mM NaCl, 0.2% (v/v) Igepal CA-630, 1 tablet of protease inhibitor cocktail (Roche complete, EDTA-free, 11873580001 and water up to 50 mL) and lysed with the help of a homogenizer. The cell lysate was then resuspended in the remain of lysis buffer, incubate on ice for 30 minutes and centrifuged at 1800 rpm for 5 minutes at 4°C. The pellet was resuspended in 1mL of 1.25X RE Buffer 2 (NEB, 1mL of 10X buffer + 7mL of water), split into four 1.5 mL tubes, and resuspended again in 358 µl of 1.25X RE Buffer 2 (NEB).

2.14.2 Restriction enzyme digestion

11 µl of SDS 10% (w/v) were added to each tube, and the chromatin was incubated for 1h. After adding 75 µl of 10% (v/v) Triton-X, the samples were incubated for 1h. Chromatin was then digested overnight with 1500 units of HindIII (NEB R0104T). A heated block shaking at 950 rpm at 37°C was used for all the incubations.

2.14.3 Biotinylation and ligation of digested ends

After placing the samples on ice, 6 µL of 10X RE Buffer 2 (NEB), 2 µL of milli-Q H_20, 1.5 µL 10 mM dCTP, 1.5 µL 10 mM dGTP, 1.5 µL 10 mM dTTP, 37.5 µL 0.4 mM biotin-14-dATP (Life Technologies 19524-016) and 10 µL of 5 U/µL Klenow DNA Polymerase large fragment (NEB M0210L) were added to each tube. The samples were then incubated for 1h at 37°C. This reaction allowed to fill in the overhangs created by HindIII and mark the fragment ends with biotin. The chromatin was added to a tube containing the ligation mix (750 µL 10x ligation buffer (NEB B0202S), 37.5 µL of 20 mg/mL BSA (NEB B9000S), 50 µL of 1 U/mL T4 DNA ligase (Invitrogen 15224-025) and 7 mL of milli-Q H_20), mixed by inversion and incubated overnight at 16°C in a water bath. At this low DNA concentration, ligation between cross-linked fragment is favoured, so that interacting-loci are joint in a single fragment. Samples were then incubated for 30 minutes at RT.

2.14.4 Crosslink reversal and DNA purification

Samples were incubated overnight at 65°C with 60 µL of 10 mg/mL Proteinase K (Roche 03115879001) to reverse crosslinks and digest proteins. 60 µL of 10 mg/mL Proteinase K were added and samples were incubating again at 65 °C for 2 hours.
Samples were cooled down to room temperature and, upon addition of 12.5 µL of 10 mg/mL RNase A (Roche 10109142001), incubated for 1h at 37°C. The DNA was purified by two phenol:chloroform extractions. The reaction mixture was transferred into 50 mL tubes with 8 mL of phenol pH 8.0 (Sigma P4557), vortexed for 1 minute and spun down at 3500 rpm for 10 minutes. The upper aqueous phase was transferred into new 50 mL tubes together with 10 mL of phenol pH8:chloroform and vortexed and

spun down as above. The upper aqueous phase was recovered and added to 10 mL of chloroform, vortexed and spun down as above. To precipitate the DNA, 1 mL of 3M sodium acetate pH 5.2 and 25 mL of ice-cold ethanol were added to the samples, that were then incubated overnight at -20 °C. Samples were centrifuged at 3500 rpm for 30 minutes, and the pellets washed twice by adding 70% (v/v) ethanol on top without resuspending. Pellets were then let resuspend in 400 µL of 1x TE on ice for 2 hours. For the second purification, 450 µL of phenol pH8:chloroform were added and samples were vortexed and spun down 10 minutes at 14000 rpm twice. The upper phase was recovered and added to 450 µL of chloroform, vortexed and spun down as above. The DNA was precipitated by adding 0.1x volumes of 3M sodium acetate pH 5.2 and 2.5x volume of ice-cold ethanol and incubating the samples overnight at -20 °C. The DNA was centrifuged at 14000 rpm 4 °C for 30 minutes, washed 3 times with 70% (v/v) ethanol and resuspended in 25 µL of 1x TE and the 4 samples were pooled together (100 µL in total). DNA yield was determined by using the Quant-iT PicoGreen kit (Life Technologies P7589) and a Qubit® 3.0 Fluorometer (Thermo Scientific).

2.14.5 Hi-C ligation efficiency and quality control

5 µL of a 1/10 dilution of the samples were resolved on a 0.8% (w/v) agarose gel, to confirm that most of the library run as a band around 10 kb (Fig. 2.6 A).

A successful fill-in and ligation of HindII sites (AAGCTT) creates a new site for the restriction enzyme NheI (GCTAGC). To test the ligation efficiency of the library, two ligation products formed by known MYC promoter interactions (a 1.8 Mb long-range interaction and a short-range interaction with an adjacent restriction fragment) were amplified with 3C PCR by using 200 ng of library as template (See tables 2.10-12).

To ensure the PCR reaction success and the presence of the expected 200 bp products, 5 µL of a 1/10 dilution of each reaction were run on a 2% (w/v) agarose gel (Fig. 2.6 B). The 3C PCR reaction was then repeated 5 times and the PCR products purified with QIAquick PCR Purification Kit (QIAGEN) following manufacturer's instruction and quantified at the Nanodrop. For each interaction, 600 ng of PCR product were digested with HindIII, NheI or both enzymes at 37 °C for 2 hours. The digestion products were resolved on a 1.5% (w/v) agarose gel, using undigested DNA was used as control (Fig. 2.6 C). Ligation products which have been efficiently ligated and biotinylated can be cut by NheI but not HindIII.

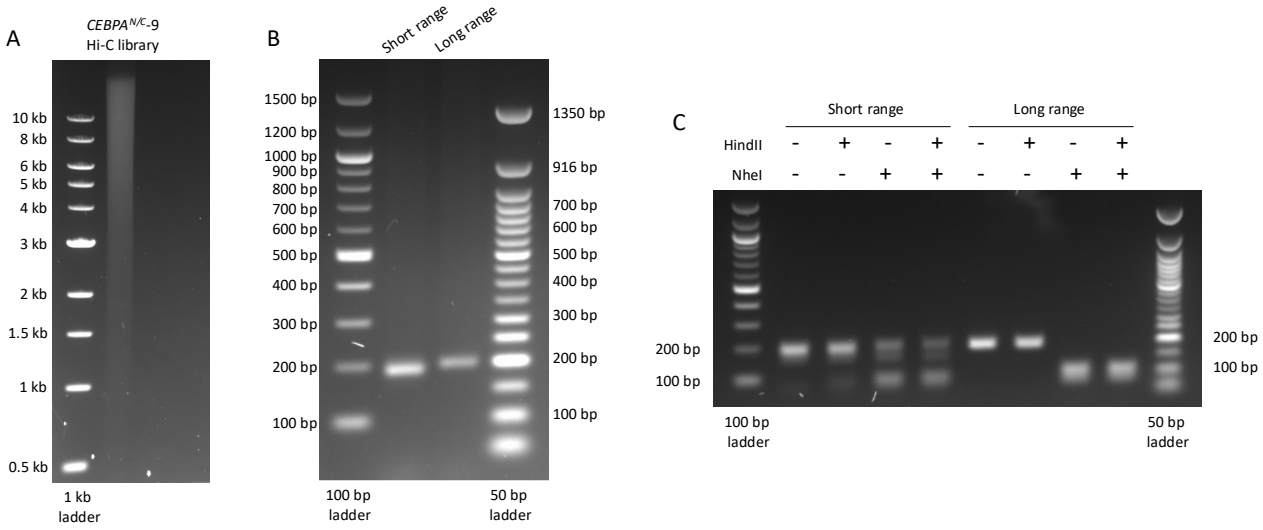

Figure 2.6: *CEBPA*$^{N/C}$-9 Hi-C library quality control.

(A) Hi-C library average size control. (B) 3C PCR amplification products of fragment generated by ligation of the MYC promoter with a neighbouring (short range) and distal (long range) fragment. (C) Fill-in and ligation quality control. Ligation products that have been efficiently ligated can be cut by NheI but not HindIII.

Reagent	Volume
Phusion buffer	5 µL
10 mM dNTP	1 µL
10 µM F primer	2.5 µL
10 µM R primer	2.5 µL
200 ng of DNA	_
Phusion enzyme	0.5 µL
H_2O	_
Final volume	25 µL

Table 2.10: 3C PCR reaction setup.

Phase	Temperature (°C)	Duration (sec)	Cycles
Initial denaturation	98	30	1
Denaturation	98	10	35
Annealing	66	30	
Extension	72	15	
Final extension	72	5	
Holding	4	∞	1

Table 2.11: 3C PCR protocol.

Target	Primer sequence
MYC promoter	GGAGAACCGGTAATGGCAAA
Short range interaction	TGAGGTCCCAGGCATTCTTT
Long range interaction	AATAACAAGGCCCCCAAATTCT

Table 2.12: 3C PCR primer sequences.

2.14.6 Removal of biotin from non-ligated DNA ends

To prevent the pull down of any non-ligated fragment, biotin from non-ligated ends was removed by using the exonuclease activity of the T4 DNA polymerase. 40 µg of Hi-C library were mixed with 4 µL of 10 mg/mL BSA, 40 µL of 10x NEB buffer 2, 16 µL of 2.5 mM dATP, 40 µL of T4 DNA polymerase (NEB M0203L) and H_2O up to 400 µL and incubated at 20 °C for 4 hours. The reaction was stopped by adding 16 µL of 0.5 M

EDTA pH 8.0, the samples were split into 4 tubes and the DNA was purified via phenol:chloroform extraction and precipitated in ethanol as previously described.

2.14.7 DNA shearing and repair

Samples were spun down at 14000 rpm at 4 °C for 30 minutes and washed once with 70% (v/v) ethanol. Air-dried pellets were resuspended in 130 µL of H_2O. DNA was fragmented by using a E220 focused-ultrasonicator (Covaris) with the duty cycle set to 10%, the intensity set to 4 and the water level set to 12 with 200 cycles per burst for 55 seconds at 7 °C. After sonication, the samples were transferred into new tubes with 18 µL of 10x ligation buffer (NEB B0202S), 18 µL of 2.5 mM dNTP mix, 6.5µl T4 DNA polymerase (NEB M0203L), 6.5µl T4 DNA Polynucleotide kinase (NEB M0201L) and 1.3µl Klenow (NEB M0210L) and incubated at room temperature for 30 minutes. Each sample was then split into two and purified with a MinElute PCR purification kit (QIAGEN) following manufacturer's instructions. Each column was eluted twice with 15 µL of TLE (10 mM Tris pH 8.0, 0.1 mM EDTA).

2.14.8 A-tailing and size selection

Each sample was mixed with 5 µL of 10x NEB buffer 2, 11.5 µL of dATP 1mM and 3.5 µL of Klenow (3´→5´ exo$^-$) (NEB M0212L) and incubated at 37 °C for 20 minutes. To inactivate the Klenow fragment, samples were incubated at 5 °C for 20 minutes and then immediately put on ice. Fragments sized between 200 and 650 bp were selected by two subsequent AMPure XP (Beckman Coulter) purifications (0.5:1 followed by 0.9:1) following manufacturer's instructions. The bead bound DNA was resuspended in 50 µL of TLE by incubating at room temperature for 5 minutes. Hi-C library were

then pooled together and quantified by using the Quant-iT PicoGreen kit (Life Technologies P7589) and a Qubit® 3.0 Fluorometer (Thermo Scientific).

2.14.9 Biotin-streptavidin pulldown and adapter ligation

For each library, 4 low-binding tubes containing 150 µL of Dynabeads MyOne Streptavidin C1 beads (Invitrogen) were prepared. Beads were washed twice with 400 µL of Tween Buffer (TB) (5 mM Tris, 0.5 mM EDTA, 1 M NaCl, 0.05% (v/v) Tween) and resuspended in 300 µL of 2x No Tween Buffer (NTB) (10 mM Tris, 1 mM EDTA, 2M NaCl). Hi-C libraries were made up to 300 µL with TLE, combined with the beads and put on slow rotation at room temperature for 30 minutes. Samples were placed on a magnetic separator and washed once with 400 µL of NTB and once with 200 µL of 1x ligation buffer (10x ligation buffer (NEB B0202S) diluted to 1x). Libraries bound beads were resuspended in 50 µL of 1x ligation buffer and transferred in new tubes. 4 µL of 15 µM paired-ends (PE) adapters (Table 2.13) and 4 µL of T4 DNA ligase (NEB M0202S) were added, and samples were incubated at room temperature on slow rotation for 2 hours. Samples were then placed on magnetic separator and washed twice with 400 µL of TB, once with 200 µL of 1x NTB (5 mM Tris, 0.5 mM EDTA, 1 M NaCl), once with 200 µL of 1x NEB buffer 2 and once with 60 µL of 1x NEB buffer 2. Beads were resuspended in 40 µL of 1x NEB buffer 2 and all reactions were pooled in a new tube and stored at 4 °C.

PE adapter primer 1	5'-P-GATCGGAAGAGCGGTTCAGCAGGAATGCCGAG-3'
PE adapter primer 2	5'-ACACTCTTTCCCTACACGACGCTCTTCCGATC*T-3'

Table 2.13: Hi-C library pair end adapter sequences.

2.14.10 Test PCRs to determine conditions for Hi-C library amplification

To determine the number of cycles needed for an optimal Hi-C library amplification, 3 PCR reaction were set up (Tables 2.14-15) and amplified for 6, 9 and 12 cycles (Table 2.16). The whole PCR reaction was run on a 1.5% (w/v) agarose gel to check libraries amplification (Fig. 2.7). Libraries usually look like a smear between 300 and 600 bp. 8 cycles were chosen for final library amplification.

PE PCR primer 1	5'-AATGATACGGCGACCACCGAGATCTACACTCTTTCCCTACACG ACGCTCTTCCGATCT-3'
PE PCR primer 2	5'-CAAGCAGAAGACGGCATACGAGATCGGTCTCGGCATTCCTGC TGAACCGCTCTTCCGA-3'

Table 2.14: Pair end adapters PCR primers

Reagent	Volume (µL)
Hi-C library DNA on beads	2.5
Buffer 5x (Phusion NEB F531)	5
dATP 10 mM	0.7
dCTP 10 mM	0.7
dGTP 10 mM	0.7
dTTP 10 mM	0.7
PE PCR primer 1 100 µM	0.075
PE PCR primer 2 100 µM	0.075
Phusion Polymerase (NEB F531)	0.3
H_2O	14.25

Table 2.15: PCR reaction setup to determine Hi-C library amplification conditions

Temperature (°C)	Duration	Cycles
98	30 sec	1
65	30 sec	
72	30 sec	
98	10 sec	n – 2
65	30 sec	
72	30 sec	
98	10 sec	1
65	30 sec	
72	7 min	

Table 2.16: PCR protocol to determine Hi-C library amplification conditions

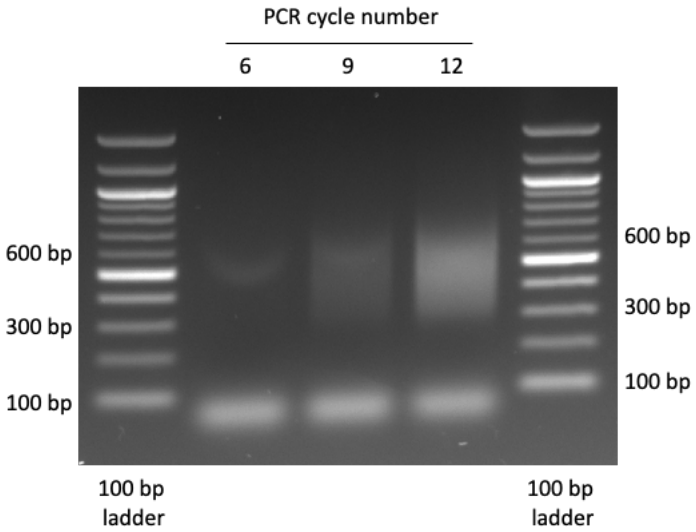

Figure 2.7: *CEBPA*$^{N/C}$-9 Hi-C library amplification products at different number of cycles.

2.14.11 Hi-C library amplification

The remaining volume of the library was amplified in 64 PCR reaction set up as previously, that were then pooled. The library was separated from the beads with a magnet, purified twice by adding 1.8x volume of AMPure XP (Beckman Coulter) following manufacturer's instructions and resuspended in 20 µL of TLE. The library

was then quantified by using the Quant-iT PicoGreen kit (Life Technologies P7589) and run on the bioanalyzer (Agilent).

2.14.12 Hybridization of the Hi-C library with the biotin-RNA baits

All the reagents used in this step are part of the SureSelect Capture Kit (Agilent Technologies).

500 ng of Hi-C library were desiccated with a SpeedVac (Thermo Fisher) at 30°C twice for 8 minutes and resuspended in 3.5 µL of H_2O by shaking for 10 minutes. After the addition of 2.5 µL of Custom Blocker 1, 2.5 µL of Custom Blocker 2 and 0.6 µL of Custom Oligo Blocker the mix was transferred in a PCR tube and kept on ice. The hybridization buffer was prepared by mixing 25 µL of SureSelect Hybridization Solution 1, 1 µL of SureSelect Hybridization Solution 2, 10 µL of SureSelect Hybridization Solution 3 and 13 µL of SureSelect Hybridization Solution 4. The buffer was then heated at 65°C for 5 minutes and transferred into PCR tubes. 5 µL of custom-made biotinylated RNA baits were mixed with 2 µL of a 1:4 dilution of SureSelect RNase Block in a PCR tube and kept on ice (for coordinates and sequences of the biotinylated Sure select RNA baits used see (Mifsud et al., 2015)). A PCR machine was set to 95°C for 5 minutes and 65°C on hold with the lid heated at 98°C. At this point, the hybridization was started. The Hi-C library was incubated in the PCR machine at 95°C for 5 minutes and, as soon as the temperature dropped to 65°C, the hybridization buffer was moved to the machine. After a 5 minutes incubation also the RNA baits mix was transferred into the machine. After 2 minutes, 13 µL of hybridization buffer and 9 µL of the Hi-C library were added to the tube containing the RNA baits and the mix was let in incubation at 65°C for 24 hours.

2.14.13 Streptavidin-biotin pulldown

60 µL of Dynabeads MyOne Strepavidin T1 (Life Technologies) were washed three times by adding 200 µL of Binding Buffer (BB, Life Technologies) and resuspended in 200 µL of BB. The hybridization reaction was transferred from the PCR machine to the tube containing the beads and incubated on a rotating wheel at room temperature for 30 minutes. The beads were then resuspended in 500 µL of Washing Buffer I (WB I, Agilent Technologies), transferred into a new tube and incubated at room temperature for 15 minutes, vortexing every 2-3 minutes for 5 seconds. The beads were then resuspended in 500 µL of Washing Buffer II (WB II, Agilent Technologies) pre-warmed at 65°C and incubated in at 65°C for 10 minutes, vortexing every 2-3 minutes for 5 seconds for three times. The beads were then resuspended in 200 µL of NEB2 1x (NEB), moved into a new tube and resuspended in 30 µL of NEB2 1x.

2.14.14 Test PCRs to determine conditions for Capture Hi-C library amplification

To determine the number of cycles needed for a sufficient Capture Hi-C library amplification, ¼ of the library on beads (i.e., 75 µL) were amplified in three separated reactions for 4 cycles following the protocol described previously in table 2.16. The supernatant containing the amplified library was separated from beads, transferred into a new tube, and mixed with 1.8x volumes of AMPure XP beads (Beckman Coulter) following the manufacturer's instructions. The beads were resuspended in 100 µL of TLE and incubated on a shaker at room temperature for 30 minutes. After another round of AMPure XP beads purification, the library was resuspended in 10 µL of TLE and quantified with the Quant-iT High-Sensitivity DNA Assay Kit (Invitrogen). The

remainder of the library was amplified in 9 separated reactions for 4 cycles as previously (see section 2.2.26). All the reactions were pooled and purified with AMPure XP beads as above. The library was finally resuspended in 10 µL of TLE, quantified with the Quant-iT High-Sensitivity DNA Assay Kit (Invitrogen) and run on the bioanalyzer (Agilent). The Promoter Capture Hi-C library was sequenced on the Illumina HiSeq 1000 platform.

2.15 DNase I-seq and ATAC-seq data analysis

2.15.1 Trimming, alignment, peak calling and annotation

Sequencing adapters and low-quality reads and were removed using Trimmomatic (Bolger et al., 2014). Reads were then mapped to the human genome version hg38 using Bowtie v2.2.3 (Langmead and Salzberg, 2012), and PCR duplicated reads were removed using Picard (http://broadinstitute.github.io/picard). Only reads aligned to unique genomic positions were retained using Samtools. The bamCoverage function from BEDTools (Quinlan and Hall, 2010) was used to generate read density profiles that were then visualized using the UCSC Genome Browser (Kent et al., 2002). DHSs, correspond to regions of open chromatin (peaks) were identified using MACS2 (Zhang et al., 2008). Peaks included in the ENCODE hg38 blacklist (Amemiya et al., 2019) were removed. Peaks were annotated to their associated gene using Promoter Capture Hi-C. Where a peak did not occur in a restriction fragment and therefore could not be mapped to a gene promoter by Hi-C, the peak was annotated to the closest gene using the annotatePeaks.pl function in Homer (Ziemann et al., 2013). Peaks were further annotated as promoter proximal if within -/+2 kb of a gene transcription start site (TSS) and were classified as distal otherwise. If two peaks had summits within 200

bp of each other, these peaks were combined into a single peak with a new summit position defined as the mid-point between the summits of the original peaks.

2.15.2 Primary blast hypersensitive site peak set definition

To maximise the precision and accuracy of peak detection, a reference peak set was created using a merged dataset of all sequencing experiments from all primary samples. To do this, the aligned reads (bam files) of all the samples were merged into a single alignment using the merge function in samtools. Peaks were then identified using this merged alignment using MACS2 as described in section 2.2.31, and these peak positions were used as the reference peak position in all further downstream analysis. Tag counts were retrieved from these peaks using featureCounts (Liao et al., 2014). Counts were then normalized as count per million (CPM) using the DEseq2 (Love et al., 2014) package in R and then further quantile normalized using quantile normalization.

2.15.3 AML subtype-specific hypersensitive sites analysis

To identify genomic regions of differential chromatin accessibility specifically enriched in *CEBPA*$^{N/C}$, t(8;21) or PBSC blasts, the average CPM values for each hypersensitive site within each group were calculated and further log2-transformed as log2(CPM +1). A genomic site was considered to be differentially accessible if the fold-difference of the CPM between two subtype was greater than 2.

2.15.4 Clustering of chromatin accessibility data from primary samples

To generate the heatmap in fig. 3.1 B, the Pearson correlation coefficients for each pair of samples were calculated using the log2 transformed CPM values. The resulting correlation matrix was then hierarchically clustered using Euclidean distance with complete linkage clustering in R.

2.16 RNA-Seq data analysis

2.16.1 Trimming, alignment and transcript assembly

Low-quality reads and sequencing adapters were removed using Trimmomatic (Bolger et al., 2014) and aligned to the human genome version hg38 using HISAT2 (Kim et al., 2015). StringTie (Pertea et al., 2015) was used to assemble reads into transcripts and calculate gene expression values as fragment per kilobase of transcript per million fragments (FPKM). Gene models from the Ensembl database were used as reference transcriptome (Howe et al., 2021). Only genes that were considered expressed with a FPKM > 1 in at least one sample were retained for further analysis. Values were log2-transformed as log2(FPKM +1).

2.16.2 Clustering of RNA-seq data from primary samples

To generate the heatmap in fig. 3.1 A, the Pearson correlation coefficients for each pair of samples were calculated using the log2 transformed FPKM values and hierarchically clustered using Euclidean distance with complete linkage clustering in R.

2.16.3 Differential gene expression analyses

Gene expression was initially measured as number of reads mapped to a transcript with featureCounts (Liao et al., 2014) using the hg38 assembly from the Ensembl database as reference transcriptome (Howe et al., 2021) (-p -s 2 parameters). Counts were filtered and normalized to Counts Per Million (CPM) using EdgeR (Robinson et al., 2010). Differential gene expression analysis were carried out using the Limma package (Law et al., 2016) in R. A gene was considered as differentially expressed between two conditions if it had a fold-change greater than 2 and a Benjamini-Hochberg adjusted p-value < 0.05. For primary samples analyses, samples within the PBSC, *CEBPA*$^{N/C}$ and t(8;21) blast groups were treated as biological replicates.

2.16.4 KEGG pathway analysis

Kyoto Encyclopaedia for Genes and Genomes (KEGG) pathway enrichment analysis were performed using the ClueGo v3.8.2 plugin (Bindea et al., 2009) for Cytoscape v2.5.7 (Shannon et al., 2003) using a right-sided hypergeometric test with Benjamini-Hochberg adjusted p-value for multiple testing. A pathway was considered significantly enriched if the adjusted p-value was < 0.05.

2.17 Promoter Capture Hi-C data analysis

Promoter Capture Hi-C data were processed with the HiCUP pipeline (Wingett et al., 2015). The paired-end sequencing reads, called di-tag, were separately mapped to the hg38 genome, repaired and filtered for experimental artifact (i.e., self-ligation and re-ligation products) and PCR duplicates. Mapped di-tags were then analysed with GOTHiC (Mifsud et al., 2017). This package uses a cumulative binomial test to assign

a p-value to each interaction and detects di-tags significantly enriched compared to a background model of random interactions. The HOMER software package was used to determine statistically significant interactions, taking into account the p-value and false discovery rate (FDR) relative to a background model.

2.18 *CEBPA$^{N/C}$*-specific gene regulatory network construction

Motif search within hypersensitive sites specific for *CEBPA$^{N/C}$* and PBSCs was performed using the findMotifGenome.pl function in HOMER (Ziemann et al., 2013). Sites were linked to their associated gene promoters using Chi-C data where possible, or otherwise to the nearest expressed gene. The number of motifs was counted for each hypothetical target gene, and the significance of motif enrichment was determined by bootstrapping analyses. To do this, the number of transcription factor motifs in the peak set being examined were counted using the annotatePeaks.pl function in Homer. A random set of peaks equal in size to the peak set being examined was then randomly sampled from the complete set of peaks across all patients. This procedure was repeated 1000 times and produced a distribution of expected motif counts. The mean (μ) and standard deviation (σ) of this distribution was then calculated, and were then used to calculate a Z-score as

$$z = \frac{x - \mu}{\sigma}$$

where x is the number of motifs in the actual peak set. Here, a positive Z-score suggests that the number of motifs in the peak set is greater than what could be expected by chance, representing an enrichment of that motif. Transcription factor family-specific motifs with positive Z-score values selected for further analysis and

were then linked to their putative target genes using either CHi-C or closest gene as described above in section 2.2.35.

2.19 ChIP-Seq data analysis

Raw sequencing reads were trimmed to remove low-quality sequences and adaptors using Trimmomatic. Processed reads were then aligned to the human genome version hg38 using Bowtie2 v2.2.3, with only uniquely aligned reads retained for further analysis. PCR duplicated reads were identified and removed from the alignments using the MarkDuplicates function in Picards tools. Peaks were called using MACS2 with default settings. The resulting peaks were then filtered using the hg38 Blacklist from ENCODE to remove potential artefacts from the data. Only peaks that were found within open chromatin regions as defined by ATAC-Seq data were retained. Peaks were then annotated to their target genes based on the Chi-C data were available or by closest gene using the annotatePeaks.pl function in Homer.

2.19.1 Motif co-localization analysis

The genomic co-ordinates for each transcription factor binding motifs were retrieved from within the KO52 ATAC-Seq peaks that were found to be bound by C/EBPα, FOS and RUNX1 using the annotatePeaks.pl function in Homer. Motif co-occurrence was then measured by counting the number of times a pair of motifs were found within 50bp of each other in this peak set. To measure the significance of this co-occurrence, we next applied a re-sampling analysis whereby we sampled a random set of ATAC peaks from the set of all ATAC peaks found in KO52 cells. The number of motif pairs in this random set was then counted. This procedure was repeated 1000 times and produced

a distribution of co-occurrence counts for each pair of motifs. A Z-score could then be computed for each pair as

$$z = \frac{x - \mu}{\sigma}$$

where x is the number of motif pairs in the C/EBPα, FOS and RUNX1 bound sites, μ is the average number of motif pairs in 1000 random peak sets and σ is the standard deviation. The resulting z-score matrix was then hierarchically clustered using complete linkage clustering of the Euclidean distance in R and displayed as a heatmap.

2.20 Single Cell RNA-Seq data analysis

Reads from single-cell RNA-Seq experiments were aligned to the human genome (version hg38) and quantified using the count function in CellRanger v3.1.0 from 10x Genomics and using gene models from Ensembl as the reference transcriptome. Unique Molecular Identifier (UMI) count data was filtered for low quality cells by removing cells with less than 500 and more than 5000 detectable genes. Cells that had more than 15% of UMIs aligned to mitochondrial transcripts were also excluded from further analysis. UMI counts were normalized using the log-normalize method in the Seurat package v3.2.2 (Stuart et al., 2019) in R v3.6.1. The cell cycle stage was then estimated for each cell using the CellCycleScoring function in Seurat and using the in-built lists of cell cycle stage specific genes. To account for the possible effect of cell cycle stage on downstream clustering analysis, S-phase and G2M-phase scores were included as variables in a linear regression model using the ScaleData function in Seurat. Principal Components Analysis (PCA) was then performed on the normalized and scaled data, with the first 25 principal components selected for further analysis. Cells were then clustered using the FindClusters function in Seurat and

visualized using Uniform Manifold Approximation and Projection (UMAP). Cluster marker genes, corresponding to genes that are significantly higher expressed in a cluster compared to all other cells outside of that cluster, were identified using the FindAllMarkers function. Genes that had an average log2-fold change of at least 0.25 with an adjusted p-value less than 0.05 were selected as marker genes.

In order to classify a single-cell cluster as either blast or LSC, we first identified blast and LSC specific gene expression signatures using bulk RNA-Seq from sorted cell populations. To do this, raw paired-end reads from bulk RNA-Seq experiments were trimmed to remove low-quality reads and sequencing adaptors using Trimmomatic v0.39 (Bolger et al., 2014). Processed reads were then aligned to the human genome (version hg38) using Hisat2 v2.1.0 (Kim et al., 2015). Gene expression was then measured as Fragments Per Kilobase of transcript per Million mapped reads (FPKM) using Stringtie v2.1.1 (Pertea et al., 2015). Only genes that were considered expressed with an FPKM greater than or equal to 1 in either LSCs or blasts were retained for further analysis. Gene expression values were normalized using upper-quartile normalization and further log2-transformed as log2(FPKM + 1). Genes were then ranked according to the log2-fold difference between blasts and LSCs. This ranked list could then be used as a reference gene expression signature for Gene Set Enrichment Analysis (GSEA).

GSEA was carried out using the fgsea package v1.10.1 (Korotkevich et al., 2021) in R. To do this, cluster marker genes from single-cell clusters were used as pathways and compared to the gene expression signatures derived from the bulk data. This analysis produced a Normalized Enrichment Score (NES) for each cluster, with a

positive NES suggesting that a cluster has a more blast-like gene expression signature and a negative NES suggesting a more LSC-like signature. Only clusters with a Benjamini-Hochberg adjusted p-value < 0.1 were considered to be positively classified as either LSC or blast.

Single-cell trajectory analysis was carried out using Monocle3 v0.2.3 (Trapnell et al., 2014). Processed data from Seurat was imported to Monocle and trajectories were inferred using the learn_graph command. Pseudotime was then calculated using the order_cells command, using cells from the earliest inferred LSC population (LSC-1). Trajectories were then plotted on the UMAP calculated by Seurat.

Chapter 3 - Results

3.1 Multi-omics analysis shows that *CEBPA*$^{N/C}$ acute myeloid leukaemia cluster with t(8;21) AML but form an independent group

Assi et al. demonstrated that different AML subtypes adopt a unique transcriptome and chromatin landscape accordingly to their mutation class and that *CEBPA*$^{N/C}$ and t(8;21) AMLs are highly related within a larger sub-cluster (Assi et al., 2019b). However, the data analysis only comprised 4 patients with *CEBPA* biallelic mutations and five patients with the t(8;21) genotype. To confirm our analysis with a larger dataset, we included additional patient samples carrying *CEBPA* biallelic mutations, bringing the total up to ten, and studied seven t(8;21) patients. CD34+ or CD117+ leukemic blasts were purified and used to perform RNA-seq and ATAC- or DNase-seq experiments (Fig. 3.1 A).

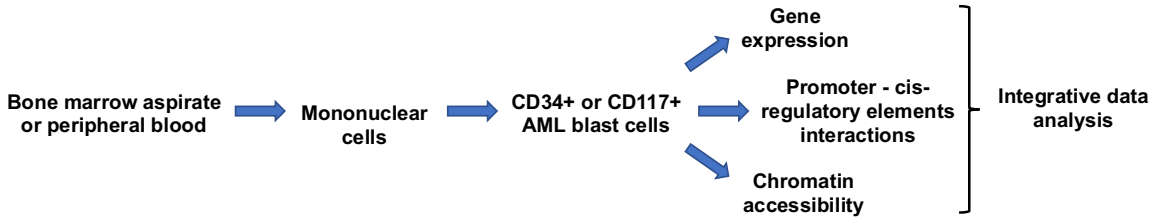

Figure 3.1: Patient-derived blast purification and experimental overview.

Unsupervised clustering analysis of RNA-seq (Fig. 3.2 A) and ATAC/DNase-seq data (Fig. 3.2 B) showed that the new *CEBPA*$^{N/C}$ patients clustered together with other *CEBPA*$^{N/C}$ mutant patients from Assi et al. (Fig. 3.2 A and B). Whilst contained in a large subcluster together with the Inv(16) and the t(8;21), *CEBPA*$^{N/C}$ patients clearly formed a separate group (Fig. 3.2 A and B). The strong correlation between chromatin landscape and gene expression within the same leukaemic subtype is exemplified by *the FOXO1, KLF12, RUNX3* and *VAV2* genes, where the expression pattern follows the chromatin accessibility profile (Fig. 3.3 A-D).

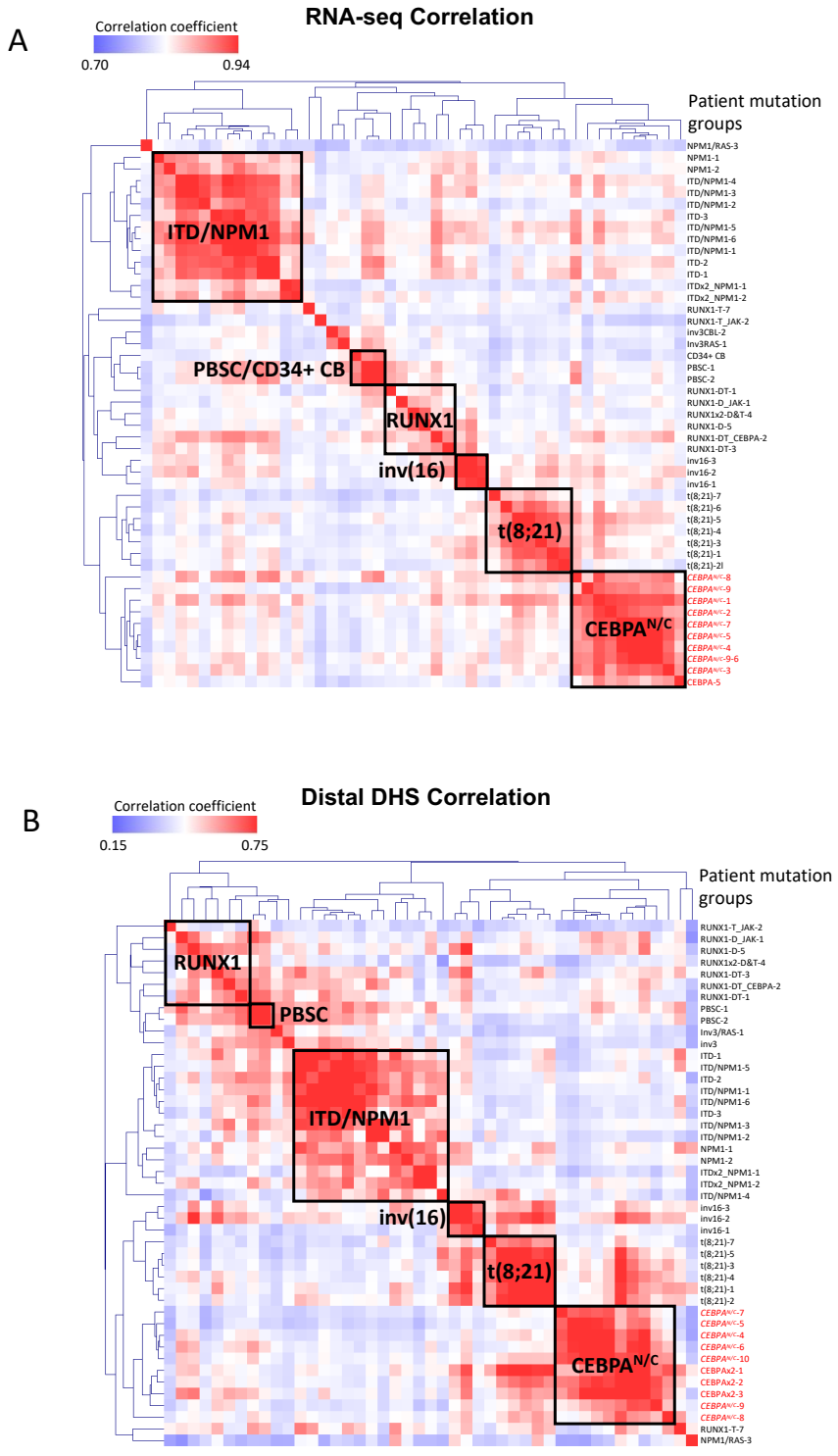

Figure 3.2: *CEBPA*$^{N/C}$ acute myeloid leukaemia cluster with t(8;21) AML but form an independent group.

(A) and (B) Hierarchical clustering of Pearson correlation coefficients of RNA-seq and DNase I/ATAC-seq data from (Assi et al., 2019b) and this study. *CEBPA*$^{N/C}$ patient samples are highlighted in red. RNA-, ATAC- and DNase I-seq were performed by Assunta Adamo, clustering analysis were performed by Dr Salam Assi (University of Birmingham).

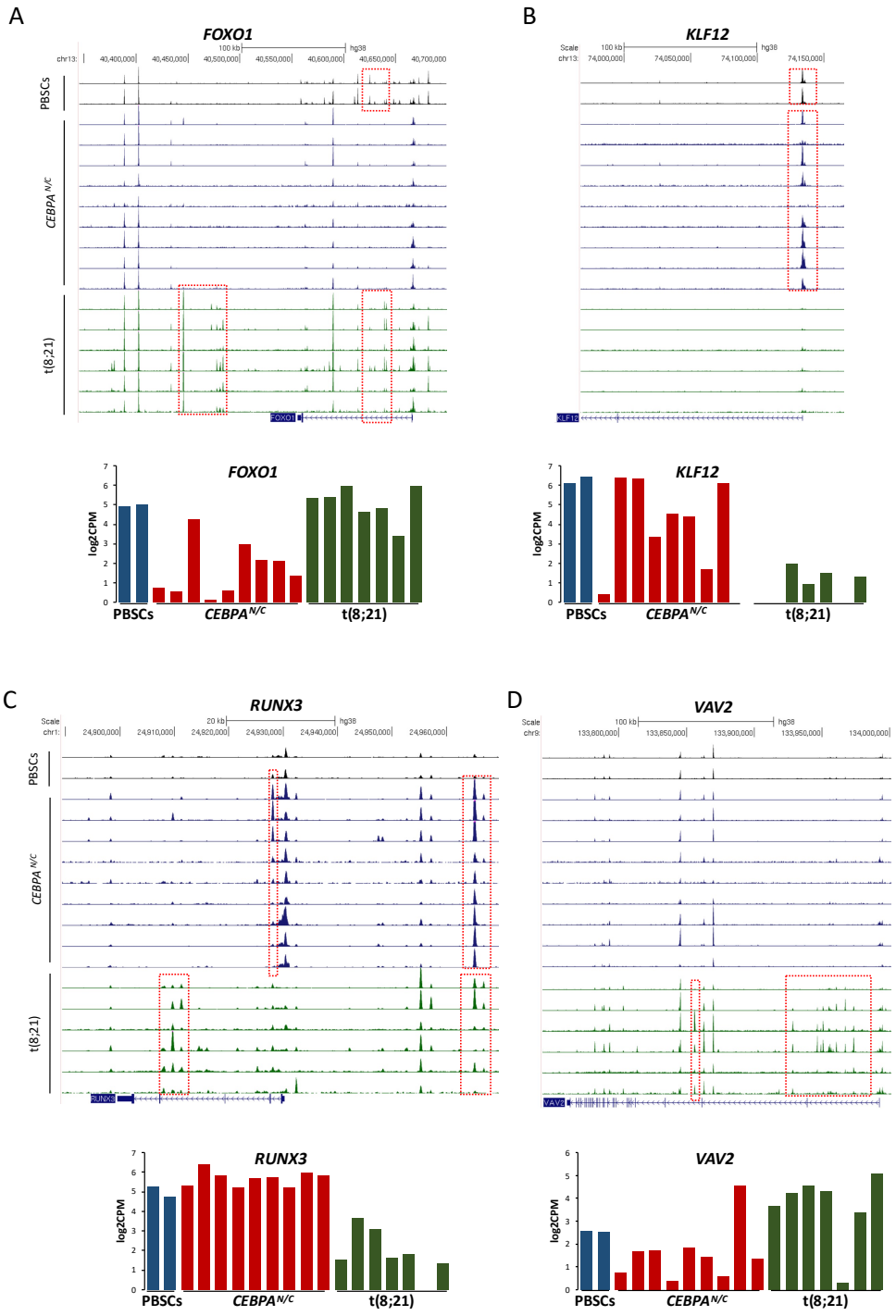

Figure 3.3: Chromatin and transcriptional profiles of PBSCs and *CEBPA*$^{N/C}$ and t(8;21) AML blasts at 4 genomic loci

The figure shows chromatin accessibility and gene expression patterns at the *FOXO1* (A), *KLF12* (B), *RUNX3* (C) and *VAV2* (D) loci. The UCSC genome browser screenshots depicting open chromatin regions (upper panels) are showed alongside gene expression data (lower histograms). Figure generated by Dr Salam Assi.

3.2 Comparison of *CEBPA*$^{N/C}$, t(8;21) and healthy blast hypersensitive sites

To substantiate this observation and to define the cis-regulatory elements specifically active in *CEBPA*$^{N/C}$ AML, we compared t(8;21) and *CEBPA*$^{N/C}$ directly (Fig. 3.4). We also compared both AML subtypes with normal PBSCs (Fig 3.5). This analysis showed that individual chromatin accessibility datasets within each AML subtype are highly similar (Fig. 3.4 A, pink and pale blue density plots) and thus could be merged. The comparison of the merged data shows that both subtypes display a large number of specific peaks when compared to each other (1738 *CEBPA*$^{N/C}$ specific and 2749 t(8;21) specific, FC > |2|) (Fig. 3.4 A, leftmost density plot). An interesting finding was the occurrence of C/EBP:AP-1 composite motifs within the *CEBPA*$^{N/C}$ specific peaks (Fig. 3.4 B). These motifs are common in regulatory elements of monocyte/macrophage-specific genes, and are bound by C/EBP:AP-1 heterodimers to induce monopoiesis to the detriment of granulopoiesis (Friedman, 2015). *CEBPA*$^{N/C}$ specific cis-regulatory elements were also enriched in PU.1 and IRF motifs (FIG. 3.4 B), while AP-1, ETS, E-box and EGR motifs were found in t(8;21) specific sites (FIG 3.4 C). Taken together, these findings suggest that the aberrant differentiation program is skewed toward monocytic differentiation in both AML subtypes.

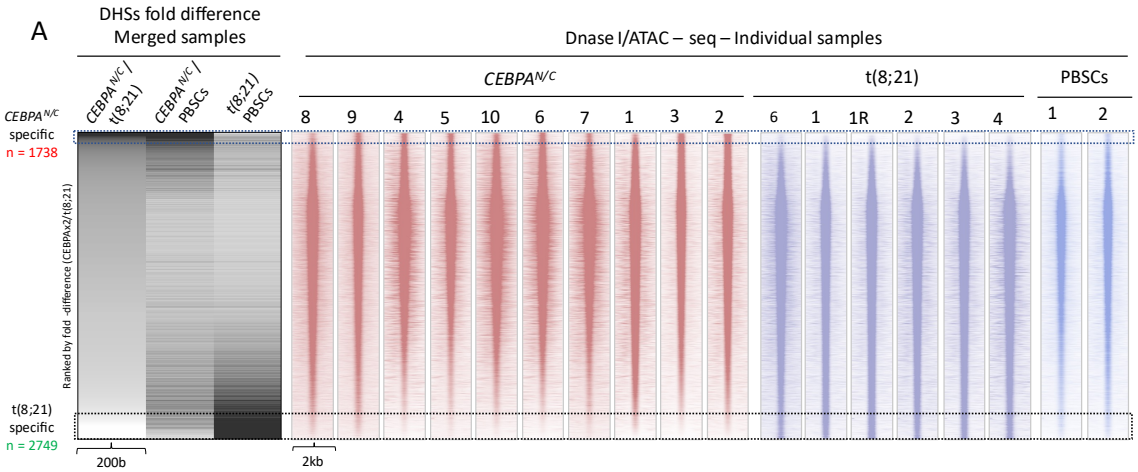

B

Motifs enriched in ***CEBPA***$^{N/C}$ specific DHSs compared to t(8;21)

Motif	% of targets	p-value	Match
	40.60	1e-126	RUNX
	33.13	1e-80	PU.1
	43.49	1e-62	C/EBP:AP-1
	11.08	1e-19	GATA
	5.78	1e-16	IRF

C

Motifs enriched t(8;21) specific DHSs compared to ***CEBPA***$^{N/C}$

Motif	% of targets	p-value	Match
	28.41	1e-244	AP-1
	52.80	1e-100	ETS
	19.06	1e-32	RUNX
	43.97	1e-25	E-box
	6.91	1e-19	EGR

Figure 3.4: Comparison of open chromatin regions between t(8;21) and *CEBPA*$^{N/C}$ AMLs

(A) Leftmost plot: Hypersensitive sites fold difference between *CEBPA*$^{N/C}$ and t(8;21), *CEBPA*$^{N/C}$ and PBSCs and t(8;21) and PBSCs samples respectively, across a 200 bp window. Rightmost plots: Density plots showing the open chromatin profile of *CEBPA*$^{N/C}$ (pink), t(8;21) (lilac) and PBSC (pale blue) across a 2kb window. Data are ranked by normalized tag count of merged *CEBPA*$^{N/C}$ peaks over merged PBSCs peaks. (B-C) Motifs analysis in *CEBPA*$^{N/C}$ (B) and t(8;21) (C) specific accessible chromatin regions. Motifs differentially enriched between the two AML subtypes are depicted in pink and green. Analyses were performed by Dr Salam Assi (University of Birmingham).

When the merged *CEBPA*$^{N/C}$ data were compared to PBSCs (360 *CEBPA*$^{N/C}$ specific sites and 426 t(8;21) specific sites, FC > |3|) (FIG. 3.4 A), motif analysis showed a strong enrichment of RUNX and, again, of the CEBP:AP-1 composite motif in *CEBPA*$^{N/C}$ specific sites (Fig. 3.5 B). Interestingly, we also found enrichment of motifs for POU4F1, which is a transcription factor aberrantly expressed in both *CEBPA*$^{N/C}$ and

t(8;21) AMLs (Assi et al., 2019b) (Fig. 3.5 B). The enrichment of GATA motifs in the PBSC-specific peaks (Fig. 3.5 A) indicates that *CEBPA*$^{N/C}$ blasts are further along the myeloid differentiation pathway as compared to healthy blasts.

A

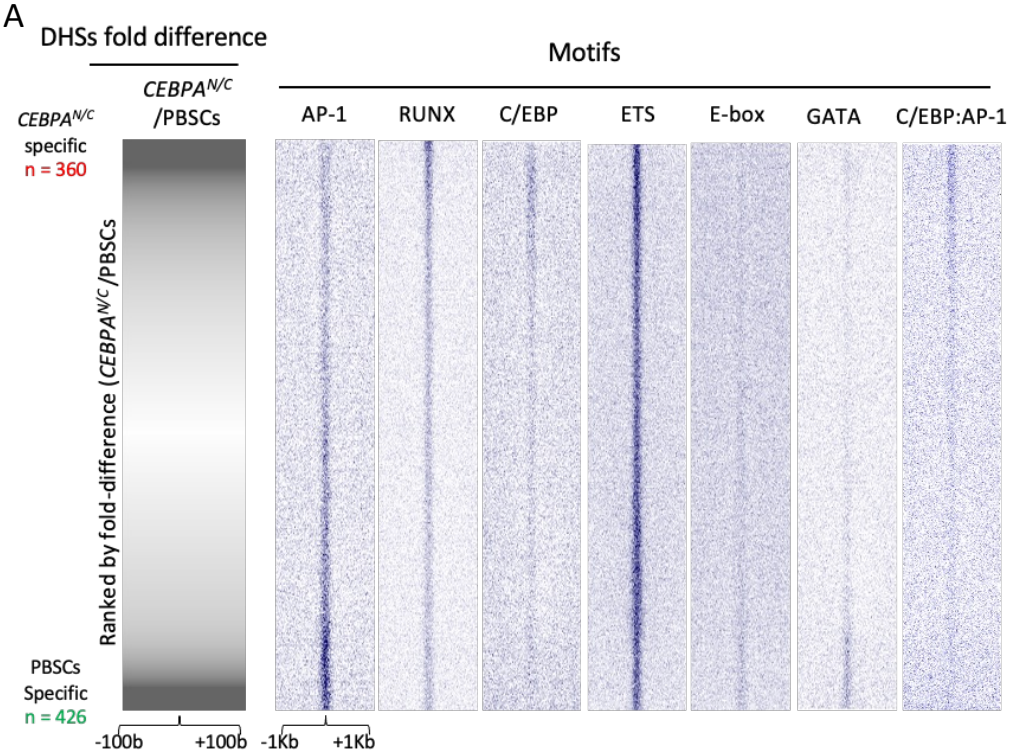

B

Motifs enriched ***CEBPA***$^{N/C}$ specific DHSs compared to ***PBSCs***

Motif	% of targets	p-value	Match
	48.38	1e-368	ETS
	51.04	1e-256	RUNX
	25.7	1e-86	C/EBP:AP-1
	2.28	1e-37	POU4F1
	29.9	1e-33	E-box

Figure 3.5: Comparison of open chromatin regions between *CEBPA*$^{N/C}$ AMLs and PBSCs

(A) Hypersensitive sites fold difference between *CEBPA*$^{N/C}$ and PBSCs across a 200 bp window. Data are ranked by normalized tag count of merged *CEBPA*$^{N/C}$ peaks over merged PBSCs peaks. TF binding motifs projected against hypersensitive sites are plotted alongside. (B) Motifs enriched in *CEBPA*$^{N/C}$ specific hypersensitive sites compared to PBSCs. Analyses were performed by Dr Salam Assi (University of Birmingham).

3.3 Global gene expression comparison between *CEBPA*$^{N/C}$ AMLs and PBSCs

To identify effector genes whose expression is deregulated by mutant C/EBPα proteins, we compared merged transcriptomic data from *CEBPA*$^{N/C}$ AML blasts and healthy PBSCs. We found that mutant C/EBPα expression was mainly associated with gene downregulation, with 1354 genes down regulated and 357 up-regulated compared to normal blasts (FC > |2|, Benjamini-Hochberg adjusted p-value < 0.05) (Fig. 3.6 A, B and supplementary table 1).

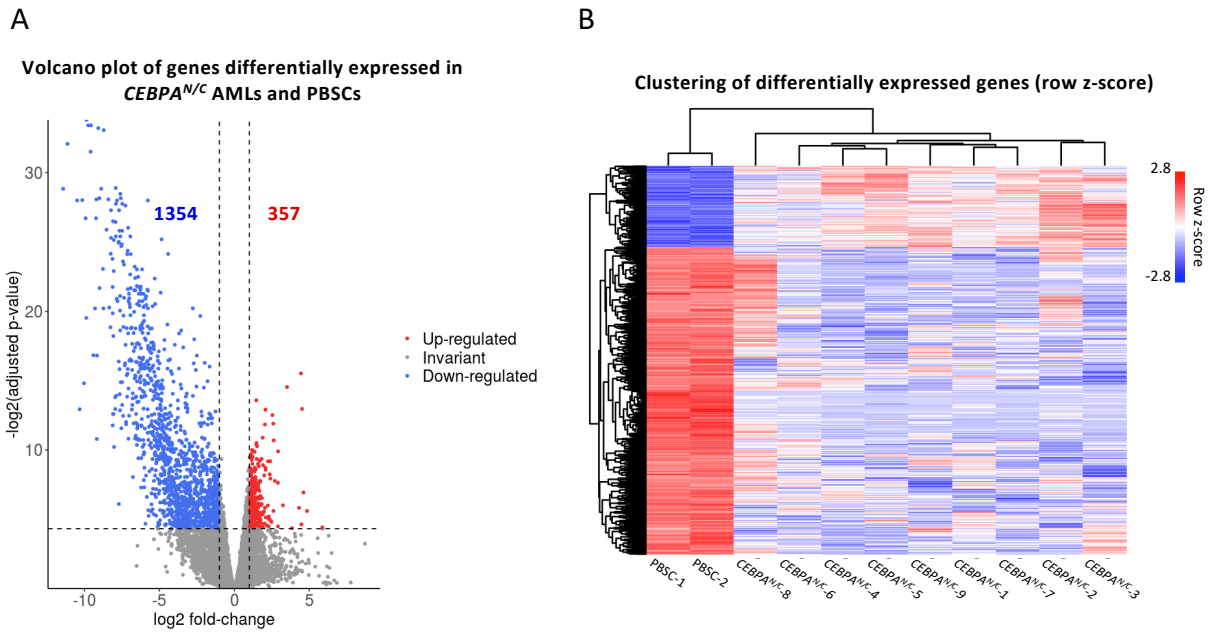

Figure 3.6: Analysis of differential gene expression patterns in *CEBPA*$^{N/C}$ AML compared to healthy cells.

(A) Volcano plot of genes deregulated in *CEBPA*$^{N/C}$ compared to PBSCs. Each dot represents a gene, the log2 fold-change indicate the mean expression level for each gene across all *CEBPA*$^{N/C}$ samples. Blue dots represent significantly downregulated genes (log2 fold-change < -1, Benjamini-Hochberg adjusted p-value < 0.05); red dots represent significantly upregulated genes (log2 fold-change > 1, Benjamini-Hochberg adjusted p-value < 0.05). (B) Hierarchical clustering heatmap of RNA-seq expression z-scores computed for genes differentially expressed between *CEBPA*$^{N/C}$ and PBSCs samples. Each row represents a gene. Analyses performed by Assunta Adamo.

CEBPA itself was amongst the most up-regulated genes (Fig. 3.7 and table 17), together with markers of myeloid differentiation such as *MPO, CTSA* and *CTSW* (Fig. 3.7). Our analysis also showed the aberrant expression of *CD7*, a marker of early T-cell differentiation (Blom and Spits, 2006) and LSCs in T-cell acute lymphoblastic leukaemia (T-ALL) (Gerby et al., 2011) (Fig. 3.7). CD7 expression has been shown to correlate with loss of wild-type C/EBPα in AML and has been proposed as marker for large-scale detection of $CEBPA^{N/C}$ AMLs (Mannelli et al., 2017; Rohrs et al., 2010). Other genes significantly upregulated in $CEBPA^{N/C}$ AMLs were the serine/threonine kinase *MAP3K8*, the RNA-binding proteins *PIWIL4* and the dual-specificity phosphatase *DUSP10* (Fig. 3.7 and table 17). Several HOX genes and their TALE interactors (i.e., MEIS1, PBX1) appeared to be strongly downregulated (Fig. 3.8 D), accordingly with previous observation that C/EBPα expression is required to sustain the expression of *Hoxa9-Meis1* in MLL-ENL transformed cells and to drive *Hoxa9-Meis1*-mediated leukaemic transformation in murine models (Collins et al., 2014; Ohlsson et al., 2014). Also MYCT1, a c-MYC target that act as tumor suppressor in AML (Fu et al., 2018; Fu et al., 2011), was among the most downregulated genes (Fig.3.8 and table 17). Recent work has reported that *MSI2* and *NT5E* are direct targets of C/EBPα-p30 and are overexpressed in $CEBPA^{N/C}$ AMLs (Heyes et al., 2021). However, in our data only *NTE5E* appeared to be upregulated (Table 17).

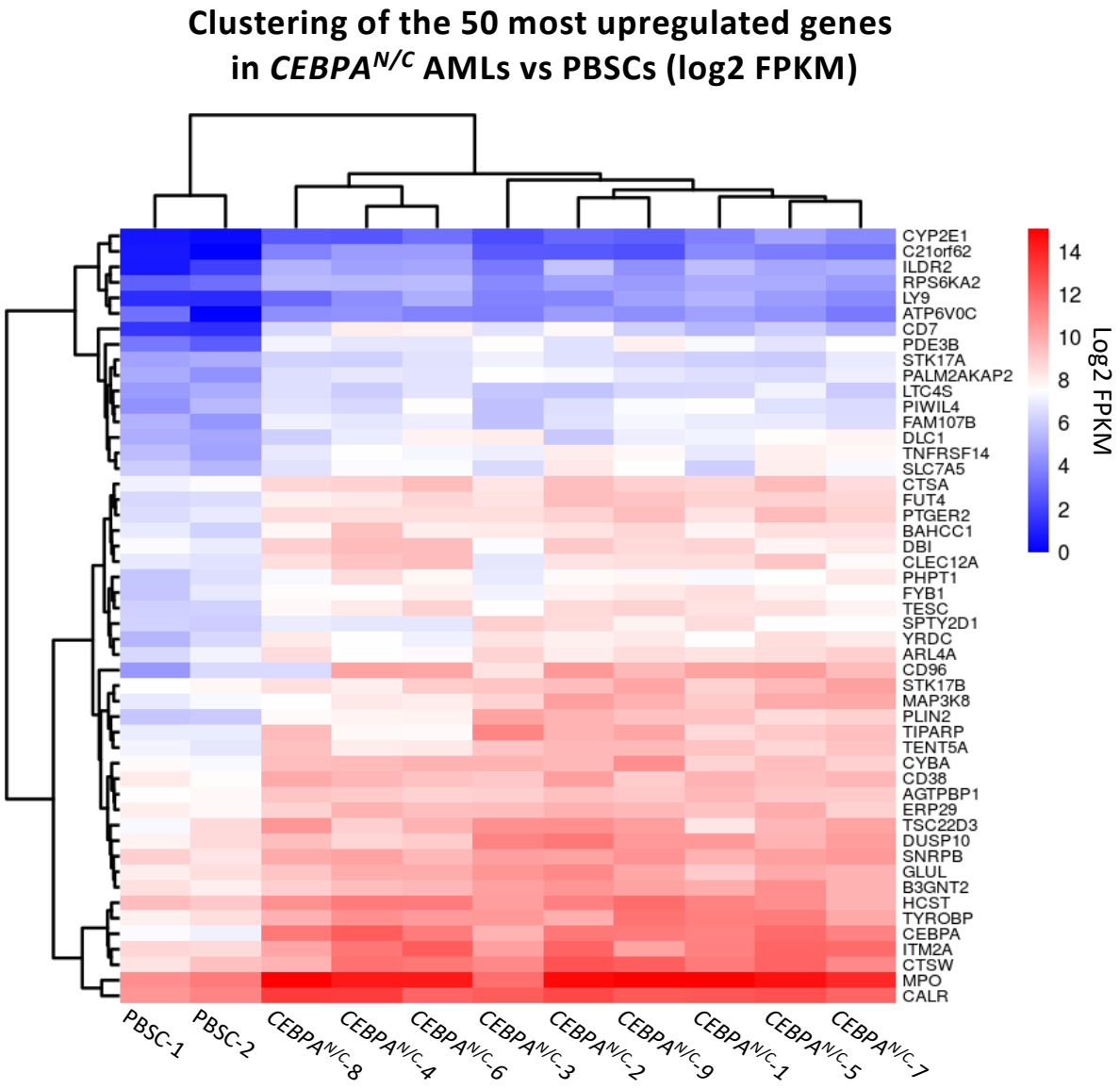

Figure 3.7: Hierarchical clustering of expression values for the 50 most upregulated in *CEBPA*$^{N/C}$ AMLs compared to PBSCs.

Expression values are reported as log2FPKM. Analyses performed by Assunta Adamo.

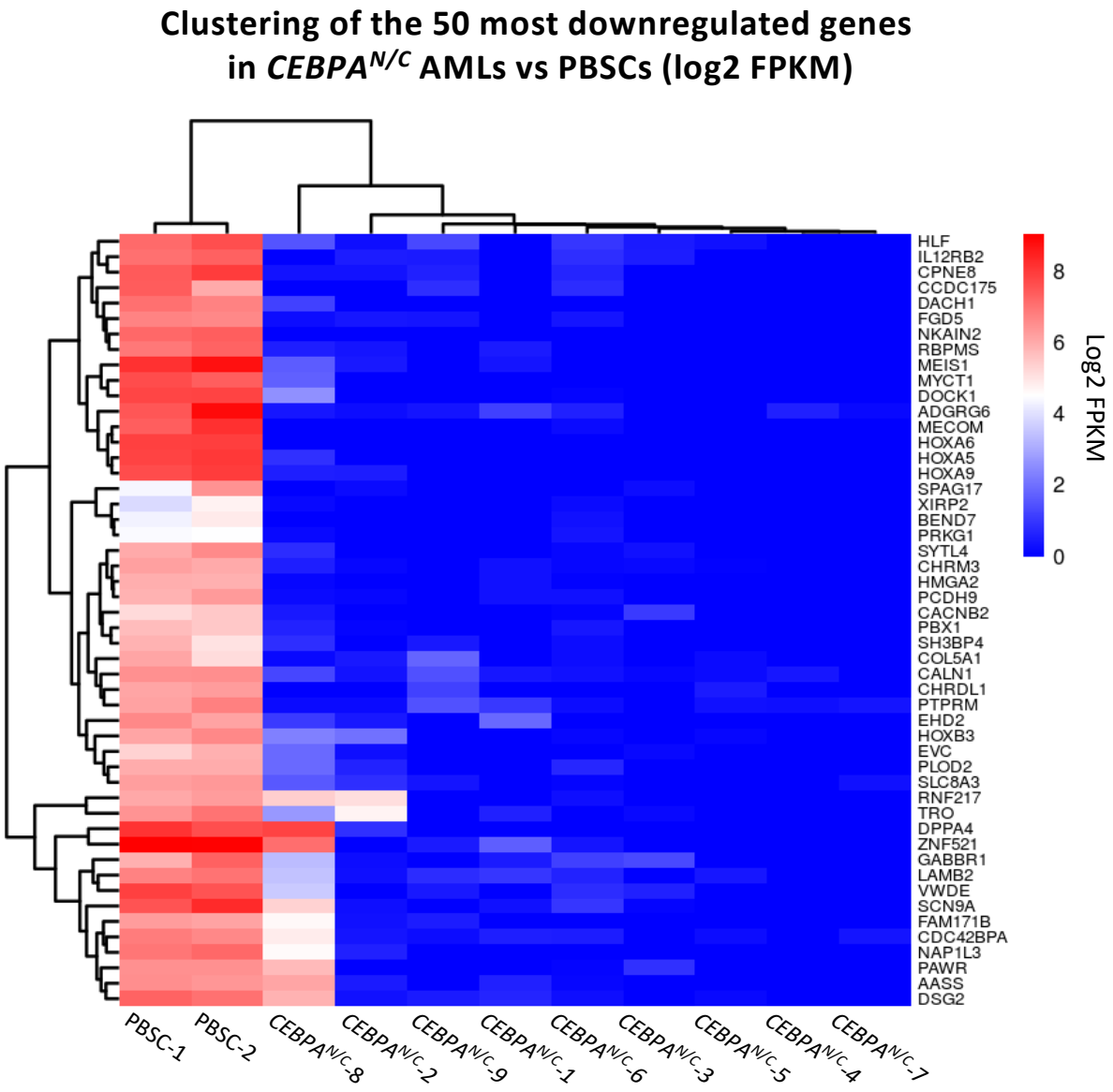

Figure 3.8: Hierarchical clustering of expression values for the 50 most downregulated in *CEBPA*$^{N/C}$ AMLs compared to PBSCs.

Expression values are reported as log2FPKM. Analyses performed by Assunta Adamo.

Gene symbol	*CEBPA* $^{N/C}$ log2CPM avg	PBSC log2CPM avg	log2FC	P.Value	adj.P.Val
NT5E	0.89	-3.29	4.97	0.279	0.507
CEBPA	9.48	5.03	4.45	0.000	0.000
MAP3K8	7.66	5.36	2.29	0.006	0.044
PIWIL4	5.65	3.46	2.10	0.003	0.029
DUSP10	8.36	6.19	2.17	0.006	0.043
MSI2	8.01	9.49	-1.48	0.001	0.013
MYCT1	-3.60	5.54	-9.21	0.000	0.000

Table 17: Expression values of selected genes across *CEBPA*$^{N/C}$ and PBSC samples.

Expression values are reported as log2CPM.

KEGG pathway analyses of up-regulated genes revealed the enrichment of pathways related to granulocyte function, such as “Antigen processing and presentation”, “Lysosome” and “Phagosome” (Fig. 3.9 A, B). Also “Ribosome” was among the most represented pathways (Fig. 3.9 A, B). Highly proliferating leukaemic blasts are characterized by increased protein synthesis and it has been previously showed that C/EBPα recruits PolI to stimulate rRNA synthesis in myeloid progenitors (Antony et al., 2021; Muller et al., 2010). “ECM-receptor interaction”, “Tight junction” and “Adherent junctions” pathways were downregulated, accordingly with previous observation that deregulation of stem cell-niche interaction are involved in the pathogenesis of AML (Majeti et al., 2009) (Fig. 3.10 A, B). Of note, RUNX1 appeared to be amongst the significantly downregulated genes (Fig. 3.10 A).

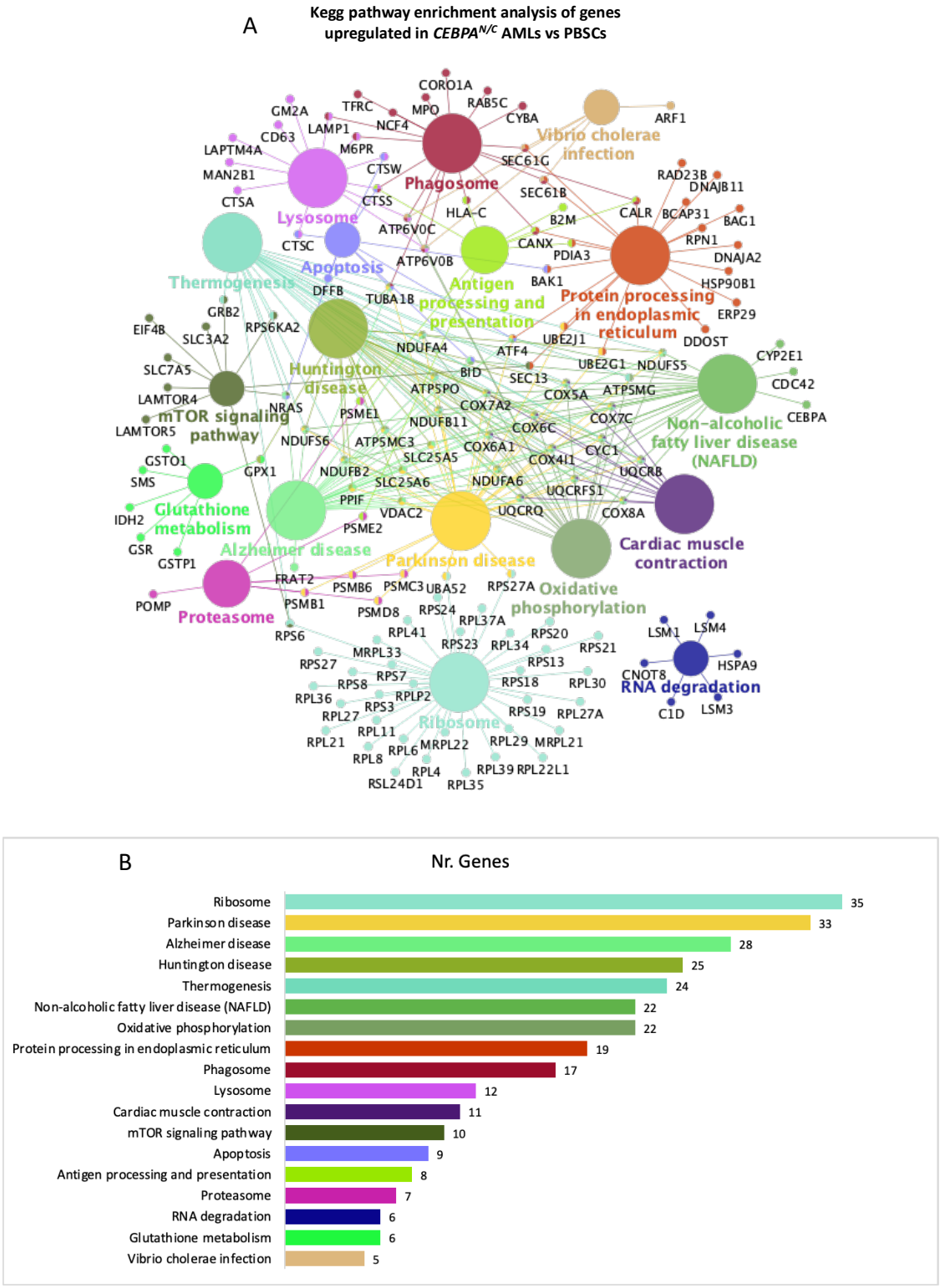

Figure 3.9: KEGG pathway analysis of genes upregulated in *CEBPA*$^{N/C}$ AML compared to healthy blasts

(A) Network of significantly enriched KEGG pathways ($p < 0.05$). (B) Number of genes included in each pathway. Analyses performed by Assunta Adamo.

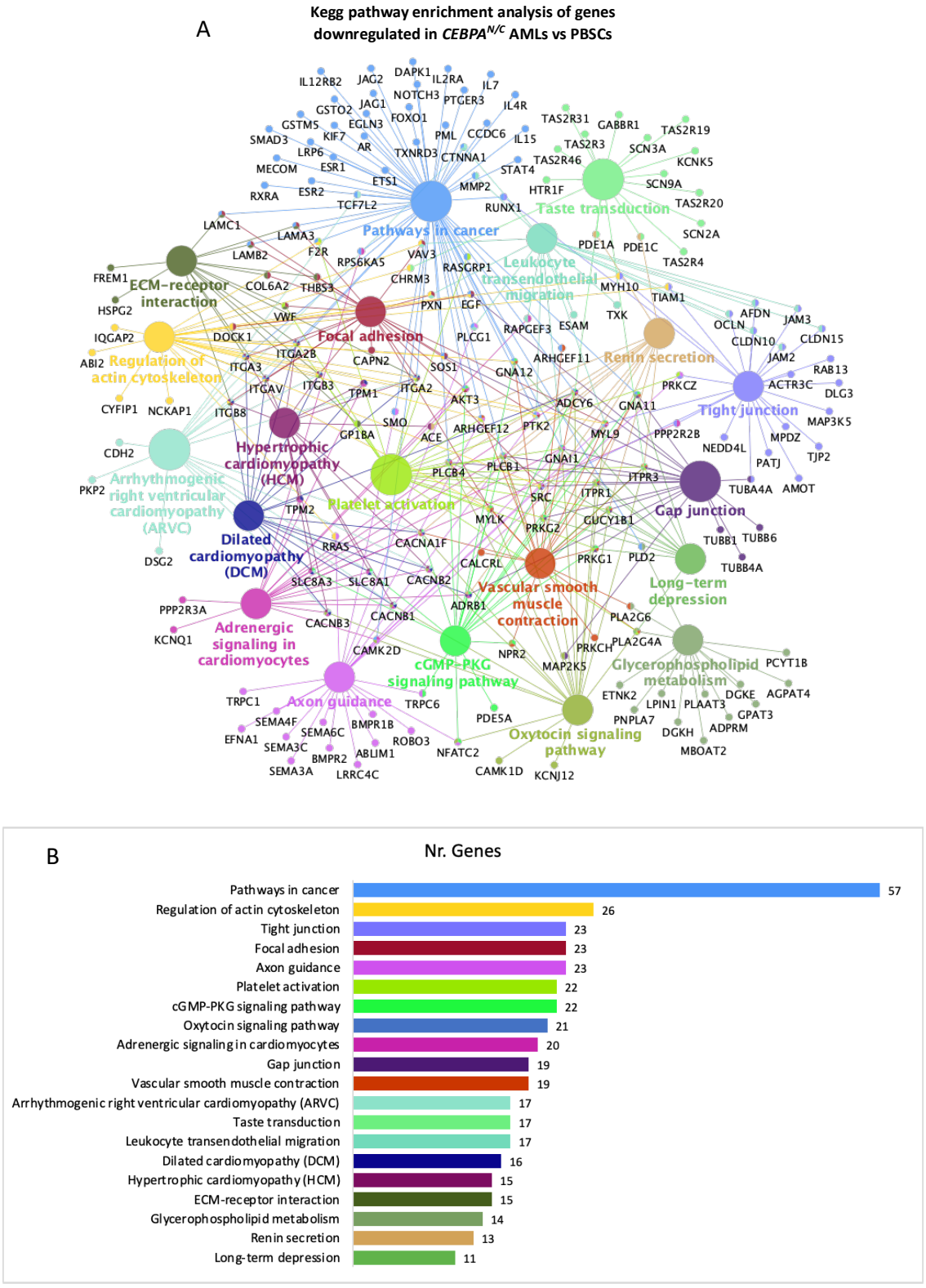

Figure 3.10: KEGG pathway analysis of genes downregulated in *CEBPA*$^{N/C}$ AML compared to healthy blasts.

(A) Network of significantly enriched KEGG pathways ($p < 0.05$). (B) Number of genes included in each pathway. Analyses performed by Assunta Adamo.

3.4 Global gene expression comparison between *CEBPA$^{N/C}$* and t(8;21) AMLs

We next wanted to identify pathways aberrantly regulated in *CEBPA$^{N/C}$* AML compared to t(8;21) leukaemia. Gene expression analysis showed 824 genes up-regulated and 454 genes down-regulated in *CEBPA$^{N/C}$* samples compared to t(8;21) (FC > |2|, Benjamini-Hochberg adjusted p-value < 0.05) (Fig. 3.11 A and supplementary table 2). KEGG pathway analysis of *CEBPA$^{N/C}$* up-regulated genes showed an enrichment of the "RAP1 signalling pathway" (Fig. 3.11 B). RAP1 regulates several biological process in hematopoietic cells, included cell adhesion, proliferation and differentiation (Stork and Dillon, 2005) and deregulation of RAP1 signalling has been suggested to contribute to the pathogenesis of myeloid disorders (Gyan et al., 2005). Several cell adhesion and signalling pathways were enriched in t(8;21) AMLs compared to *CEBPA$^{N/C}$*, including "MAPK signalling pathway", "Phospholipase D signalling pathway" and "PI3K-Akt signalling pathway" (Fig. 3.11 C). Signal transduction pathways regulates several cellular processes, such as proliferation, differentiation, apoptosis and metabolism, and their deregulation is a hallmark of AML.

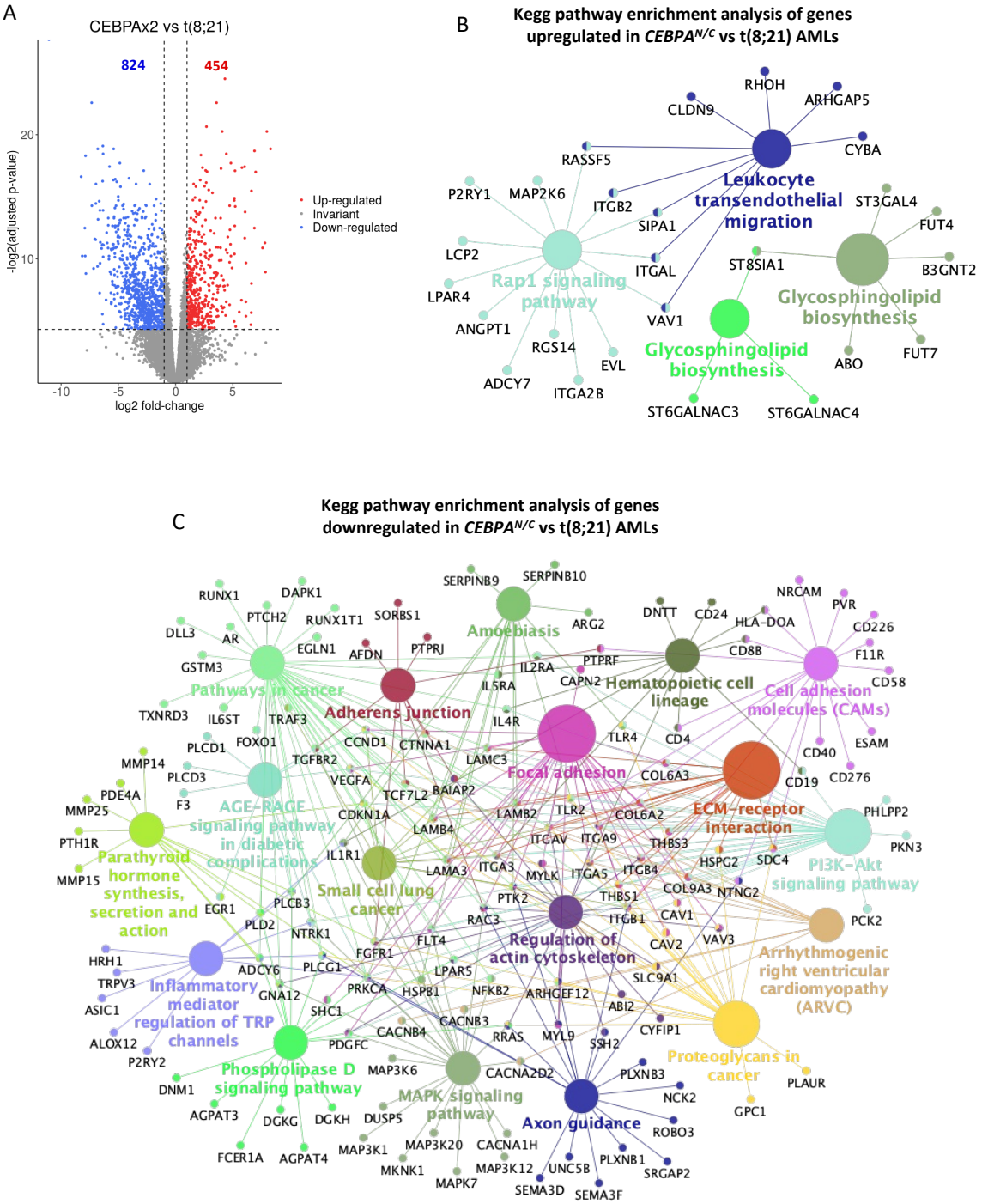

Figure 3.11: Direct comparison of t(8;21) and *CEBPA*$^{N/C}$ gene expression patterns

(A) Volcano plot of genes deregulated in *CEBPA*$^{N/C}$ compared to t(8;21) AMLs. Each dot represents a gene, the log2 fold-change indicate the mean expression level for each gene across all *CEBPA*$^{N/C}$ samples. Blue dots represent significantly downregulated genes (log2 fold-change < -1, Benjamini-Hochberg adjusted p-value < 0.05); red dots represent significantly upregulated genes (log2 fold-change > 1, Benjamini-Hochberg adjusted p-value < 0.05). (B-C) KEGG pathway enrichment analysis of genes up (E) and down (F) regulated in *CEBPA*$^{N/C}$ compared to t(8;21) AMLs. Analyses performed by Assunta Adamo.

We next defined a set of genes commonly deregulated in *CEBPA*$^{N/C}$ and t(8;21) AMLs compared to normal blasts (Fig. 3.12 A and B). GO-term analysis of upregulated genes showed an enrichment in terms related to the response to IL-7 and IL-12 (Fig. 3.12 C), two immunomodulatory cytokines with anti-tumor activity (Ferretti et al., 2010; Krawczyk et al., 2019).

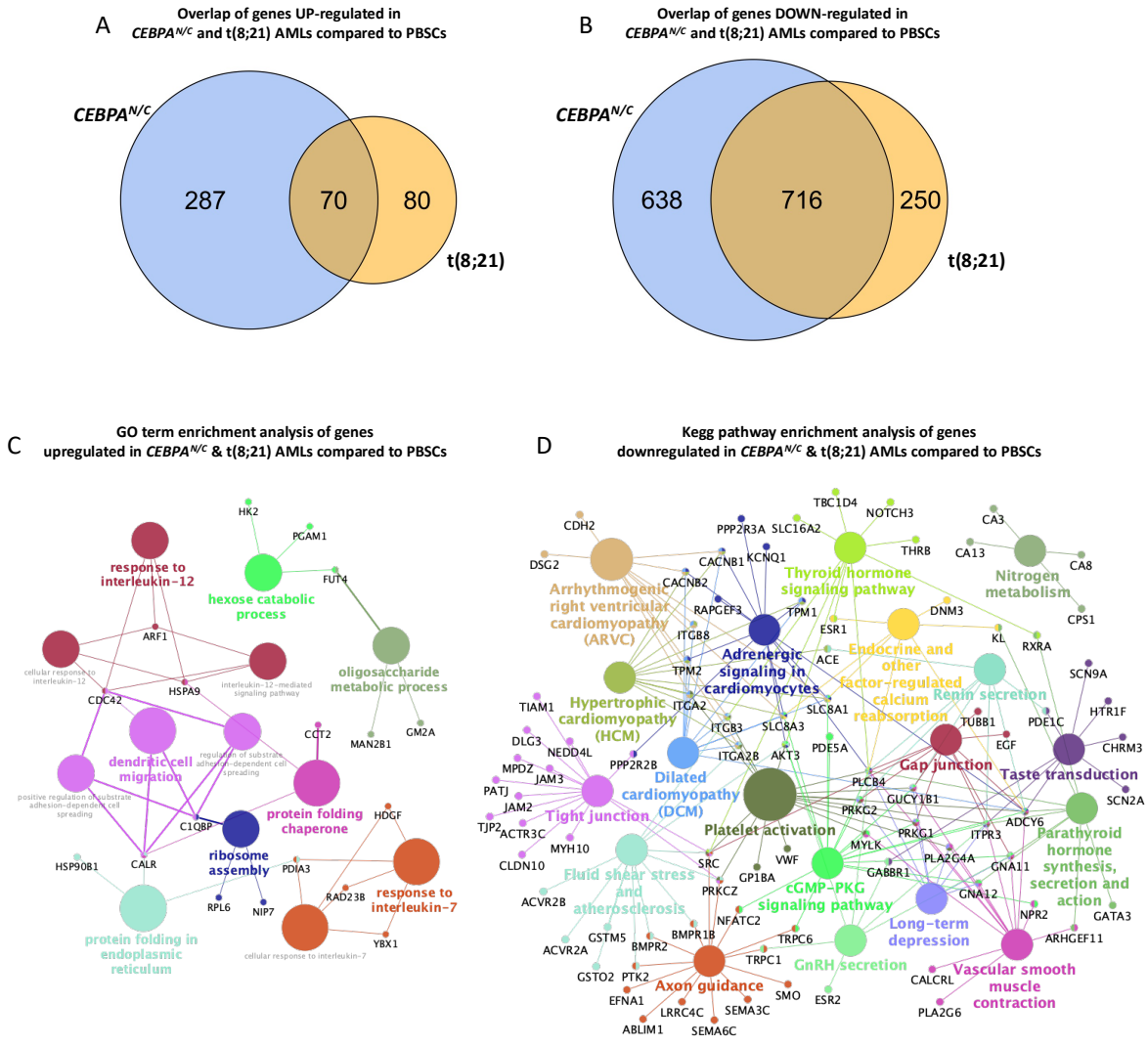

Figure 3.12: Pathways commonly deregulated in *CEBPA*$^{N/C}$ and t(8;21) AMLs compared to healthy blasts

(A-B) Venn diagrams showing the overlap of genes commonly upregulated (A) and downregulated (B) in *CEBPA*$^{N/C}$ and t(8;21) AMLs compared to PBSCs. (C-D) KEGG pathway enrichment analysis of genes commonly up (C) and down (D) regulated in *CEBPA*$^{N/C}$ and t(8;21) AMLs compared to PBSCs. Analyses performed by Assunta Adamo.

3.5 C/EBP family members may counterbalance the aberrant activity of C/EBPα in *CEBPA*$^{N/C}$ and t(8;21) AMLs

AML development is dependent on myeloid commitment of progenitors, which in turn requires C/EBPα expression (Ye et al., 2015). Several studies have suggested that C/EBP family members have redundant functions (Tsukada et al., 2011). To test whether other members of the family could compensate for C/EBPα aberrant function or low expression in affected patients, we assessed the expression of all C/EBP family members in both healthy PBSCs and *CEBPA*$^{N/C}$ and t(8;21) leukaemic blast (Fig. 3.13 A-F). We found that *CEBPA* mRNA is consistently up regulated in all *CEBPA*$^{N/C}$ patients (FC > 2, Benjamini-Hochberg adjusted p-value < 0.05) (Fig. 3.13 A). *CEBPD* was up regulated in all the AML samples but upregulation did not reach the significant threshold in our analysis (FC > 2, Benjamini-Hochberg adjusted p-value > 0.05) (Fig. 3.13 C). *CEBPB*, which is required for "emergency" granulopoiesis and can sustain normal haematopoiesis in absence of C/EBPα (Hirai et al., 2006; Jones et al., 2002), was not upregulated in either leukaemia subtype (Fig. 3.13 B). Interestingly, *CEBPE* was up regulated in t(8;21) samples compared to *CEBPA*$^{N/C}$ (Fig. 3.13 D). This transcription factor is required for terminal myeloid differentiation. We also confirmed that RUNX1 is systematically down regulated in all *CEBPA*$^{N/C}$ patients (FC < -2, Benjamini-Hochberg adjusted p-value < 0.05), with the only exception represented by a sample, *CEBPA*$^{N/C}$-8, harbouring a heterozygous *RUNX1* 292delC (FIG. 3.13 G). This variant results in the generation of a premature stop codon and is expected to result in protein truncation or nonsense mediated decay.

These results suggest that other members of the *CEBP* family are expressed and could partially compensate the impaired activity of C/EBPα in *CEBPA*$^{N/C}$ and t(8;21) AMLs.

Moreover, *RUNX1* down regulation may be a characteristic of *CEBPA*$^{N/C}$ affected patients.

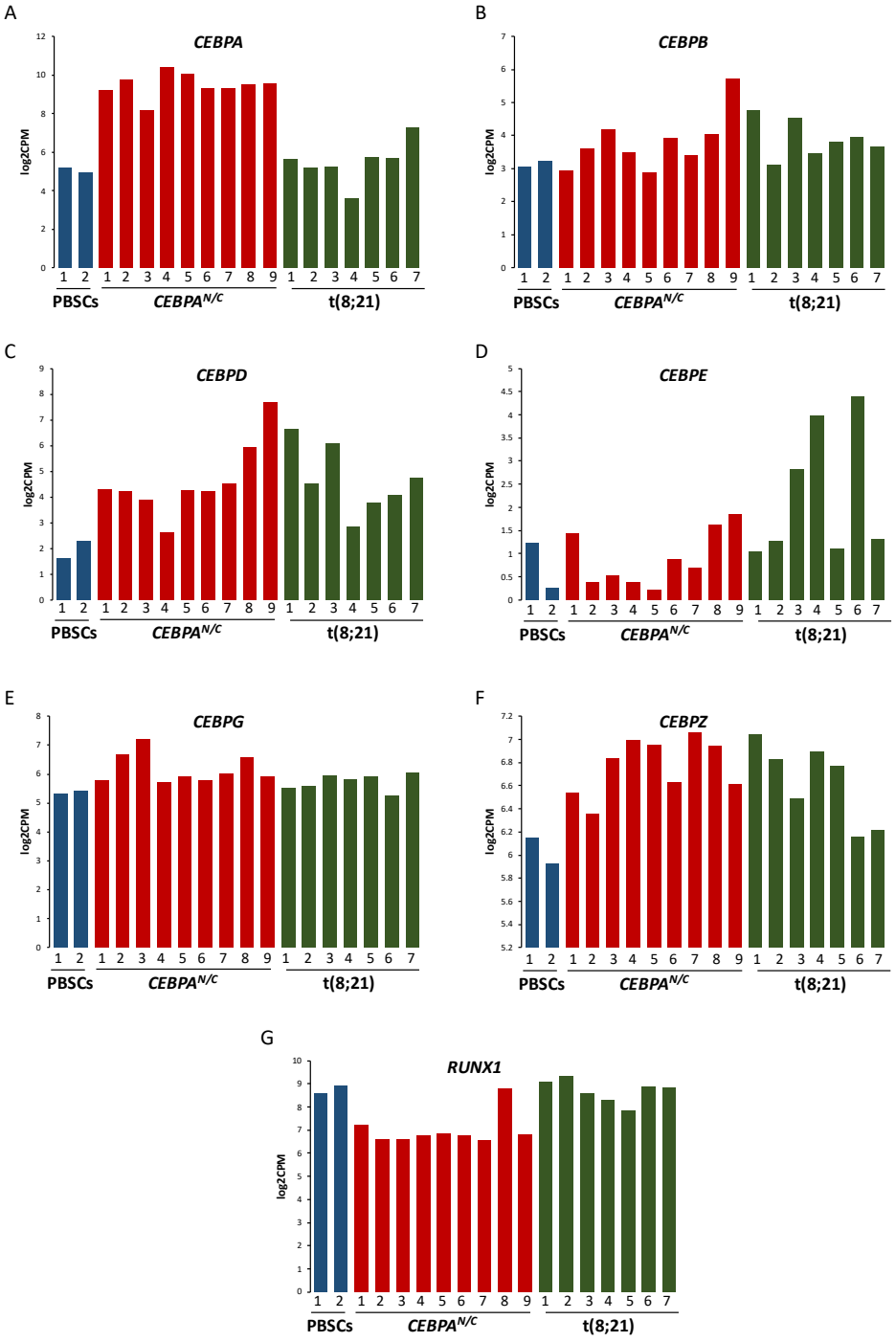

Figure 3.13: mRNA expression of *C/EBP* family members and *RUNX1* in healthy blasts and *CEBPA*$^{N/C}$ and t(8;21) AMLs

(A-G) Histograms of gene expression values (log2 CPM) for the indicated genes in PBSCs (blue), *CEBPA*$^{N/C}$ (red) and t(8;21) (green) blasts. Figure generated by Assunta Adamo.

3.6 The promoter-cis-regulatory element interactome of *CEBPA$^{N/C}$* AMLs

The accurate definition of the GRN on which *CEBPA$^{N/C}$* AMLs rely requires to unambiguously assign each active regulatory element to its target genes. By using Promoter Capture Hi-C (CHi-C), we defined the whole set of enhancer-promoter interactions for one of our *CEBPA$^{N/C}$* patient samples, *CEBPA$^{N/C}$*-9. 4x10^{7} CD34+ purified cells were fixed in formaldehyde and processed as described in detail in section 2.12. To identify significant interactions between cis-regulatory elements and promoters, Chi-C data were filtered against our DHS dataset and analyzed. The interactome for both normal CD34+ cells and t(8;21) patients has been previously characterized (Assi et al., 2019b; Mifsud et al., 2015). As seen before in healthy and t(8;21) blasts (Assi et al., 2019b), also in the *CEBPA$^{N/C}$* patient most of interactions occurred within the same chromosome, as demonstrated by the high intensity blocks centred along the diagonal of the whole genome interaction matrix (FIG. 3.14 A). In addition, the organization into TADs in both *CEBPA$^{N/C}$* and t(8;21) AMLs was not affected by the different driver mutations (Fig. 3.14 B).

More than 110000 interactions between distal open chromatin regions and promoters were identified in each sample (Fig. 3.14 C) and ~88% of *CEBPA$^{N/C}$* interactions were also present in the t(8;21) dataset (Fig. 3.14 D). A similar high overlap was also seen when compared to healthy CD34+ cells. However, given the common haematopoietic origin of all samples the overlap among leukaemic blasts and PBSCs is not surprising (Fig. 3.14 D).

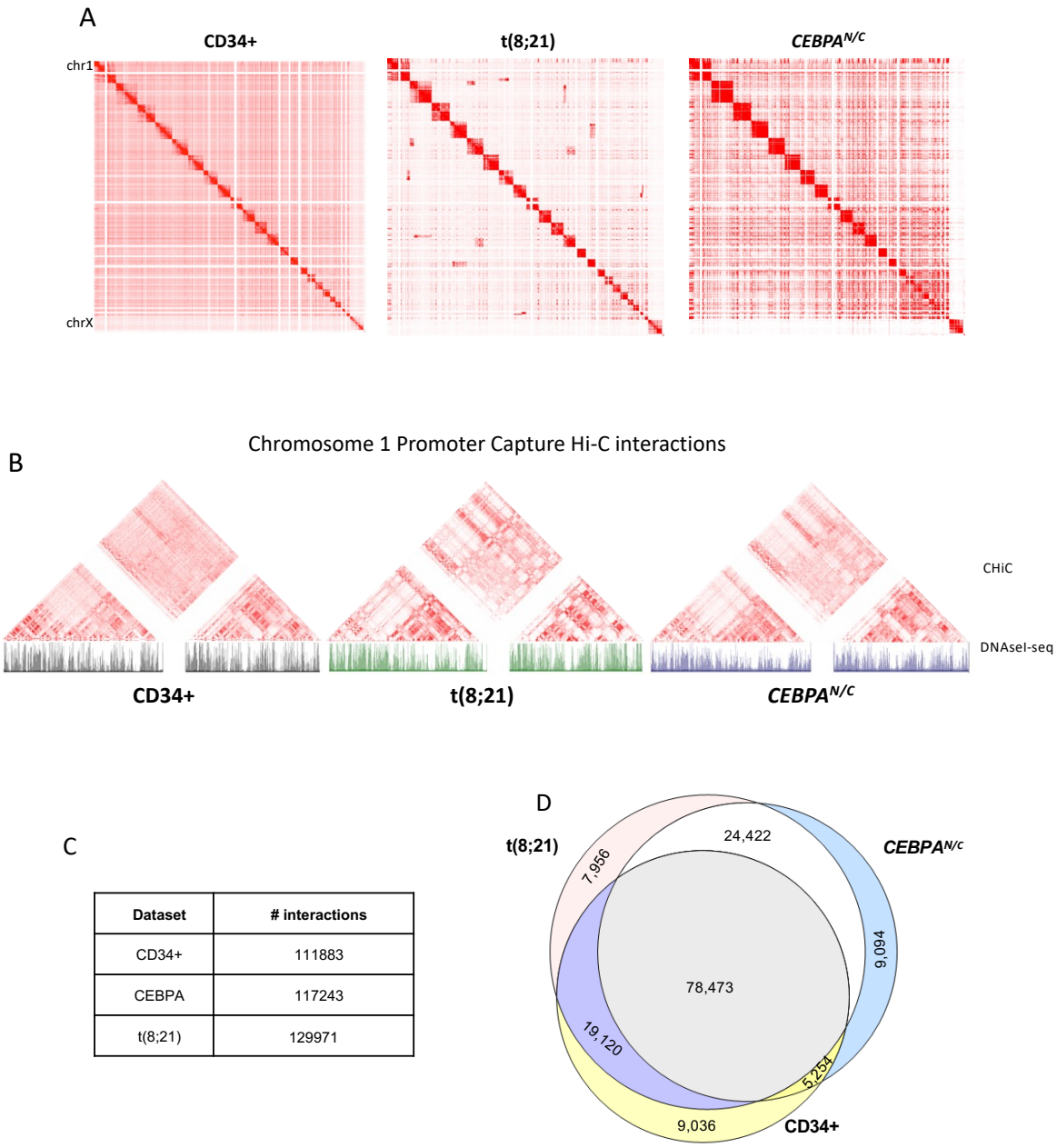

Dataset	# interactions
CD34+	111883
CEBPA	117243
t(8;21)	129971

Figure 3.14: Capture Hi-C analysis of global chromosomal structure in *CEBPA*$^{N/C}$ AML

(A) Contact matrix across all chromosomes for healthy blasts (left) and *CEBPA*$^{N/C}$ (middle) and t(8;21) (right) leukaemic blasts at 10Mb resolution. Colour intensity represents interaction frequency. (B) Contact matrix across chromosome 1 for healthy blasts (left) and *CEBPA*$^{N/C}$ (middle) and t(8;21) (right) leukaemic blasts at 10Mb resolution. A UCSC genome browser track is shown below each matrix to highlight the hypersensitive site pattern. (C) Table reporting the number of interactions identified for each cell type analysed (D) Venn diagram showing the number of interactions shared among the analysed samples. CD34+ and t(8;21) C-HiC data from (Assi et al., 2019b). C-HiC for the *CEBPA*$^{N/C}$ patient was performed by Assunta Adamo alongside with Dr Anetta Ptasinska, University of Birmingham. Analyses were performed and figure generated by Dr Salam Assi, University of Birmingham.

3.7 Healthy and leukaemic blasts differ in specific promoter-cis-regulatory element interactions

Whilst the global chromosomal interaction between the three analysed cell types were similar, differences between leukaemic and healthy cells became apparent when the interactions were analysed at a higher resolution. The heatmaps in Fig. 3.15 A represent the significance of the interactions that occur in a 10kb window within the indicated genomic positions of the *RUNX3* (Fig. 3.15 A) and *CEBPA* (Fig. 3.15 B) loci. Differences among the three cell types are highlighted with blue arrows and black rectangles. Differences were also seen at the individual gene level. The UCSC genome browser screenshots depict the interactions between the *SPI1* promoter and its surrounding DHSs in PBSCs and *CEBPA*$^{N/C}$ and t(8;21) AMLs (Fig. 3.15 C). The figure clearly shows similar promoter-enhancer binding configuration as well as comparable chromatin accessibility patterns in both leukaemia samples, while some differences with CD34+ PBSCs can be seen (indicated by arrows). This observation is in concordance with the hypothesis that the biallelic *CEBPA* mutations and t(8;21) translocation give rise to a similar aberrant gene regulatory program.

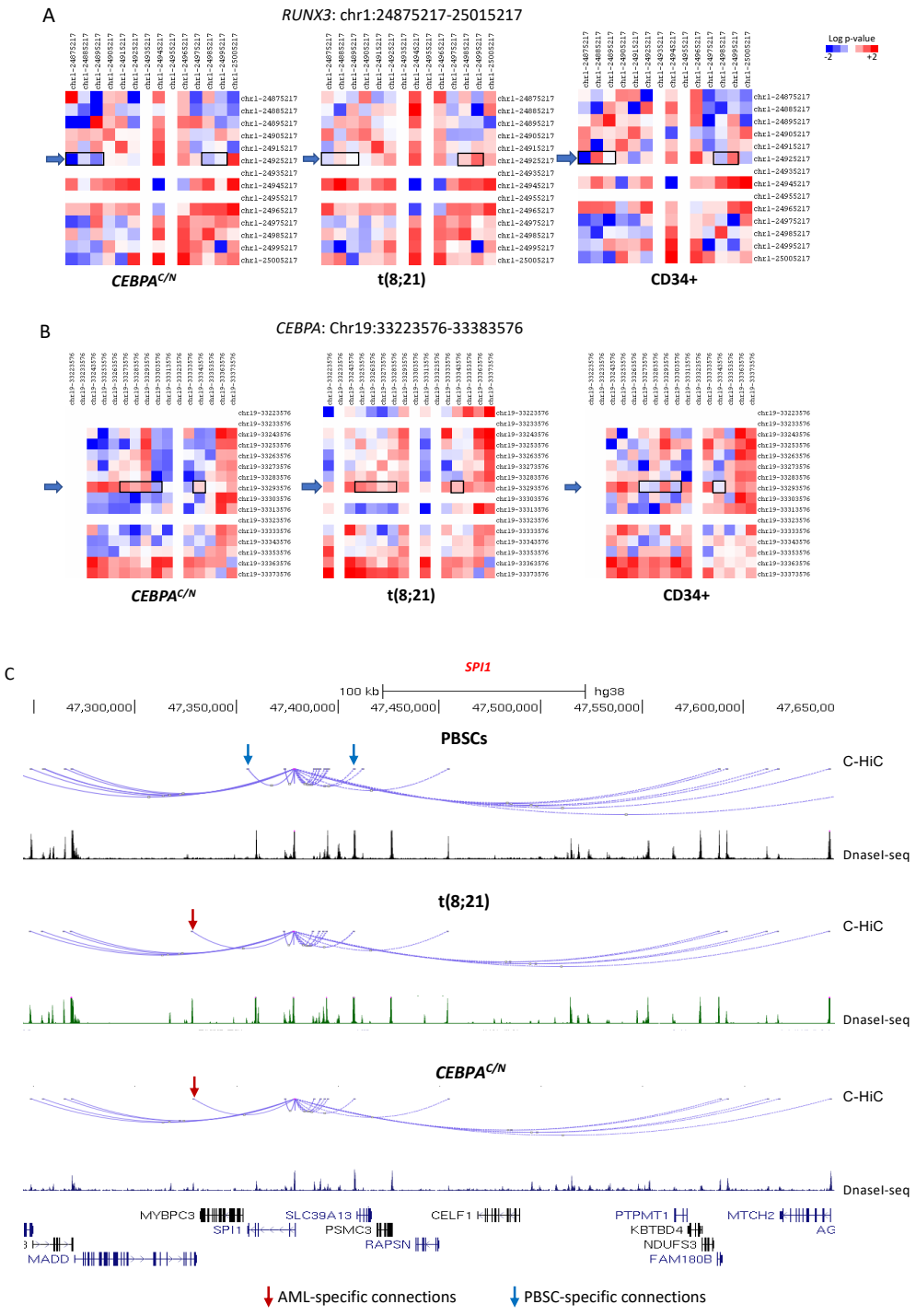

Figure 3.15: Capture Hi-C analysis of open chromatin regions in *CEBPA*$^{N/C}$ AML

(A-B) Contact matrixes at *RUNX3* (A) and *CEBPA* (B) indicated genomic positions for healthy blasts (left) and *CEBPA*$^{N/C}$ (middle) and t(8;21) (right) leukaemic blasts at 10kb resolution. The significance of the interactions is indicated by blue (less significant) and red (more significant) intensity colour. (C) UCSC genome browser screenshot depicting *SP1* promoter interaction with close cis-regulatory elements in healthy (upper), *CEBPA*$^{N/C}$ (middle) and t(8;21) (lower) blasts. A blue arrow indicates a PBSC-specific interaction, a red arrow indicates an AML-specific interaction. Figures generated by Dr Salam Assi, University of Birmingham.

3.8 Strategy to construct the *CEBPA*$^{N/C}$ AML-specific GRN

To construct the *CEBPA*$^{N/C}$-specific GRN, we integrated multiple types of genome-wide data from leukaemic and healthy blasts as previously described (Assi et al., 2019b) (Fig. 3.16). First, we defined the potential cis-regulatory elements deregulated in leukaemic blasts as compared to PBSCs. We then performed motif search within the AML-specific DHSs to infer candidate TFs that may bind these sites. To this end, we used a list of non-redundant motifs representing 80 TF families (Assi et al., 2019b). Using RNA-seq and Hi-C data, we linked each family of TFs identified to the promoter of the expressed genes that it regulates.

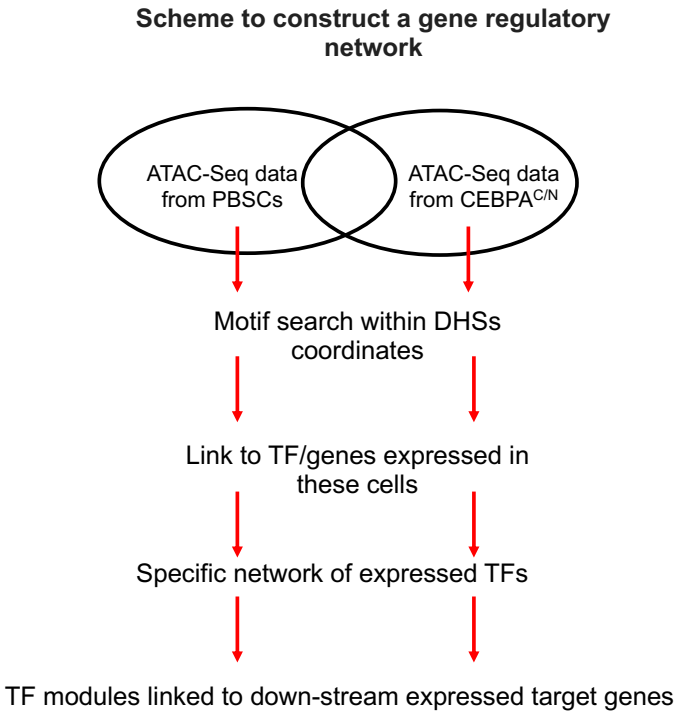

Figure 3.16: Construction of the *CEBPA*$^{N/C}$-specific GRN.

Strategy overview.

3.9 The AML subtype-specific gene regulatory network of *CEBPA$^{N/C}$* AML

The combination of motif occupancy, gene expression and promoter capture Hi-C data finally allowed us to construct the network of TF expressed in *CEBPA$^{N/C}$* AMLs (Fig. 3.17). In this network each node represents a TF coloured accordingly with its expression in *CEBPA$^{N/C}$* AMLs. TF families binding to the same motif form a composite node contained within a circle, arrows going outwards from a node to a specific gene indicate the presence of a binding motif in the locus encoding that gene. The analysis highlights nodes and edges which are specific for *CEBPA$^{N/C}$* AMLs and thus depicts how different TFs and their genes are "wired" within a network. The C/EBP and AP-1 families represents one of the major nodes of the network, with links coming in and going out and connected to 341 and 353 putative targets respectively (Supplementary table 3), suggesting a high regulatory relevance in the leukemic state maintenance. ETS, RUNX and E-box factors which are part of the haematopoietic signature (Wilson et al., 2010) are also highly connected. The RUNX family in particular was linked to 500 genes (Supplementary table 3). An interesting finding was that the TF POU4F1, a factor that was so far only known to be expressed in t(8;21) (Dunne et al., 2010), formed a node in the network. Another interesting finding was the prominence of connections emanating from the TGIF factor family, which was originally identified as a repressor of SMAD signalling (Wotton et al., 1999). In our network this family was associated to 800 putative effector targets (Supplementary table 3).

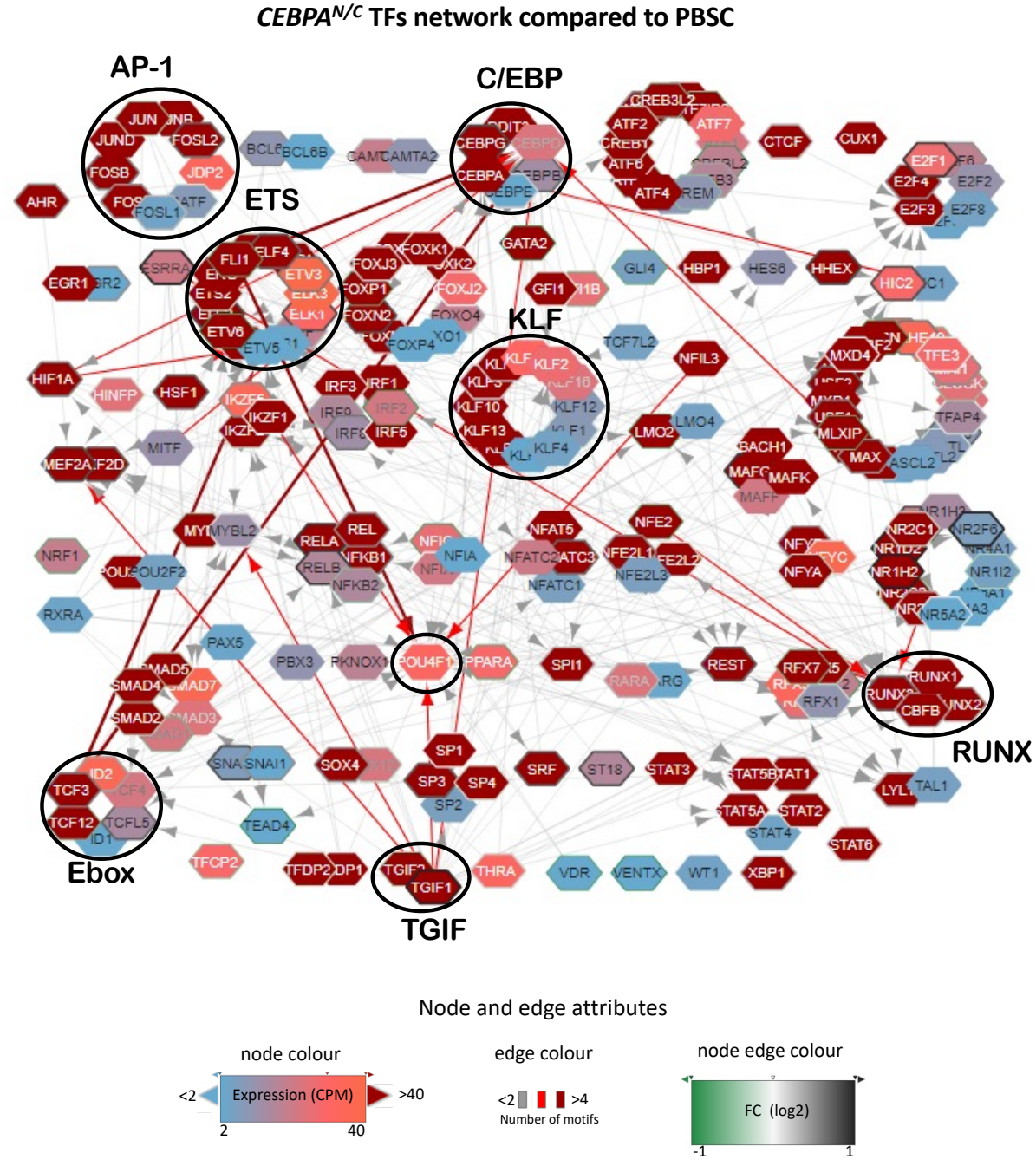

Figure 3.17: Network of TF encoding genes that are associated with sites specific for double mutant *CEBPA* AML compared to normal PBSC CD34+ cells.

TF targets determined by known motifs as determined in (Assi et al., 2019b). Arrows pointing outward from entire node highlight motifs in individual genes whereby the hypersensitive site was annotated to the gene using the C-HiC data where possible, or otherwise to the nearest gene. The expression level of the individual genes (CPM) in *CEBPA*$^{N/C}$ samples is depicted in blue (low) or red (high) colour. Edge colour is coloured accordingly with the number of motifs. Node edge colour indicates gene expression level in *CEBPA*$^{N/C}$ samples compared to PBSCs. The network was constructed by Dr Salam Assi, University of Birmingham.

3.10 C/EBPα ChIP in *CEBPA*$^{N/C}$ patient-derived blasts

Several studies based on different cell line and mouse models expressing just the C/EBPα-p30 isoform have shown that this isoform alters the respective gene expression programs (Schmidt et al., 2020). Previous work also demonstrated that a C-terminus mutated C/EBPα-p42 isoform is still able to associate with DNA (Gentle et al., 2021). However, to our knowledge, a genome-wide characterization of C/EBPα binding in *CEBPA*$^{N/C}$ patients is still missing. We thus decide to address this issue by performing ChIP-seq in patient-derived blast cells.

The C/EBPα antibody routinely used for ChIP assays in our lab, C/EBPα 14AA (sc-61, Santa Cruz), has been recently discontinued. In order to find a replacement, we tested two new antibodies, C/EBPα G-10 (sc-166258, Santa Cruz) and C/EBPα D-5 (sc-365318, Santa Cruz) in Kasumi-1 cells expressing an estrogen receptor (ER) inducible version of *CEBPA* (C/EBPα-ER) (Loke et al., 2018) after 48h of induction. We found that C/EBPα G-10 even outperformed C/EBPα 14AA when using the same experimental conditions (Fig. 3.18 A), proving to be the ideal candidate. The immunoprecipitation protocol using the C/EBPα G-10 antibody was further optimized in the SKNO-1 cell line (Fig. 3.18 B), which expresses endogenous C/EBPα at low levels, before performing the assay in *CEBPA*$^{N/C}$-8 patient purified blasts (Fig. 3.18 C) (See section 2.14 for details). C/EBPα ChIP experiments in *CEBPA*$^{N/C}$-4 and *CEBPA*$^{N/C}$-7 blasts were performed by using the C/EBPα 14AA antibody (See section 2.14 for details).

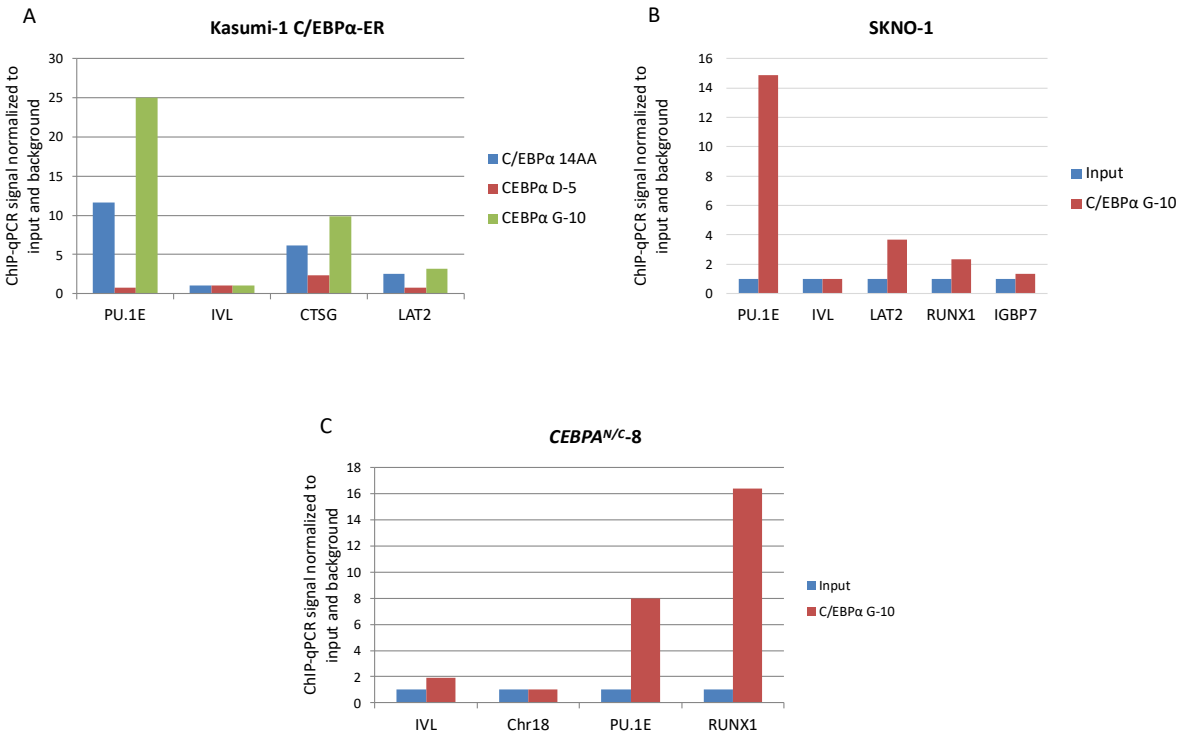

Figure 3.18: Optimization of the ChIP protocol using the C/EBPα G-10 antibody

ChIP-qPCR signal at known C/EBPα target genomic loci after chromatin immunoprecipitation with (A) the indicated C/EBPα antibodies in Kasumi-1 C/EBPα-ER cells and (B-C) the C/EBPα G-10 antibody in (B) SKNO-1 cells and (C) *CEBPA*$^{N/C}$-8 patient derived blasts. Experiment in (A) and (B) performed by Assunta Adamo, experiment in (C) performed by Dr Paulynn Chin, University of Birmingham.

ChIP data were ranked along-side the fold change between *CEBPA*$^{N/C}$ ATAC-Seq peaks and those of healthy PBSCs (Fig. 3.19 A). We found that the C/EBPα binding patterns were comparable in all samples assayed and mainly occurred in *CEBPA*$^{N/C}$ patient-specific chromatin accessible sites (Fig. 3.19 A, red plots). RUNX1 and C/EBPα often co-localise and cooperate to regulate myeloid-specific genes (Fujimoto et al., 2007; Petrovick et al., 1998). In addition, *RUNX1* is a direct target of C/EBPα (Ptasinska et al., 2014). We therefore measured RUNX1 as well and found again

similar binding patterns in all three patients closely resembling those of C/EBPα (Fig. 3.19 A, green plots).

De-novo motif analysis showed that the detected C/EBPα and RUNX1 ChIP peaks were enriched for C/EBP and RUNX motifs respectively in all patients, confirming the specificity of our immunoprecipitation experiments (Fig. 3.19 B, C and D). In addition, they again showed an enrichment for C/EBP:AP- 1 composite motifs only in *CEBPA*$^{N/C}$ patient samples, together with pure AP-1, ETS and RUNX1 motifs. RUNX1 binding sites were associated with RUNX, C/EBP, ETS and AP-1 motifs (Fig. 3.19 A blue plots, Fig. 3.19 B, C and D).

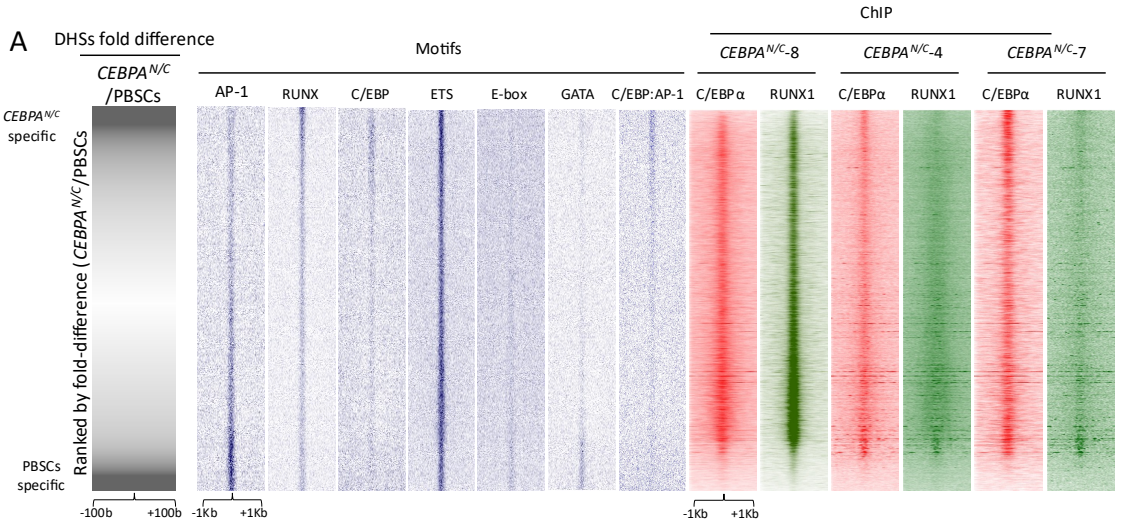

B

Motifs enriched in pat *CEBPA*$^{N/C}$-8 C/EBPα ChIP peaks (n = 1189)

Motif	match	% of targets	P-value
	C/EBP	47.74	1e-419
	PU.1	31.76	1e-63

Motifs enriched in pat *CEBPA*$^{N/C}$-8 RUNX1 ChIP peaks (n = 3386)

Motif	match	% of targets	P-value
	RUNX	44.23	1e-635
	ETS	56.24	1e-543
	AP-1	10.58	1e-125
	C/EBP	26.44	1e-110

C

Motifs enriched in pat *CEBPA*$^{N/C}$-4 C/EBP α ChIP peaks (n = 1768)

Motif	match	% of targets	P-value
	C/EBP	38.89	1e-182
	ETS	35.76	1e-133
	RUNX	27.02	1e-79
	AP-1	11.87	1e-30
	GATA	7.50	1e-28

Motifs enriched in pat *CEBPA*$^{N/C}$-4 RUNX1 ChIP peaks (n = 951)

Motif	match	% of targets	P-value
TGTGGTTT	RUNX	22.72	1e-68
CGGGAAGTG	ETS	30.99	1e-51

D

Motifs enriched in pat *CEBPA*$^{N/C}$-7 C/EBPα ChIP peaks (n = 152)

Motif	match	% of targets	P-value
TTGCAATA	C/EBP:AP-1	65.96	1e-31
AGGAAGTGGT	ETS:RUNX	45.74	1e-23
TTGCGTAA	C/EBP	58.51	1e-15

Motifs enriched in pat *CEBPA*$^{N/C}$-7 RUNX1 ChIP peaks (n = 130)

Motif	match	% of targets	P-value
CTGTGGTTTT	RUNX	28.00	1e-15

Figure 3.19: C/EBPα and RUNX1 binding patterns in *CEBPA*$^{N/C}$ patient samples

(A) Density plot of C/EBPα (red) and RUNX1 (green) ChIP peaks in CEBPAN/C patient samples across a 2kb window. Chip data and TF binding motifs (blue plots) are plotted alongside hypersensitive sites ranked by normalized tag count of merged CEBPAN/C peaks over merged PBSCs peaks (leftmost plot). RUNX1 ChIP in patient ID216 performed by Assunta Adamo; all the other ChIP experiments performed by Dr Paulynn Chin, University of Birmingham.

3.11 Validation of *CEBPA*$^{N/C}$ and t(8;21) cell line models

Patient derived blasts represent the most faithful model of *CEBPA*$^{N/C}$ AML and are a valuable source to extract biologically significant data. However working with primary cells is not always possible, due to scarcity of samples and technical limitations. To overcome this issue, we employed the *CEBPA*$^{N/C}$ cell line model KO52 (Broad, 2020; Heyes et al., 2021) and the well-established t(8;21) cell line model Kasumi-1 (Asou et al., 1991). To validate these cell line models, we performed ATAC-seq assays to map their open chromatin regions and compared them to the merged DHS dataset from patient cells (Fig. 3.20 A). We found that more than 70% of all KO52 and Kasumi-1 peaks overlapped with those from *CEBPA*$^{N/C}$ and t(8;21) patients respectively, demonstrating that the identity of the two leukaemic subtypes is largely preserved in these cell line models (Fig. 3.20 B and C).

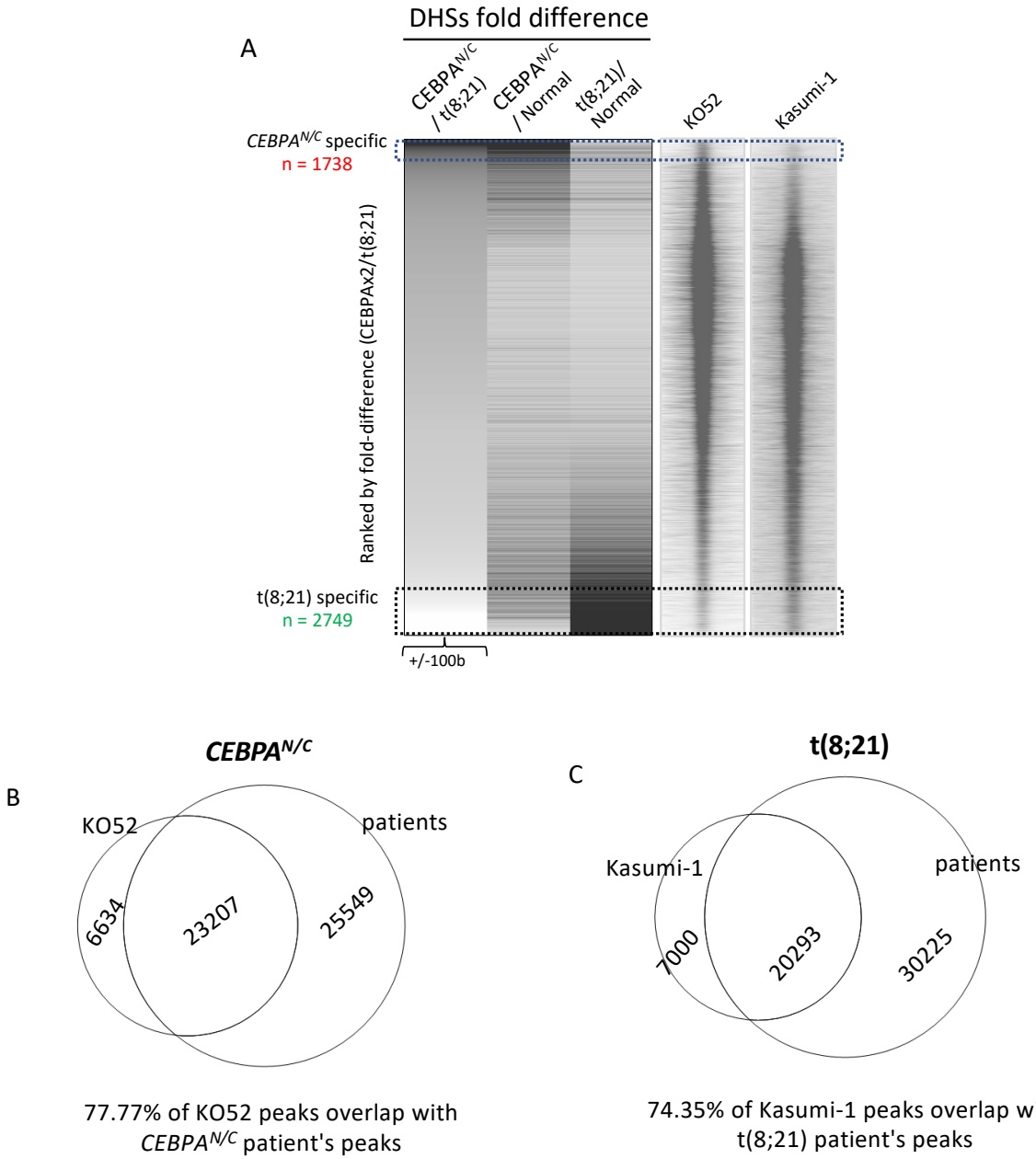

Figure 3.20: Validation of the KO52 *CEBPA*$^{N/C}$ cell line model

(A) Density plot of KO52 and Kasumi-1 hypersensitive sites across a 2kb window (rightmost plots). Data are showed alongside hypersensitive sites fold difference between *CEBPA*$^{N/C}$ and t(8;21), *CEBPA*$^{N/C}$ and PBSCs and t(8;21) and PBSCs samples respectively and ranked by normalized tag count of merged *CEBPA*$^{N/C}$ peaks over merged PBSCs peaks. (B-C) Venn diagram showing the number of hypersensitive sites shared between KO52 cell line and *CEBPA*$^{N/C}$ patient samples (B) and Kasumi-1 and t(8;21) AMLs (C). ATAC-seq in KO52 and Kasumi-1 performed by Assunta Adamo, figures generated by Dr Salam Assi, University of Birmingham.

To further validate and characterize our *CEBPA*$^{N/C}$ cell line model, we performed a ChIP-seq assay for C/EBPα, RUNX1 and c-FOS, one of the AP-1 family members represented in the *CEBPA*$^{N/C}$-specific GRN (Fig. 3.17). The binding pattern of C/EBPα and RUNX1 resembled that previously observed in patients (Fig. 3.21 A), with most peaks observed in both KO52 and primary samples (Fig. 3.21 B and C).

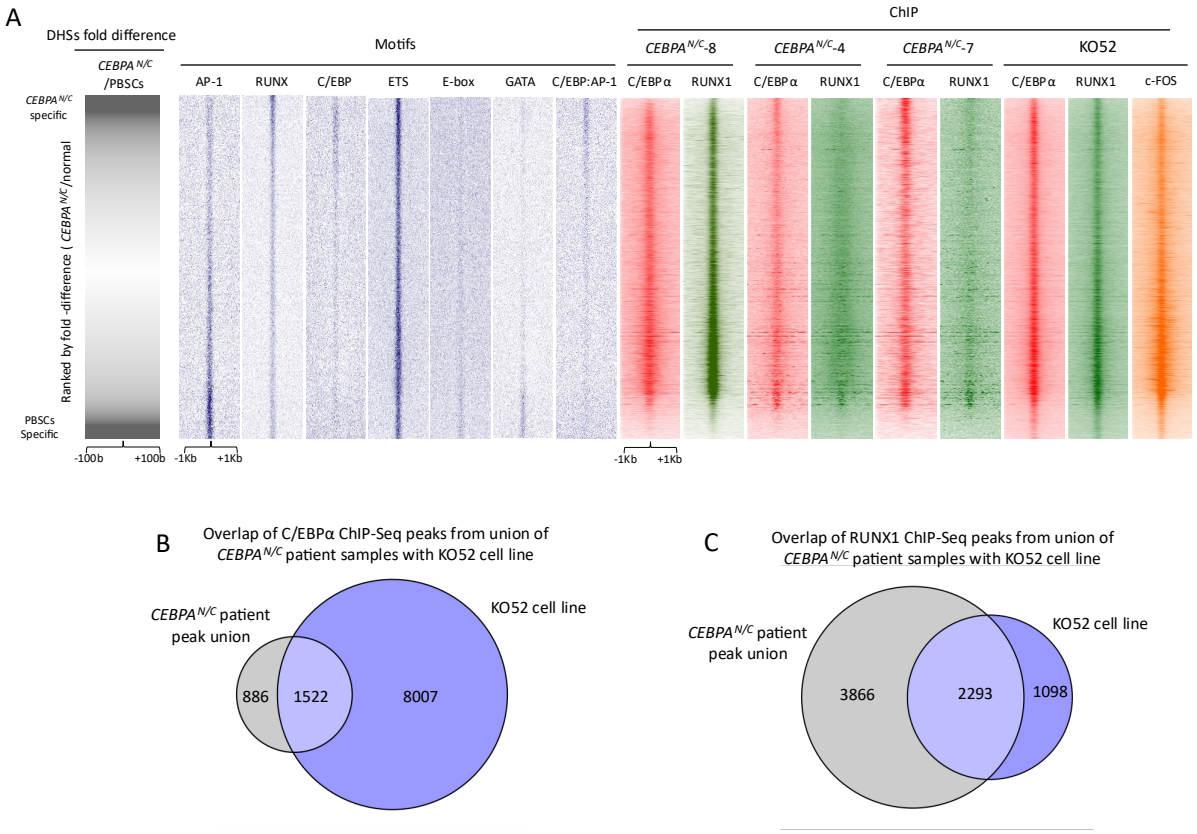

Figure 3.21: C/EBPα, RUNX1 and c-FOS binding profile in the KO52 cell line

(A) Density plot of C/EBPα (red), RUNX1 (green) and FOS (orange) ChIP peaks in *CEBPA*$^{N/C}$ and KO52 cell line across a 2kb window. ChIP data and TF binding motifs (blue plots) are plotted alongside hypersensitive sites ranked by normalized tag count of merged *CEBPA*$^{N/C}$ peaks over merged PBSCs peaks (leftmost plot). ChIP experiments in KO52 cell line were performed by Dr Paulynn Chin, University of Birmingham. (B-C) Venn diagrams showing the number of C/EBPα (C) and RUNX1 (C) ChIP peaks shared between KO52 cell line and *CEBPA*$^{N/C}$ patient samples. ChIP experiments in KO52 cell line were performed by Dr Paulynn Chin, University of Birmingham. Overlap analysis were performed by Dr Peter Keane, University of Birmingham.

Motif analysis showed an enrichment of ETS, RUNX, GATA and AP-1 motifs in the ChIP peaks of all the TFs assayed (FIG. 3.22 A-C). We found that around 50% of C/EBPα and AP-1 binding sites overlap. The overlap for RUNX1 sites was even larger, with the majority of RUNX1 peaks overlapping with either C/EBPα (30%) or AP-1 (50%) (FIG.3.22 D).

A

C/EBPα ChIP in KO52
Motifs enriched in distal peaks (n = 4380)

Motif	match	% of targets	P-value
	C/EBP	52.03	1e-869
	ETS	58.17	1e-571
	RUNX	38.39	1e-390
	AP-1	17.01	1e-111
	GATA	13.51	1e-47

B

RUNX1 ChIP in KO52
Motifs enriched in distal peaks (n = 2596)

Motif	match	% of targets	P-value
	RUNX	70.07	1e-773
	ETS	65.99	1e-390
	GATA	18.76	1e-79
	AP-1	8.65	1e-52

C

C-FOS ChIP in KO52
Motifs enriched in distal peaks (n = 4605)

Motif	match	% of targets	P-value
	ETS	61.49	1e-805
	RUNX	49.93	1e-532
	GATA	26.06	1e-176
	AP-1	9.87	1e-110

D

KO52 ChIP peaks overlap

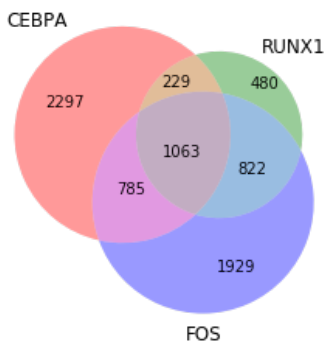

Figure 3.22: C/EBPα binds with a high frequency together with RUNX1 and AP-1

(A-C) Motifs enriched in C/EBPα (A), RUNX1 (B) and c-FOS (C) distal ChIP peaks in KO52 cell line. (G) Venn diagram showing the overlap of C/EBPα, RUNX1 and c-FOS ChIP peaks in KO52 cell line. Analyses performed by Assunta Adamo.

The C/EBP:AP-1 composite motif signature observed in *CEBPA*$^{N/C}$ AML specific open chromatin sites and the extensive overlap between C/EBPα and FOS ChIP peaks in KO52 cell line suggested that mutant C/EBPα and FOS may co-operate. To test this hypothesis, we measured the distribution of the distance between C/EBP and AP-1 motifs in open chromatin regions that are bound by both C/EBPα and FOS in KO52 cells. We found that C/EBP and AP-1 motifs tend to occur close together (Fig.3.23 A, left histogram) more frequently than expected by chance (Fig. 3.23 A, right histogram, and Fig. B). This is true also for C/EBP and RUNX motifs (Fig. 3.23 C and D) but not for AP-1 and RUNX motifs (Fig. 3.23 E and F). Interestingly, motif distribution in hypersensitive sites bound by both C/EBPα and c-FOS showed a multi-modal pattern that is not observed in sites not bound by both TFs, indicating that protein complexes may bind in a distinct spatial arrangement.

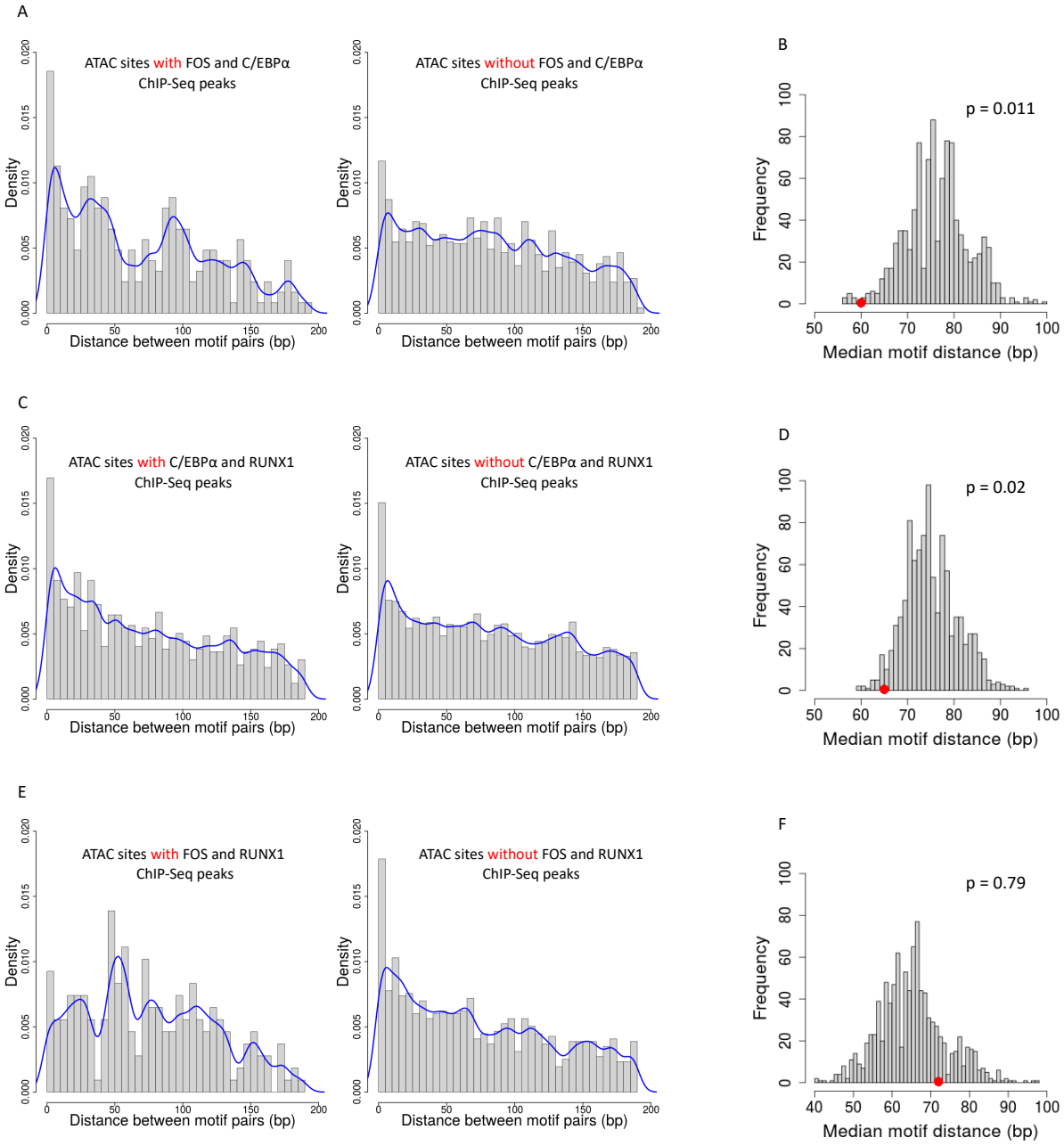

Figure 3.23: C/EBPα and c-FOS bound regions show a specific C/EBP and AP-1 motif spacing

(A, C, E) Histograms showing the distribution of the distances between (A) C/EBP and AP-1, (C) RUNX and AP-1 and (E) C/EBP and RUNX1 motifs in sites bound (left) or not bound (right) by C/EBPα and c-FOS, RUNX1 and c-FOS and C/EBPα and RUNX1 respectively in KO52 cell line. (B, D, F) Histograms showing the median distance between C/EBP and AP-1 motif pairs in 1000 random peak sets compared to median of peaks with C/EBPα and c-FOS signal. Analyses performed by Dr Peter Keane, University of Birmingham.

3.12 Creation of a merged ChIP-seq dataset

Our analyses showed that most of C/EBPα binding sites are shared among patient-derived blasts and KO52 cell line. We thus created a merged ChIP dataset encompassing all the C/EBPα and RUNX1 peaks identified in primary samples and cell line model, identifying 7982 and 5723 target genes respectively. To gain an insight in biological processes that are directly affected by C/EBPα mutant proteins, we performed a KEGG pathway enrichment analysis of C/EBPα targets. “Acute myeloid leukaemia” and “Pathways in cancer” appeared among the most enriched pathways together with “NOD-like receptor signalling pathway”, which deregulation has been linked to hematopoietic malignancies (Buteyn et al., 2020; Sallman and List, 2019) (Fig.3.24 A). We then combined ChIP-seq and RNA-seq data to identify C/EBPα targets that were deregulated in *CEBPA*$^{N/C}$ AMLs compared to healthy blasts. Upregulated targets (n = 170) were linked to the “Ribosome” pathway, which we previously found specifically enriched in *CEBPA*$^{N/C}$ AMLs (Fig.3.9 A), and “RNA transport” and “RNA degradation”, suggesting that aberrant regulation of RNA turnover may be an oncogenic mechanism in these patients (Fig. 3.24 B). Also “Protein processing in endoplasmic reticulum” and “Proteasome” figured among the upregulated pathways (Fig. 3.24 B). Our analysis also showed that some of the genes most overexpressed in leukemic blasts, such as MAP3K8, PIWIL4 and DUSP10 (Fig. 3.7 and table 17), were C/EBPα targets. KEGG pathway analysis of downregulated C/EBPα targets (n = 461) showed enrichment in “Pathways in cancer” and “Gap junction” pathways (Fig. 3.24 C). The lysine methyltransferase KMT2A and SETD7, which play an essential role in gene expression regulation during hematopoiesis

(Nakamura et al., 2002), figured among the downregulated target genes (Fig. 3.24 C).

Of note, RUNX1 appeared among the downregulated C/EBPα targets (Fig. 3.24 C).

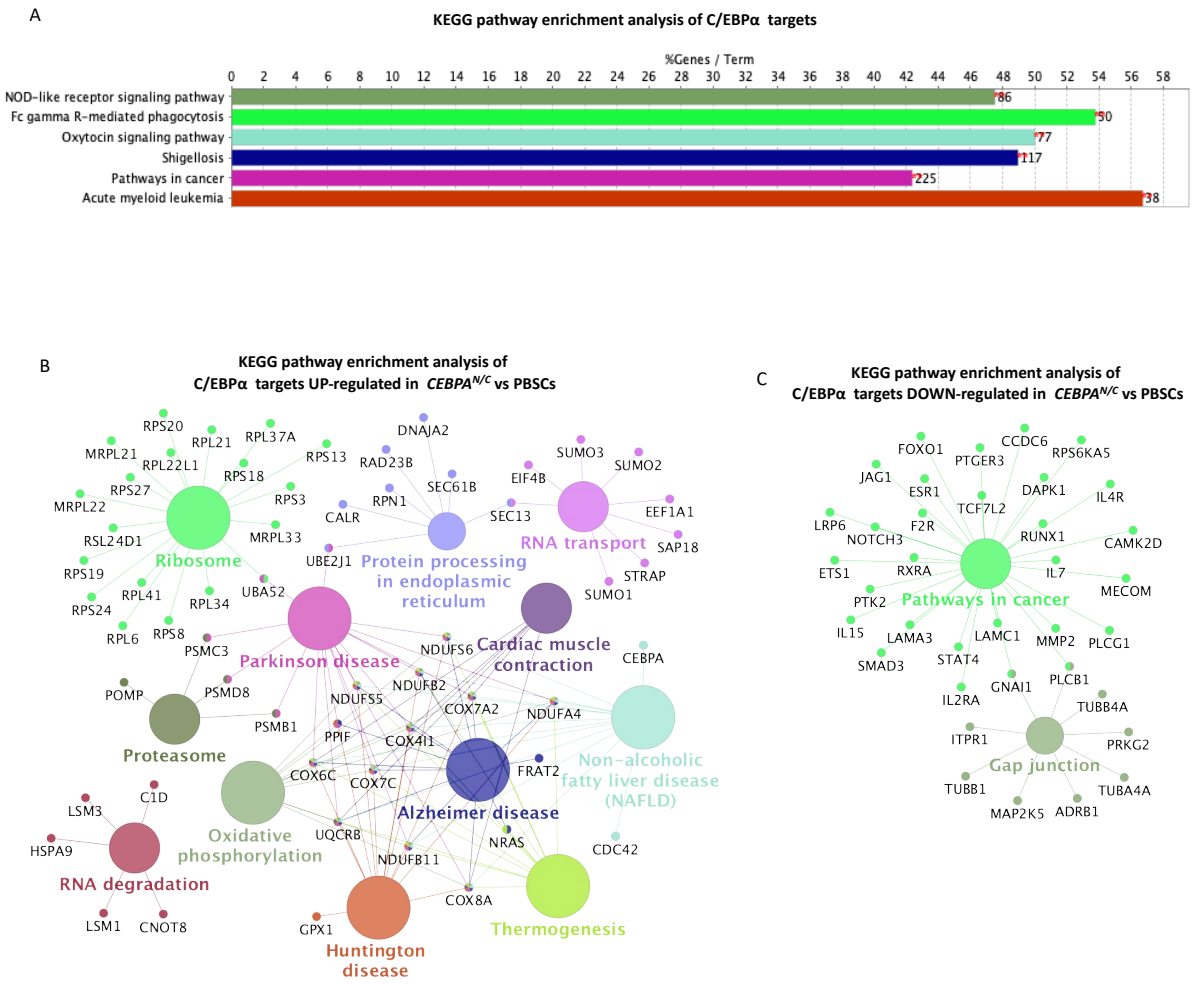

Figure 3.24: KEGG pathway analyses of C/EBPα targets

KEGG pathway enrichment analyses of (A) all C/EBPα targets and C/EBPα targets (B) upregulated and (C) downregulated in *CEBPA*$^{N/C}$ AMLs compared to PBSCs. Analyses performed by Assunta Adamo.

3.13 Integration of ChIP data and GRN modules

Our GRN construction strategy relies on the identification of TF binding motifs within promoters and cis-regulatory elements to infer TF binding. To validate this approach, we compared C/EBP, RUNX and AP-1 targets identified in the *CEBPA*$^{N/C}$-specific GRNs with C/EBPα, RUNX1 and c-FOS ChIP data respectively. Almost 50% of AP-1 family targets identified in our GRNs were bound by c-FOS in KO52 cell lines (Fig. 3.25, left pie chart). The percentage was even higher for the RUNX and C/EBP modules, where the overlap was over 60% for the RUNX1 (Fig. 3.25, right pie chart) and over 80% for the C/EBP targets (Fig. 3.25, middle pie chart) defined from the merged KO52 and *CEBPA*$^{N/C}$ ChIP peak dataset. Of note, a DNA binding motif is recognized by multiple members of a TF family, and in our ChIP experiments only one TF belonging to each family was assayed. Taken together these results demonstrated the reliability of our GRN construction strategy.

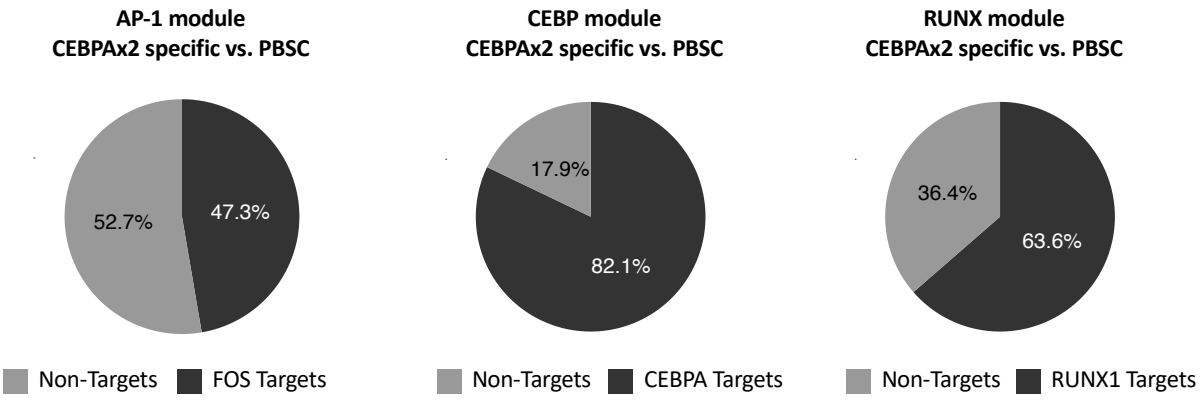

Figure 3.25: Integration of AP-1, C/EBP and RUNX network modules with ChIP-Seq data for c-FOS, C/EBPα and RUNX1

The pie charts show the overlap between targets genes identified in the AP-1, C/EBP and RUNX network modules and target genes identified by ChIP-seq. c-FOS target genes (left pie chart) were defined based on c-FOS ChIP data in KO52 only. C/EBPα (middle pie chart) and RUNX1 targets (right pie chart) were defined based on merged C/EBPα and RUNX1 ChIP-seq data from KO52 and *CEBPA*$^{N/C}$ patient-derived blasts. Analyses performed by Dr Peter Keane, University of Birmingham.

3.14 Gene regulatory network perturbation

Our analysis showed that C/EBP and AP-1 families constitute prominent nodes of both the *CEBPA*$^{N/C}$-specific and the *CEBPA*$^{N/C}$-t(8;21) shared GRNs. We next wanted to investigate the mechanisms through which these TFs sustain the aberrant leukaemic program. To this end, we exploited a dominant negative C/EBP peptide (dnC/EBP) (Olive et al., 1996) and a dominant negative FOS peptide (dnFOS) (Olive et al., 1997). These peptides heterodimerize with multiple members of the C/EBP and JUN families respectively and abolish their binding to the DNA (Fig. 3.26 A). In fig. 3.26 B the nucleotide and amino acid sequences of dnC/EBP are showed. The dominant negatives or a control were subcloned in a doxycycline-inducible lentiviral vector upstream an IRES-GFP (for details see section 2.5 and (Martinez-Soria et al., 2018)).

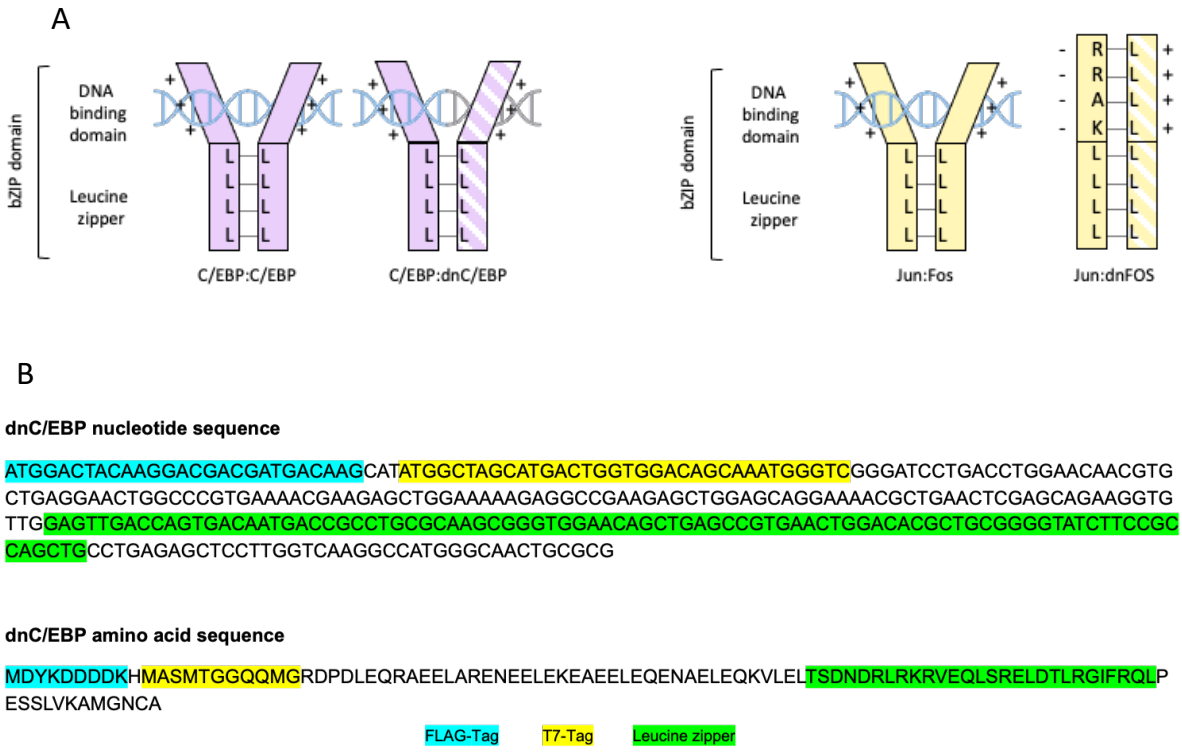

Figure 3.26: Structure of dominant negative versions of AP-1 and C/EBP

(A) Representation of dnC/EBP and dnFOS mechanism of action. Both peptides heterodimerize with C/EBP and AP-1 family members respectively, interfering with their DNA binding ability. (B) Nucleotide and amino acid sequence of dnC/EBP. FLAG and T7 tags and the leucin zipper domain are highlighted.

The constructs were transduced in KO52 and Kasumi-1, a *CEBPA*$^{N/C}$ and t(8;21) cell line model respectively (Fig. 3.27 A). To obtain homogeneous clonal populations, we set up multiple single-cell cultures for each cell line and construct and applied Puromycin selection to enrich for stably integrated transgenes. Unfortunately, we failed to expand any of the isolated KO52 clones. Therefore, the following experiments were conducted in GFP+ cells isolated from the bulk population. The efficiency of the induction was assessed by real time-qPCR (Fig. 3.27 B and D) and western blot (Fig. 3.27 C).

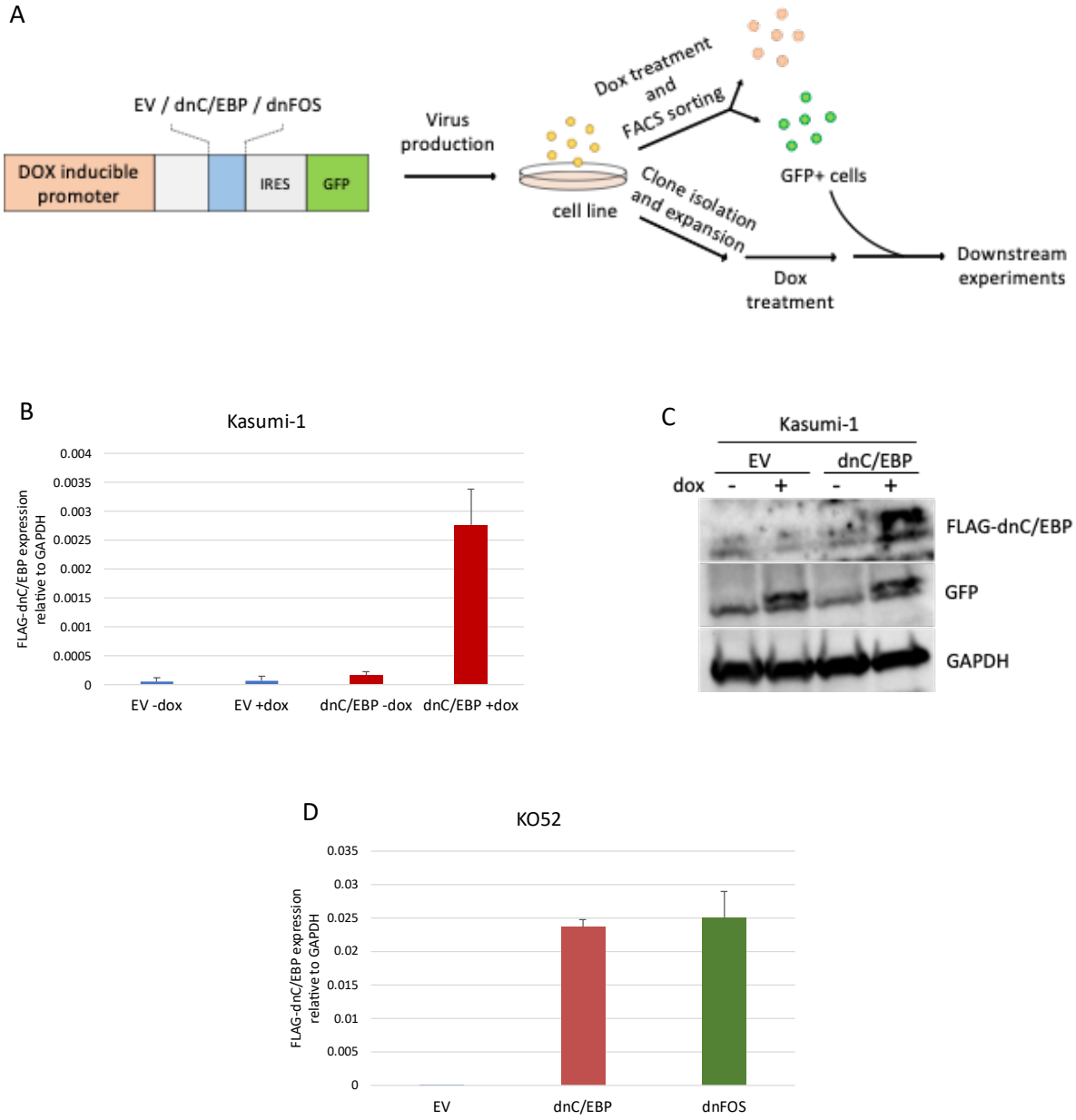

Figure 3.27: Inducible expression of dnC/EBP and dnFOS in Kasumi-1 and KO52 cell lines. (A) Perturbation experiment overview. (B-C) dnC/EBP mRNA and (C) protein expression assessed by RT-qPCR and western blot in Kasumi-1 after 48h of doxycycline induction. (D) dnC/EBP and dnFOS mRNA expression in KO52 GFP+ FACS sorted cells after 48h of doxycycline induction. Experiments performed by Assunta Adamo.

After 48h of doxycycline treatment and FACS sorting for GFP positive cells, we performed ATAC-seq and RNA-seq with KO52 cells expressing either a control vector or the dominant negative peptides. The expression of dnC/EBP had a very mild impact on chromatin accessibility, as only 87 and 60 open chromatin regions were gained and lost upon interference with C/EBPs binding, respectively (FC > |2|, Benjamini-Hochberg adjusted p-value < 0.05) (Fig. 3.28 A and B). The new open chromatin sites were enriched in AP-1, RUNX-1 and GATA motifs (Fig.3.28 C) whereas lost sites were enriched in PU.1 and C/EBP motifs (Fig. 3.28 D), suggesting that CEBP binding was lost. Enrichment of GATA and loss of PU.1 motifs suggest that KO52 cells became more immature upon induction of dnC/EBP. In addition, minimal changes in gene expression were observed (Fig. 3.29).

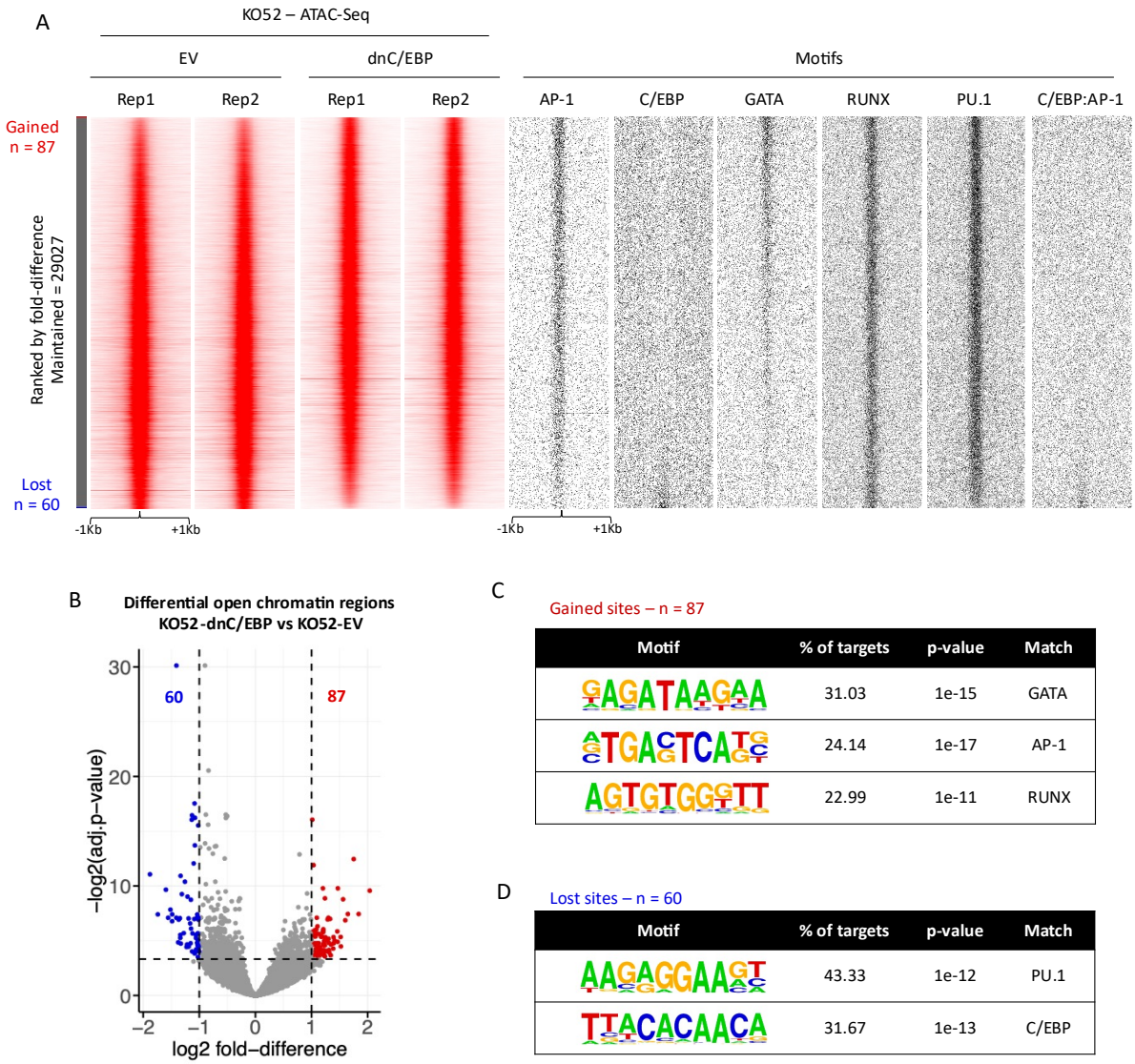

Figure 3.28: dnC/EBP expression leads to a loss of open chromatin regions with C/EBP motifs in KO52 cells

(A) Density plots showing the ATAC-seq profile of KO52 cells expressing dnC/EBP or a control vector across a 2kb window. Data are ranked by normalized tag counts of dnC/EBP expressing cells over control. TF binding motifs projected against hypersensitive sites are plotted alongside. (B) Volcano plot of hypersensitive sites deregulated in KO52 cells expressing dnC/EBP compared to control. Blue dots represent significantly downregulated genes (log2 fold-change < -1, Benjamini-Hochberg adjusted p-value < 0.05); red dots represent significantly upregulated genes (log2 fold-change > 1, Benjamini-Hochberg adjusted p-value < 0.05). (C-D) Motif enriched in dnC/EBP-specific (C) and control-specific (D) hypersensitive sites. (E) Volcano plot of genes deregulated in KO52 cells expressing dnC/EBP compared to control. Blue dots represent significantly downregulated genes (log2 fold-change < -1, Benjamini-Hochberg adjusted p-value < 0.05); red dots represent significantly upregulated genes (log2 fold-change > 1, Benjamini-Hochberg adjusted p-value < 0.05). ATAC-seq and analyses performed by Assunta Adamo.

Figure 3.29: dnC/EBP expression has little impact on gene expression in KO52 cells

Volcano plot of genes deregulated in KO52 cells expressing dnC/EBP compared to control. Blue dots represent significantly downregulated genes (log2 fold-change < -1, Benjamini-Hochberg adjusted p-value < 0.05); red dots represent significantly upregulated genes (log2 fold-change > 1, Benjamini-Hochberg adjusted p-value < 0.05). RNA-seq and analyses performed by Assunta Adamo.

The induction of dnFOS resulted in gain of 191 open chromatin sites (FC > 2, Benjamini-Hochberg adjusted p-value < 0.05) (Fig. 3.30 A and B), which were enriched in PU.1 and ETS motifs (Fig. 3.30 A and C), and loss of 857 sites (FC < -2, Benjamini-Hochberg adjusted p-value < 0.05). We observed a significant enrichment of RUNX, GATA and AP-1 motifs in lost sites, again suggesting that closing of chromatin was a consequence of loss of AP-1 binding (Fig. 3.30 A and D).

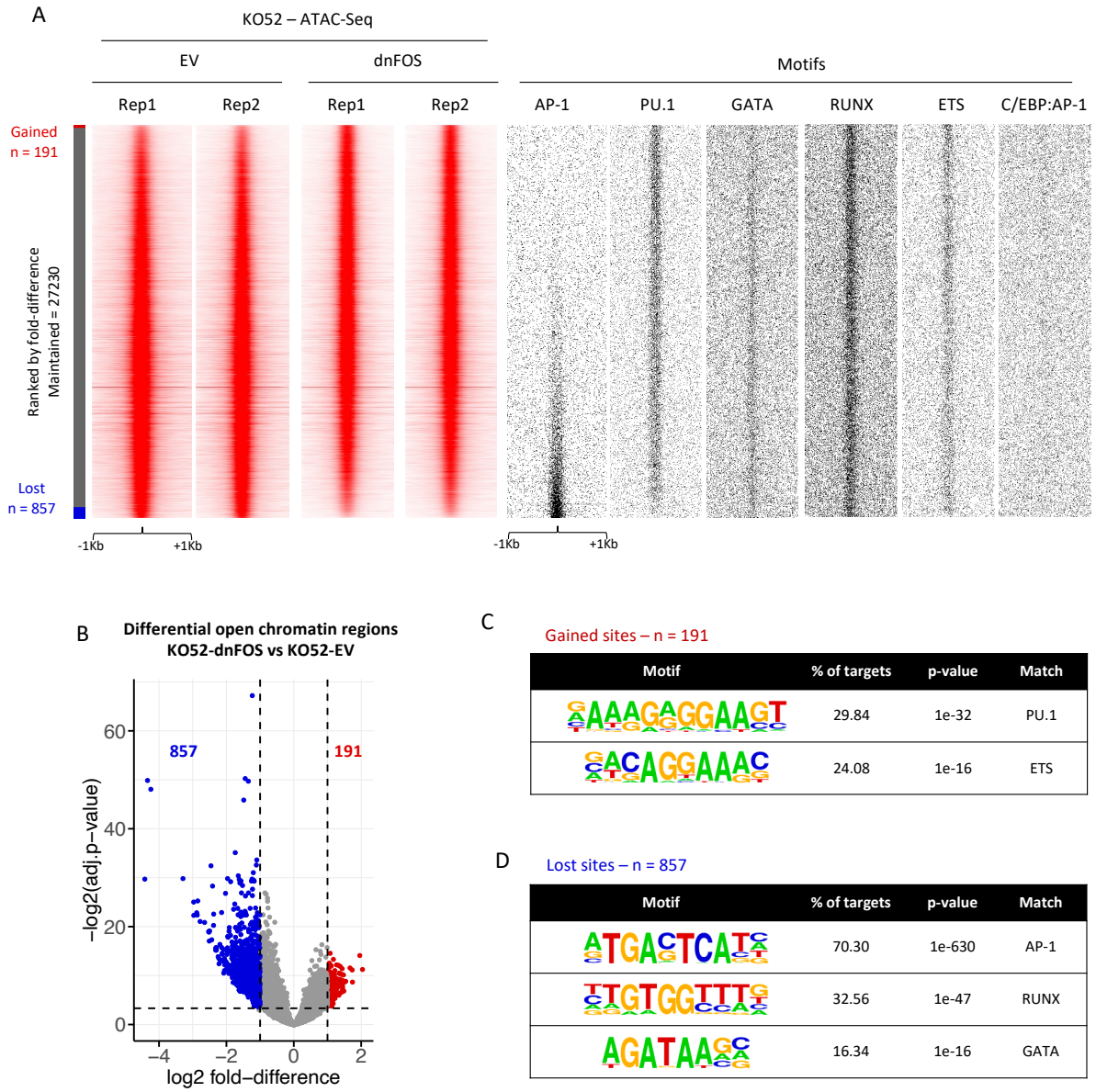

Figure 3.30: Expression of dnFOS has a strong effect on the chromatin landscape in KO52 cells and leads to a loss of open chromatin regions with AP-1 motifs

(A) Density plots showing the ATAC-seq profile of KO52 cells expressing dnFOS or a control vector across a 2kb window. Data are ranked by normalized tag counts of dnFOS expressing cells over control. TF binding motifs projected against hypersensitive sites are plotted alongside. (B) Volcano plot of hypersensitive sites deregulated in KO52 cells expressing dnFOS compared to control. Blue dots represent significantly downregulated genes (log2 fold-change < -1, Benjamini-Hochberg adjusted p-value < 0.05); red dots represent significantly upregulated genes (log2 fold-change > 1, Benjamini-Hochberg adjusted p-value < 0.05). (C-D) Motif enriched in dnFOS-specific (C) and control-specific (D) hypersensitive sites. ATAC-seq and analyses performed by Assunta Adamo.

We next performed a gene expression analysis of dnFOS expressing cells, demonstrating the deregulation of 288 genes, with most genes (180) being down-regulated (Fig. 3.31 A). KEGG pathway analysis showed that a large number of downregulated genes encodes for cell signalling component such as SRC and multiple chemokines (Fig. 3.31 B).

Note that *CEBPE* appeared among the significantly downregulated genes upon dnFOS expression (Fig. 3.31 B). Interestingly, our ChIP data showed that both C/EBPα and FOS bound a *CEBPE* enhancer, suggesting that these TFs control C/EBPε expression (Fig. 3.31 C).

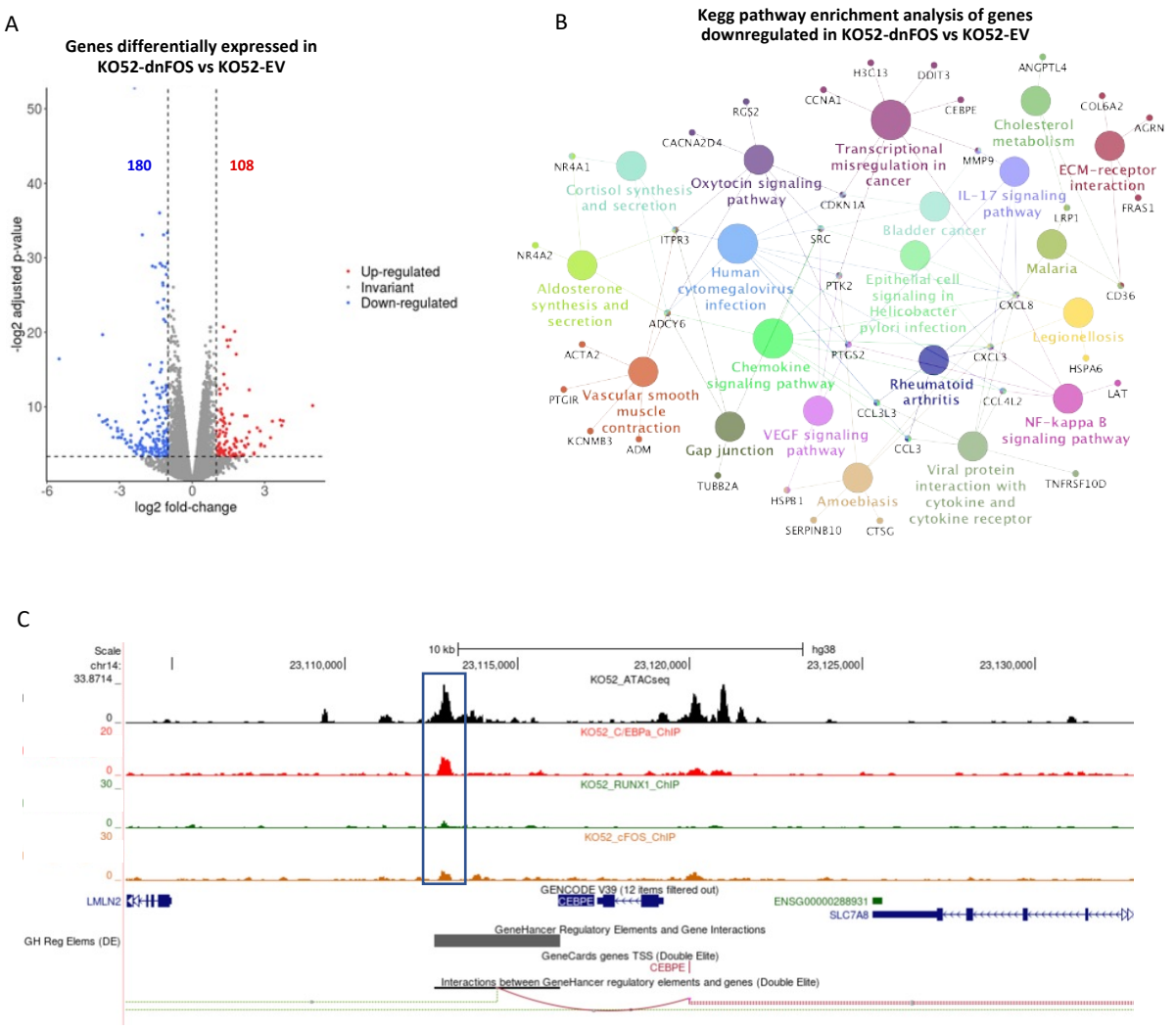

Figure 3.31: Expression of dnFOS has a strong effect on gene expression landscape in KO52 cells

(A) Volcano plot of genes deregulated in KO52 cells expressing dnFOS compared to control. Blue dots represent significantly downregulated genes (log2 fold-change < -1, Benjamini-Hochberg adjusted p-value < 0.05); red dots represent significantly upregulated genes (log2 fold-change > 1, Benjamini-Hochberg adjusted p-value < 0.05). (B) KEGG pathway enrichment analysis of genes downregulated in KO52 cells expressing dnFOS compared to control. (C) UCSC genome browser screenshot depicting the *CEBPE* gene locus with nearby cis-regulatory elements and the genome track of hypersensitive site (black) and C/EBPα (red), RUNX1 (green) and c-FOS (ochre) ChIP peaks. A *CEBPE* enhancer bound by all three TFs is highlighted. RNA-seq and analyses performed by Assunta Adamo.

The expression of dnC/EBP in Kasumi-1 resulted in the gain of 706 open chromatin sites and loss of 805 ones (Fig. 3.32 A). PU.1, CTCF and RUNX motifs were enriched within both gained and lost sites, indicating that these TFs may rearrange their binding position and establish a new chromatin landscape (Fig. 3.32 A and B). The enrichment of AP-1, C/EBP and the composite C/EBP:AP-1 motifs within the lost sites suggested that C/EBP binding in our t(8;21) model is, at least in part, dependent on the AP-1 family members activity (Fig. 3.32 A and C). The experiment also validated the integrity of the expression construct.

A

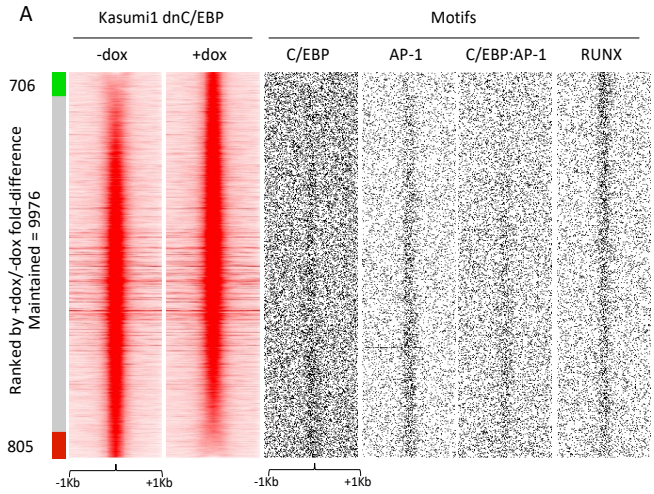

B

Motifs enriched in DHSs gained upon dnC/EBP expression

Logo	% of targets	p-value	Match
	24.32%	1e-65	PU.1
	8.71%	1e-33	CTCF
	20.15%	1e-32	RUNX

C

Motifs enriched in DHSs lost upon dnC/EBP expression

Logo	% of targets	p-value	Match
	26.86%	1e-46	PU.1
	7.28%	1e-28	CTCF
	13.92%	1e-18	RUNX
	12.46%	1e-14	AP-1
	21.04%	1e-13	C/EBP

Figure 3.32: dnC/EBP expression leads to a loss of open chromatin regions with C/EBP motifs in t(8;21) cells

(A) Density plots showing the DNase I-seq profile of Kasumi-1 cells expressing dnC/EBP or a control vector across a 2kb window. Data are ranked by normalized tag counts of dnC/EBP expressing cells over control. TF binding motifs projected against hypersensitive sites are plotted alongside. (B-C) Motif enriched in dnC/EBP-specific (B) and control-specific (C) hypersensitive sites. DNase I-seq and analyses performed by Assunta Adamo.

3.15 C/EBP and AP-1 transcription factors regulates cell growth

To test whether C/EBPs and AP-1 family members are required for leukemic cell growth, we performed proliferation assays with KO52 and Kasumi-1 expressing our dominant negative constructs. We found that both dnC/EBP and dnFOS expression decreased cell growth in our *CEBPA*$^{N/C}$ and t(8;21) cell line models (Fig. 3.33 A-C and (Assi et al., 2019b)). Taken together, these data show that both AP-1 and C/EBP are essential parts of the gene regulatory networks regulating the growth of *CEBPA*$^{N/C}$ and t(8;21) cells.

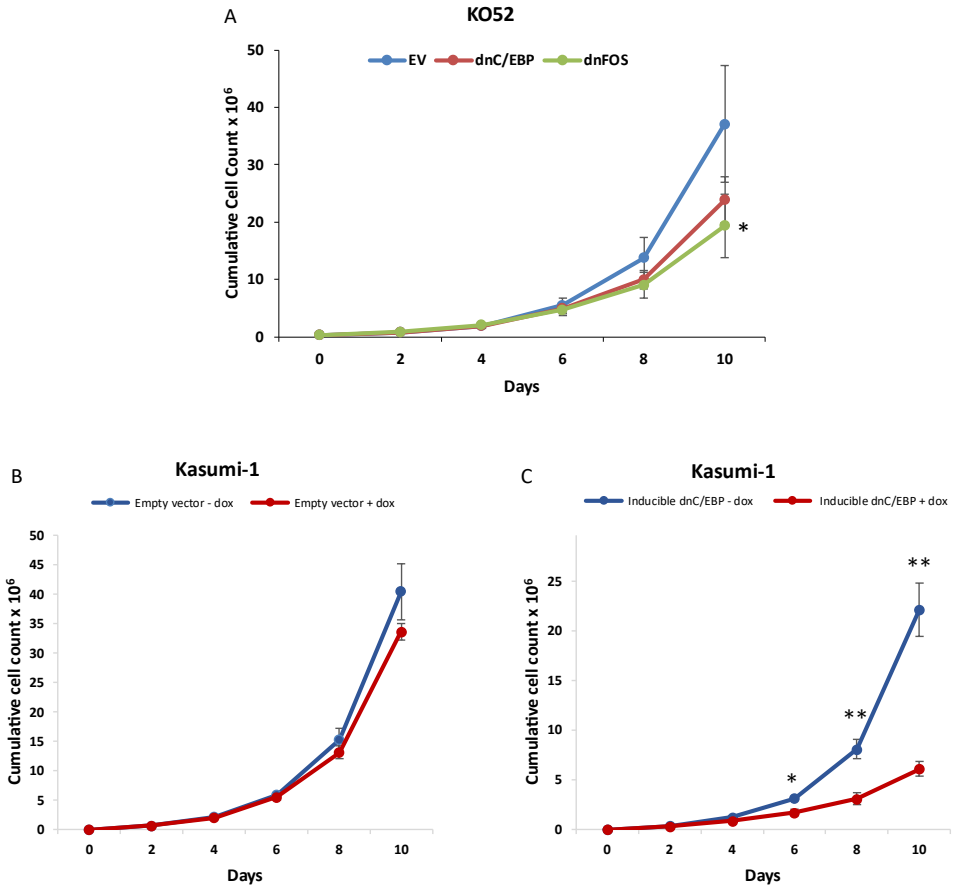

Figure 3.33: C/EBP family members are important for the growth of KO52 cells

(A-C) Cumulative cell growth time course. (A) KO52 GFP+ cells expressing either a control vector (blue), dnC/EBP (red) or dnFOS (green). KO52 were treated with doxycycline for 48h before GFP+ cells FACS sorting and experiment setup. (B) Kasumi-1 cells expressing an inducible control vector with (blue) or without (red) doxycycline. (C) Kasumi-1 cells expressing an inducible dnC/EBP with (blue) or without (red) doxycycline. Experiment performed by Adamo Assunta.

3.16 LSCs and blasts derived from a *CEBPA$^{N/C}$* patient show a different motif signature

Despite *CEBPA$^{N/C}$* AMLs have a favourable prognosis, relapse occurs in around 40% of patients (Pastore et al., 2014). Leukaemia regeneration is due to the presence of a rare subpopulation of LSCs among the leukaemic blasts, which survive chemotherapy and persist after remission (Ishikawa et al., 2007). Thus eradication of these cells to achieve long-term remission and cure therefore represents an important clinical need. To identify potential LSC-specific vulnerabilities, we used multi-omics approaches to characterize LSCs (CD34+ CD90- CD38-) and leukaemic blasts (CD34+ CD90- CD38+) purified from a *CEBPA$^{N/C}$* sample (Fig. 3.34 A). ATAC-seq analysis showed large differences in the accessible chromatin landscape between the two populations, with 3263 open chromatin sites enriched in LSCs and 5761 enriched in blasts (Fig. 3.34 B). Motif analysis showed enrichment of C/EBP motifs in blast-specific sites while GATA motifs were more represented in LSC-specific sites, in accordance with their stage of differentiation (Fig. 3.34 C and D). The RUNX signature was stronger in LSCs when compared to blasts (Fig. 3.34 C and D), consistent with the observation that RUNX factors are critical for the maintenance of both healthy and leukaemic stem cells (Staber et al., 2014; Wesely et al., 2020). The composite C/EBP:AP-1 motif was specifically enriched in the blast-specific hypersensitive sites (Fig. 3.34 B).

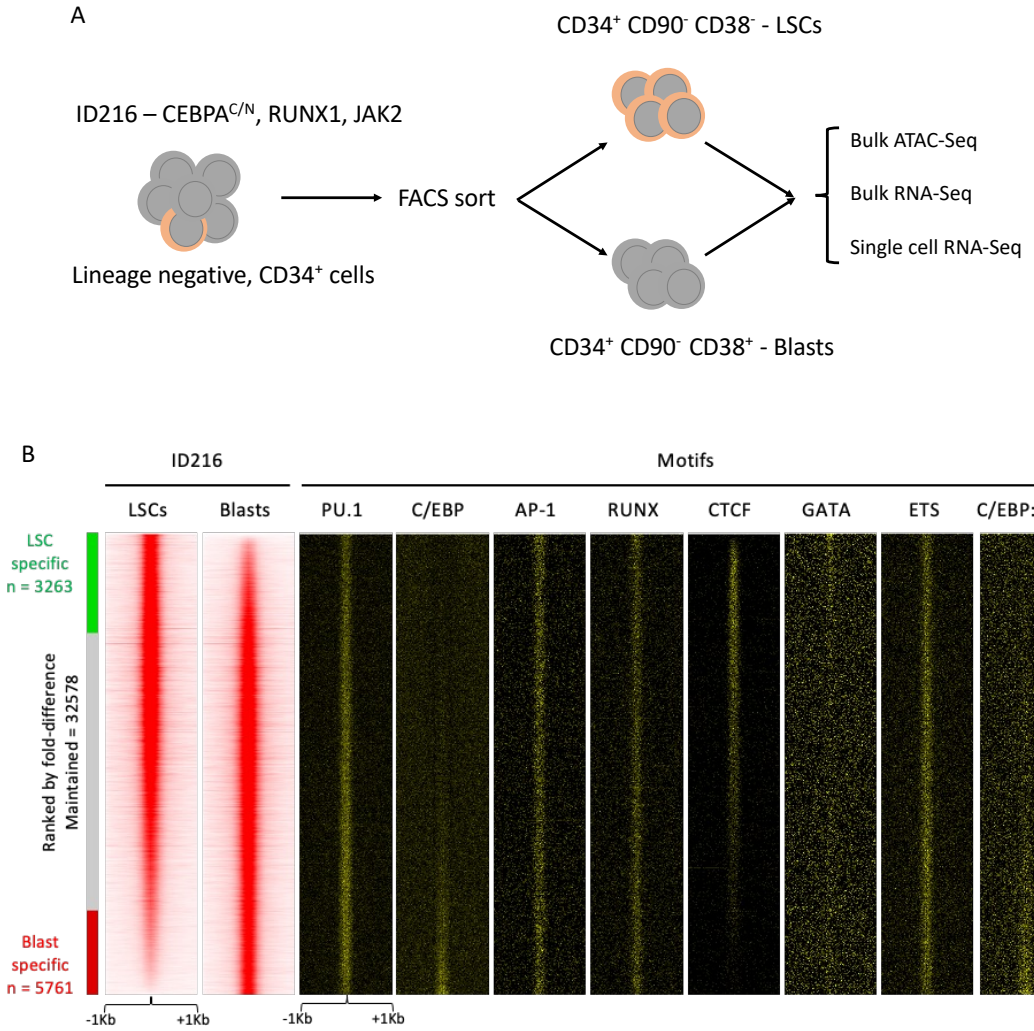

C

Motifs enriched in LSC specific DHSs

Motif	% of targets	p-value	Match
	15.98	1e-349	CTCF
	34.98	1e-200	PU.1
	40.91	1e-111	RUNX
	13.53	1e-97	AP-1

D

Motifs enriched in blast specific DHSs

Motif	% of targets	p-value	Match
	40.96	1e-570	PU.1
	35.25	1e-393	C/EBP
	11.55	1e-132	AP-1
	12.81	1e-121	RUNX

Figure 3.34: Leukaemic stem and blast cells from a *CEBPA*$^{N/C}$ patient show different open chromatin patterns

(A) LSCs/blast purification and experimental overview. Sorting was performed by Dr Sandeep Potluri, University of Birmingham (B) Density plot showing the ATAC-seq peak profile of LSCs and blast cells purified from a *CEBPA*$^{N/C}$ patient sample across a 2kb window (red plots). Data are ranked by normalized tag count of LSCs peaks over blast. TF binding motifs projected against hypersensitive sites are plotted alongside. (C-D) Motifs enriched in LSC-specific (C) and blast-specific (D) hypersensitive sites. ATAC-seq performed by Dr Sandeep Potluri, analyses performed by Assunta Adamo.

3.17 scRNA-seq highlights the heterogeneity of LSC and blast populations

AML is a highly complex and heterogeneous disease. Bulk ATAC-seq analysis highlighted differences in the LSCs and blasts motif signatures; however they do not take into account that each of these populations is made up of cells with a continuum of mixed differentiation stages. To investigate this, we performed scRNA-seq of purified LSC and blast populations from the same *CEBPA*$^{N/C}$ patient sample. Clustering analysis found that these cells could be separated into 8 distinct populations accordingly to their gene expression pattern (Fig. 3.35 A-C). To determine which of these could be classified as either LSC or blast, we compared the cluster marker genes from each cluster to an LSC/blast gene expression signature derived from bulk-RNA-seq data using Gene Set Enrichment Analysis (GSEA) (Fig. 3.35 B and C).

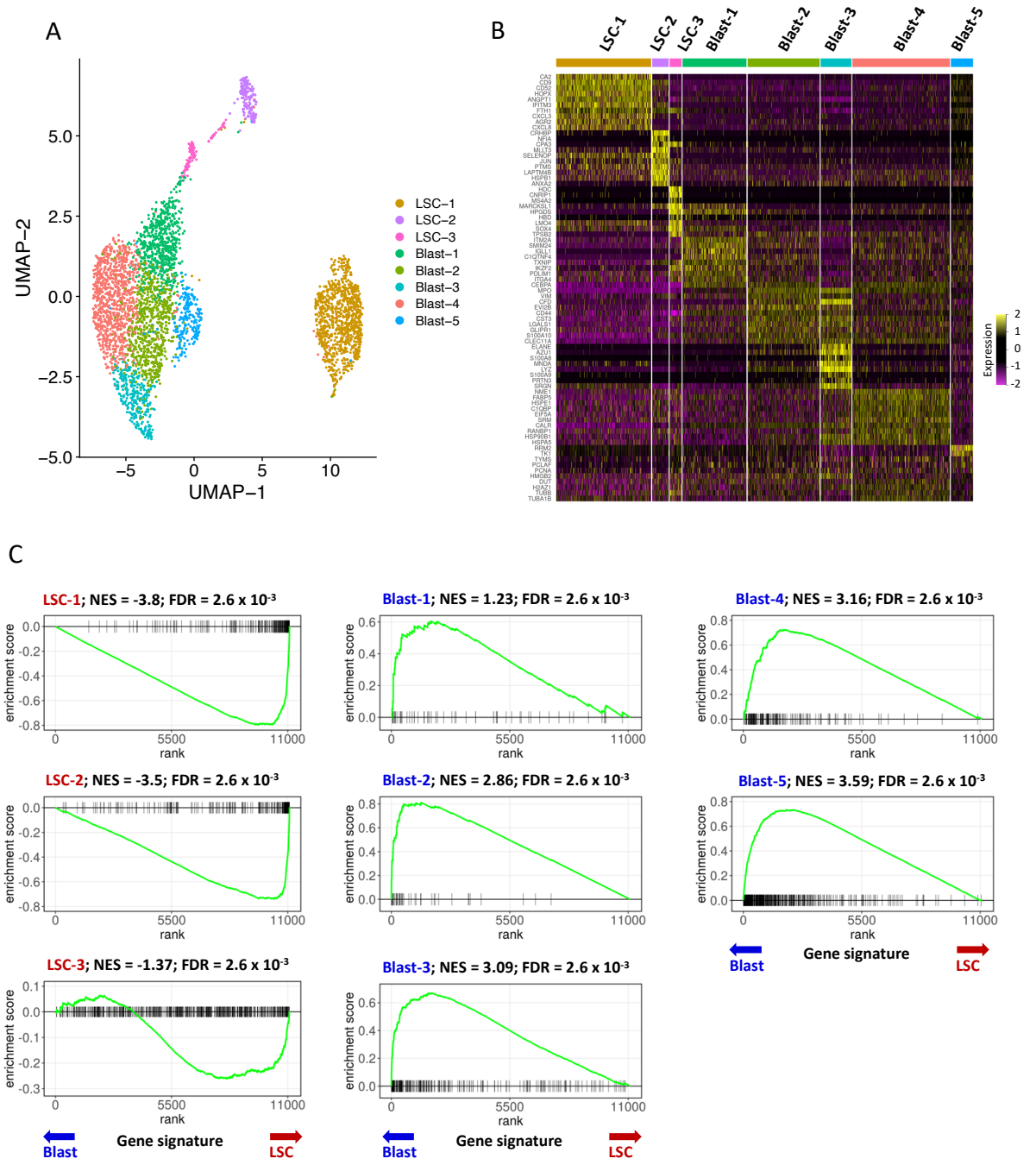

Figure 3.35: Identification of LSC and blast sub-populations.

(A) Uniform Manifold Approximation and Projection for Dimensional Reduction (UMAP) map displaying LSC and blast clusters as identified with GSEA analysis. Each dot in the map represents a cell and is coloured accordingly to cluster assignment.(B) Heatmap depicting the top 10 most upregulated marker genes identified in each cluster. (C) Gene Set Enrichment Analysis of cluster marker genes identified in scRNA-seq populations. Plots show the enrichment of a blast or LSC signature, as derived from bulk-RNA-seq. NES = Normalized Enrichment Score; FDR = False Discovery Rate. Analyses were performed by Dr Peter Keane, University of Birmingham.

The analysis of genes which are expressed in different phases of the cell cycle in individual cells is a good measure of the growth status of the overall cell population. This analysis showed that LSCs were mainly in G0/G1 phase, consistent with their quiescent state; the cell cycle status of blast cells was more variable, with the Blast-5 cluster showing the highest proliferation rate (Fig. 3.36 A and B).

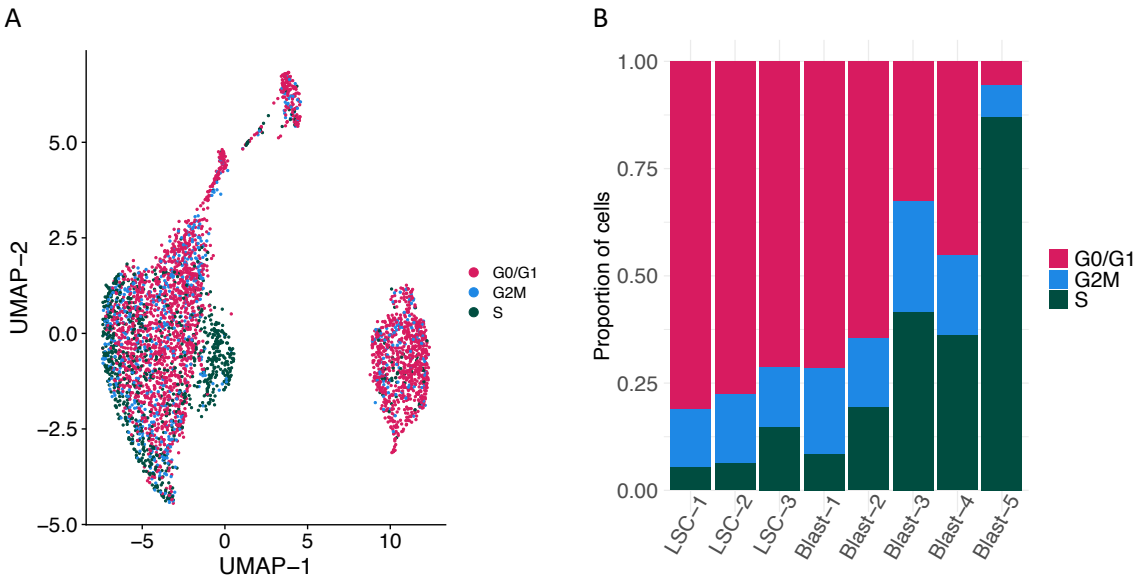

Figure 3.36: Cell-cycle analysis

(A) Expression of cell-cycle phase-specific genes (G0-G1, G2-M, S) projected on the UMAP map of scRNA populations. (B) Histogram showing the proportion of cells in each cell cycle phase within each cluster as identified by the expression of cell-cycle regulated genes. Analyses performed by Dr Peter Keane, University of Birmingham.

Each individual cell displays a specific gene expression pattern that is characteristic of its differentiation stage. This feature allows to order cells within a population of differentiating cells according to their similarity to a next neighbour and thus to visualize a differentiation trajectory within this population (pseudo-time analysis). This type of information highlights the hierarchical (progenitor - product) relationship between cell types. To gain more insight into the cellular hierarchy within the LSCs and blast populations, we therefore performed such analysis using our scRNA-Seq data. The LSC-1 cluster localized at the apex of the differentiation trajectory (Fig. 3.37 A and B), consistent with the strong enrichment of a LSC gene signature (Fig. 3.35 A). The analysis also showed that Blast-1 give rise to Blast-2, that subsequently branched into other three blast populations (Fig. 3.37 A). *HOXP*, encoding for an atypical homeodomain protein (Chen et al., 2002), was among the genes most upregulated in the LSC-1 (Fig. 3.35 B). This gene is enriched in LSCs compared to more differentiated progenitors and associated with adverse outcome in AML patients (Gentles et al., 2010). Another gene enriched in LSC-2, MLLT3 (Fig. 3.35 B), has been previously shown to be crucial for the maintenance of HSC self-renewal (Calvanese et al., 2019). Blast subgroups were characterized by elevated expression of genes related to a more mature phenotype, such as AZU1, MPO and ELANE (Fig. 3.35 B)

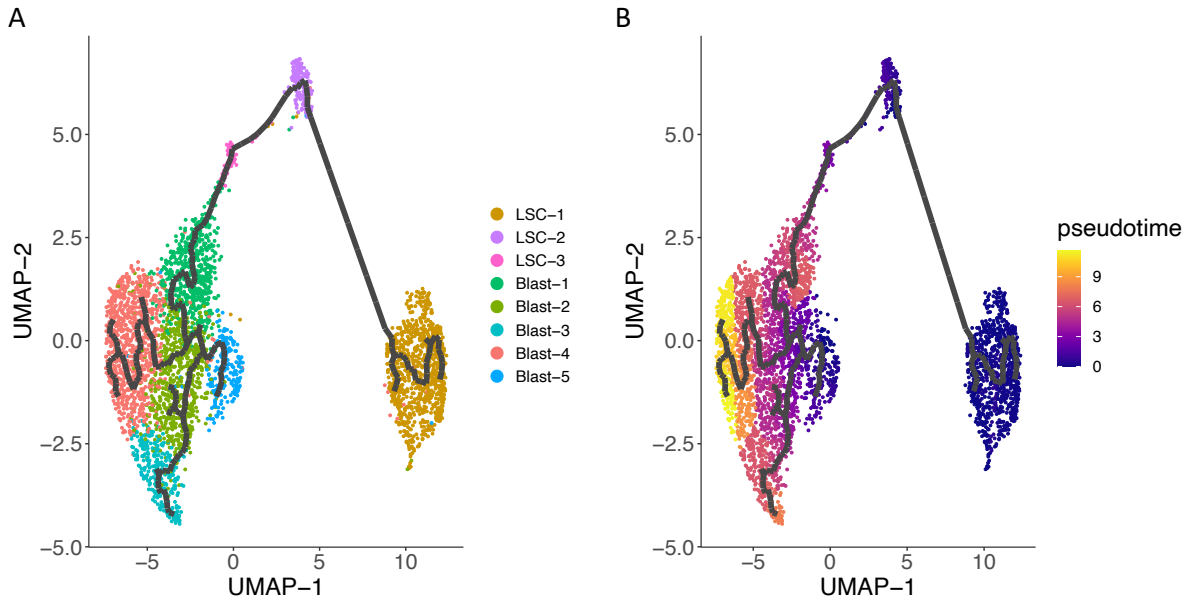

Figure 3.37: Pseudo-time analysis of LSC and Blast cells

Monocle pseudo-time trajectory of LSC and blast cells projected on the UMAP map of scRNA clusters. In (B) cells are coloured according to their pseudo-time value. Analyses performed by Dr Peter Keane, University of Birmingham.

We then projected the expression of some important hematopoietic TFs on cell clusters (Fig. 3.38). As expected, *CEBPA* expression was increased in all blast clusters compared to LSCs. On the contrary, *SOX4* was expressed at higher levels in the LSC compartment, coherently with previous observation that SOX4 is repressed by C/EBPα and is required for self-renewal in *CEBPA*$^{N/C}$ LSCs (Zhang et al., 2013).

The transcription factor POU4F1, that has been only recently associated with *CEBPA*$^{N/C}$ AMLs (Assi et al., 2019b), is widely expressed only within the LSC-1 cluster. The AP-1 family member FOS was expressed across all clusters, while JUN was preferentially expressed in the LSC compartment.

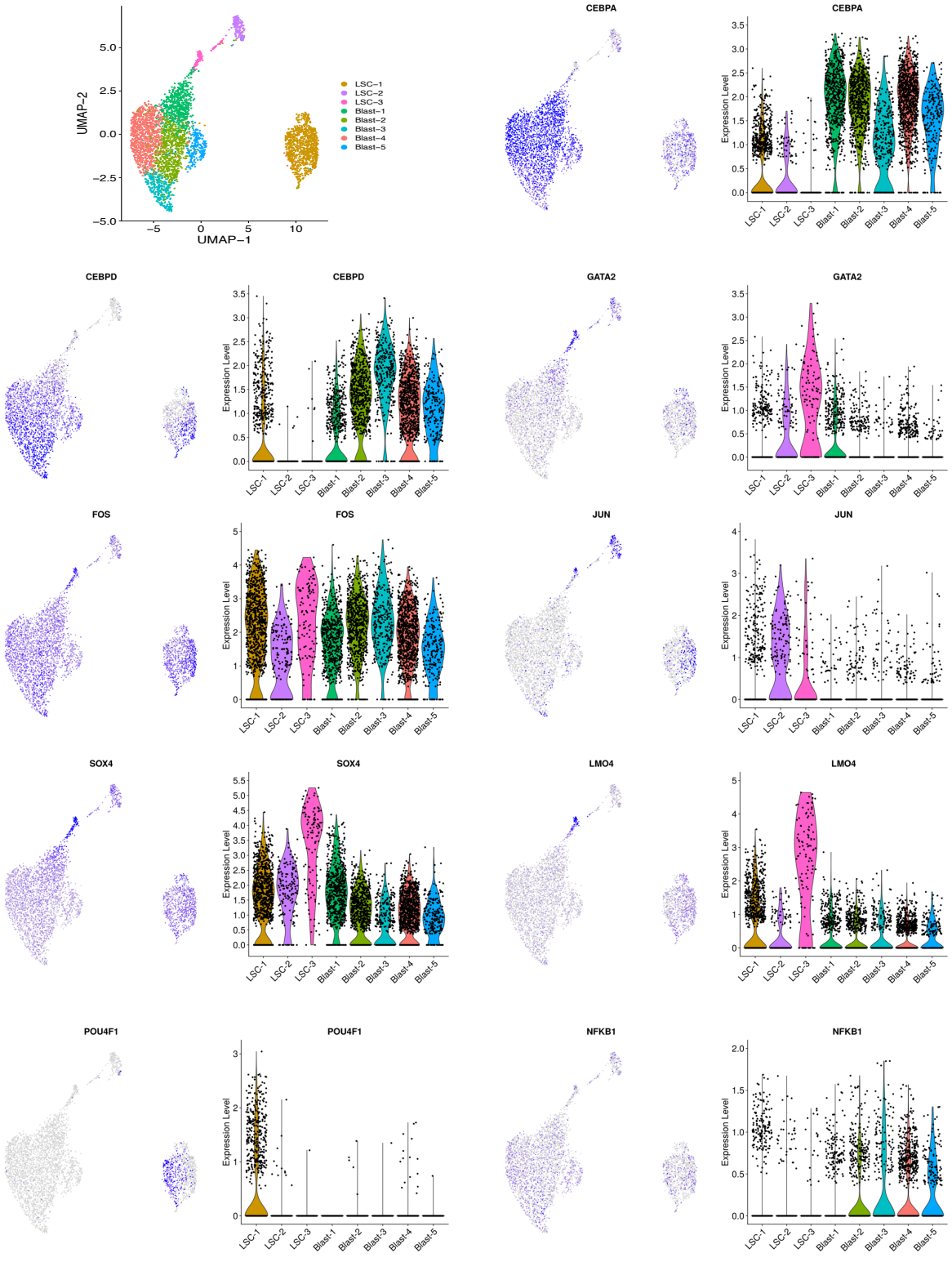

Figure 3.38: Examples of differential gene expression in LSCs and blast cells using scRNA-Seq analysis

(A) Expression of indicated genes projected on the UMAP map. Colour intensity represent expression data log2 normalized unique molecular identifier (UMI) counts. Analyses performed by Dr Peter Keane, University of Birmingham.

3.18 Pharmacological inhibition of RUNX and MAPK signalling in *CEBPA*$^{N/C}$ AMLs

Together with C/EBP and AP-1, the CBF family represented another major node of the *CEBPA*$^{N/C}$ GRN (Fig. 3.13). It has been previously demonstrated that RUNX1 is required for the growth of MLL-AF4 (Wilkinson et al., 2013), t(8;21) and inv(16) leukaemic cells (Ben-Ami et al., 2013). To test whether RUNX proteins are also required for *CEBPA*$^{N/C}$ leukaemic cells proliferation, we treated KO52 or patient derived blasts with the AI-14-91 inhibitor (CBFβi), which binds to CBFβ and impedes its binding to RUNX (Illendula et al., 2016). The CBFβi significantly reduced the proliferation of KO52 (Fig. 3.39 A) but did not have major effects on patient derived blasts (Fig. 3.39 B-D) or healthy PBSCs (Fig. 3.39 E).

Aberrant activation of the MAPK signalling pathway promotes cell proliferation and prevent apoptosis, and is a common feature of haematological malignancies (Platanias, 2003). We probed the relevance of the MAPK signalling in *CEBPA*$^{N/C}$ AMLs by using the MEK inhibitor CH5126766 (henceforth indicated as MEKi) (Ishii et al., 2013). This molecule causes the formation of a stable MEK/RAF complex, causing the simultaneous inhibition of both proteins and a strong suppression of the ERK signalling. We found that the MEKi did not affect proliferation of KO52 (Fig. 3.39 A), whereas all the patient derived blast showed impaired cell growth (Fig. 3.39 B-D).

The conflicting results observed in KO52 and blasts upon inhibitors treatment are likely to be due to the different culture conditions used (Section 2.4). KO52 is a cell line adapted to grow in serum containing basic cell culture media whereas patient cells are grown in serum-free stem cell media rich in cytokines. The full composition of the media used for CD34+ progenitor expansion is unknown because this information is protected

by a patent. It is likely that the additional cytokines necessary for the growth of primary cells activate growth regulatory pathways in the primary cells that are sensitive to MEK/RAF inhibition. In turn, the same pathways make the cells independent of RUNX1. The results of these experiments highlight the difficulties of judging drug responsiveness from in vitro culture only.

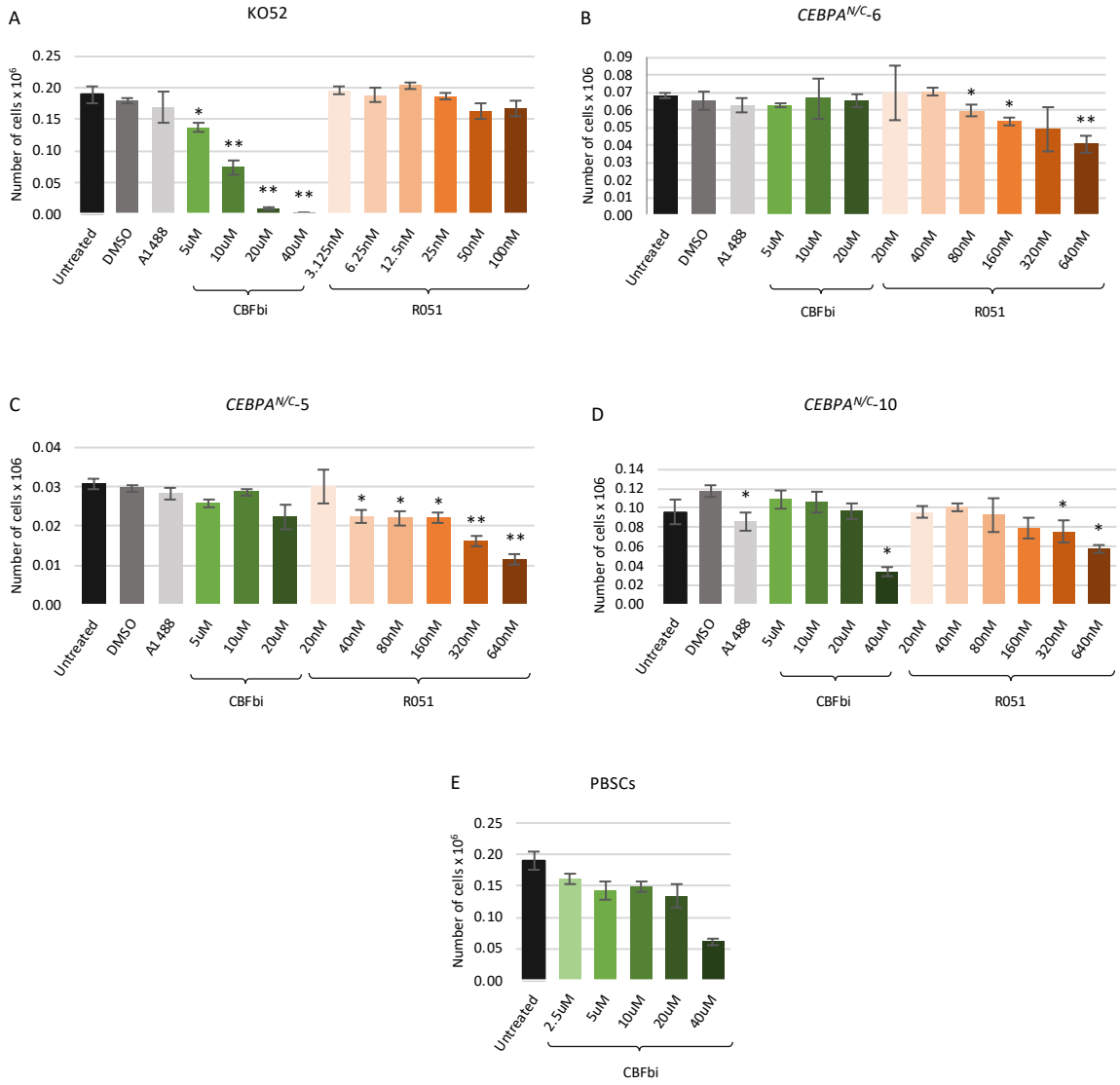

Figure 3.39: Response of CEBPA$^{N/C}$ cells to RUNX and MEK inhibitors

(A-E) Cumulative cell growth after one week of CBFβi (green) or MEKi (orange) treatment at the indicated concentration. (A) KO52 cell line. (B-D) *CEBPA*$^{N/C}$ patient derived blasts. (E) PBSCs. The experiment in (E) was performed by Dan Coleman (University of Birmingham), all other experiments were performed by Assunta Adamo.

Chapter 4 - Discussion

Acute myeloid leukaemia with biallelic *CEBPA* mutations are characterized by a distinctive gene expression profile and are associated with a favourable prognosis (Pabst et al., 2009; Wouters et al., 2009). However, in spite of many years of studies in mice, the molecular mechanism through which mutant C/EBPα proteins drive leukaemogenesis and how leukaemic cells are maintained is not completely understood (Koschmieder et al., 2009). In particular, very few experiments directly analysed patient derived cells. In this work we used multi-omics approaches to comprehensively characterize *CEBPA*$^{N/C}$ AMLs using purified primary patient-derived blasts and gain a better insight in the molecular pathogenesis of biallelic *CEBPA* mutated AMLs. We studied the gene expression at both the bulk and single cell level, determined open chromatin regions and linked these regions to their rightful genes. Assi et.al clearly demonstrated that *CEBPA*$^{N/C}$ and t(8;21) AMLs are epigenetically related (Assi et al., 2019b). In this study we confirmed this observation with a larger dataset, including 10 *CEBPA*$^{N/C}$ and 7 t(8;21) AML samples. Finally, we determined the gene regulatory network of *CEBPA*$^{N/C}$ AML and compared it to normal cells.

4.1 *CEBPA*$^{N/C}$ and t(8;21) AML show commonalities and differences in their gene expression and open chromatin patterns

We compared *CEBPA*$^{N/C}$ blasts to t(8;21) blasts and healthy PBSCs to define how *CEBPA* biallelic mutations shape the genomic and transcriptomic landscape in affected patients and to define common druggable target to treat leukaemic subtypes. Gene expression analysis showed *CEBPA* upregulation in leukaemic blasts compared to PBSCs, which is a common feature of *CEBPA*$^{N/C}$ AMLs.

Recent work showed that the duplication of lysine K313 (C/EBPα-K313), a typical C-terminal mutation associated with this type of AML, drives the overexpression of *CEBPA*, but not other members of the family, in a mouse model of granulocyte progenitors (Gentle et al., 2021). The authors also confirmed that C/EBPα-K313 is unable to bind the DNA and suggested that the mutant protein may regulate gene expression by interacting with other factors. This may be a common feature of *CEBPA*$^{N/C}$ AMLs, where p42 isoforms harbouring C-terminal mutations different from K313 may drive an oncogenic program by dimerizing with other transcription factors. This idea is also suggested by our open chromatin analyses.

We also found that the serine/threonine kinase *MAP3K8* is upregulated in *CEBPA*$^{N/C}$ AMLs compared to both t(8;21) and healthy blasts (see supplementary tables 1 and 3). MAP3K8 is involved in the regulation of several kinase pathways related to cell proliferation, differentiation, survival and chemotherapy resistance, included the MERK-ERK and NF-κB signalling (Chiariello et al., 2000; Chorzalska et al., 2018; Patriotis et al., 1994; Sanchez et al., 2017). Our GRN and ChIP experiments also showed that it is a C/EBPα and FOS target (see supplementary table 3).

Another C/EBPα and AP-1 target upregulated in *CEBPA*$^{N/C}$ AML is *PIWIL4* (see supplementary tables 1 and 3), This gene encodes a protein that belongs to the family of Argonauta proteins and is involved in the maintenance of germline stem cells (Sasaki et al., 2003). It has been found overexpressed in most AML patients and associated with increased cell proliferation and clonogenicity of leukemic cells (Bamezai et al., 2013; Bamezai et al., 2018).

MYCT1 appeared among the genes commonly downregulated in biallelic *CEBPA* mutated and t(8;21) AMLs (see supplementary table 1 and 3). This finding is in contrast

with previous reports, where it was shown that *RUNX1-ETO* expression in human cord blood-derived CD34+ progenitor cells increases proliferation by upregulating MYCT1 (Liddiard et al., 2012; Tonks et al., 2007). In contrast, another group found that *MYCT1* expression is significantly lower in the bone marrow of AML patients compared to healthy individuals, and its overexpression blocks proliferation and triggers apoptosis in AML cell line models (Fu et al., 2018). *MYCT1* was also found downregulated in a subtype of AML characterized by *CEBPA* hypermethylation and silencing, and identified as target normally activated by C/EBPα (Taskesen et al., 2011), observation confirmed by our ChIP analysis (see supplementary table 4).

Our open chromatin analyses enforced the idea that mutant C/EBPα proteins may cooperate with other TFs. Indeed an interesting finding in this study was the presence of the composite C/EPB:AP-1 motif in *CEBPA*$^{N/C}$-specific hypersensitive sites, in contrast to the AP-1 canonical motif that was enriched in both t(8;21) and healthy blasts-specific sites. AP-1 - in this case the JUN and FOS - are crucial for normal haematopoiesis (Schorpp-Kistner et al., 1999; Wang et al., 1992). In hematopoietic malignancies AP-1 can behave both as oncogene and tumor suppressor (Kesarwani et al., 2017; Passegue et al., 2001). Previous work from our lab using a dnFOS peptide has shown that global AP-1 activity is required for the maintenance of the leukaemic phenotype in t(8;21) AMLs (Assi et al., 2019b; Martinez-Soria et al., 2018; Ptasinska et al., 2019) and that the AP-1 family represents an important node of the GRNs specific for different leukaemia subtypes, included *CEBPA*$^{N/C}$ (Assi et al., 2019b). It has been reported that C/EBP and AP-1 transcription factors form heterodimers (Gombart et al., 2007; Hai and Curran, 1991; Hsu et al., 1994), and C/EBPα:AP-1

interaction is required to drive monocytic lineage commitment (Cai et al., 2008). The enrichment of C/EBP:AP-1 motifs at *CEBPA*$^{N/C}$-specific sites suggests that in this context the two transcription factors may collaborate to maintain the leukemic phenotype.

4.2 Specific network nodes of *CEBPA*$^{N/C}$ AML form regulatory modules that drive the expression of specific target genes which are distinct from those of t(8;21) AML

Assi et al. (Assi et al., 2019b) have previously defined the GRN of different leukaemia subtypes, including *CEBPA*$^{N/C}$. In this work we refined this network, using a larger dataset and including C-HiC data. Since not all open chromatin regions are associated with their nearest gene, an essential part of GRN construction is the determination of which cis-regulatory element belongs to its rightful promoter by performing Capture Hi-C (C-HIC). This work describes such a dataset for the *CEBPA*$^{N/C}$ subtype for the first time. It should be noted that our group has now generated data from 3 different sub-types (t(8;21), FT3-ITD/NPM1, *CEBPA*$^{N/C}$) and combined them with published data from healthy CD34+ cells ((Assi et al., 2019b; Mifsud et al., 2015) and this work). In each case, we find a large (>70%) overlap of DHSs with interactions but also several thousand AML-sub-type specific hypersensitive sites. t(8;21), FLT3-ITD and *CEBPA*$^{N/C}$ make up about 85% of all AMLs. In light of the fact that all AML subtypes are of the myeloid lineage, and that the majority of DHSs of all sub-types overlap (Assi et al., 2019), our combined dataset therefore can serve as a “Master” dataset for the majority of AML subtypes to assign cis-elements to their rightful promoters.

The *CEBPA*$^{N/C}$-specific core GRN emphasizes the AML-specific connections (binding events) between TF-coding genes that are distinct from those found in PBSCs, and highlighted a number of interesting results. The analysis of the TF modules (supplementary table 4), i.e. the downstream targets of TFs forming nodes, shows that these differences are responsible for the alterations in gene expression in AML. It is of importance to note that whilst our GRN construction involves the identification of binding motifs, our ChIP experiments confirmed that the majority of C/EBP, RUNX and AP-1 motifs are bound by at least one member of the family (Fig. 3.23). This result demonstrates that motif analysis is valid to identify connections between genes, provided the TF family is expressed.

Another interesting result is the finding that, despite one essential member being mutated, the C/EBP family itself represents one of the most connected nodes of the *CEBPA*$^{N/C}$ specific GRN, indicating an important regulatory function. The RUNX family shows numerous connections going inward, suggesting that the expression of this transcription factor is strictly regulated in the *CEBPA*$^{N/C}$ AML subtype and is likely to be important for the maintenance of *CEBPA*$^{N/C}$ AMLs. Targets of RUNX1 in the AML-specific GRN include, for example, the apoptosis regulator *BCL2,* which is highly expressed in *CEBPA*$^{N/C}$ AML blasts and can be inhibited by the drug Venetoclax (Souers et al., 2013).

As seen in other AML subtypes (Assi et al., 2019), the AP-1 family forms an important node in the *CEBPA*$^{N/C}$ AML GRN, indicating that MAPK signalling plays an essential role in regulating cellular growth. For FLT3-ITD and t(8;21) AML this idea has been confirmed *in vitro* and *in vivo* by employing an inducible dnFOS (Assi et al., 2019b; Martinez-Soria et al., 2018). Moreover, inspection of the *CEBPA*$^{N/C}$ AML-specific AP-

1 module showed an association with the *CCND2* gene which has been shown to be up-regulated in t(8;21) AML, indicating that this pathway is also used in *CEBPA*$^{N/C}$ AML. In t(8;21), this phenotype mediated a vulnerability of AML cells to treatment with the FDA approved drug Palbociclib (Martinez-Soria et al., 2018). However, in *CEBPA*$^{N/C}$ AML the gene is not up-regulated as compared to PBSCs, but the AP-1 connection makes it susceptible to up-regulation in response to inflammatory stimuli during treatment. Taken together, and with the caveat that these experiments need to be further substantiated in primary cells as discussed further below, these ideas were confirmed by our perturbation experiments using dnC/EBP, dnFOS, MEKi and CBFβi.

An important result is the finding that the gene encoding the TF POU4F1 (BRN3) is one of the most connected nodes. This transcription factor is important for neuronal development (Xiang et al., 1996) but is not normally expressed in blood progenitors (Assi et al., 2019b). It is upregulated in *CEBPA*$^{N/C}$ AMLs (Supplementary table 1) and was confirmed to be a C/EBPα and RUNX1 target in our ChIP experiments (see supplementary table 4). The binding motif for POU4F1 was found to be occupied in both *CEBPA*$^{N/C}$ and t(8;21) AMLs as determined by digital footprinting, indicating that it binds to its target genes and plays a functional role in maintaining the leukaemic phenotype for both AML sub-types (Assi et al., 2019b). *POU4F1* is indeed also upregulated in t(8;21) AMLs, and synergizes with RUNX1-ETO to suppress myeloid differentiation (Dunne et al., 2010; Dunne et al., 2012; Fortier et al., 2010). Moreover, it is ectopically expressed in several different solid tumours (Ahmed et al., 2010; Diss et al., 2006; Hohenauer et al., 2013).

Another major node of our network is the E2F family, involved in the control of differentiation, cell cycle progression and apoptosis (Irwin et al., 2000; Muller et al., 2001), Direct repression of E2F by C/EBPα N-terminal domain is critical to inhibit cell proliferation and induce granulocyte differentiation (Porse et al., 2001; Slomiany et al., 2000). This control mechanism is abrogated in the N-terminal truncated p30 isoform leading to uncontrolled myeloid progenitor expansion (D'Alo et al., 2003; Porse et al., 2005).

The TGIF factor family, belonging to the TALE class of homeodomain proteins (Burglin, 1997), represents one of the most connected nodes of the *CEBPA*$^{N/C}$ specific GRN, with identified targets (See supplementary table 4). The family member TGIF1 was originally identified as co-repressor of the retinoic acid and TGF-β signalling (Bertolino et al., 1995; Wotton et al., 1999), both known to play an important role in hematopoiesis and, in particular, in myelopoiesis. Loss of TGIF1 in murine HSC promoted quiescence and self-renewal (Yan et al., 2013), while TGIF1 knock-down in AML cell lines reduced proliferation and decreased the expression of the myeloid TFs CEBPβ, CEBPϵ, PU.1 and RUNX1 (Hamid and Brandt, 2009). Moreover, in mouse models of AML or CML, loss of TGIF1 in hematopoietic stem and progenitor cells resulted in increased frequency of leukaemia-initiating cells (LICs), chemotherapy resistance and an overall worst prognosis (Yan et al., 2020).

In summary, as the examples outlined above demonstrate, the identification of the *CEBPA*$^{N/C}$ AML-specific core GRN highlights several leukaemia subtype-specific connections between TFs, as well as target genes that code for “druggable” gene products. Our work will be an important resource for researchers developing combination therapies aimed at treating this particular AML subtype.

4.3 Binding of C/EBPα proteins to their targets

Several studies have exploited cell line and mouse models expressing exogenous mutant C/EBPα proteins to identify target genes whose expression is affected in *CEBPA*$^{N/C}$ AMLs. However, to our knowledge, the global C/EBPα binding pattern in *CEBPA*$^{N/C}$ human cell lines and affected patients has never been characterized.

CEBPA$^{N/C}$ AMLs are characterized by two distinct genetic alterations: a frameshift mutation at the N-terminal, which result in the exclusive expression of the p30 isoform, and an in-frame C-terminal mutation, that affect the bZIP domain altering DNA binding or dimerization ability. Recent works have investigated the global genomic occupancy of mutant C/EBPα in an AML mouse model exclusively expressing the C/EBPα-p30 isoform (Kirstetter et al., 2008), enabling the discovery of new druggable targets. Using this model, it has been demonstrated that the 5'-ribonucleotide phosphohydrolase CD73 and the RNA-binding protein MSI2, both overexpressed in *CEBPA*$^{N/C}$ AMLs, are direct targets of C/EBPα-p30 and are critical for leukaemic growth and survival (Heyes et al., 2021; Jakobsen et al., 2019). Of note, our human data confirmed the upregulation of CD73 (*NT5E*) but not *MSI2* (Supplementary table 1). The exploitation of the *CEBPA*$^{p30/p30}$ mouse as *CEBPA*$^{N/C}$ AML model assumes that C/EBPα-p30 but not the mutated C/EBPα-p42 is able to bind the DNA and drive the oncogenic program. This idea is challenged by previous work suggesting that p42 may still associate to DNA (Gentle et al., 2021) and recent studies showing that mutations in the bZIP domain, occurring either as biallelic or single mutations, are associated to a better prognosis and that *CEBPA*$^{N/C}$ and *CEBPA*-bZIP AMLs have a similar gene expression profile (Tarlock et al., 2021; Taube et al., 2022; Wakita et al., 2022). These results

suggest that the p42 isoform, despite the presence of mutations in the bZIP domain, may still conserve some activities. An important result of our work therefore was the genome-wide mapping of C/EBPα targets in primary human samples and a human cell line model of *CEBPA* biallelic mutated AML expressing both the p30 and p42 isoforms. Unfortunately, the antibody used for our ChIP experiments recognizes a C-terminal epitope present in both isoforms, thus cannot discriminate between C/EBPα-p30 and the eventual C/EBPα-p42 DNA binding. Future experiments using tagged versions of the mutant proteins should enable to distinguish which isoform is binding to chromatin.

The presence of a C/EBP:AP-1 signature in $CEBPA^{N/C}$ AMLs and the significant C/EBPα and c-FOS ChIP peak overlap in KO52 cells suggested that the two transcription factors may cooperate to drive the oncogenic program. It is possible that instead of p42:p30 dimers, C/EBP:AP-1 dimers that bind to a sub-set of C/EBP binding motifs are formed. Previous studies pointed to an involvement of FOS and JUN but not MAF (Cai et al., 2008) and since we see a composite binding motif in DNA, it is likely that the C/EBP partner is the DNA-binding p30 isoform. Future pull-down experiments followed by Western blotting should clarify whether this is indeed true, and which AP-1 family member is involved. Our analysis of the spacing between C/EBP and AP-1 motifs at sites bound by both factors showed a periodic structure which indicates that the two proteins may not just heterodimerise, but also physically cooperate as they seem to both bind to the same side of the DNA-helix. A similar picture was seen with C/EBP and RUNX1, but not with AP-1 and RUNX1 motifs, suggesting that the former but not the latter cooperate. Again, additional experiments are required to elucidate the molecular details of such possible cooperation.

4.4 The chromatin and gene expression landscape of CEBPA$^{N/C}$ AML leukaemic stem and blast cells

AML is characterized by abnormal proliferation of immature and dysfunctional cells, which accumulate in the bone marrow and in the blood interfering with the normal haematopoietic process. Current treatments have increased the percentage of patients that achieve complete remission; however, relapse occurs often and the survival rate remains low. Several lines of evidence suggest that relapse is caused by LSCs, a rare population within the tumor bulk characterized by quiescence, self-renewal ability and drug resistance. Thus, a better characterization of LSCs is required to identify new therapeutic strategies for their complete eradication. We used ATAC-seq to define the chromatin landscape of LSCs and leukaemic blasts purified from a *CEBPA*$^{N/C}$ primary sample. We found that LSCs open chromatin regions were enriched in CTCF and RUNX binding motifs, whereas the C/EBP signature was mainly confined to blast cells, indicating a more mature phenotype. The enrichment of C/EBP:AP-1 motifs in the blast-specific hypersensitive sites suggested that C/EBPs and AP-1 cooperation may not have a preeminent role in LSCs maintenance.

Several studies demonstrated that RUNX1 is required for the maintenance of LSCs in different leukaemia subtypes, as RUNX1 depletion resulted in stem cell exhaustion and impaired engraftment in mice models (Jacob et al., 2010; Wesely et al., 2020). A similar role has been described for the chromatin organizer CTCF, which is required to switch off the core stem-cell program and enable the LT-HSC to exit from quiescent state, and transit to ST-HSC state with reduced stemness (Takayama et al., 2021). However, in contrast to the other TFs which form large complexes, CTCF tends to bind as single protein and motif protection / enrichment is highly sensitive to small variation

in nuclease concentrations. Further experiments using ChIP are needed to clarify whether the high enrichment of this motif in LSC-specific open chromatin regions is of functional significance.

Our single cell experiments confirmed the differences between LSCs and blast cells. *CEBPA* and *CEBPD* were mainly expressed in blast cells which is consistent with a more mature phenotype, however the expression of both transcription factors was still widely detectable in one of the LSC subpopulations. C/EBPα is required to maintain adult HSCs in a quiescent state and preserve their self-renew ability (Hasemann et al., 2014; Ye et al., 2013). The expression pattern of *CEBPD* in our scRNA-seq analysis suggested that this transcription factor may play a similar role. On the other hand, *CEBPD* may be part of the oncogenic hub sustaining LSC maintenance in *CEBPA*$^{N/C}$ AMLs. It would be interesting to test this hypothesis by comparing *CEBPD* expression in LSCs derived from other leukaemic subtypes and healthy HSCs.

Our expression analyses showed that the AP-1 family members were uniformly expressed throughout all the LSC and blast subpopulations, except for *JUN*. *JUN* was downregulated in the blast compartment following an expression pattern inversely correlated to *CEBPA*. During granulocyte differentiation C/EBPα heterodimerizes with c-JUN, impeding the formation of JUN:FOS complexes and preventing JUN from autoregulate its own promoter. The consequent JUN downregulation promotes granulocytic differentiation (Rangatia et al., 2002). This result explains the expression pattern of JUN observed in our scRNA-seq data. Another interesting finding was the expression of *POU4F1* almost exclusively in the most primitive LSC cluster. POU4F1 has been shown to prevent apoptosis and induce cell cycle arrest in neurons (Budram-Mahadeo et al., 2002), thus may protect LSCs through similar mechanisms.

4.5 AP-1 and C/EBP shape the regulatory phenotype of CEBPA$^{N/C}$ AMLs

Our perturbation experiments in KO52 cells were informed by our gene regulatory network analysis, which highlighted the important role of both C/EBP and AP-1 families in maintaining the leukaemic phenotype of *CEBPA*$^{N/C}$ AMLs. Unfortunately, we have not been able to test the effects of dnC/EBP and dnFOS expression in *CEBPA*$^{N/C}$ patient blasts. These cells were extremely difficult to transduce and, after doxycycline induction, we recovered only a small number of GFP+ blasts which were insufficient to perform further experiments. We were also not able to establish a KO52 clonal cell line stably transduced with the inducible dnC/EBP and dnFOS constructs. This may be due to excessive stress following single cell FACS sorting, which causes loss of our single-cell cultures. Another possibility is that even the transient expression of these constructs blocks the growth of such cells which then drop out of the culture. This possibility is supported by the fact that it took several attempts to generate an inducible dnC/EBP expressing Kasumi-1 cell line where uninduced expression was low enough (data not shown).

Block of C/EBP binding in KO52 did not show major chromatin or transcriptional changes. However hypersensitive sites lost and gained upon dnC/EBP expression were enriched in C/EBP and PU.1 motifs and GATA motifs respectively, consistent with the loss of C/EBP binding and the acquisition of a more immature phenotype. These results suggest that the dnC/EBP peptide was blocking C/EBPs binding as expected, and longer time of doxycycline induction may be required to appreciate marked changes in chromatin accessibility and gene expression. Time constraints prohibited a repetition of this experiment.

Expression of dnFOS had a stronger effect on the chromatin landscape of KO52 cell, mainly causing loss of open chromatin sites. This result agrees with previous studies showing that AP-1 transcription factors have an important role in recruiting chromatin remodellers and promoting and maintaining chromatin accessibility (Bevington et al., 2016; Biddie et al., 2011; Vierbuchen et al., 2017). Interestingly, C/EBP:AP-1 composite motifs were enriched in hypersensitive sites lost upon dnC/EBP expression in KO52, but not in Kasumi-1. This result suggests that the cooperation between these TFs is a specific feature of *CEBPA*$^{N/C}$ AMLs. Our gene expression analysis showed that loss of AP-1 binding in KO52 was accompanied by downregulation of several signalling pathways, suggesting that these factors promote the survival of *CEBPA*$^{N/C}$ leukaemic cells through an autocrine loop.

Finally, we found that the expression of dnC/EBP or dnFOS induced growth arrest in both KO52 (this study) and Kasumi-1 cells (this study and (Potluri et al., 2021)). Further experiments in KO52 cells will clarify whether proliferation impairment is caused by increased rate of apoptosis or a block in the cell cycle.

4.6 The response of *CEBPA*$^{N/C}$ AMLs to pharmacological inhibitors differs between KO52 cells and primary cells

The CBF family of transcription factors was one of the principal nodes of our GRN. Previous works have shown that different AML subtypes, including t(8;21), inv(16) and MLL-AF9 leukaemia, require RUNX1 activity for their survival (Ben-Ami et al., 2013; Goyama et al., 2013); however a similar dependence for *CEBPA*$^{N/C}$ AMLs has never been established. The Ras/Raf/MEK/ERK pathway is often deregulated in hematopoietic malignancies and is implicated in increased proliferation and drug

resistance of leukaemic blasts by regulating gene expression and activity of several targets including FOS, JUN and NF-κB (McCubrey et al., 2007; Steelman et al., 2011). These observations prompted us to test the effect of pharmacological inhibition of RUNX and the ERK signalling on cell proliferation in KO52 cells and *CEBPA*$^{N/C}$ patient blasts. However, these experiments yielded conflicting results. We found that KO52 cells were sensitive to the CBFβi but not the MEKi, whereas the opposite was true for the patient derived blasts. This inconsistency is likely to be due to the different culture systems used. *CEBPA*$^{N/C}$ and t(8;21) blasts are associated to a good prognosis and are extremely difficult to maintain both *in vitro,* in contrast to *FLT3-ITD* primary cells. KO52 cells are grown in standard cell culture media, but our primary patient samples were cultured in serum-free media rich in cytokines, which may render blast cells dependent on MEK/ERK activation and independent of RUNX transcription factors for their survival. We observed a similar culture-medium dependent difference in drug response with primary cells from FLT3-ITD AML patients (Dr Daniel Coleman, University of Birmingham, personal communication). *In vivo* drug testing would be a preferable and more reliable alternative. However, our attempts to expand *CEBPA*$^{N/C}$ leukaemic blasts in an immunodeficient mouse recipient failed, due to lack of engraftment (Dr Helen Blair and Dr Olaf Heidenreich, University of Newcastle, unpublished results). A t(8;21) sample obtained from a patient on relapse harbouring a *KIT* mutation, associated with a poor prognosis (Ishikawa et al., 2020) did engraft. Interestingly, previous studies suggested that the ability of leukemic blasts to engraft in NOD/SCID mice is an intrinsic property of AML cells and correlates with response to therapy (Pearce et al., 2006). Taken together, our preliminary experiments show

that great care has to be taken to design drug response experiments in cultured primary cells.

4.7 Limitations and future directions

Our study will provide an important resource for researchers working on *CEBPA*$^{N/C}$ AML. However, a few more mechanistic studies need to be done to finalise this work for publication.

(i) Pulldown experiments followed by Western Blotting using primary cells need to be done to test whether C/EBP:AP-1 heterodimers exist in *CEBPA*$^{N/C}$ AML.

(ii) Tagged versions of the endogenous p42 and p30 mutant alleles have to be generated using the CRISPR/Cas9 to test by ChIP which one of the two isoforms is associated with chromatin.

(iii) We will selectively silence the C/EBPα-p30 or p42 allele in KO52 by CRISPR/Cas9 to test which mutant protein is required for cellular viability.

(iv) We will repeat the dnFOS and dnC/EBP expression experiments in KO52 cells and wait longer before harvesting the cells to perform ATAC- and RNA-seq experiments.

(v) We will compare *CEBPA*$^{N/C}$ blasts and LSCs scRNA-seq data with publicly available PBSC scRNA-seq data to define therapeutic targets specifically expressed in the leukaemic stem cells and suitable for LSCs eradication.

(vi) Our GRN analysis will inform a targeted CRISPR screen to see which genes are required for the maintenance of *CEBPA*$^{N/C}$ AML. Our group used a similar strategy to target genes forming important nodes in the FLT3-ITD

GRN (unpublished results from the Bonifer/Cockerill group). The hit rate in this screen was between 30% and 70% making it (i) much more efficient than genome-wide screens and (ii) eliminates the assay being swamped by guide RNAs hitting genes generally essential for the growth of all cells. This experiment will help us to validate multiple druggable candidate targets defined by our GRN.

References

Adya, N., Stacy, T., Speck, N.A., and Liu, P.P. (1998). The leukemic protein core binding factor beta (CBFbeta)-smooth-muscle myosin heavy chain sequesters CBFalpha2 into cytoskeletal filaments and aggregates. Mol Cell Biol *18*, 7432-7443.

Ahmed, N., Latifi, A., Riley, C.B., Findlay, J.K., and Quinn, M.A. (2010). Neuronal transcription factor Brn-3a(l) is over expressed in high-grade ovarian carcinomas and tumor cells from ascites of patients with advanced-stage ovarian cancer. J Ovarian Res *3*, 17.

Aikawa, Y., Katsumoto, T., Zhang, P., Shima, H., Shino, M., Terui, K., Ito, E., Ohno, H., Stanley, E.R., Singh, H.*, et al.* (2010). PU.1-mediated upregulation of CSF1R is crucial for leukemia stem cell potential induced by MOZ-TIF2. Nat Med *16*, 580-585, 581p following 585.

Akashi, K., Traver, D., Miyamoto, T., and Weissman, I.L. (2000). A clonogenic common myeloid progenitor that gives rise to all myeloid lineages. Nature *404*, 193-197.

Amann, J.M., Nip, J., Strom, D.K., Lutterbach, B., Harada, H., Lenny, N., Downing, J.R., Meyers, S., and Hiebert, S.W. (2001). ETO, a target of t(8;21) in acute leukemia, makes distinct contacts with multiple histone deacetylases and binds mSin3A through its oligomerization domain. Mol Cell Biol *21*, 6470-6483.

Amemiya, H.M., Kundaje, A., and Boyle, A.P. (2019). The ENCODE Blacklist: Identification of Problematic Regions of the Genome. Sci Rep *9*, 9354.

Angel, P., and Karin, M. (1991). The role of Jun, Fos and the AP-1 complex in cell-proliferation and transformation. Biochim Biophys Acta *1072*, 129-157.

Antony, C., George, S.S., Blum, J., Somers, P., Wu-corts, D., Pimkin, M., and Paralkar, V.R. (2021). CEBPA Directly Binds Ribosomal DNA and Promotes Ribosomal RNA Transcription in Myeloid Progenitors. Blood *138*, 3269-3269.

Arber, D.A., Orazi, A., Hasserjian, R., Thiele, J., Borowitz, M.J., Le Beau, M.M., Bloomfield, C.D., Cazzola, M., and Vardiman, J.W. (2016). The 2016 revision to the World Health Organization classification of myeloid neoplasms and acute leukemia. Blood *127*, 2391-2405.

Asou, H., Gombart, A.F., Takeuchi, S., Tanaka, H., Tanioka, M., Matsui, H., Kimura, A., Inaba, T., and Koeffler, H.P. (2003). Establishment of the acute myeloid leukemia cell line Kasumi-6 from a patient with a dominant-negative mutation in the DNA-binding region of the C/EBPalpha gene. Genes Chromosomes Cancer *36*, 167-174.

Asou, H., Tashiro, S., Hamamoto, K., Otsuji, A., Kita, K., and Kamada, N. (1991). Establishment of a human acute myeloid leukemia cell line (Kasumi-1) with 8;21 chromosome translocation. Blood *77*, 2031-2036.

Assi, S.A., Bonifer, C., and Cockerill, P.N. (2019a). Rewiring of the Transcription Factor Network in Acute Myeloid Leukemia. Cancer Inform *18*, 1176935119859863.

Assi, S.A., Imperato, M.R., Coleman, D.J.L., Pickin, A., Potluri, S., Ptasinska, A., Chin, P.S., Blair, H., Cauchy, P., James, S.R.*, et al.* (2019b). Subtype-specific regulatory network rewiring in acute myeloid leukemia. Nat Genet *51*, 151-162.

Bamezai, S., Mulaw, M.M., Zhou, F., Rohde, C., Muller-Tidow, C., Dohner, K., Dohner, H., Buske, M.F., Buske, C., and Rawat, V.P.S. (2013). Knockdown Of The Piwi - Like Protein 4 (PIWIL4) Delays Leukemic Growth and Is Associated With Gross Changes In The Global Histone Methylation Marks In Human MLL - Rearranged AML. Blood *122*, 597-597.

Bamezai, S., Vegi, N., Pulikkottil Jose, A., Müller, J., Grummt, I., Song, C., Döhner, K., Döhner, H., Feuring-Buske, M., Rawat, V.P.S.*, et al.* (2018). The Non-Canonical, R-Loop Regulatory Function of PIWIL4 Maintains Genomic Integrity and Leukemic Potential of AML Cells. Blood *132*, 879-879.

Banerji, J., Rusconi, S., and Schaffner, W. (1981). Expression of a beta-globin gene is enhanced by remote SV40 DNA sequences. Cell *27*, 299-308.

Barakat, T.S., Halbritter, F., Zhang, M., Rendeiro, A.F., Perenthaler, E., Bock, C., and Chambers, I. (2018). Functional Dissection of the Enhancer Repertoire in Human Embryonic Stem Cells. Cell Stem Cell *23*, 276-288 e278.

Barreyro, L., Will, B., Bartholdy, B., Zhou, L., Todorova, T.I., Stanley, R.F., Ben-Neriah, S., Montagna, C., Parekh, S., Pellagatti, A.*, et al.* (2012). Overexpression of IL-1 receptor accessory protein in stem and progenitor cells and outcome correlation in AML and MDS. Blood *120*, 1290-1298.

Begley, C.G., Aplan, P.D., Davey, M.P., Nakahara, K., Tchorz, K., Kurtzberg, J., Hershfield, M.S., Haynes, B.F., Cohen, D.I., Waldmann, T.A.*, et al.* (1989). Chromosomal translocation in a human leukemic stem-cell line disrupts the T-cell antigen receptor delta-chain diversity region and results in a previously unreported fusion transcript. Proc Natl Acad Sci U S A *86*, 2031-2035.

Behre, G., Whitmarsh, A.J., Coghlan, M.P., Hoang, T., Carpenter, C.L., Zhang, D.E., Davis, R.J., and Tenen, D.G. (1999). c-Jun is a JNK-independent coactivator of the PU.1 transcription factor. J Biol Chem *274*, 4939-4946.

Bejerano, G., Pheasant, M., Makunin, I., Stephen, S., Kent, W.J., Mattick, J.S., and Haussler, D. (2004). Ultraconserved elements in the human genome. Science *304*, 1321-1325.

Bell, A.C., West, A.G., and Felsenfeld, G. (1999). The protein CTCF is required for the enhancer blocking activity of vertebrate insulators. Cell *98*, 387-396.

Ben-Ami, O., Friedman, D., Leshkowitz, D., Goldenberg, D., Orlovsky, K., Pencovich, N., Lotem, J., Tanay, A., and Groner, Y. (2013). Addiction of t(8;21) and inv(16) acute myeloid leukemia to native RUNX1. Cell Rep *4*, 1131-1143.

Bennett, J.M., Catovsky, D., Daniel, M.T., Flandrin, G., Galton, D.A., Gralnick, H.R., and Sultan, C. (1985). Criteria for the diagnosis of acute leukemia of megakaryocyte lineage (M7). A report of the French-American-British Cooperative Group. Ann Intern Med *103*, 460-462.

Bereshchenko, O., Mancini, E., Moore, S., Bilbao, D., Mansson, R., Luc, S., Grover, A., Jacobsen, S.E., Bryder, D., and Nerlov, C. (2009). Hematopoietic stem cell expansion precedes the generation of committed myeloid leukemia-initiating cells in C/EBPalpha mutant AML. Cancer Cell *16*, 390-400.

Beri-Dexheimer, M., Latger-Cannard, V., Philippe, C., Bonnet, C., Chambon, P., Roth, V., Gregoire, M.J., Bordigoni, P., Lecompte, T., Leheup, B.*, et al.* (2008). Clinical phenotype of germline RUNX1 haploinsufficiency: from point mutations to large genomic deletions. Eur J Hum Genet *16*, 1014-1018.

Bernstein, B.E., Mikkelsen, T.S., Xie, X., Kamal, M., Huebert, D.J., Cuff, J., Fry, B., Meissner, A., Wernig, M., Plath, K.*, et al.* (2006). A bivalent chromatin structure marks key developmental genes in embryonic stem cells. Cell *125*, 315-326.

Bertolino, E., Reimund, B., Wildt-Perinic, D., and Clerc, R.G. (1995). A novel homeobox protein which recognizes a TGT core and functionally interferes with a retinoid-responsive motif. J Biol Chem *270*, 31178-31188.

Bevington, S.L., Cauchy, P., Piper, J., Bertrand, E., Lalli, N., Jarvis, R.C., Gilding, L.N., Ott, S., Bonifer, C., and Cockerill, P.N. (2016). Inducible chromatin priming is associated with the establishment of immunological memory in T cells. EMBO J *35*, 515-535.

Biddie, S.C., John, S., Sabo, P.J., Thurman, R.E., Johnson, T.A., Schiltz, R.L., Miranda, T.B., Sung, M.H., Trump, S., Lightman, S.L.*, et al.* (2011). Transcription factor AP1 potentiates chromatin accessibility and glucocorticoid receptor binding. Mol Cell *43*, 145-155.

Bindea, G., Mlecnik, B., Hackl, H., Charoentong, P., Tosolini, M., Kirilovsky, A., Fridman, W.H., Pages, F., Trajanoski, Z., and Galon, J. (2009). ClueGO: a Cytoscape plug-in to decipher functionally grouped gene ontology and pathway annotation networks. Bioinformatics *25*, 1091-1093.

Biondi, A., Cimino, G., Pieters, R., and Pui, C.H. (2000). Biological and therapeutic aspects of infant leukemia. Blood *96*, 24-33.

Blair, A., Hogge, D.E., Ailles, L.E., Lansdorp, P.M., and Sutherland, H.J. (1997). Lack of expression of Thy-1 (CD90) on acute myeloid leukemia cells with long-term proliferative ability in vitro and in vivo. Blood *89*, 3104-3112.

Blom, B., and Spits, H. (2006). Development of human lymphoid cells. Annu Rev Immunol *24*, 287-320.

Blomquist, P., Li, Q., and Wrange, O. (1996). The affinity of nuclear factor 1 for its DNA site is drastically reduced by nucleosome organization irrespective of its rotational or translational position. J Biol Chem *271*, 153-159.

Boisset, J.C., van Cappellen, W., Andrieu-Soler, C., Galjart, N., Dzierzak, E., and Robin, C. (2010). In vivo imaging of haematopoietic cells emerging from the mouse aortic endothelium. Nature *464*, 116-120.

Bolger, A.M., Lohse, M., and Usadel, B. (2014). Trimmomatic: a flexible trimmer for Illumina sequence data. Bioinformatics *30*, 2114-2120.

Bonifer, C., and Bowen, D.T. (2010). Epigenetic mechanisms regulating normal and malignant haematopoiesis: new therapeutic targets for clinical medicine. Expert Rev Mol Med *12*, e6.

Bonnet, D., and Dick, J.E. (1997). Human acute myeloid leukemia is organized as a hierarchy that originates from a primitive hematopoietic cell. Nat Med *3*, 730-737.

Boyle, A.P., Davis, S., Shulha, H.P., Meltzer, P., Margulies, E.H., Weng, Z., Furey, T.S., and Crawford, G.E. (2008). High-resolution mapping and characterization of open chromatin across the genome. Cell *132*, 311-322.

Brand, A.H., Breeden, L., Abraham, J., Sternglanz, R., and Nasmyth, K. (1985). Characterization of a "silencer" in yeast: a DNA sequence with properties opposite to those of a transcriptional enhancer. Cell *41*, 41-48.

Broad, D. (2020). Depmap achilles 20q1 public (Cambridge, MA: Broad Institute).

Budram-Mahadeo, V., Morris, P.J., and Latchman, D.S. (2002). The Brn-3a transcription factor inhibits the pro-apoptotic effect of p53 and enhances cell cycle arrest by differentially regulating the activity of the p53 target genes encoding Bax and p21(CIP1/Waf1). Oncogene *21*, 6123-6131.

Buenrostro, J.D., Giresi, P.G., Zaba, L.C., Chang, H.Y., and Greenleaf, W.J. (2013). Transposition of native chromatin for fast and sensitive epigenomic profiling of open chromatin, DNA-binding proteins and nucleosome position. Nat Methods *10*, 1213-1218.

Buenrostro, J.D., Wu, B., Chang, H.Y., and Greenleaf, W.J. (2015). ATAC-seq: A Method for Assaying Chromatin Accessibility Genome-Wide. Curr Protoc Mol Biol *109*, 21 29 21-21 29 29.

Bulger, M., and Groudine, M. (1999). Looping versus linking: toward a model for long-distance gene activation. Genes Dev *13*, 2465-2477.

Burglin, T.R. (1997). Analysis of TALE superclass homeobox genes (MEIS, PBC, KNOX, Iroquois, TGIF) reveals a novel domain conserved between plants and animals. Nucleic Acids Res *25*, 4173-4180.

Busque, L., Patel, J.P., Figueroa, M.E., Vasanthakumar, A., Provost, S., Hamilou, Z., Mollica, L., Li, J., Viale, A., Heguy, A.*, et al.* (2012). Recurrent somatic TET2 mutations in normal elderly individuals with clonal hematopoiesis. Nat Genet *44*, 1179-1181.

Bussmann, L.H., Schubert, A., Vu Manh, T.P., De Andres, L., Desbordes, S.C., Parra, M., Zimmermann, T., Rapino, F., Rodriguez-Ubreva, J., Ballestar, E.*, et al.* (2009). A robust and highly efficient immune cell reprogramming system. Cell Stem Cell *5*, 554-566.

Buteyn, N.J., Santhanam, R., Merchand-Reyes, G., Murugesan, R.A., Dettorre, G.M., Byrd, J.C., Sarkar, A., Vasu, S., Mundy-Bosse, B.L., Butchar, J.P.*, et al.* (2020). Activation of the Intracellular Pattern Recognition Receptor NOD2 Promotes Acute Myeloid Leukemia (AML) Cell Apoptosis and Provides a Survival Advantage in an Animal Model of AML. J Immunol *204*, 1988-1997.

Cai, D.H., Wang, D., Keefer, J., Yeamans, C., Hensley, K., and Friedman, A.D. (2008). C/EBP alpha:AP-1 leucine zipper heterodimers bind novel DNA elements, activate the PU.1 promoter and direct monocyte lineage commitment more potently than C/EBP alpha homodimers or AP-1. Oncogene *27*, 2772-2779.

Calvanese, V., Nguyen, A.T., Bolan, T.J., Vavilina, A., Su, T., Lee, L.K., Wang, Y., Lay, F.D., Magnusson, M., Crooks, G.M.*, et al.* (2019). MLLT3 governs human haematopoietic stem-cell self-renewal and engraftment. Nature *576*, 281-286.

Cancer Genome Atlas Research, N., Ley, T.J., Miller, C., Ding, L., Raphael, B.J., Mungall, A.J., Robertson, A., Hoadley, K., Triche, T.J., Jr., Laird, P.W.*, et al.* (2013). Genomic and epigenomic landscapes of adult de novo acute myeloid leukemia. N Engl J Med *368*, 2059-2074.

Castilla, L.H., Garrett, L., Adya, N., Orlic, D., Dutra, A., Anderson, S., Owens, J., Eckhaus, M., Bodine, D., and Liu, P.P. (1999). The fusion gene Cbfb-MYH11 blocks myeloid differentiation and predisposes mice to acute myelomonocytic leukaemia. Nat Genet *23*, 144-146.

Castilla, L.H., Perrat, P., Martinez, N.J., Landrette, S.F., Keys, R., Oikemus, S., Flanegan, J., Heilman, S., Garrett, L., Dutra, A.*, et al.* (2004). Identification of genes that synergize with Cbfb-MYH11 in the pathogenesis of acute myeloid leukemia. Proc Natl Acad Sci U S A *101*, 4924-4929.

Castilla, L.H., Wijmenga, C., Wang, Q., Stacy, T., Speck, N.A., Eckhaus, M., Marin-Padilla, M., Collins, F.S., Wynshaw-Boris, A., and Liu, P.P. (1996). Failure of embryonic hematopoiesis and lethal hemorrhages in mouse embryos heterozygous for a knocked-in leukemia gene CBFB-MYH11. Cell *87*, 687-696.

Chen, F., Kook, H., Milewski, R., Gitler, A.D., Lu, M.M., Li, J., Nazarian, R., Schnepp, R., Jen, K., Biben, C.*, et al.* (2002). Hop is an unusual homeobox gene that modulates cardiac development. Cell *110*, 713-723.

Chen, L., and Widom, J. (2005). Mechanism of transcriptional silencing in yeast. Cell *120*, 37-48.

Chen, M.J., Yokomizo, T., Zeigler, B.M., Dzierzak, E., and Speck, N.A. (2009). Runx1 is required for the endothelial to haematopoietic cell transition but not thereafter. Nature *457*, 887-891.

Cheng, J.T., Hsu, H.L., Hwang, L.Y., and Baer, R. (1993). Products of the TAL1 oncogene: basic helix-loop-helix proteins phosphorylated at serine residues. Oncogene *8*, 677-683.

Chiariello, M., Marinissen, M.J., and Gutkind, J.S. (2000). Multiple mitogen-activated protein kinase signaling pathways connect the cot oncoprotein to the c-jun promoter and to cellular transformation. Mol Cell Biol *20*, 1747-1758.

Chinenov, Y., and Kerppola, T.K. (2001). Close encounters of many kinds: Fos-Jun interactions that mediate transcription regulatory specificity. Oncogene *20*, 2438-2452.

Choi, Y., Elagib, K.E., Delehanty, L.L., and Goldfarb, A.N. (2006). Erythroid inhibition by the leukemic fusion AML1-ETO is associated with impaired acetylation of the major erythroid transcription factor GATA-1. Cancer Res *66*, 2990-2996.

Chorzalska, A., Ahsan, N., Rao, R.S.P., Roder, K., Yu, X., Morgan, J., Tepper, A., Hines, S., Zhang, P., Treaba, D.O.*, et al.* (2018). Overexpression of Tpl2 is linked to imatinib resistance and activation of MEK-ERK and NF-kappaB pathways in a model of chronic myeloid leukemia. Mol Oncol *12*, 630-647.

Chou, F.S., Wunderlich, M., Griesinger, A., and Mulloy, J.C. (2011). N-Ras(G12D) induces features of stepwise transformation in preleukemic human umbilical cord blood cultures expressing the AML1-ETO fusion gene. Blood *117*, 2237-2240.

Christen, F., Hoyer, K., Yoshida, K., Hou, H.A., Waldhueter, N., Heuser, M., Hills, R.K., Chan, W., Hablesreiter, R., Blau, O.*, et al.* (2019). Genomic landscape and clonal evolution of acute myeloid leukemia with t(8;21): an international study on 331 patients. Blood *133*, 1140-1151.

Chung, J.H., Whiteley, M., and Felsenfeld, G. (1993). A 5' element of the chicken beta-globin domain serves as an insulator in human erythroid cells and protects against position effect in Drosophila. Cell *74*, 505-514.

Cirillo, L.A., Lin, F.R., Cuesta, I., Friedman, D., Jarnik, M., and Zaret, K.S. (2002). Opening of compacted chromatin by early developmental transcription factors HNF3 (FoxA) and GATA-4. Mol Cell *9*, 279-289.

Cleaves, R., Wang, Q.F., and Friedman, A.D. (2004). C/EBPalphap30, a myeloid leukemia oncoprotein, limits G-CSF receptor expression but not terminal granulopoiesis via site-selective inhibition of C/EBP DNA binding. Oncogene *23*, 716-725.

Cockerill, P.N. (2011). Structure and function of active chromatin and DNase I hypersensitive sites. FEBS J *278*, 2182-2210.

Collins, C., Wang, J., Miao, H., Bronstein, J., Nawer, H., Xu, T., Figueroa, M., Muntean, A.G., and Hess, J.L. (2014). C/EBPalpha is an essential collaborator in Hoxa9/Meis1-mediated leukemogenesis. Proc Natl Acad Sci U S A *111*, 9899-9904.

Collombet, S., van Oevelen, C., Sardina Ortega, J.L., Abou-Jaoude, W., Di Stefano, B., Thomas-Chollier, M., Graf, T., and Thieffry, D. (2017). Logical modeling of lymphoid and myeloid cell specification and transdifferentiation. Proc Natl Acad Sci U S A *114*, 5792-5799.

Consortium, E.P. (2012). An integrated encyclopedia of DNA elements in the human genome. Nature *489*, 57-74.

Consortium, E.P., Birney, E., Stamatoyannopoulos, J.A., Dutta, A., Guigo, R., Gingeras, T.R., Margulies, E.H., Weng, Z., Snyder, M., Dermitzakis, E.T.*, et al.* (2007). Identification and analysis of functional elements in 1% of the human genome by the ENCODE pilot project. Nature *447*, 799-816.

Corces, M.R., Granja, J.M., Shams, S., Louie, B.H., Seoane, J.A., Zhou, W., Silva, T.C., Groeneveld, C., Wong, C.K., Cho, S.W.*, et al.* (2018). The chromatin accessibility landscape of primary human cancers. Science *362*.

Corces, M.R., Trevino, A.E., Hamilton, E.G., Greenside, P.G., Sinnott-Armstrong, N.A., Vesuna, S., Satpathy, A.T., Rubin, A.J., Montine, K.S., Wu, B.*, et al.* (2017). An improved ATAC-seq protocol reduces background and enables interrogation of frozen tissues. Nat Methods *14*, 959-962.

Corces-Zimmerman, M.R., Hong, W.J., Weissman, I.L., Medeiros, B.C., and Majeti, R. (2014). Preleukemic mutations in human acute myeloid leukemia affect epigenetic regulators and persist in remission. Proc Natl Acad Sci U S A *111*, 2548-2553.

Cozzio, A., Passegue, E., Ayton, P.M., Karsunky, H., Cleary, M.L., and Weissman, I.L. (2003). Similar MLL-associated leukemias arising from self-renewing stem cells and short-lived myeloid progenitors. Genes Dev *17*, 3029-3035.

Creyghton, M.P., Cheng, A.W., Welstead, G.G., Kooistra, T., Carey, B.W., Steine, E.J., Hanna, J., Lodato, M.A., Frampton, G.M., Sharp, P.A.*, et al.* (2010). Histone H3K27ac separates active from poised enhancers and predicts developmental state. Proc Natl Acad Sci U S A *107*, 21931-21936.

Cuddapah, S., Jothi, R., Schones, D.E., Roh, T.Y., Cui, K., and Zhao, K. (2009). Global analysis of the insulator binding protein CTCF in chromatin barrier regions reveals demarcation of active and repressive domains. Genome Res *19*, 24-32.

D'Alo, F., Johansen, L.M., Nelson, E.A., Radomska, H.S., Evans, E.K., Zhang, P., Nerlov, C., and Tenen, D.G. (2003). The amino terminal and E2F interaction domains are critical for C/EBP alpha-mediated induction of granulopoietic development of hematopoietic cells. Blood *102*, 3163-3171.

Davis, R.R., Campbell, M., Izumiya, Y., and Tepper, C.G. (2020). Chapter Twenty-One - Capture Hi-C: Characterization of chromatin contacts. In Epigenetics Methods, T. Tollefsbol, ed. (Academic Press), pp. 419-444.

Deaton, A.M., and Bird, A. (2011). CpG islands and the regulation of transcription. Genes Dev *25*, 1010-1022.

Dekker, J., Rippe, K., Dekker, M., and Kleckner, N. (2002). Capturing chromosome conformation. Science *295*, 1306-1311.

Dick, J.E. (2008). Stem cell concepts renew cancer research. Blood *112*, 4793-4807.

Diss, J.K., Faulkes, D.J., Walker, M.M., Patel, A., Foster, C.S., Budhram-Mahadeo, V., Djamgoz, M.B., and Latchman, D.S. (2006). Brn-3a neuronal transcription factor functional expression in human prostate cancer. Prostate Cancer Prostatic Dis *9*, 83-91.

Dixon, J.R., Selvaraj, S., Yue, F., Kim, A., Li, Y., Shen, Y., Hu, M., Liu, J.S., and Ren, B. (2012). Topological domains in mammalian genomes identified by analysis of chromatin interactions. Nature *485*, 376-380.

Dogan, N., Wu, W., Morrissey, C.S., Chen, K.B., Stonestrom, A., Long, M., Keller, C.A., Cheng, Y., Jain, D., Visel, A.*, et al.* (2015). Occupancy by key transcription factors is a more accurate predictor of enhancer activity than histone modifications or chromatin accessibility. Epigenetics Chromatin *8*, 16.

Dohner, H., Weisdorf, D.J., and Bloomfield, C.D. (2015). Acute Myeloid Leukemia. N Engl J Med *373*, 1136-1152.

Doni Jayavelu, N., Jajodia, A., Mishra, A., and Hawkins, R.D. (2020). Candidate silencer elements for the human and mouse genomes. Nat Commun *11*, 1061.

Dorigo, B., Schalch, T., Bystricky, K., and Richmond, T.J. (2003). Chromatin fiber folding: requirement for the histone H4 N-terminal tail. J Mol Biol *327*, 85-96.

Downing, J.R., Head, D.R., Curcio-Brint, A.M., Hulshof, M.G., Motroni, T.A., Raimondi, S.C., Carroll, A.J., Drabkin, H.A., Willman, C., Theil, K.S.*, et al.* (1993). An AML1/ETO fusion transcript is consistently detected by RNA-based polymerase chain reaction in acute myelogenous leukemia containing the (8;21)(q22;q22) translocation. Blood *81*, 2860-2865.

Dufour, A., Schneider, F., Metzeler, K.H., Hoster, E., Schneider, S., Zellmeier, E., Benthaus, T., Sauerland, M.C., Berdel, W.E., Buchner, T.*, et al.* (2010). Acute myeloid leukemia with biallelic CEBPA gene mutations and normal karyotype represents a distinct genetic entity associated with a favorable clinical outcome. J Clin Oncol *28*, 570-577.

Dunne, J., Gascoyne, D.M., Lister, T.A., Brady, H.J., Heidenreich, O., and Young, B.D. (2010). AML1/ETO proteins control POU4F1/BRN3A expression and function in t(8;21) acute myeloid leukemia. Cancer Res *70*, 3985-3995.

Dunne, J., Mannari, D., Farzaneh, T., Gessner, A., van Delft, F.W., Heidenreich, O., Young, B.D., and Gascoyne, D.M. (2012). AML1/ETO and POU4F1 synergy drives B-lymphoid gene expression typical of t(8;21) acute myeloid leukemia. Leukemia *26*, 1131-1135.

Dynlacht, B.D. (1997). Regulation of transcription by proteins that control the cell cycle. Nature *389*, 149-152.

Edginton-White, B., and Bonifer, C. (2022). The transcriptional regulation of normal and malignant blood cell development. FEBS J *289*, 1240-1255.

Fasan, A., Haferlach, C., Alpermann, T., Jeromin, S., Grossmann, V., Eder, C., Weissmann, S., Dicker, F., Kohlmann, A., Schindela, S.*, et al.* (2014). The role of different genetic subtypes of CEBPA mutated AML. Leukemia *28*, 794-803.

Fathi, A.T., and Abdel-Wahab, O. (2012). Mutations in epigenetic modifiers in myeloid malignancies and the prospect of novel epigenetic-targeted therapy. Adv Hematol *2012*, 469592.

Ferrando, A.A., Herblot, S., Palomero, T., Hansen, M., Hoang, T., Fox, E.A., and Look, A.T. (2004). Biallelic transcriptional activation of oncogenic transcription factors in T-cell acute lymphoblastic leukemia. Blood *103*, 1909-1911.

Ferrari, K.J., Scelfo, A., Jammula, S., Cuomo, A., Barozzi, I., Stutzer, A., Fischle, W., Bonaldi, T., and Pasini, D. (2014). Polycomb-dependent H3K27me1 and H3K27me2 regulate active transcription and enhancer fidelity. Mol Cell *53*, 49-62.

Ferretti, E., Di Carlo, E., Cocco, C., Ribatti, D., Sorrentino, C., Ognio, E., Montagna, D., Pistoia, V., and Airoldi, I. (2010). Direct inhibition of human acute myeloid leukemia cell growth by IL-12. Immunol Lett *133*, 99-105.

Fink, M., Imholz, D., and Thoma, F. (2007). Contribution of the serine 129 of histone H2A to chromatin structure. Mol Cell Biol *27*, 3589-3600.

Fortier, J.M., Payton, J.E., Cahan, P., Ley, T.J., Walter, M.J., and Graubert, T.A. (2010). POU4F1 is associated with t(8;21) acute myeloid leukemia and contributes directly to its unique transcriptional signature. Leukemia *24*, 950-957.

Friedman, A.D. (2007). Transcriptional control of granulocyte and monocyte development. Oncogene *26*, 6816-6828.

Friedman, A.D. (2015). C/EBPalpha in normal and malignant myelopoiesis. Int J Hematol *101*, 330-341.

Frohling, S., Scholl, C., Gilliland, D.G., and Levine, R.L. (2005). Genetics of myeloid malignancies: pathogenetic and clinical implications. J Clin Oncol *23*, 6285-6295.

Fu, S., Fu, Y., Chen, F., Hu, Y., Quan, B., and Zhang, J. (2018). Overexpression of MYCT1 Inhibits Proliferation and Induces Apoptosis in Human Acute Myeloid Leukemia HL-60 and KG-1a Cells in vitro and in vivo. Front Pharmacol *9*, 1045.

Fu, S., Guo, Y., Chen, H., Xu, Z.M., Qiu, G.B., Zhong, M., Sun, K.L., and Fu, W.N. (2011). MYCT1-TV, a novel MYCT1 transcript, is regulated by c-Myc and may participate in laryngeal carcinogenesis. PLoS One *6*, e25648.

Fujimoto, T., Anderson, K., Jacobsen, S.E., Nishikawa, S.I., and Nerlov, C. (2007). Cdk6 blocks myeloid differentiation by interfering with Runx1 DNA binding and Runx1-C/EBPalpha interaction. EMBO J *26*, 2361-2370.

Fujita, Y., Nishimura, M., Taniwaki, M., Abe, T., and Okuda, T. (2001). Identification of an alternatively spliced form of the mouse AML1/RUNX1 gene transcript AML1c and its expression in early hematopoietic development. Biochem Biophys Res Commun *281*, 1248-1255.

Gaidzik, V.I., Teleanu, V., Papaemmanuil, E., Weber, D., Paschka, P., Hahn, J., Wallrabenstein, T., Kolbinger, B., Kohne, C.H., Horst, H.A.*, et al.* (2016). RUNX1 mutations in acute myeloid leukemia are associated with distinct clinico-pathologic and genetic features. Leukemia *30*, 2282.

Galas, D.J., and Schmitz, A. (1978). DNAse footprinting: a simple method for the detection of protein-DNA binding specificity. Nucleic Acids Res *5*, 3157-3170.

Gao, Y., Chen, L., Han, Y., Wu, F., Yang, W.S., Zhang, Z., Huo, T., Zhu, Y., Yu, C., Kim, H.*, et al.* (2020). Acetylation of histone H3K27 signals the transcriptional elongation for estrogen receptor alpha. Commun Biol *3*, 165.

Geiger, J.H., Hahn, S., Lee, S., and Sigler, P.B. (1996). Crystal structure of the yeast TFIIA/TBP/DNA complex. Science *272*, 830-836.

Gelmetti, V., Zhang, J., Fanelli, M., Minucci, S., Pelicci, P.G., and Lazar, M.A. (1998). Aberrant recruitment of the nuclear receptor corepressor-histone deacetylase complex by the acute myeloid leukemia fusion partner ETO. Mol Cell Biol *18*, 7185-7191.

Genovese, G., Kahler, A.K., Handsaker, R.E., Lindberg, J., Rose, S.A., Bakhoum, S.F., Chambert, K., Mick, E., Neale, B.M., Fromer, M.*, et al.* (2014). Clonal hematopoiesis and blood-cancer risk inferred from blood DNA sequence. N Engl J Med *371*, 2477-2487.

Gentle, I.E., Moelter, I., Badr, M.T., Dohner, K., Lubbert, M., and Hacker, G. (2021). The AML-associated K313 mutation enhances C/EBPalpha activity by leading to C/EBPalpha overexpression. Cell Death Dis *12*, 675.

Gentles, A.J., Plevritis, S.K., Majeti, R., and Alizadeh, A.A. (2010). Association of a leukemic stem cell gene expression signature with clinical outcomes in acute myeloid leukemia. JAMA *304*, 2706-2715.

Gerby, B., Clappier, E., Armstrong, F., Deswarte, C., Calvo, J., Poglio, S., Soulier, J., Boissel, N., Leblanc, T., Baruchel, A.*, et al.* (2011). Expression of CD34 and CD7 on human T-cell acute lymphoblastic leukemia discriminates functionally heterogeneous cell populations. Leukemia *25*, 1249-1258.

Ghozi, M.C., Bernstein, Y., Negreanu, V., Levanon, D., and Groner, Y. (1996). Expression of the human acute myeloid leukemia gene AML1 is regulated by two promoter regions. Proc Natl Acad Sci U S A *93*, 1935-1940.

Gilliland, D.G., and Griffin, J.D. (2002). The roles of FLT3 in hematopoiesis and leukemia. Blood *100*, 1532-1542.

Goardon, N., Marchi, E., Atzberger, A., Quek, L., Schuh, A., Soneji, S., Woll, P., Mead, A., Alford, K.A., Rout, R.*, et al.* (2011). Coexistence of LMPP-like and GMP-like leukemia stem cells in acute myeloid leukemia. Cancer Cell *19*, 138-152.

Gombart, A.F., Grewal, J., and Koeffler, H.P. (2007). ATF4 differentially regulates transcriptional activation of myeloid-specific genes by C/EBPepsilon and C/EBPalpha. J Leukoc Biol *81*, 1535-1547.

Goyama, S., Schibler, J., Cunningham, L., Zhang, Y., Rao, Y., Nishimoto, N., Nakagawa, M., Olsson, A., Wunderlich, M., Link, K.A.*, et al.* (2013). Transcription factor RUNX1 promotes survival of acute myeloid leukemia cells. J Clin Invest *123*, 3876-3888.

Grass, J.A., Boyer, M.E., Pal, S., Wu, J., Weiss, M.J., and Bresnick, E.H. (2003). GATA-1-dependent transcriptional repression of GATA-2 via disruption of positive autoregulation and domain-wide chromatin remodeling. Proc Natl Acad Sci U S A *100*, 8811-8816.

Greif, P.A., Dufour, A., Konstandin, N.P., Ksienzyk, B., Zellmeier, E., Tizazu, B., Sturm, J., Benthaus, T., Herold, T., Yaghmaie, M.*, et al.* (2012a). GATA2 zinc finger 1 mutations associated with biallelic CEBPA mutations define a unique genetic entity of acute myeloid leukemia. Blood *120*, 395-403.

Greif, P.A., Konstandin, N.P., Metzeler, K.H., Herold, T., Pasalic, Z., Ksienzyk, B., Dufour, A., Schneider, F., Schneider, S., Kakadia, P.M.*, et al.* (2012b). RUNX1 mutations in cytogenetically normal acute myeloid leukemia are associated with a poor prognosis and up-regulation of lymphoid genes. Haematologica *97*, 1909-1915.

Groschel, S., Sanders, M.A., Hoogenboezem, R., de Wit, E., Bouwman, B.A.M., Erpelinck, C., van der Velden, V.H.J., Havermans, M., Avellino, R., van Lom, K.*, et al.* (2014). A single oncogenic enhancer rearrangement causes concomitant EVI1 and GATA2 deregulation in leukemia. Cell *157*, 369-381.

Grossmann, V., Haferlach, C., Nadarajah, N., Fasan, A., Weissmann, S., Roller, A., Eder, C., Stopp, E., Kern, W., Haferlach, T.*, et al.* (2013). CEBPA double-mutated acute myeloid leukaemia harbours concomitant molecular mutations in 76.8% of cases with TET2 and GATA2 alterations impacting prognosis. Br J Haematol *161*, 649-658.

Guan, Y., Gerhard, B., and Hogge, D.E. (2003). Detection, isolation, and stimulation of quiescent primitive leukemic progenitor cells from patients with acute myeloid leukemia (AML). Blood *101*, 3142-3149.

Guo, H., Ma, O., Speck, N.A., and Friedman, A.D. (2012). Runx1 deletion or dominant inhibition reduces Cebpa transcription via conserved promoter and distal enhancer sites to favor monopoiesis over granulopoiesis. Blood *119*, 4408-4418.

Gyan, E., Frew, M., Bowen, D., Beldjord, C., Preudhomme, C., Lacombe, C., Mayeux, P., Dreyfus, F., Porteu, F., and Fontenay, M. (2005). Mutation in RAP1 is a rare event in myelodysplastic syndromes. Leukemia *19*, 1678-1680.

Hahn, S. (2004). Structure and mechanism of the RNA polymerase II transcription machinery. Nat Struct Mol Biol *11*, 394-403.

Hai, T., and Curran, T. (1991). Cross-family dimerization of transcription factors Fos/Jun and ATF/CREB alters DNA binding specificity. Proc Natl Acad Sci U S A *88*, 3720-3724.

Hamid, R., and Brandt, S.J. (2009). Transforming growth-interacting factor (TGIF) regulates proliferation and differentiation of human myeloid leukemia cells. Mol Oncol *3*, 451-463.

Harada, H., Harada, Y., Niimi, H., Kyo, T., Kimura, A., and Inaba, T. (2004). High incidence of somatic mutations in the AML1/RUNX1 gene in myelodysplastic syndrome and low blast percentage myeloid leukemia with myelodysplasia. Blood *103*, 2316-2324.

Hargreaves, D.C., and Crabtree, G.R. (2011). ATP-dependent chromatin remodeling: genetics, genomics and mechanisms. Cell Res *21*, 396-420.

Hasemann, M.S., Lauridsen, F.K., Waage, J., Jakobsen, J.S., Frank, A.K., Schuster, M.B., Rapin, N., Bagger, F.O., Hoppe, P.S., Schroeder, T.*, et al.* (2014). C/EBPalpha is required for long-term self-renewal and lineage priming of hematopoietic stem cells and for the maintenance of epigenetic configurations in multipotent progenitors. PLoS Genet *10*, e1004079.

Heintzman, N.D., Stuart, R.K., Hon, G., Fu, Y., Ching, C.W., Hawkins, R.D., Barrera, L.O., Van Calcar, S., Qu, C., Ching, K.A.*, et al.* (2007). Distinct and predictive chromatin signatures of transcriptional promoters and enhancers in the human genome. Nat Genet *39*, 311-318.

Heinz, S., Benner, C., Spann, N., Bertolino, E., Lin, Y.C., Laslo, P., Cheng, J.X., Murre, C., Singh, H., and Glass, C.K. (2010). Simple combinations of lineage-determining transcription factors prime cis-regulatory elements required for macrophage and B cell identities. Mol Cell *38*, 576-589.

Hesselberth, J.R., Chen, X., Zhang, Z., Sabo, P.J., Sandstrom, R., Reynolds, A.P., Thurman, R.E., Neph, S., Kuehn, M.S., Noble, W.S.*, et al.* (2009). Global mapping of protein-DNA interactions in vivo by digital genomic footprinting. Nat Methods *6*, 283-289.

Heyes, E., Schmidt, L., Manhart, G., Eder, T., Proietti, L., and Grebien, F. (2021). Identification of gene targets of mutant C/EBPalpha reveals a critical role for MSI2 in CEBPA-mutated AML. Leukemia *35*, 2526-2538.

Hirai, H., Zhang, P., Dayaram, T., Hetherington, C.J., Mizuno, S., Imanishi, J., Akashi, K., and Tenen, D.G. (2006). C/EBPbeta is required for 'emergency' granulopoiesis. Nat Immunol *7*, 732-739.

Hirsch, P., Zhang, Y., Tang, R., Joulin, V., Boutroux, H., Pronier, E., Moatti, H., Flandrin, P., Marzac, C., Bories, D.*, et al.* (2016). Genetic hierarchy and temporal variegation in the clonal history of acute myeloid leukaemia. Nat Commun *7*, 12475.

Hohaus, S., Petrovick, M.S., Voso, M.T., Sun, Z., Zhang, D.E., and Tenen, D.G. (1995). PU.1 (Spi-1) and C/EBP alpha regulate expression of the granulocyte-macrophage colony-stimulating factor receptor alpha gene. Mol Cell Biol *15*, 5830-5845.

Hohenauer, T., Berking, C., Schmidt, A., Haferkamp, S., Senft, D., Kammerbauer, C., Fraschka, S., Graf, S.A., Irmler, M., Beckers, J.*, et al.* (2013). The neural crest transcription factor Brn3a is expressed in melanoma and required for cell cycle progression and survival. EMBO Mol Med *5*, 919-934.

Hong, S., Skaist, A.M., Wheelan, S.J., and Friedman, A.D. (2011). AP-1 protein induction during monopoiesis favors C/EBP: AP-1 heterodimers over C/EBP homodimerization and stimulates FosB transcription. J Leukoc Biol *90*, 643-651.

Hoogenkamp, M., Krysinska, H., Ingram, R., Huang, G., Barlow, R., Clarke, D., Ebralidze, A., Zhang, P., Tagoh, H., Cockerill, P.N.*, et al.* (2007). The Pu.1 locus is differentially regulated at the level of chromatin structure and noncoding transcription by alternate mechanisms at distinct developmental stages of hematopoiesis. Mol Cell Biol *27*, 7425-7438.

Horikoshi, M., Hai, T., Lin, Y.S., Green, M.R., and Roeder, R.G. (1988). Transcription factor ATF interacts with the TATA factor to facilitate establishment of a preinitiation complex. Cell *54*, 1033-1042.

Howe, K.L., Achuthan, P., Allen, J., Allen, J., Alvarez-Jarreta, J., Amode, M.R., Armean, I.M., Azov, A.G., Bennett, R., Bhai, J.*, et al.* (2021). Ensembl 2021. Nucleic Acids Res *49*, D884-D891.

Hsu, W., Kerppola, T.K., Chen, P.L., Curran, T., and Chen-Kiang, S. (1994). Fos and Jun repress transcription activation by NF-IL6 through association at the basic zipper region. Mol Cell Biol *14*, 268-276.

Hu, Z., Gu, X., Baraoidan, K., Ibanez, V., Sharma, A., Kadkol, S., Munker, R., Ackerman, S., Nucifora, G., and Sauntharajah, Y. (2011). RUNX1 regulates corepressor interactions of PU.1. Blood *117*, 6498-6508.

Huber, H.E., Edwards, G., Goodhart, P.J., Patrick, D.R., Huang, P.S., Ivey-Hoyle, M., Barnett, S.F., Oliff, A., and Heimbrook, D.C. (1993). Transcription factor E2F binds DNA as a heterodimer. Proc Natl Acad Sci U S A *90*, 3525-3529.

Illendula, A., Gilmour, J., Grembecka, J., Tirumala, V.S.S., Boulton, A., Kuntimaddi, A., Schmidt, C., Wang, L., Pulikkan, J.A., Zong, H.*, et al.* (2016). Small Molecule Inhibitor of CBFbeta-RUNX Binding for RUNX Transcription Factor Driven Cancers. EBioMedicine *8*, 117-131.

Imperato, M.R., Cauchy, P., Obier, N., and Bonifer, C. (2015). The RUNX1-PU.1 axis in the control of hematopoiesis. Int J Hematol *101*, 319-329.

Irwin, M., Marin, M.C., Phillips, A.C., Seelan, R.S., Smith, D.I., Liu, W., Flores, E.R., Tsai, K.Y., Jacks, T., Vousden, K.H.*, et al.* (2000). Role for the p53 homologue p73 in E2F-1-induced apoptosis. Nature *407*, 645-648.

Ishii, N., Harada, N., Joseph, E.W., Ohara, K., Miura, T., Sakamoto, H., Matsuda, Y., Tomii, Y., Tachibana-Kondo, Y., Iikura, H.*, et al.* (2013). Enhanced inhibition of ERK signaling by a novel allosteric MEK inhibitor, CH5126766, that suppresses feedback reactivation of RAF activity. Cancer Res *73*, 4050-4060.

Ishikawa, F., Yoshida, S., Saito, Y., Hijikata, A., Kitamura, H., Tanaka, S., Nakamura, R., Tanaka, T., Tomiyama, H., Saito, N.*, et al.* (2007). Chemotherapy-resistant human AML stem cells home to and engraft within the bone-marrow endosteal region. Nat Biotechnol *25*, 1315-1321.

Ishikawa, Y., Kawashima, N., Atsuta, Y., Sugiura, I., Sawa, M., Dobashi, N., Yokoyama, H., Doki, N., Tomita, A., Kiguchi, T.*, et al.* (2020). Prospective evaluation of prognostic impact of KIT mutations on acute myeloid leukemia with RUNX1-RUNX1T1 and CBFB-MYH11. Blood Adv *4*, 66-75.

Jacob, B., Osato, M., Yamashita, N., Wang, C.Q., Taniuchi, I., Littman, D.R., Asou, N., and Ito, Y. (2010). Stem cell exhaustion due to Runx1 deficiency is prevented by Evi5 activation in leukemogenesis. Blood *115*, 1610-1620.

Jaiswal, S., and Ebert, B.L. (2019). Clonal hematopoiesis in human aging and disease. Science *366*.

Jaiswal, S., Fontanillas, P., Flannick, J., Manning, A., Grauman, P.V., Mar, B.G., Lindsley, R.C., Mermel, C.H., Burtt, N., Chavez, A.*, et al.* (2014). Age-related clonal hematopoiesis associated with adverse outcomes. N Engl J Med *371*, 2488-2498.

Jakobsen, J.S., Laursen, L.G., Schuster, M.B., Pundhir, S., Schoof, E., Ge, Y., d'Altri, T., Vitting-Seerup, K., Rapin, N., Gentil, C.*, et al.* (2019). Mutant CEBPA directly drives the expression of the targetable tumor-promoting factor CD73 in AML. Sci Adv *5*, eaaw4304.

Jin, C., Zang, C., Wei, G., Cui, K., Peng, W., Zhao, K., and Felsenfeld, G. (2009). H3.3/H2A.Z double variant-containing nucleosomes mark 'nucleosome-free regions' of active promoters and other regulatory regions. Nat Genet *41*, 941-945.

Johnson, B.V., Bert, A.G., Ryan, G.R., Condina, A., and Cockerill, P.N. (2004). Granulocyte-macrophage colony-stimulating factor enhancer activation requires cooperation between NFAT and AP-1 elements and is associated with extensive nucleosome reorganization. Mol Cell Biol *24*, 7914-7930.

Johnson, D.S., Mortazavi, A., Myers, R.M., and Wold, B. (2007). Genome-wide mapping of in vivo protein-DNA interactions. Science *316*, 1497-1502.

Jolma, A., Yan, J., Whitington, T., Toivonen, J., Nitta, K.R., Rastas, P., Morgunova, E., Enge, M., Taipale, M., Wei, G.*, et al.* (2013). DNA-binding specificities of human transcription factors. Cell *152*, 327-339.

Jones, L.C., Lin, M.L., Chen, S.S., Krug, U., Hofmann, W.K., Lee, S., Lee, Y.H., and Koeffler, H.P. (2002). Expression of C/EBPbeta from the C/ebpalpha gene locus is sufficient for normal hematopoiesis in vivo. Blood *99*, 2032-2036.

Jordan, C.T., Guzman, M.L., and Noble, M. (2006). Cancer stem cells. N Engl J Med *355*, 1253-1261.

Kanno, Y., Kanno, T., Sakakura, C., Bae, S.C., and Ito, Y. (1998). Cytoplasmic sequestration of the polyomavirus enhancer binding protein 2 (PEBP2)/core binding factor alpha (CBFalpha) subunit by the leukemia-related PEBP2/CBFbeta-SMMHC fusion protein inhibits PEBP2/CBF-mediated transactivation. Mol Cell Biol *18*, 4252-4261.

Keegan, L., Gill, G., and Ptashne, M. (1986). Separation of DNA binding from the transcription-activating function of a eukaryotic regulatory protein. Science *231*, 699-704.

Kellaway, S., Chin, P.S., Barneh, F., Bonifer, C., and Heidenreich, O. (2020). t(8;21) Acute Myeloid Leukemia as a Paradigm for the Understanding of Leukemogenesis at the Level of Gene Regulation and Chromatin Programming. Cells *9*.

Kellaway, S.G., Keane, P., Edginton-White, B., Regha, K., Kennett, E., and Bonifer, C. (2021). Different mutant RUNX1 oncoproteins program alternate haematopoietic differentiation trajectories. Life Sci Alliance *4*.

Kelly, L.M., and Gilliland, D.G. (2002). Genetics of myeloid leukemias. Annu Rev Genomics Hum Genet *3*, 179-198.

Kent, W.J., Sugnet, C.W., Furey, T.S., Roskin, K.M., Pringle, T.H., Zahler, A.M., and Haussler, D. (2002). The human genome browser at UCSC. Genome Res *12*, 996-1006.

Kesarwani, M., Kincaid, Z., Gomaa, A., Huber, E., Rohrabaugh, S., Siddiqui, Z., Bouso, M.F., Latif, T., Xu, M., Komurov, K.*, et al.* (2017). Targeting c-FOS and DUSP1 abrogates intrinsic resistance to tyrosine-kinase inhibitor therapy in BCR-ABL-induced leukemia. Nat Med *23*, 472-482.

Kim, D., Langmead, B., and Salzberg, S.L. (2015). HISAT: a fast spliced aligner with low memory requirements. Nat Methods *12*, 357-360.

Kirstetter, P., Schuster, M.B., Bereshchenko, O., Moore, S., Dvinge, H., Kurz, E., Theilgaard-Monch, K., Mansson, R., Pedersen, T.A., Pabst, T.*, et al.* (2008). Modeling of C/EBPalpha mutant acute myeloid leukemia reveals a common expression signature of committed myeloid leukemia-initiating cells. Cancer Cell *13*, 299-310.

Klampfer, L., Zhang, J., Zelenetz, A.O., Uchida, H., and Nimer, S.D. (1996). The AML1/ETO fusion protein activates transcription of BCL-2. Proc Natl Acad Sci U S A *93*, 14059-14064.

Klemsz, M.J., and Maki, R.A. (1996). Activation of transcription by PU.1 requires both acidic and glutamine domains. Mol Cell Biol *16*, 390-397.

Klemsz, M.J., McKercher, S.R., Celada, A., Van Beveren, C., and Maki, R.A. (1990). The macrophage and B cell-specific transcription factor PU.1 is related to the ets oncogene. Cell *61*, 113-124.

Kodandapani, R., Pio, F., Ni, C.Z., Piccialli, G., Klemsz, M., McKercher, S., Maki, R.A., and Ely, K.R. (1996). A new pattern for helix-turn-helix recognition revealed by the PU.1 ETS-domain-DNA complex. Nature *380*, 456-460.

Kondo, M., Weissman, I.L., and Akashi, K. (1997). Identification of clonogenic common lymphoid progenitors in mouse bone marrow. Cell *91*, 661-672.

Konstandin, N.P., Pastore, F., Herold, T., Dufour, A., Rothenberg-Thurley, M., Hinrichsen, T., Ksienzyk, B., Tschuri, S., Schneider, S., Hoster, E.*, et al.* (2018). Genetic heterogeneity of cytogenetically normal AML with mutations of CEBPA. Blood Adv *2*, 2724-2731.

Kornberg, R.D. (1977). Structure of chromatin. Annu Rev Biochem *46*, 931-954.

Korotkevich, G., Sukhov, V., Budin, N., Shpak, B., Artyomov, M.N., and Sergushichev, A. (2021). Fast gene set enrichment analysis. bioRxiv, 060012.

Koschmieder, S., D'Alo, F., Radomska, H., Schoneich, C., Chang, J.S., Konopleva, M., Kobayashi, S., Levantini, E., Suh, N., Di Ruscio, A.*, et al.* (2007). CDDO induces granulocytic differentiation of myeloid leukemic blasts through translational up-regulation of p42 CCAAT enhancer binding protein alpha. Blood *110*, 3695-3705.

Koschmieder, S., Halmos, B., Levantini, E., and Tenen, D.G. (2009). Dysregulation of the C/EBPalpha differentiation pathway in human cancer. J Clin Oncol *27*, 619-628.

Krawczyk, E., Zolov, S.N., Huang, K., and Bonifant, C.L. (2019). T-cell Activity against AML Improved by Dual-Targeted T Cells Stimulated through T-cell and IL7 Receptors. Cancer Immunol Res *7*, 683-692.

Kucinski, I., Wilson, N.K., Hannah, R., Kinston, S.J., Cauchy, P., Lenaerts, A., Grosschedl, R., and Gottgens, B. (2020). Interactions between lineage-associated transcription factors govern haematopoietic progenitor states. EMBO J *39*, e104983.

Kvon, E.Z., Kazmar, T., Stampfel, G., Yanez-Cuna, J.O., Pagani, M., Schernhuber, K., Dickson, B.J., and Stark, A. (2014). Genome-scale functional characterization of Drosophila developmental enhancers in vivo. Nature *512*, 91-95.

Lambert, S.A., Jolma, A., Campitelli, L.F., Das, P.K., Yin, Y., Albu, M., Chen, X., Taipale, J., Hughes, T.R., and Weirauch, M.T. (2018). The Human Transcription Factors. Cell *175*, 598-599.

Lancrin, C., Sroczynska, P., Stephenson, C., Allen, T., Kouskoff, V., and Lacaud, G. (2009). The haemangioblast generates haematopoietic cells through a haemogenic endothelium stage. Nature *457*, 892-895.

Landschulz, W.H., Johnson, P.F., and McKnight, S.L. (1988). The leucine zipper: a hypothetical structure common to a new class of DNA binding proteins. Science *240*, 1759-1764.

Langmead, B., and Salzberg, S.L. (2012). Fast gapped-read alignment with Bowtie 2. Nat Methods *9*, 357-359.

Lapidot, T., Sirard, C., Vormoor, J., Murdoch, B., Hoang, T., Caceres-Cortes, J., Minden, M., Paterson, B., Caligiuri, M.A., and Dick, J.E. (1994). A cell initiating human acute myeloid leukaemia after transplantation into SCID mice. Nature *367*, 645-648.

Lavallee, V.P., Krosl, J., Lemieux, S., Boucher, G., Gendron, P., Pabst, C., Boivin, I., Marinier, A., Guidos, C.J., Meloche, S.*, et al.* (2016). Chemo-genomic interrogation of CEBPA mutated AML reveals recurrent CSF3R mutations and subgroup sensitivity to JAK inhibitors. Blood *127*, 3054-3061.

Law, C.W., Alhamdoosh, M., Su, S., Dong, X., Tian, L., Smyth, G.K., and Ritchie, M.E. (2016). RNA-seq analysis is easy as 1-2-3 with limma, Glimma and edgeR. F1000Res *5*.

Leroy, H., Roumier, C., Huyghe, P., Biggio, V., Fenaux, P., and Preudhomme, C. (2005). CEBPA point mutations in hematological malignancies. Leukemia *19*, 329-334.

Li, J., Mahata, B., Escobar, M., Goell, J., Wang, K., Khemka, P., and Hilton, I.B. (2021). Programmable human histone phosphorylation and gene activation using a CRISPR/Cas9-based chromatin kinase. Nat Commun *12*, 896.

Li, L.M., and Arnosti, D.N. (2011). Long- and short-range transcriptional repressors induce distinct chromatin states on repressed genes. Curr Biol *21*, 406-412.

Liang, G., Lin, J.C., Wei, V., Yoo, C., Cheng, J.C., Nguyen, C.T., Weisenberger, D.J., Egger, G., Takai, D., Gonzales, F.A.*, et al.* (2004). Distinct localization of histone H3 acetylation and H3-K4 methylation to the transcription start sites in the human genome. Proc Natl Acad Sci U S A *101*, 7357-7362.

Liao, Y., Smyth, G.K., and Shi, W. (2014). featureCounts: an efficient general purpose program for assigning sequence reads to genomic features. Bioinformatics *30*, 923-930.

Liddiard, K., Burnett, A.K., Darley, R.L., and Tonks, A. (2012). RUNX1-ETO deregulates the proliferation and growth factor responsiveness of human hematopoietic progenitor cells downstream of the myeloid transcription factor, MYCT1. Leukemia *26*, 177-179.

Lieberman-Aiden, E., van Berkum, N.L., Williams, L., Imakaev, M., Ragoczy, T., Telling, A., Amit, I., Lajoie, B.R., Sabo, P.J., Dorschner, M.O*., et al.* (2009). Comprehensive mapping of long-range interactions reveals folding principles of the human genome. Science *326*, 289-293.

Lin, F.T., MacDougald, O.A., Diehl, A.M., and Lane, M.D. (1993). A 30-kDa alternative translation product of the CCAAT/enhancer binding protein alpha message: transcriptional activator lacking antimitotic activity. Proc Natl Acad Sci U S A *90*, 9606-9610.

Lin, S., Ptasinska, A., Chen, X., Shrestha, M., Assi, S.A., Chin, P.S., Imperato, M.R., Aronow, B.J., Zhang, J., Weirauch, M.T*., et al.* (2017). A FOXO1-induced oncogenic network defines the AML1-ETO preleukemic program. Blood *130*, 1213-1222.

Liu, P., Tarle, S.A., Hajra, A., Claxton, D.F., Marlton, P., Freedman, M., Siciliano, M.J., and Collins, F.S. (1993). Fusion between transcription factor CBF beta/PEBP2 beta and a myosin heavy chain in acute myeloid leukemia. Science *261*, 1041-1044.

Loke, J., Assi, S.A., Imperato, M.R., Ptasinska, A., Cauchy, P., Grabovska, Y., Soria, N.M., Raghavan, M., Delwel, H.R., Cockerill, P.N*., et al.* (2017). RUNX1-ETO and RUNX1-EVI1 Differentially Reprogram the Chromatin Landscape in t(8;21) and t(3;21) AML. Cell Rep *19*, 1654-1668.

Loke, J., Chin, P.S., Keane, P., Pickin, A., Assi, S.A., Ptasinska, A., Imperato, M.R., Cockerill, P.N., and Bonifer, C. (2018). C/EBPalpha overrides epigenetic reprogramming by oncogenic transcription factors in acute myeloid leukemia. Blood Adv *2*, 271-284.

Lord, K.A., Abdollahi, A., Hoffman-Liebermann, B., and Liebermann, D.A. (1993). Proto-oncogenes of the fos/jun family of transcription factors are positive regulators of myeloid differentiation. Mol Cell Biol *13*, 841-851.

Louder, R.K., He, Y., Lopez-Blanco, J.R., Fang, J., Chacon, P., and Nogales, E. (2016). Structure of promoter-bound TFIID and model of human pre-initiation complex assembly. Nature *531*, 604-609.

Love, M.I., Huber, W., and Anders, S. (2014). Moderated estimation of fold change and dispersion for RNA-seq data with DESeq2. Genome Biol *15*, 550.

Luger, K., Dechassa, M.L., and Tremethick, D.J. (2012). New insights into nucleosome and chromatin structure: an ordered state or a disordered affair? Nat Rev Mol Cell Biol *13*, 436-447.

Luger, K., Mader, A.W., Richmond, R.K., Sargent, D.F., and Richmond, T.J. (1997). Crystal structure of the nucleosome core particle at 2.8 A resolution. Nature *389*, 251-260.

Lupianez, D.G., Spielmann, M., and Mundlos, S. (2016). Breaking TADs: How Alterations of Chromatin Domains Result in Disease. Trends Genet *32*, 225-237.

Lutterbach, B., Westendorf, J.J., Linggi, B., Patten, A., Moniwa, M., Davie, J.R., Huynh, K.D., Bardwell, V.J., Lavinsky, R.M., Rosenfeld, M.G.*, et al.* (1998). ETO, a target of t(8;21) in acute leukemia, interacts with the N-CoR and mSin3 corepressors. Mol Cell Biol *18*, 7176-7184.

Ma, O., Hong, S., Guo, H., Ghiaur, G., and Friedman, A.D. (2014). Granulopoiesis requires increased C/EBPalpha compared to monopoiesis, correlated with elevated Cebpa in immature G-CSF receptor versus M-CSF receptor expressing cells. PLoS One *9*, e95784.

Macaulay, I.C., Svensson, V., Labalette, C., Ferreira, L., Hamey, F., Voet, T., Teichmann, S.A., and Cvejic, A. (2016). Single-Cell RNA-Sequencing Reveals a Continuous Spectrum of Differentiation in Hematopoietic Cells. Cell Rep *14*, 966-977.

Madrigal, P., and Alasoo, K. (2018). AP-1 Takes Centre Stage in Enhancer Chromatin Dynamics. Trends Cell Biol *28*, 509-511.

Majeti, R., Becker, M.W., Tian, Q., Lee, T.L., Yan, X., Liu, R., Chiang, J.H., Hood, L., Clarke, M.F., and Weissman, I.L. (2009). Dysregulated gene expression networks in human acute myelogenous leukemia stem cells. Proc Natl Acad Sci U S A *106*, 3396-3401.

Mandoli, A., Singh, A.A., Jansen, P.W., Wierenga, A.T., Riahi, H., Franci, G., Prange, K., Saeed, S., Vellenga, E., Vermeulen, M.*, et al.* (2014). CBFB-MYH11/RUNX1 together with a compendium of hematopoietic regulators, chromatin modifiers and basal transcription factors occupies self-renewal genes in inv(16) acute myeloid leukemia. Leukemia *28*, 770-778.

Mandoli, A., Singh, A.A., Prange, K.H.M., Tijchon, E., Oerlemans, M., Dirks, R., Ter Huurne, M., Wierenga, A.T.J., Janssen-Megens, E.M., Berentsen, K.*, et al.* (2016). The Hematopoietic Transcription Factors RUNX1 and ERG Prevent AML1-ETO Oncogene Overexpression and Onset of the Apoptosis Program in t(8;21) AMLs. Cell Rep *17*, 2087-2100.

Mannelli, F., Ponziani, V., Bencini, S., Bonetti, M.I., Benelli, M., Cutini, I., Gianfaldoni, G., Scappini, B., Pancani, F., Piccini, M.*, et al.* (2017). CEBPA-double-mutated acute myeloid leukemia displays a unique phenotypic profile: a reliable screening method and insight into biological features. Haematologica *102*, 529-540.

Martinez-Soria, N., McKenzie, L., Draper, J., Ptasinska, A., Issa, H., Potluri, S., Blair, H.J., Pickin, A., Isa, A., Chin, P.S.*, et al.* (2018). The Oncogenic Transcription Factor RUNX1/ETO Corrupts Cell Cycle Regulation to Drive Leukemic Transformation. Cancer Cell *34*, 626-642 e628.

Matheny, C.J., Speck, M.E., Cushing, P.R., Zhou, Y., Corpora, T., Regan, M., Newman, M., Roudaia, L., Speck, C.L., Gu, T.L.*, et al.* (2007). Disease mutations in RUNX1 and RUNX2 create nonfunctional, dominant-negative, or hypomorphic alleles. EMBO J *26*, 1163-1175.

Maxson, J.E., Gotlib, J., Pollyea, D.A., Fleischman, A.G., Agarwal, A., Eide, C.A., Bottomly, D., Wilmot, B., McWeeney, S.K., Tognon, C.E.*, et al.* (2013). Oncogenic CSF3R mutations in chronic neutrophilic leukemia and atypical CML. N Engl J Med *368*, 1781-1790.

McCubrey, J.A., Steelman, L.S., Chappell, W.H., Abrams, S.L., Wong, E.W., Chang, F., Lehmann, B., Terrian, D.M., Milella, M., Tafuri, A.*, et al.* (2007). Roles of the Raf/MEK/ERK pathway in cell growth, malignant transformation and drug resistance. Biochim Biophys Acta *1773*, 1263-1284.

McKercher, S.R., Torbett, B.E., Anderson, K.L., Henkel, G.W., Vestal, D.J., Baribault, H., Klemsz, M., Feeney, A.J., Wu, G.E., Paige, C.J.*, et al.* (1996). Targeted disruption of the PU.1 gene results in multiple hematopoietic abnormalities. EMBO J *15*, 5647-5658.

McKinley, K.L., and Cheeseman, I.M. (2016). The molecular basis for centromere identity and function. Nat Rev Mol Cell Biol *17*, 16-29.

Medvinsky, A.L., Samoylina, N.L., Muller, A.M., and Dzierzak, E.A. (1993). An early pre-liver intraembryonic source of CFU-S in the developing mouse. Nature *364*, 64-67.

Meyer, S.C., and Levine, R.L. (2014). Translational implications of somatic genomics in acute myeloid leukaemia. Lancet Oncol *15*, e382-394.

Meyers, S., Downing, J.R., and Hiebert, S.W. (1993). Identification of AML-1 and the (8;21) translocation protein (AML-1/ETO) as sequence-specific DNA-binding proteins: the runt homology domain is required for DNA binding and protein-protein interactions. Mol Cell Biol *13*, 6336-6345.

Mifsud, B., Martincorena, I., Darbo, E., Sugar, R., Schoenfelder, S., Fraser, P., and Luscombe, N.M. (2017). GOTHiC, a probabilistic model to resolve complex biases and to identify real interactions in Hi-C data. PLoS One *12*, e0174744.

Mifsud, B., Tavares-Cadete, F., Young, A.N., Sugar, R., Schoenfelder, S., Ferreira, L., Wingett, S.W., Andrews, S., Grey, W., Ewels, P.A.*, et al.* (2015). Mapping long-range promoter contacts in human cells with high-resolution capture Hi-C. Nat Genet *47*, 598-606.

Mikkola, H.K., Klintman, J., Yang, H., Hock, H., Schlaeger, T.M., Fujiwara, Y., and Orkin, S.H. (2003). Haematopoietic stem cells retain long-term repopulating activity

and multipotency in the absence of stem-cell leukaemia SCL/tal-1 gene. Nature *421*, 547-551.

Miyoshi, H., Kozu, T., Shimizu, K., Enomoto, K., Maseki, N., Kaneko, Y., Kamada, N., and Ohki, M. (1993). The t(8;21) translocation in acute myeloid leukemia results in production of an AML1-MTG8 fusion transcript. EMBO J *12*, 2715-2721.

Mollinedo, F., Vaquerizo, M.J., and Naranjo, J.R. (1991). Expression of c-jun, jun B and jun D proto-oncogenes in human peripheral-blood granulocytes. Biochem J *273(Pt 2)*, 477-479.

Moore, M.A., and Metcalf, D. (1970). Ontogeny of the haemopoietic system: yolk sac origin of in vivo and in vitro colony forming cells in the developing mouse embryo. Br J Haematol *18*, 279-296.

Mori, N., Fujii, M., Iwai, K., Ikeda, S., Yamasaki, Y., Hata, T., Yamada, Y., Tanaka, Y., Tomonaga, M., and Yamamoto, N. (2000). Constitutive activation of transcription factor AP-1 in primary adult T-cell leukemia cells. Blood *95*, 3915-3921.

Motoda, L., Osato, M., Yamashita, N., Jacob, B., Chen, L.Q., Yanagida, M., Ida, H., Wee, H.J., Sun, A.X., Taniuchi, I.*, et al.* (2007). Runx1 protects hematopoietic stem/progenitor cells from oncogenic insult. Stem Cells *25*, 2976-2986.

Mouthon, M.A., Bernard, O., Mitjavila, M.T., Romeo, P.H., Vainchenker, W., and Mathieu-Mahul, D. (1993). Expression of tal-1 and GATA-binding proteins during human hematopoiesis. Blood *81*, 647-655.

Mueller, B.U., and Pabst, T. (2006). C/EBPalpha and the pathophysiology of acute myeloid leukemia. Curr Opin Hematol *13*, 7-14.

Mueller, B.U., Pabst, T., Osato, M., Asou, N., Johansen, L.M., Minden, M.D., Behre, G., Hiddemann, W., Ito, Y., and Tenen, D.G. (2002). Heterozygous PU.1 mutations are associated with acute myeloid leukemia. Blood *100*, 998-1007.

Mulet-Lazaro, R., van Herk, S., Erpelinck, C., Bindels, E., Sanders, M.A., Vermeulen, C., Renkens, I., Valk, P., Melnick, A.M., de Ridder, J.*, et al.* (2021). Allele-specific expression of GATA2 due to epigenetic dysregulation in CEBPA double-mutant AML. Blood *138*, 160-177.

Mullen, A.C., Orlando, D.A., Newman, J.J., Loven, J., Kumar, R.M., Bilodeau, S., Reddy, J., Guenther, M.G., DeKoter, R.P., and Young, R.A. (2011). Master transcription factors determine cell-type-specific responses to TGF-beta signaling. Cell *147*, 565-576.

Muller, C., Bremer, A., Schreiber, S., Eichwald, S., and Calkhoven, C.F. (2010). Nucleolar retention of a translational C/EBPalpha isoform stimulates rDNA transcription and cell size. EMBO J *29*, 897-909.

Muller, C., Calkhoven, C.F., Sha, X., and Leutz, A. (2004). The CCAAT enhancer-binding protein alpha (C/EBPalpha) requires a SWI/SNF complex for proliferation arrest. J Biol Chem *279*, 7353-7358.

Muller, H., Bracken, A.P., Vernell, R., Moroni, M.C., Christians, F., Grassilli, E., Prosperini, E., Vigo, E., Oliner, J.D., and Helin, K. (2001). E2Fs regulate the expression of genes involved in differentiation, development, proliferation, and apoptosis. Genes Dev *15*, 267-285.

Muller-Sieburg, C.E., Whitlock, C.A., and Weissman, I.L. (1986). Isolation of two early B lymphocyte progenitors from mouse marrow: a committed pre-pre-B cell and a clonogenic Thy-1-lo hematopoietic stem cell. Cell *44*, 653-662.

Mumbach, M.R., Granja, J.M., Flynn, R.A., Roake, C.M., Satpathy, A.T., Rubin, A.J., Qi, Y., Jiang, Z., Shams, S., Louie, B.H.*, et al.* (2019). HiChIRP reveals RNA-associated chromosome conformation. Nat Methods *16*, 489-492.

Nakabeppu, Y., Ryder, K., and Nathans, D. (1988). DNA binding activities of three murine Jun proteins: stimulation by Fos. Cell *55*, 907-915.

Nakamura, T., Mori, T., Tada, S., Krajewski, W., Rozovskaia, T., Wassell, R., Dubois, G., Mazo, A., Croce, C.M., and Canaani, E. (2002). ALL-1 is a histone methyltransferase that assembles a supercomplex of proteins involved in transcriptional regulation. Mol Cell *10*, 1119-1128.

Neph, S., Stergachis, A.B., Reynolds, A., Sandstrom, R., Borenstein, E., and Stamatoyannopoulos, J.A. (2012a). Circuitry and dynamics of human transcription factor regulatory networks. Cell *150*, 1274-1286.

Neph, S., Vierstra, J., Stergachis, A.B., Reynolds, A.P., Haugen, E., Vernot, B., Thurman, R.E., John, S., Sandstrom, R., Johnson, A.K.*, et al.* (2012b). An expansive human regulatory lexicon encoded in transcription factor footprints. Nature *489*, 83-90.

Nerlov, C. (2004). C/EBPalpha mutations in acute myeloid leukaemias. Nat Rev Cancer *4*, 394-400.

Nerlov, C., Querfurth, E., Kulessa, H., and Graf, T. (2000). GATA-1 interacts with the myeloid PU.1 transcription factor and represses PU.1-dependent transcription. Blood *95*, 2543-2551.

Nerlov, C., and Ziff, E.B. (1995). CCAAT/enhancer binding protein-alpha amino acid motifs with dual TBP and TFIIB binding ability co-operate to activate transcription in both yeast and mammalian cells. EMBO J *14*, 4318-4328.

Nonaka, L., Maruyama, F., Onishi, Y., Kobayashi, T., Ogura, Y., Hayashi, T., Suzuki, S., and Masuda, M. (2014). Various pAQU plasmids possibly contribute to disseminate tetracycline resistance gene tet(M) among marine bacterial community. Front Microbiol *5*, 152.

Nora, E.P., Lajoie, B.R., Schulz, E.G., Giorgetti, L., Okamoto, I., Servant, N., Piolot, T., van Berkum, N.L., Meisig, J., Sedat, J.*, et al.* (2012). Spatial partitioning of the regulatory landscape of the X-inactivation centre. Nature *485*, 381-385.

North, T., Gu, T.L., Stacy, T., Wang, Q., Howard, L., Binder, M., Marin-Padilla, M., and Speck, N.A. (1999). Cbfa2 is required for the formation of intra-aortic hematopoietic clusters. Development *126*, 2563-2575.

North, T.E., Stacy, T., Matheny, C.J., Speck, N.A., and de Bruijn, M.F. (2004). Runx1 is expressed in adult mouse hematopoietic stem cells and differentiating myeloid and lymphoid cells, but not in maturing erythroid cells. Stem Cells *22*, 158-168.

Nutt, S.L., Metcalf, D., D'Amico, A., Polli, M., and Wu, L. (2005). Dynamic regulation of PU.1 expression in multipotent hematopoietic progenitors. J Exp Med *201*, 221-231.

Obier, N., and Bonifer, C. (2016). Chromatin programming by developmentally regulated transcription factors: lessons from the study of haematopoietic stem cell specification and differentiation. FEBS Lett *590*, 4105-4115.

Obier, N., Cauchy, P., Assi, S.A., Gilmour, J., Lie, A.L.M., Lichtinger, M., Hoogenkamp, M., Noailles, L., Cockerill, P.N., Lacaud, G.*, et al.* (2016). Cooperative binding of AP-1 and TEAD4 modulates the balance between vascular smooth muscle and hemogenic cell fate. Development *143*, 4324-4340.

Ohlsson, E., Hasemann, M.S., Willer, A., Lauridsen, F.K., Rapin, N., Jendholm, J., and Porse, B.T. (2014). Initiation of MLL-rearranged AML is dependent on C/EBPalpha. J Exp Med *211*, 5-13.

Okuda, T., van Deursen, J., Hiebert, S.W., Grosveld, G., and Downing, J.R. (1996). AML1, the target of multiple chromosomal translocations in human leukemia, is essential for normal fetal liver hematopoiesis. Cell *84*, 321-330.

Olive, M., Krylov, D., Echlin, D.R., Gardner, K., Taparowsky, E., and Vinson, C. (1997). A dominant negative to activation protein-1 (AP1) that abolishes DNA binding and inhibits oncogenesis. J Biol Chem *272*, 18586-18594.

Olive, M., Williams, S.C., Dezan, C., Johnson, P.F., and Vinson, C. (1996). Design of a C/EBP-specific, dominant-negative bZIP protein with both inhibitory and gain-of-function properties. J Biol Chem *271*, 2040-2047.

Osada, S., Yamamoto, H., Nishihara, T., and Imagawa, M. (1996). DNA binding specificity of the CCAAT/enhancer-binding protein transcription factor family. J Biol Chem *271*, 3891-3896.

Pabst, T., Eyholzer, M., Fos, J., and Mueller, B.U. (2009). Heterogeneity within AML with CEBPA mutations; only CEBPA double mutations, but not single CEBPA mutations are associated with favourable prognosis. Br J Cancer *100*, 1343-1346.

Pabst, T., Eyholzer, M., Haefliger, S., Schardt, J., and Mueller, B.U. (2008). Somatic CEBPA mutations are a frequent second event in families with germline CEBPA mutations and familial acute myeloid leukemia. J Clin Oncol *26*, 5088-5093.

Pabst, T., Mueller, B.U., Harakawa, N., Schoch, C., Haferlach, T., Behre, G., Hiddemann, W., Zhang, D.E., and Tenen, D.G. (2001a). AML1-ETO downregulates the granulocytic differentiation factor C/EBPalpha in t(8;21) myeloid leukemia. Nat Med *7*, 444-451.

Pabst, T., Mueller, B.U., Zhang, P., Radomska, H.S., Narravula, S., Schnittger, S., Behre, G., Hiddemann, W., and Tenen, D.G. (2001b). Dominant-negative mutations of CEBPA, encoding CCAAT/enhancer binding protein-alpha (C/EBPalpha), in acute myeloid leukemia. Nat Genet *27*, 263-270.

Papaemmanuil, E., Gerstung, M., Bullinger, L., Gaidzik, V.I., Paschka, P., Roberts, N.D., Potter, N.E., Heuser, M., Thol, F., Bolli, N.*, et al.* (2016). Genomic Classification and Prognosis in Acute Myeloid Leukemia. N Engl J Med *374*, 2209-2221.

Park, S., Speck, N.A., and Bushweller, J.H. (2009). The role of CBFbeta in AML1-ETO's activity. Blood *114*, 2849-2850.

Passegue, E., Jochum, W., Schorpp-Kistner, M., Mohle-Steinlein, U., and Wagner, E.F. (2001). Chronic myeloid leukemia with increased granulocyte progenitors in mice lacking junB expression in the myeloid lineage. Cell *104*, 21-32.

Passegue, E., Wagner, E.F., and Weissman, I.L. (2004). JunB deficiency leads to a myeloproliferative disorder arising from hematopoietic stem cells. Cell *119*, 431-443.

Pastore, F., Kling, D., Hoster, E., Dufour, A., Konstandin, N.P., Schneider, S., Sauerland, M.C., Berdel, W.E., Buechner, T., Woermann, B.*, et al.* (2014). Long-term follow-up of cytogenetically normal CEBPA-mutated AML. J Hematol Oncol *7*, 55.

Patikoglou, G.A., Kim, J.L., Sun, L., Yang, S.H., Kodadek, T., and Burley, S.K. (1999). TATA element recognition by the TATA box-binding protein has been conserved throughout evolution. Genes Dev *13*, 3217-3230.

Patriotis, C., Makris, A., Chernoff, J., and Tsichlis, P.N. (1994). Tpl-2 acts in concert with Ras and Raf-1 to activate mitogen-activated protein kinase. Proc Natl Acad Sci U S A *91*, 9755-9759.

Pearce, D.J., Taussig, D., Zibara, K., Smith, L.L., Ridler, C.M., Preudhomme, C., Young, B.D., Rohatiner, A.Z., Lister, T.A., and Bonnet, D. (2006). AML engraftment in the NOD/SCID assay reflects the outcome of AML: implications for our understanding of the heterogeneity of AML. Blood *107*, 1166-1173.

Pearson, J.C., Lemons, D., and McGinnis, W. (2005). Modulating Hox gene functions during animal body patterning. Nat Rev Genet *6*, 893-904.

Pertea, M., Pertea, G.M., Antonescu, C.M., Chang, T.C., Mendell, J.T., and Salzberg, S.L. (2015). StringTie enables improved reconstruction of a transcriptome from RNA-seq reads. Nat Biotechnol *33*, 290-295.

Peter, I.S., and Davidson, E.H. (2011). A gene regulatory network controlling the embryonic specification of endoderm. Nature *474*, 635-639.

Petrovick, M.S., Hiebert, S.W., Friedman, A.D., Hetherington, C.J., Tenen, D.G., and Zhang, D.E. (1998). Multiple functional domains of AML1: PU.1 and C/EBPalpha synergize with different regions of AML1. Mol Cell Biol *18*, 3915-3925.

Phillips, J.E., and Corces, V.G. (2009). CTCF: master weaver of the genome. Cell *137*, 1194-1211.

Pikaart, M.J., Recillas-Targa, F., and Felsenfeld, G. (1998). Loss of transcriptional activity of a transgene is accompanied by DNA methylation and histone deacetylation and is prevented by insulators. Genes Dev *12*, 2852-2862.

Pilon, A.M., Ajay, S.S., Kumar, S.A., Steiner, L.A., Cherukuri, P.F., Wincovitch, S., Anderson, S.M., Center, N.C.S., Mullikin, J.C., Gallagher, P.G.*, et al.* (2011). Genome-wide ChIP-Seq reveals a dramatic shift in the binding of the transcription factor erythroid Kruppel-like factor during erythrocyte differentiation. Blood *118*, e139-148.

Pimanda, J.E., and Gottgens, B. (2010). Gene regulatory networks governing haematopoietic stem cell development and identity. Int J Dev Biol *54*, 1201-1211.

Piper, J., Elze, M.C., Cauchy, P., Cockerill, P.N., Bonifer, C., and Ott, S. (2013). Wellington: a novel method for the accurate identification of digital genomic footprints from DNase-seq data. Nucleic Acids Res *41*, e201.

Platanias, L.C. (2003). Map kinase signaling pathways and hematologic malignancies. Blood *101*, 4667-4679.

Pongubala, J.M., Nagulapalli, S., Klemsz, M.J., McKercher, S.R., Maki, R.A., and Atchison, M.L. (1992). PU.1 recruits a second nuclear factor to a site important for immunoglobulin kappa 3' enhancer activity. Mol Cell Biol *12*, 368-378.

Pongubala, J.M., Van Beveren, C., Nagulapalli, S., Klemsz, M.J., McKercher, S.R., Maki, R.A., and Atchison, M.L. (1993). Effect of PU.1 phosphorylation on interaction with NF-EM5 and transcriptional activation. Science *259*, 1622-1625.

Porse, B.T., Bryder, D., Theilgaard-Monch, K., Hasemann, M.S., Anderson, K., Damgaard, I., Jacobsen, S.E., and Nerlov, C. (2005). Loss of C/EBP alpha cell cycle control increases myeloid progenitor proliferation and transforms the neutrophil granulocyte lineage. J Exp Med *202*, 85-96.

Porse, B.T., Pedersen, T.A., Xu, X., Lindberg, B., Wewer, U.M., Friis-Hansen, L., and Nerlov, C. (2001). E2F repression by C/EBPalpha is required for adipogenesis and granulopoiesis in vivo. Cell *107*, 247-258.

Potluri, S., Assi, S.A., Chin, P.S., Coleman, D.J.L., Pickin, A., Moriya, S., Seki, N., Heidenreich, O., Cockerill, P.N., and Bonifer, C. (2021). Isoform-specific and signaling-dependent propagation of acute myeloid leukemia by Wilms tumor 1. Cell Rep *35*, 109010.

Ptashne, M. (1967). Specific binding of the lambda phage repressor to lambda DNA. Nature *214*, 232-234.

Ptashne, M. (1986). Gene regulation by proteins acting nearby and at a distance. Nature *322*, 697-701.

Ptasinska, A., Assi, S.A., Mannari, D., James, S.R., Williamson, D., Dunne, J., Hoogenkamp, M., Wu, M., Care, M., McNeill, H.*, et al.* (2012). Depletion of RUNX1/ETO in t(8;21) AML cells leads to genome-wide changes in chromatin structure and transcription factor binding. Leukemia *26*, 1829-1841.

Ptasinska, A., Assi, S.A., Martinez-Soria, N., Imperato, M.R., Piper, J., Cauchy, P., Pickin, A., James, S.R., Hoogenkamp, M., Williamson, D.*, et al.* (2014). Identification of a dynamic core transcriptional network in t(8;21) AML that regulates differentiation block and self-renewal. Cell Rep *8*, 1974-1988.

Ptasinska, A., Pickin, A., Assi, S.A., Chin, P.S., Ames, L., Avellino, R., Groschel, S., Delwel, R., Cockerill, P.N., Osborne, C.S.*, et al.* (2019). RUNX1-ETO Depletion in t(8;21) AML Leads to C/EBPalpha- and AP-1-Mediated Alterations in Enhancer-Promoter Interaction. Cell Rep *29*, 2120.

Quinlan, A.R., and Hall, I.M. (2010). BEDTools: a flexible suite of utilities for comparing genomic features. Bioinformatics *26*, 841-842.

Radomska, H.S., Huettner, C.S., Zhang, P., Cheng, T., Scadden, D.T., and Tenen, D.G. (1998). CCAAT/enhancer binding protein alpha is a regulatory switch sufficient for induction of granulocytic development from bipotential myeloid progenitors. Mol Cell Biol *18*, 4301-4314.

Rangatia, J., Vangala, R.K., Treiber, N., Zhang, P., Radomska, H., Tenen, D.G., Hiddemann, W., and Behre, G. (2002). Downregulation of c-Jun expression by transcription factor C/EBPalpha is critical for granulocytic lineage commitment. Mol Cell Biol *22*, 8681-8694.

Rao, S.S., Huntley, M.H., Durand, N.C., Stamenova, E.K., Bochkov, I.D., Robinson, J.T., Sanborn, A.L., Machol, I., Omer, A.D., Lander, E.S.*, et al.* (2014). A 3D map of the human genome at kilobase resolution reveals principles of chromatin looping. Cell *159*, 1665-1680.

Rauscher, F.J., 3rd, Voulalas, P.J., Franza, B.R., Jr., and Curran, T. (1988). Fos and Jun bind cooperatively to the AP-1 site: reconstitution in vitro. Genes Dev *2*, 1687-1699.

Regha, K., Assi, S.A., Tsoulaki, O., Gilmour, J., Lacaud, G., and Bonifer, C. (2015). Developmental-stage-dependent transcriptional response to leukaemic oncogene expression. Nat Commun *6*, 7203.

Renneville, A., Roumier, C., Biggio, V., Nibourel, O., Boissel, N., Fenaux, P., and Preudhomme, C. (2008). Cooperating gene mutations in acute myeloid leukemia: a review of the literature. Leukemia *22*, 915-931.

Robb, L., Lyons, I., Li, R., Hartley, L., Kontgen, F., Harvey, R.P., Metcalf, D., and Begley, C.G. (1995). Absence of yolk sac hematopoiesis from mice with a targeted disruption of the scl gene. Proc Natl Acad Sci U S A *92*, 7075-7079.

Robinson, M.D., McCarthy, D.J., and Smyth, G.K. (2010). edgeR: a Bioconductor package for differential expression analysis of digital gene expression data. Bioinformatics *26*, 139-140.

Robinson, P.J., Fairall, L., Huynh, V.A., and Rhodes, D. (2006). EM measurements define the dimensions of the "30-nm" chromatin fiber: evidence for a compact, interdigitated structure. Proc Natl Acad Sci U S A *103*, 6506-6511.

Rohrs, S., Scherr, M., Romani, J., Zaborski, M., Drexler, H.G., and Quentmeier, H. (2010). CD7 in acute myeloid leukemia: correlation with loss of wild-type CEBPA, consequence of epigenetic regulation. J Hematol Oncol *3*, 15.

Rosenbauer, F., Wagner, K., Kutok, J.L., Iwasaki, H., Le Beau, M.M., Okuno, Y., Akashi, K., Fiering, S., and Tenen, D.G. (2004). Acute myeloid leukemia induced by graded reduction of a lineage-specific transcription factor, PU.1. Nat Genet *36*, 624-630.

Roudaia, L., Cheney, M.D., Manuylova, E., Chen, W., Morrow, M., Park, S., Lee, C.T., Kaur, P., Williams, O., Bushweller, J.H.*, et al.* (2009). CBFbeta is critical for AML1-ETO and TEL-AML1 activity. Blood *113*, 3070-3079.

Sachs, K., Sarver, A.L., Noble-Orcutt, K.E., LaRue, R.S., Antony, M.L., Chang, D., Lee, Y., Navis, C.M., Hillesheim, A.L., Nykaza, I.R.*, et al.* (2020). Single-Cell Gene Expression Analyses Reveal Distinct Self-Renewing and Proliferating Subsets in the Leukemia Stem Cell Compartment in Acute Myeloid Leukemia. Cancer Res *80*, 458-470.

Sainsbury, S., Bernecky, C., and Cramer, P. (2015). Structural basis of transcription initiation by RNA polymerase II. Nat Rev Mol Cell Biol *16*, 129-143.

Sallman, D.A., and List, A. (2019). The central role of inflammatory signaling in the pathogenesis of myelodysplastic syndromes. Blood *133*, 1039-1048.

Sanchez, A., Relano, C., Carrasco, A., Contreras-Jurado, C., Martin-Duce, A., Aranda, A., and Alemany, S. (2017). Map3k8 controls granulocyte colony-stimulating factor production and neutrophil precursor proliferation in lipopolysaccharide-induced emergency granulopoiesis. Sci Rep *7*, 5010.

Sandelin, A., Carninci, P., Lenhard, B., Ponjavic, J., Hayashizaki, Y., and Hume, D.A. (2007). Mammalian RNA polymerase II core promoters: insights from genome-wide studies. Nat Rev Genet *8*, 424-436.

Santaguida, M., Schepers, K., King, B., Sabnis, A.J., Forsberg, E.C., Attema, J.L., Braun, B.S., and Passegue, E. (2009). JunB protects against myeloid malignancies by limiting hematopoietic stem cell proliferation and differentiation without affecting self-renewal. Cancer Cell *15*, 341-352.

Sardina, J.L., Collombet, S., Tian, T.V., Gomez, A., Di Stefano, B., Berenguer, C., Brumbaugh, J., Stadhouders, R., Segura-Morales, C., Gut, M.*, et al.* (2018). Transcription Factors Drive Tet2-Mediated Enhancer Demethylation to Reprogram Cell Fate. Cell Stem Cell *23*, 905-906.

Sasaki, T., Shiohama, A., Minoshima, S., and Shimizu, N. (2003). Identification of eight members of the Argonaute family in the human genome. Genomics *82*, 323-330.

Sauer, P.V., Gu, Y., Liu, W.H., Mattiroli, F., Panne, D., Luger, K., and Churchill, M.E. (2018). Mechanistic insights into histone deposition and nucleosome assembly by the chromatin assembly factor-1. Nucleic Acids Res *46*, 9907-9917.

Saxonov, S., Berg, P., and Brutlag, D.L. (2006). A genome-wide analysis of CpG dinucleotides in the human genome distinguishes two distinct classes of promoters. Proc Natl Acad Sci U S A *103*, 1412-1417.

Schalch, T., Duda, S., Sargent, D.F., and Richmond, T.J. (2005). X-ray structure of a tetranucleosome and its implications for the chromatin fibre. Nature *436*, 138-141.

Schessl, C., Rawat, V.P., Cusan, M., Deshpande, A., Kohl, T.M., Rosten, P.M., Spiekermann, K., Humphries, R.K., Schnittger, S., Kern, W.*, et al.* (2005). The AML1-ETO fusion gene and the FLT3 length mutation collaborate in inducing acute leukemia in mice. J Clin Invest *115*, 2159-2168.

Schmidt, L., Heyes, E., and Grebien, F. (2020). Gain-of-Function Effects of N-Terminal CEBPA Mutations in Acute Myeloid Leukemia. Bioessays *42*, e1900178.

Schneider, T.D., and Stephens, R.M. (1990). Sequence logos: a new way to display consensus sequences. Nucleic Acids Res *18*, 6097-6100.

Schnittger, S., Dicker, F., Kern, W., Wendland, N., Sundermann, J., Alpermann, T., Haferlach, C., and Haferlach, T. (2011). RUNX1 mutations are frequent in de novo AML with noncomplex karyotype and confer an unfavorable prognosis. Blood *117*, 2348-2357.

Schoenfelder, S., and Fraser, P. (2019). Long-range enhancer-promoter contacts in gene expression control. Nat Rev Genet *20*, 437-455.

Schorpp-Kistner, M., Wang, Z.Q., Angel, P., and Wagner, E.F. (1999). JunB is essential for mammalian placentation. EMBO J *18*, 934-948.

Scott, E.W., Simon, M.C., Anastasi, J., and Singh, H. (1994). Requirement of transcription factor PU.1 in the development of multiple hematopoietic lineages. Science *265*, 1573-1577.

Shannon, P., Markiel, A., Ozier, O., Baliga, N.S., Wang, J.T., Ramage, D., Amin, N., Schwikowski, B., and Ideker, T. (2003). Cytoscape: a software environment for integrated models of biomolecular interaction networks. Genome Res *13*, 2498-2504.

Shima, T., Miyamoto, T., Kikushige, Y., Yuda, J., Tochigi, T., Yoshimoto, G., Kato, K., Takenaka, K., Iwasaki, H., Mizuno, S.*, et al.* (2014). The ordered acquisition of Class II and Class I mutations directs formation of human t(8;21) acute myelogenous leukemia stem cell. Exp Hematol *42*, 955-965 e951-955.

Shivdasani, R.A., Mayer, E.L., and Orkin, S.H. (1995). Absence of blood formation in mice lacking the T-cell leukaemia oncoprotein tal-1/SCL. Nature *373*, 432-434.

Shivdasani, R.A., and Orkin, S.H. (1996). The transcriptional control of hematopoiesis. Blood *87*, 4025-4039.

Shlush, L.I., Zandi, S., Mitchell, A., Chen, W.C., Brandwein, J.M., Gupta, V., Kennedy, J.A., Schimmer, A.D., Schuh, A.C., Yee, K.W.*, et al.* (2014). Identification of pre-leukaemic haematopoietic stem cells in acute leukaemia. Nature *506*, 328-333.

Slomiany, B.A., D'Arigo, K.L., Kelly, M.M., and Kurtz, D.T. (2000). C/EBPalpha inhibits cell growth via direct repression of E2F-DP-mediated transcription. Mol Cell Biol *20*, 5986-5997.

Souers, A.J., Leverson, J.D., Boghaert, E.R., Ackler, S.L., Catron, N.D., Chen, J., Dayton, B.D., Ding, H., Enschede, S.H., Fairbrother, W.J.*, et al.* (2013). ABT-199, a potent and selective BCL-2 inhibitor, achieves antitumor activity while sparing platelets. Nat Med *19*, 202-208.

Speck, N.A., and Baltimore, D. (1987). Six distinct nuclear factors interact with the 75-base-pair repeat of the Moloney murine leukemia virus enhancer. Mol Cell Biol *7*, 1101-1110.

Staber, P.B., Zhang, P., Ye, M., Welner, R.S., Levantini, E., Di Ruscio, A., Ebralidze, A.K., Bach, C., Zhang, H., Zhang, J.*, et al.* (2014). The Runx-PU.1 pathway preserves normal and AML/ETO9a leukemic stem cells. Blood *124*, 2391-2399.

Staber, P.B., Zhang, P., Ye, M., Welner, R.S., Nombela-Arrieta, C., Bach, C., Kerenyi, M., Bartholdy, B.A., Zhang, H., Alberich-Jorda, M.*, et al.* (2013). Sustained PU.1 levels balance cell-cycle regulators to prevent exhaustion of adult hematopoietic stem cells. Mol Cell *49*, 934-946.

Steelman, L.S., Franklin, R.A., Abrams, S.L., Chappell, W., Kempf, C.R., Basecke, J., Stivala, F., Donia, M., Fagone, P., Nicoletti, F.*, et al.* (2011). Roles of the Ras/Raf/MEK/ERK pathway in leukemia therapy. Leukemia *25*, 1080-1094.

Stengel, K.R., Ellis, J.D., Spielman, C.L., Bomber, M.L., and Hiebert, S.W. (2021). Definition of a small core transcriptional circuit regulated by AML1-ETO. Mol Cell *81*, 530-545 e535.

Stergachis, A.B., Neph, S., Reynolds, A., Humbert, R., Miller, B., Paige, S.L., Vernot, B., Cheng, J.B., Thurman, R.E., Sandstrom, R.*, et al.* (2013). Developmental fate and cellular maturity encoded in human regulatory DNA landscapes. Cell *154*, 888-903.

Stork, P.J., and Dillon, T.J. (2005). Multiple roles of Rap1 in hematopoietic cells: complementary versus antagonistic functions. Blood *106*, 2952-2961.

Stormo, G.D., and Zhao, Y. (2010). Determining the specificity of protein-DNA interactions. Nat Rev Genet *11*, 751-760.

Stuart, T., Butler, A., Hoffman, P., Hafemeister, C., Papalexi, E., Mauck, W.M., 3rd, Hao, Y., Stoeckius, M., Smibert, P., and Satija, R. (2019). Comprehensive Integration of Single-Cell Data. Cell *177*, 1888-1902 e1821.

Su, L., Gao, S., Tan, Y., Lin, H., Liu, X., Liu, S., Yang, Y., Sun, J., and Li, W. (2019). CSF3R mutations were associated with an unfavorable prognosis in patients with acute myeloid leukemia with CEBPA double mutations. Ann Hematol *98*, 1641-1646.

Sun, F.L., and Elgin, S.C. (1999). Putting boundaries on silence. Cell *99*, 459-462.

Sun, X.J., Wang, Z., Wang, L., Jiang, Y., Kost, N., Soong, T.D., Chen, W.Y., Tang, Z., Nakadai, T., Elemento, O.*, et al.* (2013). A stable transcription factor complex nucleated by oligomeric AML1-ETO controls leukaemogenesis. Nature *500*, 93-97.

Takahashi, S. (2011). Current findings for recurring mutations in acute myeloid leukemia. J Hematol Oncol *4*, 36.

Takayama, N., Murison, A., Takayanagi, S.I., Arlidge, C., Zhou, S., Garcia-Prat, L., Chan-Seng-Yue, M., Zandi, S., Gan, O.I., Boutzen, H.*, et al.* (2021). The Transition from Quiescent to Activated States in Human Hematopoietic Stem Cells Is Governed by Dynamic 3D Genome Reorganization. Cell Stem Cell *28*, 488-501 e410.

Talbert, P.B., and Henikoff, S. (2010). Histone variants--ancient wrap artists of the epigenome. Nat Rev Mol Cell Biol *11*, 264-275.

Tarlock, K., Lamble, A.J., Wang, Y.C., Gerbing, R.B., Ries, R.E., Loken, M.R., Brodersen, L.E., Pardo, L., Leonti, A., Smith, J.L.*, et al.* (2021). CEBPA-bZip mutations are associated with favorable prognosis in de novo AML: a report from the Children's Oncology Group. Blood *138*, 1137-1147.

Taskesen, E., Avellino, R., AlberichJorda, M., Tenen, D.G., de, J.R., Valk, P., Wouters, B., Erpelinck, C., Reinders, M., and Delwel, R. (2011). CEBPα Is a Transcriptional Repressor of T-Cell Related Genes Explaining the Myeloid/T-Lymphoid Features of CEBPα-Silenced AML. Blood *118*, 554-554.

Taube, F., Georgi, J.A., Kramer, M., Stasik, S., Middeke, J.M., Rollig, C., Krug, U., Kramer, A., Scholl, S., Hochhaus, A.*, et al.* (2022). CEBPA mutations in 4708 patients with acute myeloid leukemia: differential impact of bZIP and TAD mutations on outcome. Blood *139*, 87-103.

Tawana, K., Rio-Machin, A., Preudhomme, C., and Fitzgibbon, J. (2017). Familial CEBPA-mutated acute myeloid leukemia. Semin Hematol *54*, 87-93.

Tawana, K., Wang, J., Renneville, A., Bodor, C., Hills, R., Loveday, C., Savic, A., Van Delft, F.W., Treleaven, J., Georgiades, P.*, et al.* (2015). Disease evolution and outcomes in familial AML with germline CEBPA mutations. Blood *126*, 1214-1223.

Tefferi, A., and Vardiman, J.W. (2009). Myelodysplastic syndromes. N Engl J Med *361*, 1872-1885.

Thoma, F., Koller, T., and Klug, A. (1979). Involvement of histone H1 in the organization of the nucleosome and of the salt-dependent superstructures of chromatin. J Cell Biol *83*, 403-427.

Thomas, M.C., and Chiang, C.M. (2006). The general transcription machinery and general cofactors. Crit Rev Biochem Mol Biol *41*, 105-178.

Thurman, R.E., Rynes, E., Humbert, R., Vierstra, J., Maurano, M.T., Haugen, E., Sheffield, N.C., Stergachis, A.B., Wang, H., Vernot, B.*, et al.* (2012). The accessible chromatin landscape of the human genome. Nature *489*, 75-82.

Timchenko, N., Wilson, D.R., Taylor, L.R., Abdelsayed, S., Wilde, M., Sawadogo, M., and Darlington, G.J. (1995). Autoregulation of the human C/EBP alpha gene by stimulation of upstream stimulatory factor binding. Mol Cell Biol *15*, 1192-1202.

Tonks, A., Pearn, L., Musson, M., Gilkes, A., Mills, K.I., Burnett, A.K., and Darley, R.L. (2007). Transcriptional dysregulation mediated by RUNX1-RUNX1T1 in normal human progenitor cells and in acute myeloid leukaemia. Leukemia *21*, 2495-2505.

Trapnell, C., Cacchiarelli, D., Grimsby, J., Pokharel, P., Li, S., Morse, M., Lennon, N.J., Livak, K.J., Mikkelsen, T.S., and Rinn, J.L. (2014). The dynamics and regulators of cell fate decisions are revealed by pseudotemporal ordering of single cells. Nat Biotechnol *32*, 381-386.

Tsukada, J., Yoshida, Y., Kominato, Y., and Auron, P.E. (2011). The CCAAT/enhancer (C/EBP) family of basic-leucine zipper (bZIP) transcription factors is a multifaceted highly-regulated system for gene regulation. Cytokine *54*, 6-19.

Valk, P.J., Verhaak, R.G., Beijen, M.A., Erpelinck, C.A., Barjesteh van Waalwijk van Doorn-Khosrovani, S., Boer, J.M., Beverloo, H.B., Moorhouse, M.J., van der Spek, P.J., Lowenberg, B.*, et al.* (2004). Prognostically useful gene-expression profiles in acute myeloid leukemia. N Engl J Med *350*, 1617-1628.

van Oevelen, C., Collombet, S., Vicent, G., Hoogenkamp, M., Lepoivre, C., Badeaux, A., Bussmann, L., Sardina, J.L., Thieffry, D., Beato, M.*, et al.* (2015). C/EBPalpha

Activates Pre-existing and De Novo Macrophage Enhancers during Induced Pre-B Cell Transdifferentiation and Myelopoiesis. Stem Cell Reports *5*, 232-247.

Vangala, R.K., Heiss-Neumann, M.S., Rangatia, J.S., Singh, S.M., Schoch, C., Tenen, D.G., Hiddemann, W., and Behre, G. (2003). The myeloid master regulator transcription factor PU.1 is inactivated by AML1-ETO in t(8;21) myeloid leukemia. Blood *101*, 270-277.

Velten, L., Haas, S.F., Raffel, S., Blaszkiewicz, S., Islam, S., Hennig, B.P., Hirche, C., Lutz, C., Buss, E.C., Nowak, D.*, et al.* (2017). Human haematopoietic stem cell lineage commitment is a continuous process. Nat Cell Biol *19*, 271-281.

Vierbuchen, T., Ling, E., Cowley, C.J., Couch, C.H., Wang, X., Harmin, D.A., Roberts, C.W.M., and Greenberg, M.E. (2017). AP-1 Transcription Factors and the BAF Complex Mediate Signal-Dependent Enhancer Selection. Mol Cell *68*, 1067-1082 e1012.

Villasenor, R., and Baubec, T. (2021). Regulatory mechanisms governing chromatin organization and function. Curr Opin Cell Biol *70*, 10-17.

Vinson, C.R., Sigler, P.B., and McKnight, S.L. (1989). Scissors-grip model for DNA recognition by a family of leucine zipper proteins. Science *246*, 911-916.

Visvader, J., Begley, C.G., and Adams, J.M. (1991). Differential expression of the LYL, SCL and E2A helix-loop-helix genes within the hemopoietic system. Oncogene *6*, 187-194.

Wade, P.A., Pruss, D., and Wolffe, A.P. (1997). Histone acetylation: chromatin in action. Trends Biochem Sci *22*, 128-132.

Wadman, I.A., Osada, H., Grutz, G.G., Agulnick, A.D., Westphal, H., Forster, A., and Rabbitts, T.H. (1997). The LIM-only protein Lmo2 is a bridging molecule assembling an erythroid, DNA-binding complex which includes the TAL1, E47, GATA-1 and Ldb1/NLI proteins. EMBO J *16*, 3145-3157.

Wakita, S., Sakaguchi, M., Oh, I., Kako, S., Toya, T., Najima, Y., Doki, N., Kanda, J., Kuroda, J., Mori, S.*, et al.* (2022). Prognostic impact of CEBPA bZIP domain mutation in acute myeloid leukemia. Blood Adv *6*, 238-247.

Wang, H., Iakova, P., Wilde, M., Welm, A., Goode, T., Roesler, W.J., and Timchenko, N.A. (2001). C/EBPalpha arrests cell proliferation through direct inhibition of Cdk2 and Cdk4. Mol Cell *8*, 817-828.

Wang, J., Hoshino, T., Redner, R.L., Kajigaya, S., and Liu, J.M. (1998). ETO, fusion partner in t(8;21) acute myeloid leukemia, represses transcription by interaction with the human N-CoR/mSin3/HDAC1 complex. Proc Natl Acad Sci U S A *95*, 10860-10865.

Wang, Q., Stacy, T., Binder, M., Marin-Padilla, M., Sharpe, A.H., and Speck, N.A. (1996a). Disruption of the Cbfa2 gene causes necrosis and hemorrhaging in the central

nervous system and blocks definitive hematopoiesis. Proc Natl Acad Sci U S A *93*, 3444-3449.

Wang, Q., Stacy, T., Miller, J.D., Lewis, A.F., Gu, T.L., Huang, X., Bushweller, J.H., Bories, J.C., Alt, F.W., Ryan, G.*, et al.* (1996b). The CBFbeta subunit is essential for CBFalpha2 (AML1) function in vivo. Cell *87*, 697-708.

Wang, Z.Q., Ovitt, C., Grigoriadis, A.E., Mohle-Steinlein, U., Ruther, U., and Wagner, E.F. (1992). Bone and haematopoietic defects in mice lacking c-fos. Nature *360*, 741-745.

Watcham, S., Kucinski, I., and Gottgens, B. (2019). New insights into hematopoietic differentiation landscapes from single-cell RNA sequencing. Blood *133*, 1415-1426.

Weintraub, H., and Groudine, M. (1976). Chromosomal subunits in active genes have an altered conformation. Science *193*, 848-856.

Welch, J.S., Ley, T.J., Link, D.C., Miller, C.A., Larson, D.E., Koboldt, D.C., Wartman, L.D., Lamprecht, T.L., Liu, F., Xia, J.*, et al.* (2012). The origin and evolution of mutations in acute myeloid leukemia. Cell *150*, 264-278.

Wendt, K.S., Yoshida, K., Itoh, T., Bando, M., Koch, B., Schirghuber, E., Tsutsumi, S., Nagae, G., Ishihara, K., Mishiro, T.*, et al.* (2008). Cohesin mediates transcriptional insulation by CCCTC-binding factor. Nature *451*, 796-801.

Wesely, J., Kotini, A.G., Izzo, F., Luo, H., Yuan, H., Sun, J., Georgomanoli, M., Zviran, A., Deslauriers, A.G., Dusaj, N.*, et al.* (2020). Acute Myeloid Leukemia iPSCs Reveal a Role for RUNX1 in the Maintenance of Human Leukemia Stem Cells. Cell Rep *31*, 107688.

Wichmann, C., Quagliano-Lo Coco, I., Yildiz, O., Chen-Wichmann, L., Weber, H., Syzonenko, T., Doring, C., Brendel, C., Ponnusamy, K., Kinner, A.*, et al.* (2015). Activating c-KIT mutations confer oncogenic cooperativity and rescue RUNX1/ETO-induced DNA damage and apoptosis in human primary CD34+ hematopoietic progenitors. Leukemia *29*, 279-289.

Wiemels, J.L., Xiao, Z., Buffler, P.A., Maia, A.T., Ma, X., Dicks, B.M., Smith, M.T., Zhang, L., Feusner, J., Wiencke, J.*, et al.* (2002). In utero origin of t(8;21) AML1-ETO translocations in childhood acute myeloid leukemia. Blood *99*, 3801-3805.

Wilhelmson, A.S., and Porse, B.T. (2020). CCAAT enhancer binding protein alpha (CEBPA) biallelic acute myeloid leukaemia: cooperating lesions, molecular mechanisms and clinical relevance. Br J Haematol *190*, 495-507.

Wilkinson, A.C., Ballabio, E., Geng, H., North, P., Tapia, M., Kerry, J., Biswas, D., Roeder, R.G., Allis, C.D., Melnick, A.*, et al.* (2013). RUNX1 is a key target in t(4;11) leukemias that contributes to gene activation through an AF4-MLL complex interaction. Cell Rep *3*, 116-127.

Wilkinson, A.C., Nakauchi, H., and Gottgens, B. (2017). Mammalian Transcription Factor Networks: Recent Advances in Interrogating Biological Complexity. Cell Syst *5*, 319-331.

Williams, S.C., Cantwell, C.A., and Johnson, P.F. (1991). A family of C/EBP-related proteins capable of forming covalently linked leucine zipper dimers in vitro. Genes Dev *5*, 1553-1567.

Wilson, N.K., Foster, S.D., Wang, X., Knezevic, K., Schutte, J., Kaimakis, P., Chilarska, P.M., Kinston, S., Ouwehand, W.H., Dzierzak, E.*, et al.* (2010). Combinatorial transcriptional control in blood stem/progenitor cells: genome-wide analysis of ten major transcriptional regulators. Cell Stem Cell *7*, 532-544.

Wingett, S., Ewels, P., Furlan-Magaril, M., Nagano, T., Schoenfelder, S., Fraser, P., and Andrews, S. (2015). HiCUP: pipeline for mapping and processing Hi-C data. F1000Res *4*, 1310.

Wotton, D., Lo, R.S., Swaby, L.A., and Massague, J. (1999). Multiple modes of repression by the Smad transcriptional corepressor TGIF. J Biol Chem *274*, 37105-37110.

Wouters, B.J., Lowenberg, B., Erpelinck-Verschueren, C.A., van Putten, W.L., Valk, P.J., and Delwel, R. (2009). Double CEBPA mutations, but not single CEBPA mutations, define a subgroup of acute myeloid leukemia with a distinctive gene expression profile that is uniquely associated with a favorable outcome. Blood *113*, 3088-3091.

Wouters, B.J., Sanders, M.A., Lugthart, S., Geertsma-Kleinekoort, W.M., van Drunen, E., Beverloo, H.B., Lowenberg, B., Valk, P.J., and Delwel, R. (2007). Segmental uniparental disomy as a recurrent mechanism for homozygous CEBPA mutations in acute myeloid leukemia. Leukemia *21*, 2382-2384.

Xiang, M., Gan, L., Zhou, L., Klein, W.H., and Nathans, J. (1996). Targeted deletion of the mouse POU domain gene Brn-3a causes selective loss of neurons in the brainstem and trigeminal ganglion, uncoordinated limb movement, and impaired suckling. Proc Natl Acad Sci U S A *93*, 11950-11955.

Yan, L., Dave, U.P., Engel, M., Brandt, S.J., and Hamid, R. (2020). Loss of TG-Interacting Factor 1 decreases survival in mouse models of myeloid leukaemia. J Cell Mol Med *24*, 13472-13480.

Yan, L., Womack, B., Wotton, D., Guo, Y., Shyr, Y., Dave, U., Li, C., Hiebert, S., Brandt, S., and Hamid, R. (2013). Tgif1 regulates quiescence and self-renewal of hematopoietic stem cells. Mol Cell Biol *33*, 4824-4833.

Ye, M., Zhang, H., Amabile, G., Yang, H., Staber, P.B., Zhang, P., Levantini, E., Alberich-Jorda, M., Zhang, J., Kawasaki, A.*, et al.* (2013). C/EBPa controls acquisition and maintenance of adult haematopoietic stem cell quiescence. Nat Cell Biol *15*, 385-394.

Ye, M., Zhang, H., Yang, H., Koche, R., Staber, P.B., Cusan, M., Levantini, E., Welner, R.S., Bach, C.S., Zhang, J.*, et al.* (2015). Hematopoietic Differentiation Is Required for Initiation of Acute Myeloid Leukemia. Cell Stem Cell *17*, 611-623.

Yokomizo, T., Ogawa, M., Osato, M., Kanno, T., Yoshida, H., Fujimoto, T., Fraser, S., Nishikawa, S., Okada, H., Satake, M.*, et al.* (2001). Requirement of Runx1/AML1/PEBP2alphaB for the generation of haematopoietic cells from endothelial cells. Genes Cells *6*, 13-23.

Yuan, Y., Zhou, L., Miyamoto, T., Iwasaki, H., Harakawa, N., Hetherington, C.J., Burel, S.A., Lagasse, E., Weissman, I.L., Akashi, K.*, et al.* (2001). AML1-ETO expression is directly involved in the development of acute myeloid leukemia in the presence of additional mutations. Proc Natl Acad Sci U S A *98*, 10398-10403.

Yvernogeau, L., Gautier, R., Khoury, H., Menegatti, S., Schmidt, M., Gilles, J.F., and Jaffredo, T. (2016). An in vitro model of hemogenic endothelium commitment and hematopoietic production. Development *143*, 1302-1312.

Zaret, K.S. (2020). Pioneer Transcription Factors Initiating Gene Network Changes. Annu Rev Genet *54*, 367-385.

Zaret, K.S., and Carroll, J.S. (2011). Pioneer transcription factors: establishing competence for gene expression. Genes Dev *25*, 2227-2241.

Zentner, G.E., Tesar, P.J., and Scacheri, P.C. (2011). Epigenetic signatures distinguish multiple classes of enhancers with distinct cellular functions. Genome Res *21*, 1273-1283.

Zhang, D.E., Zhang, P., Wang, N.D., Hetherington, C.J., Darlington, G.J., and Tenen, D.G. (1997). Absence of granulocyte colony-stimulating factor signaling and neutrophil development in CCAAT enhancer binding protein alpha-deficient mice. Proc Natl Acad Sci U S A *94*, 569-574.

Zhang, H., Alberich-Jorda, M., Amabile, G., Yang, H., Staber, P.B., Di Ruscio, A., Welner, R.S., Ebralidze, A., Zhang, J., Levantini, E.*, et al.* (2013). Sox4 is a key oncogenic target in C/EBPalpha mutant acute myeloid leukemia. Cancer Cell *24*, 575-588.

Zhang, P., Iwama, A., Datta, M.W., Darlington, G.J., Link, D.C., and Tenen, D.G. (1998). Upregulation of interleukin 6 and granulocyte colony-stimulating factor receptors by transcription factor CCAAT enhancer binding protein alpha (C/EBP alpha) is critical for granulopoiesis. J Exp Med *188*, 1173-1184.

Zhang, Y., Liu, T., Meyer, C.A., Eeckhoute, J., Johnson, D.S., Bernstein, B.E., Nusbaum, C., Myers, R.M., Brown, M., Li, W.*, et al.* (2008). Model-based analysis of ChIP-Seq (MACS). Genome Biol *9*, R137.

Zheng, R., and Small, D. (2005). Mutant FLT3 signaling contributes to a block in myeloid differentiation. Leuk Lymphoma *46*, 1679-1687.

Zhu, J., He, F., Hu, S., and Yu, J. (2008). On the nature of human housekeeping genes. Trends Genet *24*, 481-484.

Ziemann, M., Kaspi, A., Lazarus, R., and El-Osta, A. (2013). Motif analysis in DNAse hypersensitivity regions uncovers distal cis elements associated with gene expression. Bioinformation *9*, 212-215.

Zinn, K., DiMaio, D., and Maniatis, T. (1983). Identification of two distinct regulatory regions adjacent to the human beta-interferon gene. Cell *34*, 865-879.

Zinzen, R.P., Girardot, C., Gagneur, J., Braun, M., and Furlong, E.E. (2009). Combinatorial binding predicts spatio-temporal cis-regulatory activity. Nature *462*, 65-70.

Appendix

Supplementary table 1: DEG in *CEBPA*$^{N/C}$ AML compared to PBSCs.

gene_symbol	CEBPAx2_log2CPM_avg	PBSC_log2CPM_avg	log2FC	P.Value	adj.P.Val
CD7	4.80	-0.97	5.87	0.007	0.047
C21orf62	2.20	-2.50	4.85	0.002	0.021
ILDR2	5.40	0.72	4.62	0.001	0.008
PDE3B	7.44	2.94	4.52	0.000	0.000
CYP2E1	3.09	-1.34	4.48	0.006	0.040
CEBPA	9.48	5.03	4.45	0.000	0.000
CD96	8.74	4.36	4.32	0.002	0.018
LY9	4.18	0.29	3.85	0.007	0.049
MPO	12.88	9.38	3.52	0.000	0.000
PLIN2	7.90	4.66	3.24	0.001	0.016
CTSW	8.98	6.05	2.92	0.000	0.001
ITM2A	9.09	6.16	2.92	0.000	0.005
ATP6V0C	1.37	-1.56	2.91	0.007	0.045
TYROBP	7.27	4.54	2.71	0.000	0.005
TNFRSF14	6.81	4.22	2.63	0.000	0.001
TIPARP	8.23	5.64	2.61	0.002	0.021
FUT4	8.06	5.47	2.60	0.000	0.000
PALM2AKAP2	7.79	5.26	2.54	0.000	0.000
DLC1	7.59	5.10	2.48	0.005	0.036
CYBA	8.02	5.63	2.41	0.000	0.004
PTGER2	6.82	4.42	2.39	0.000	0.002
TESC	5.94	3.54	2.38	0.004	0.032
TENT5A	8.38	6.03	2.36	0.000	0.003
RPS6KA2	4.67	2.36	2.31	0.004	0.031
YRDC	5.55	3.20	2.31	0.003	0.027
MAP3K8	7.66	5.36	2.29	0.006	0.044
FAM107B	6.29	4.06	2.25	0.000	0.002
TSC22D3	8.92	6.67	2.24	0.001	0.016
DUSP10	8.36	6.19	2.17	0.006	0.043
PIWIL4	5.65	3.46	2.10	0.003	0.029
BAHCC1	8.83	6.74	2.09	0.000	0.003
CALR	10.79	8.72	2.07	0.000	0.000
B3GNT2	8.24	6.18	2.07	0.000	0.002
CTSA	8.24	6.19	2.04	0.000	0.000
CD38	9.12	7.09	2.04	0.002	0.018
CLEC12A	6.90	4.88	2.02	0.005	0.039
GLUL	10.37	8.38	2.00	0.000	0.003

HCST	6.91	4.93	1.98	0.002	0.021
SNRPB	7.30	5.41	1.92	0.000	0.002
SPTY2D1	7.02	5.10	1.92	0.007	0.046
SLC7A5	6.21	4.35	1.90	0.002	0.022
ERP29	7.81	5.92	1.90	0.000	0.001
STK17B	8.69	6.80	1.89	0.003	0.024
ARL4A	6.92	5.06	1.84	0.001	0.011
STK17A	5.67	3.85	1.83	0.001	0.015
AGTPBP1	8.21	6.39	1.82	0.000	0.002
LTC4S	3.28	1.51	1.80	0.005	0.038
DBI	6.73	4.94	1.79	0.001	0.016
FYB1	7.68	5.89	1.77	0.007	0.047
PHPT1	5.09	3.32	1.76	0.004	0.032
RAB32	6.76	4.98	1.74	0.001	0.010
IGFBP7	8.06	6.33	1.73	0.001	0.015
CD48	6.73	4.97	1.73	0.001	0.015
TMSB4X	10.42	8.69	1.73	0.000	0.005
RAB5C	5.10	3.35	1.73	0.003	0.026
ITM2C	8.75	7.04	1.70	0.000	0.005
MPND	4.83	3.15	1.70	0.004	0.033
SNX30	6.14	4.42	1.70	0.000	0.005
PDIA3	8.81	7.12	1.70	0.000	0.002
ARID5A	5.52	3.84	1.67	0.005	0.039
MRPS36	4.99	3.36	1.67	0.002	0.022
AKIRIN1	6.83	5.16	1.67	0.001	0.008
ATP5PO	5.86	4.22	1.67	0.001	0.015
OSBPL5	6.32	4.65	1.67	0.006	0.043
MRPL33	5.75	4.10	1.65	0.004	0.031
GZF1	5.66	3.97	1.64	0.003	0.026
GAS7	7.53	5.89	1.63	0.001	0.011
ATP6V0B	7.04	5.39	1.63	0.000	0.002
DNAJB11	6.51	4.87	1.63	0.001	0.011
PAG1	6.55	4.95	1.62	0.005	0.038
PLEKHF2	6.32	4.68	1.62	0.006	0.043
GPX1	8.13	6.52	1.61	0.001	0.014
POLE4	4.02	2.35	1.61	0.000	0.007
SEC61G	5.43	3.89	1.60	0.006	0.041
C1D	4.99	3.44	1.60	0.002	0.017
TADA1	5.60	4.00	1.58	0.007	0.046
SNRPC	6.41	4.84	1.58	0.000	0.006
CMTM6	8.16	6.58	1.58	0.000	0.002
NOP16	4.72	3.30	1.56	0.007	0.046

STAP1	5.89	4.37	1.55	0.001	0.011
BUD23	5.25	3.70	1.55	0.006	0.042
PPIF	6.66	5.11	1.55	0.004	0.030
RAP2C	6.72	5.19	1.54	0.005	0.037
LAT2	8.60	7.06	1.54	0.001	0.016
RPL22L1	7.44	5.92	1.52	0.001	0.010
ATF4	9.32	7.80	1.52	0.002	0.021
MRPL54	5.48	3.95	1.52	0.003	0.025
DDX21	8.52	7.00	1.52	0.000	0.001
LAPTM4A	6.87	5.36	1.51	0.002	0.021
FRAT2	5.20	3.68	1.51	0.004	0.030
RAD23B	8.02	6.53	1.50	0.000	0.002
ATP5MG	6.39	4.92	1.49	0.002	0.019
DFFB	5.26	3.74	1.49	0.006	0.040
MYDGF	5.44	3.95	1.49	0.002	0.019
TMEM167B	6.68	5.20	1.49	0.003	0.029
SH3KBP1	7.21	5.73	1.48	0.000	0.001
JTB	5.62	4.18	1.48	0.002	0.023
CORO1A	8.66	7.19	1.47	0.002	0.021
NDUFB11	6.27	4.82	1.47	0.001	0.011
PTMA	10.80	9.33	1.47	0.000	0.000
NIP7	5.37	3.94	1.47	0.000	0.006
UQCRB	8.27	6.80	1.47	0.000	0.001
PLD1	7.10	5.62	1.46	0.000	0.005
NDUFB2	5.76	4.29	1.46	0.003	0.024
UBE2M	5.39	3.94	1.46	0.000	0.006
MEX3C	7.91	6.46	1.46	0.002	0.023
TFB2M	5.35	3.87	1.45	0.006	0.043
TSEN54	5.60	4.14	1.45	0.002	0.021
HLA-C	9.50	8.06	1.45	0.002	0.023
SLC25A6	8.89	7.45	1.45	0.000	0.006
PGAM1	6.19	4.71	1.45	0.000	0.006
LSM14B	6.26	4.84	1.44	0.000	0.007
FTL	10.22	8.78	1.44	0.003	0.024
RNF138	7.20	5.77	1.44	0.005	0.038
EEF1B2	10.48	9.05	1.43	0.000	0.004
PTDSS1	8.38	6.95	1.42	0.000	0.003
BLOC1S2	5.45	4.04	1.42	0.001	0.007
MOAP1	6.17	4.75	1.42	0.007	0.048
GET3	5.82	4.39	1.41	0.001	0.010
RPL37A	11.22	9.80	1.41	0.004	0.030
LAMTOR4	6.37	4.95	1.41	0.000	0.005

PM20D2	7.69	6.28	1.41	0.002	0.019
COPS9	4.62	3.27	1.40	0.007	0.047
GSR	6.51	5.12	1.40	0.000	0.004
ALYREF	6.40	5.00	1.40	0.001	0.013
RNF139	7.14	5.74	1.39	0.002	0.018
ABT1	5.57	4.20	1.39	0.003	0.024
SCCPDH	7.80	6.42	1.39	0.003	0.026
CAPG	7.16	5.75	1.39	0.005	0.039
MPZL1	6.90	5.51	1.38	0.003	0.028
HK2	7.06	5.68	1.38	0.000	0.007
STK26	8.38	7.00	1.38	0.000	0.003
HENMT1	6.82	5.44	1.38	0.007	0.049
RPN1	8.68	7.30	1.38	0.001	0.016
MRPL44	5.70	4.34	1.38	0.007	0.047
COX6C	7.10	5.74	1.37	0.001	0.008
LSM3	5.68	4.31	1.37	0.000	0.002
JPT1	6.42	5.07	1.37	0.004	0.029
GRAMD4	7.50	6.14	1.36	0.001	0.012
GM2A	6.87	5.51	1.36	0.000	0.001
FAM53B	6.11	4.78	1.36	0.000	0.006
BAK1	5.25	3.90	1.36	0.007	0.045
ETF1	7.97	6.62	1.36	0.004	0.030
BZW1	8.48	7.13	1.36	0.000	0.004
TXNRD1	8.26	6.92	1.35	0.000	0.003
TUBA1B	9.51	8.17	1.34	0.000	0.006
NUDT15	4.40	3.05	1.34	0.008	0.050
RPS27	11.10	9.76	1.34	0.002	0.017
DAZAP2	8.40	7.06	1.34	0.003	0.024
UBE2J1	8.05	6.72	1.34	0.004	0.033
RSL24D1	8.39	7.06	1.33	0.002	0.020
RPL39	10.73	9.40	1.33	0.003	0.028
GNA15	7.86	6.55	1.32	0.003	0.024
SF3B6	6.62	5.30	1.32	0.000	0.004
NDUFS5	6.94	5.63	1.32	0.002	0.019
MAPRE1	7.55	6.24	1.31	0.002	0.019
CYC1	6.29	4.98	1.30	0.004	0.032
CENPU	6.98	5.68	1.30	0.001	0.009
HSP90B1	9.43	8.14	1.30	0.006	0.041
HNRNPL	8.22	6.92	1.29	0.000	0.005
TRIR	6.73	5.42	1.29	0.005	0.038
FEM1A	6.18	4.90	1.29	0.007	0.045
BRIX1	5.81	4.54	1.29	0.000	0.004

NDUFS6	4.53	3.25	1.29	0.001	0.014
TMED1	4.64	3.38	1.29	0.003	0.024
COX6A1	5.92	4.65	1.28	0.002	0.021
RPS21	8.70	7.42	1.28	0.001	0.016
ZNF92	6.41	5.14	1.28	0.007	0.048
IRF2BP2	9.29	8.02	1.27	0.000	0.006
TMEM9B	5.32	4.07	1.27	0.003	0.027
HNRNPA0	7.19	5.94	1.27	0.000	0.004
NHP2	6.16	4.91	1.27	0.001	0.012
YBX1	9.44	8.18	1.26	0.000	0.001
ZFP91	7.23	5.97	1.26	0.002	0.017
C16orf54	7.32	6.06	1.26	0.000	0.006
ELOC	5.52	4.26	1.26	0.002	0.018
UBE2Q2	7.21	5.95	1.26	0.001	0.012
BTF3L4	7.11	5.86	1.26	0.000	0.004
HNRNPAB	7.42	6.18	1.25	0.000	0.003
NRBP1	7.20	5.94	1.25	0.002	0.023
RPL6	10.82	9.56	1.25	0.001	0.012
MOB1A	9.12	7.87	1.25	0.000	0.004
H2AZ1	7.97	6.72	1.25	0.005	0.036
TIMM17A	5.83	4.61	1.24	0.000	0.004
CDC42	9.58	8.35	1.24	0.001	0.008
UQCRFS1	6.65	5.40	1.24	0.002	0.018
GSTO1	6.65	5.41	1.24	0.002	0.023
C1QBP	7.46	6.23	1.23	0.001	0.008
MRPL21	5.28	4.05	1.23	0.007	0.046
CCT2	8.72	7.49	1.22	0.000	0.001
PTP4A2	8.53	7.32	1.22	0.005	0.036
HPS6	4.95	3.76	1.22	0.005	0.040
PNO1	4.71	3.51	1.22	0.004	0.030
HDGF	8.58	7.36	1.22	0.000	0.001
PPP2CA	7.74	6.53	1.22	0.002	0.019
BAG1	6.82	5.60	1.22	0.005	0.036
UTP11	5.78	4.58	1.21	0.001	0.008
NDUFA4	7.32	6.10	1.21	0.000	0.004
EIF5A	8.19	6.99	1.21	0.001	0.010
MRPL22	4.44	3.22	1.21	0.006	0.040
VASP	6.91	5.71	1.21	0.001	0.013
LAMP1	7.66	6.45	1.21	0.000	0.002
CMTM3	6.48	5.29	1.20	0.002	0.020
TRIM26	5.46	4.27	1.20	0.002	0.019
CLIP2	7.88	6.68	1.20	0.001	0.014

RBM14	7.49	6.29	1.20	0.005	0.036
RPS24	11.46	10.27	1.20	0.002	0.019
RPL35	10.01	8.83	1.20	0.006	0.044
ARPC4	6.58	5.40	1.19	0.001	0.012
TOMM40	5.86	4.66	1.19	0.007	0.045
ZBTB33	7.02	5.83	1.19	0.001	0.015
RPL27A	10.60	9.41	1.19	0.001	0.008
APLP2	9.06	7.89	1.19	0.005	0.039
HMGN1	8.94	7.75	1.19	0.000	0.003
DNAJC14	5.62	4.48	1.19	0.005	0.036
RPL41	10.14	8.94	1.19	0.005	0.035
BID	5.91	4.71	1.18	0.001	0.011
CDV3	8.52	7.34	1.18	0.000	0.001
DYNLL2	6.50	5.34	1.17	0.000	0.007
NAXE	5.18	4.01	1.17	0.005	0.039
RPS18	11.71	10.53	1.17	0.004	0.030
PSMD8	6.71	5.54	1.17	0.002	0.019
PSMB1	7.32	6.15	1.17	0.001	0.010
PGK1	9.33	8.16	1.17	0.000	0.004
PSMB6	5.69	4.55	1.16	0.005	0.035
SLC38A2	9.43	8.27	1.16	0.004	0.030
DDOST	8.20	7.04	1.16	0.000	0.002
UFC1	7.07	5.92	1.16	0.001	0.016
NCF4	7.13	5.97	1.16	0.005	0.036
PPP4C	6.14	4.97	1.16	0.005	0.036
NDUFA6	5.49	4.34	1.16	0.008	0.050
RPF1	5.95	4.80	1.16	0.001	0.011
GSTP1	8.29	7.14	1.16	0.002	0.021
GTF3A	8.11	6.96	1.16	0.001	0.016
UBE2E1	7.62	6.47	1.15	0.000	0.003
TFRC	9.45	8.29	1.15	0.001	0.008
COX8A	5.99	4.84	1.15	0.002	0.023
TUFM	7.54	6.39	1.15	0.000	0.005
COMMD9	6.51	5.33	1.15	0.005	0.037
LSM4	6.06	4.91	1.15	0.001	0.011
SEC61B	5.96	4.84	1.15	0.007	0.049
DRAP1	6.27	5.12	1.15	0.003	0.029
SMYD2	5.63	4.49	1.14	0.004	0.033
CD63	7.51	6.36	1.14	0.004	0.030
LAMTOR5	5.99	4.85	1.14	0.000	0.005
ACTR3	8.82	7.68	1.14	0.000	0.001
TMSB10	9.79	8.65	1.14	0.006	0.044

FAM168B	7.03	5.90	1.14	0.006	0.044
ZDHHC20	7.56	6.43	1.14	0.005	0.039
TCP1	8.51	7.37	1.14	0.000	0.005
VDAC2	7.43	6.29	1.14	0.000	0.003
DHRS7	6.24	5.11	1.14	0.001	0.014
BACH1	8.05	6.92	1.13	0.005	0.037
COPS3	7.21	6.08	1.13	0.001	0.014
ZPR1	6.80	5.67	1.13	0.001	0.010
SLC3A2	6.85	5.72	1.13	0.001	0.009
NDRG1	7.15	6.02	1.13	0.003	0.025
SUMO1	6.85	5.74	1.13	0.001	0.011
HMGN3	7.37	6.24	1.13	0.002	0.016
RPL21	10.40	9.28	1.13	0.007	0.048
SET	9.91	8.78	1.12	0.000	0.003
RPS3	11.04	9.91	1.12	0.003	0.029
B2M	11.54	10.43	1.12	0.005	0.039
PSMC3	6.64	5.52	1.12	0.000	0.006
TPI1	8.67	7.55	1.12	0.001	0.011
GUCD1	7.45	6.34	1.12	0.001	0.013
POLE3	6.94	5.82	1.12	0.000	0.006
SLBP	6.66	5.55	1.12	0.007	0.049
RPL27	9.53	8.42	1.12	0.007	0.046
MAN2B1	7.03	5.90	1.11	0.003	0.027
RPS7	10.50	9.39	1.11	0.007	0.047
PPIB	8.02	6.91	1.11	0.000	0.006
UTP18	6.39	5.29	1.10	0.001	0.013
ARF1	8.18	7.08	1.10	0.001	0.014
GALNT1	8.15	7.05	1.10	0.000	0.001
SUB1	8.41	7.32	1.10	0.001	0.012
SMS	6.42	5.32	1.10	0.001	0.013
CNOT8	7.81	6.71	1.10	0.001	0.009
LRRC59	7.07	5.97	1.10	0.000	0.003
UBL5	6.37	5.28	1.10	0.004	0.032
FAM162A	4.92	3.82	1.10	0.008	0.050
SEC13	6.53	5.43	1.10	0.000	0.004
GLRX5	5.08	4.00	1.10	0.005	0.035
RPS6	12.02	10.92	1.10	0.007	0.048
COX7C	8.00	6.90	1.09	0.002	0.017
ARF4	6.60	5.51	1.09	0.002	0.021
EMC4	5.76	4.68	1.09	0.004	0.031
GTPBP4	6.62	5.54	1.09	0.000	0.007
DNAJA2	7.01	5.92	1.09	0.000	0.007

SPAG7	5.71	4.64	1.09	0.001	0.013
IDH2	7.92	6.84	1.08	0.002	0.021
RPLP2	9.76	8.67	1.08	0.006	0.041
SAP18	7.61	6.53	1.08	0.005	0.035
EEF1A1	14.30	13.22	1.08	0.005	0.039
EIF4B	10.61	9.53	1.08	0.003	0.023
PPP1CA	7.41	6.33	1.08	0.001	0.016
RPL34	10.35	9.28	1.07	0.007	0.045
TMA7	6.98	5.91	1.07	0.002	0.021
STOM	7.79	6.71	1.07	0.000	0.007
UBA52	9.39	8.32	1.07	0.006	0.043
CNPY3	7.41	6.34	1.07	0.000	0.006
PAK1IP1	4.74	3.66	1.07	0.006	0.044
PHF5A	5.41	4.38	1.07	0.005	0.037
COX7A2	6.39	5.34	1.07	0.005	0.039
FUNDC2	5.92	4.86	1.07	0.001	0.015
NACA	10.04	8.97	1.07	0.002	0.020
PUF60	6.84	5.78	1.06	0.003	0.029
SLC25A5	7.80	6.74	1.06	0.001	0.009
COX4I1	8.00	6.94	1.06	0.000	0.005
LSM1	4.97	3.93	1.06	0.006	0.041
RPL11	10.84	9.78	1.05	0.003	0.029
RPIA	5.06	4.03	1.05	0.002	0.023
RPS27A	10.74	9.68	1.05	0.004	0.031
RPS19	10.68	9.63	1.05	0.005	0.037
RPS23	11.15	10.09	1.05	0.004	0.033
RNF6	6.56	5.52	1.05	0.002	0.020
NRAS	7.67	6.62	1.05	0.004	0.033
SEC11A	7.09	6.04	1.05	0.001	0.016
ATP5MC3	6.99	5.95	1.05	0.000	0.005
CANX	10.18	9.13	1.05	0.001	0.010
C9orf78	6.75	5.71	1.05	0.004	0.035
MRPS35	6.34	5.32	1.04	0.001	0.016
POMP	5.65	4.63	1.04	0.002	0.017
RPS20	10.76	9.72	1.04	0.006	0.040
RPL36	9.45	8.41	1.04	0.004	0.030
TOMM22	6.61	5.58	1.04	0.002	0.017
AZIN1	8.22	7.19	1.04	0.001	0.013
ARPC3	8.17	7.14	1.03	0.001	0.011
HSPA9	8.59	7.56	1.03	0.000	0.006
CDC123	6.52	5.49	1.03	0.000	0.001
CTSC	7.85	6.82	1.03	0.003	0.026

RPS8	11.44	10.41	1.03	0.004	0.033
TMX4	7.42	6.39	1.03	0.002	0.018
RPL30	10.55	9.52	1.03	0.008	0.050
SUMO3	6.74	5.73	1.03	0.004	0.032
CTSS	8.04	7.01	1.03	0.007	0.046
PPM1G	6.95	5.93	1.03	0.000	0.002
GRB2	7.79	6.77	1.03	0.006	0.044
UQCRQ	6.20	5.18	1.02	0.002	0.021
RPS13	9.89	8.87	1.02	0.004	0.033
RPL4	11.67	10.65	1.02	0.003	0.023
COX5A	6.22	5.20	1.02	0.002	0.021
NPM1	10.70	9.67	1.02	0.001	0.015
UBE2G1	6.37	5.36	1.02	0.001	0.012
M6PR	7.47	6.45	1.02	0.003	0.029
EDF1	7.04	6.02	1.02	0.001	0.012
ZBTB1	7.49	6.47	1.02	0.007	0.045
STRAP	6.92	5.91	1.02	0.002	0.020
PSME1	8.07	7.05	1.02	0.003	0.023
BCAP31	6.94	5.92	1.01	0.002	0.019
RPL8	9.70	8.69	1.01	0.001	0.012
YTHDF2	7.45	6.45	1.01	0.003	0.027
SUMO2	7.76	6.75	1.01	0.001	0.009
SLC39A7	5.41	4.45	1.01	0.004	0.035
PSME2	6.99	5.98	1.01	0.003	0.024
RPL29	10.17	9.16	1.00	0.005	0.039
MIS18BP1	8.66	7.67	1.00	0.002	0.022
ZNF785	3.94	4.99	-1.00	0.004	0.033
PCNT	6.68	7.69	-1.00	0.002	0.021
SLC25A12	4.66	5.64	-1.01	0.003	0.023
OGT	9.66	10.67	-1.02	0.001	0.008
KMT2D	7.31	8.33	-1.02	0.008	0.049
GANC	5.13	6.11	-1.02	0.000	0.006
PARP14	7.45	8.46	-1.02	0.003	0.024
EXD3	3.42	4.49	-1.02	0.007	0.049
TBCK	6.16	7.18	-1.03	0.005	0.035
NHLRC2	6.01	7.03	-1.03	0.001	0.009
TRRAP	7.06	8.09	-1.03	0.001	0.016
ATP11C	5.47	6.51	-1.03	0.006	0.044
CCDC14	7.01	8.05	-1.03	0.003	0.025
LUC7L3	7.78	8.81	-1.03	0.004	0.029
DMTF1	7.06	8.10	-1.03	0.001	0.013
MON2	6.75	7.77	-1.04	0.002	0.019

ATXN2	5.67	6.68	-1.04	0.002	0.018
MRNIP	3.87	4.93	-1.04	0.003	0.026
CARF	5.31	6.35	-1.04	0.000	0.002
SIK3	6.07	7.11	-1.04	0.005	0.035
SUPT3H	3.89	4.94	-1.04	0.005	0.035
C1QTNF3	2.82	3.84	-1.05	0.002	0.017
PRORP	4.11	5.21	-1.05	0.001	0.015
MARF1	6.43	7.48	-1.05	0.002	0.020
IQGAP2	8.14	9.19	-1.05	0.004	0.032
RNF213	8.54	9.60	-1.05	0.001	0.009
ZNF605	4.35	5.41	-1.06	0.003	0.028
ZNF17	3.26	4.42	-1.06	0.006	0.043
UTRN	8.55	9.62	-1.07	0.001	0.009
ZNF397	4.87	6.00	-1.07	0.002	0.023
CSAD	3.88	4.92	-1.07	0.001	0.010
VPS8	6.79	7.85	-1.07	0.004	0.032
RNPC3	5.83	6.92	-1.08	0.000	0.004
LPP	6.17	7.23	-1.08	0.003	0.023
ZNF169	3.22	4.42	-1.08	0.004	0.030
CCDC6	5.90	6.98	-1.08	0.001	0.008
NFXL1	4.05	5.17	-1.08	0.000	0.007
PRDM11	4.37	5.43	-1.08	0.004	0.033
SLC16A5	3.88	4.93	-1.08	0.006	0.041
NEK1	4.83	5.87	-1.08	0.006	0.044
INPP5F	4.48	5.55	-1.08	0.004	0.030
NBPF14	4.49	5.54	-1.08	0.001	0.016
BORCS5	3.76	4.87	-1.08	0.004	0.033
DTNBP1	3.28	4.24	-1.08	0.007	0.049
ZNF70	5.03	6.10	-1.08	0.007	0.049
TOM1L2	4.54	5.59	-1.09	0.000	0.002
MLYCD	4.61	5.73	-1.09	0.004	0.031
ZNF514	5.02	6.16	-1.09	0.001	0.014
BRD4	5.50	6.59	-1.09	0.003	0.029
ZNRF1	5.60	6.71	-1.09	0.003	0.026
AGO2	6.12	7.21	-1.09	0.000	0.006
ARID1B	8.00	9.10	-1.10	0.000	0.003
HSD17B7	3.09	4.27	-1.10	0.007	0.045
CCM2	5.51	6.61	-1.10	0.002	0.022
PML	5.76	6.87	-1.10	0.001	0.010
RNF8	3.92	5.00	-1.10	0.002	0.020
LRSAM1	4.58	5.72	-1.11	0.001	0.010
RAD51B	4.36	5.47	-1.11	0.001	0.009

FAM120B	5.12	6.22	-1.11	0.001	0.013
ADPRM	4.53	5.71	-1.11	0.000	0.007
CDC16	5.81	6.94	-1.12	0.000	0.003
TECPR2	3.93	5.09	-1.12	0.003	0.024
TTC14	6.72	7.85	-1.12	0.003	0.029
ATF7	4.80	5.89	-1.12	0.005	0.035
KIAA0825	3.48	4.58	-1.12	0.004	0.030
ZNF621	5.32	6.48	-1.13	0.000	0.004
KMT2A	7.76	8.89	-1.13	0.001	0.009
SLC48A1	3.63	4.77	-1.13	0.002	0.018
ELMO1	7.82	8.96	-1.13	0.007	0.045
TARBP1	8.02	9.16	-1.14	0.000	0.007
RPS6KA5	4.82	5.92	-1.14	0.005	0.039
ACP2	3.50	4.73	-1.14	0.004	0.032
MBTPS2	3.14	4.26	-1.14	0.002	0.023
CSRP1	4.95	6.10	-1.14	0.001	0.012
SOS1	6.48	7.62	-1.15	0.007	0.047
KLHL6	6.63	7.78	-1.15	0.003	0.027
ZNF33B	5.83	7.02	-1.16	0.000	0.007
ZNF620	3.00	4.23	-1.16	0.002	0.019
SIN3B	4.67	5.81	-1.16	0.002	0.020
VAV3	7.02	8.18	-1.16	0.000	0.007
PHACTR4	5.64	6.81	-1.16	0.001	0.009
ZC3H6	4.75	5.88	-1.16	0.002	0.016
SCAPER	5.27	6.39	-1.16	0.001	0.015
MLKL	4.67	5.78	-1.16	0.006	0.040
CPLANE1	6.75	7.90	-1.16	0.000	0.002
MFGE8	4.13	5.33	-1.17	0.007	0.049
TRDMT1	4.53	5.65	-1.17	0.002	0.017
ZNF445	6.34	7.52	-1.17	0.000	0.005
GATAD2B	5.64	6.79	-1.17	0.000	0.003
TFB1M	4.07	5.29	-1.18	0.004	0.030
ZFP36L2	7.73	8.92	-1.18	0.003	0.023
DGKE	5.05	6.18	-1.19	0.002	0.020
CCDC191	3.45	4.64	-1.19	0.002	0.023
PKNOX1	4.11	5.28	-1.19	0.000	0.007
GPR89B	2.99	4.22	-1.19	0.001	0.008
STK36	3.93	5.21	-1.19	0.003	0.029
STX16	5.28	6.45	-1.20	0.001	0.008
MAP2K5	4.24	5.38	-1.20	0.000	0.004
CLDN15	3.78	4.97	-1.20	0.000	0.007
TMEM91	3.03	4.32	-1.20	0.003	0.024

ALG10B	4.72	5.99	-1.20	0.001	0.008
EXOG	3.60	4.85	-1.21	0.002	0.018
TAMM41	3.68	4.94	-1.21	0.001	0.008
PIK3C2B	4.56	5.74	-1.21	0.003	0.028
ZNF133	3.67	4.94	-1.21	0.001	0.016
SLC23A2	5.07	6.24	-1.21	0.001	0.008
WWP1	4.52	5.71	-1.22	0.005	0.035
MTHFR	5.09	6.29	-1.22	0.001	0.013
SYNRG	5.60	6.81	-1.23	0.005	0.038
WDR27	4.89	6.15	-1.23	0.002	0.018
ZBTB37	6.22	7.47	-1.24	0.001	0.015
FAM222B	3.34	4.62	-1.24	0.002	0.019
CARD8	6.92	8.15	-1.24	0.005	0.035
SYNE1	6.16	7.39	-1.24	0.000	0.004
MAPKBP1	5.15	6.41	-1.24	0.002	0.021
MRTFB	4.41	5.64	-1.25	0.002	0.023
ZFP90	5.13	6.41	-1.25	0.003	0.029
ENOSF1	5.67	6.92	-1.25	0.004	0.033
SP2	2.50	3.76	-1.25	0.005	0.039
FNBP1	7.23	8.49	-1.25	0.000	0.000
ZSCAN30	5.06	6.34	-1.26	0.000	0.006
ANKRD36	7.10	8.36	-1.26	0.001	0.009
SHPK	1.33	2.59	-1.26	0.007	0.048
IGF2BP2	5.51	6.77	-1.26	0.006	0.041
PIAS3	3.42	4.70	-1.26	0.000	0.006
ALPK1	5.44	6.70	-1.26	0.000	0.004
ZNF891	4.41	5.66	-1.26	0.000	0.005
ZNF572	2.46	3.79	-1.27	0.006	0.044
SERAC1	3.93	5.27	-1.27	0.001	0.014
CAMTA2	3.31	4.62	-1.27	0.003	0.025
WSB1	7.17	8.45	-1.27	0.000	0.005
PIGM	4.33	5.72	-1.28	0.002	0.022
SSBP2	7.28	8.57	-1.29	0.004	0.033
TMEM234	3.21	4.60	-1.29	0.001	0.014
ERG	7.03	8.32	-1.29	0.005	0.039
SNAPC3	5.03	6.38	-1.29	0.002	0.023
SLC24A1	3.85	5.13	-1.29	0.003	0.026
C1RL	4.93	6.20	-1.30	0.000	0.003
ATXN7L1	4.28	5.54	-1.30	0.002	0.017
ZNF862	4.58	5.88	-1.30	0.002	0.023
ERICH1	5.26	6.62	-1.30	0.000	0.005
NUDT6	2.62	3.85	-1.30	0.007	0.045

ARMC2	3.10	4.38	-1.31	0.000	0.006
NBEAL2	6.80	8.11	-1.31	0.004	0.035
ALG13	5.95	7.26	-1.31	0.000	0.002
KIAA0753	4.46	5.77	-1.31	0.000	0.001
SCAI	5.48	6.80	-1.31	0.000	0.005
PARP11	4.41	5.72	-1.31	0.001	0.008
TRANK1	6.56	7.88	-1.31	0.002	0.018
SLC26A6	2.77	3.99	-1.32	0.004	0.031
NEK7	5.55	6.86	-1.33	0.005	0.036
ABCC1	7.16	8.49	-1.33	0.000	0.002
SLC38A6	2.50	3.83	-1.33	0.001	0.016
SCYL3	4.17	5.57	-1.33	0.001	0.010
PRH1	2.70	3.94	-1.34	0.002	0.023
LENG8	7.43	8.78	-1.34	0.001	0.012
DNHD1	5.08	6.45	-1.34	0.000	0.007
USP54	3.66	4.99	-1.34	0.001	0.010
UAP1L1	3.48	4.90	-1.34	0.003	0.024
ZNF83	6.07	7.42	-1.35	0.000	0.002
LRRC37A3	3.20	4.40	-1.35	0.006	0.041
ICA1L	3.44	4.65	-1.35	0.003	0.023
ABR	4.82	6.20	-1.35	0.006	0.041
PEA15	3.31	4.59	-1.35	0.003	0.024
ZC4H2	2.83	4.14	-1.36	0.003	0.024
ACOT7	2.61	3.90	-1.36	0.003	0.028
ITPR1	7.55	8.92	-1.37	0.001	0.011
FRA10AC1	3.88	5.27	-1.37	0.003	0.026
PLCB1	6.04	7.37	-1.37	0.004	0.031
ZNF619	4.10	5.52	-1.37	0.000	0.001
ZC3HAV1L	3.10	4.58	-1.37	0.001	0.014
SNX10	3.56	5.04	-1.37	0.004	0.032
ARHGAP33	3.20	4.61	-1.38	0.007	0.046
IFT81	3.19	4.62	-1.38	0.000	0.003
C21orf58	3.98	5.40	-1.38	0.001	0.012
NPHP3	3.40	4.83	-1.38	0.000	0.004
ANKRD36C	7.33	8.73	-1.39	0.002	0.023
SAMD9L	6.45	7.84	-1.39	0.004	0.032
ANO10	3.66	4.95	-1.40	0.004	0.029
BMP2K	6.52	7.91	-1.40	0.000	0.001
CASP10	5.88	7.29	-1.40	0.001	0.011
BCORL1	3.86	5.25	-1.40	0.002	0.023
HDAC8	4.44	5.85	-1.41	0.002	0.016
CEMIP2	3.81	5.17	-1.41	0.002	0.019

EXOC1	5.88	7.30	-1.41	0.000	0.002
ZSWIM6	3.78	5.26	-1.42	0.007	0.047
SYNGAP1	4.68	6.13	-1.42	0.001	0.009
C20orf96	3.32	4.75	-1.43	0.000	0.001
ZMAT1	5.46	6.85	-1.43	0.000	0.004
RBM12B	5.67	7.14	-1.44	0.002	0.019
NEK11	2.60	4.01	-1.44	0.002	0.022
PHC1	4.83	6.28	-1.45	0.004	0.033
SMAD3	4.59	6.07	-1.46	0.001	0.008
TRIM66	4.74	6.18	-1.46	0.003	0.027
ZNF518B	4.57	6.06	-1.47	0.000	0.006
ERMP1	6.19	7.65	-1.47	0.001	0.008
MBD5	5.60	7.07	-1.47	0.000	0.000
MSI2	8.01	9.49	-1.48	0.001	0.013
ARID5B	4.89	6.33	-1.49	0.007	0.047
ZNF69	4.71	6.23	-1.50	0.000	0.000
PGGHG	4.37	5.86	-1.51	0.003	0.025
SUN1	4.15	5.73	-1.51	0.000	0.002
ZNF599	1.33	2.84	-1.51	0.002	0.023
PRPF40B	2.00	3.60	-1.53	0.004	0.032
MFSD4B	5.28	6.85	-1.55	0.000	0.003
RIPOR1	3.42	4.91	-1.55	0.001	0.014
RFX3	5.03	6.59	-1.56	0.000	0.001
DTNB	3.33	4.83	-1.56	0.001	0.009
TRPV1	1.99	3.64	-1.56	0.000	0.003
ACSS2	4.03	5.52	-1.57	0.003	0.026
LRRC37A2	3.52	4.95	-1.57	0.004	0.031
OSGIN1	0.83	2.42	-1.57	0.008	0.050
THBS3	4.67	6.24	-1.58	0.001	0.011
ETFBKMT	1.45	3.00	-1.58	0.002	0.022
PLA2G6	4.75	6.35	-1.59	0.001	0.007
STXBP4	4.07	5.64	-1.59	0.000	0.000
BCL9L	3.02	4.59	-1.59	0.004	0.035
GBP4	6.28	7.88	-1.60	0.004	0.031
ZNF347	3.53	5.21	-1.61	0.000	0.004
CLSTN3	4.18	5.82	-1.61	0.000	0.001
YAE1	2.11	3.88	-1.61	0.005	0.037
ELOVL6	2.89	4.61	-1.61	0.006	0.043
TTC21A	1.71	3.24	-1.61	0.002	0.020
IQSEC1	3.42	5.01	-1.62	0.000	0.005
GLMP	2.32	3.90	-1.62	0.003	0.029
CCDC171	5.82	7.42	-1.63	0.001	0.011

ZNF66	4.45	6.04	-1.63	0.000	0.000
LMO7	2.61	4.31	-1.63	0.000	0.001
CROCC	3.38	5.07	-1.64	0.004	0.030
HGSNAT	5.29	6.92	-1.64	0.000	0.005
CAPRIN2	3.96	5.60	-1.64	0.000	0.007
CDKL1	1.78	3.55	-1.64	0.001	0.015
ZKSCAN8P1	1.06	2.75	-1.64	0.003	0.027
RABGAP1	5.65	7.28	-1.65	0.000	0.000
ZHX3	3.27	4.91	-1.65	0.001	0.008
ARL15	2.97	4.63	-1.65	0.001	0.014
SCARF1	4.50	6.13	-1.65	0.000	0.007
PLA2G4A	4.04	5.65	-1.66	0.000	0.004
NAPEPLD	3.26	5.02	-1.66	0.000	0.007
GET4	1.51	3.11	-1.66	0.004	0.033
SVIL	4.95	6.63	-1.67	0.000	0.002
AOPEP	3.81	5.52	-1.68	0.000	0.000
OR2W3	1.93	3.57	-1.68	0.006	0.040
TIAM2	1.23	2.92	-1.68	0.002	0.019
GNAI1	5.15	6.86	-1.68	0.000	0.004
XRRA1	4.26	5.96	-1.69	0.005	0.039
GLCCI1	3.03	4.88	-1.69	0.002	0.018
ZNF283	3.14	4.95	-1.69	0.002	0.023
MAP3K5	5.41	7.03	-1.70	0.003	0.023
ZNF780B	4.48	6.25	-1.70	0.000	0.006
PARP15	3.79	5.60	-1.70	0.004	0.033
KANTR	4.18	5.86	-1.71	0.000	0.001
P2RX7	3.75	5.46	-1.73	0.001	0.013
CCDC121	0.90	2.68	-1.73	0.005	0.038
RMND5B	2.75	4.51	-1.73	0.000	0.004
ULK4	5.02	6.71	-1.74	0.000	0.000
TXK	3.70	5.47	-1.74	0.004	0.033
SLC15A2	5.26	6.97	-1.74	0.002	0.021
PXN	4.08	5.81	-1.75	0.005	0.039
MAST4	5.24	6.97	-1.76	0.000	0.002
RUNX1	6.97	8.74	-1.78	0.001	0.010
C1QTNF6	1.41	3.29	-1.78	0.001	0.010
ANKRD36B	5.76	7.51	-1.78	0.000	0.000
BTBD8	3.69	5.45	-1.78	0.002	0.018
LPIN1	6.05	7.84	-1.78	0.000	0.000
KIAA1549	3.57	5.39	-1.79	0.001	0.013
PIGZ	1.62	3.31	-1.79	0.001	0.011
PRR5	2.43	4.21	-1.80	0.000	0.001

LRRC69	0.56	2.43	-1.80	0.003	0.027
HK1	4.50	6.25	-1.80	0.006	0.043
HIPK2	4.52	6.23	-1.81	0.000	0.002
FLOT1	3.91	5.63	-1.81	0.006	0.042
MICAL3	4.05	5.91	-1.81	0.000	0.003
SBF2	4.93	6.69	-1.81	0.003	0.028
TRIM3	1.32	3.07	-1.82	0.005	0.036
TMEM25	2.30	4.08	-1.82	0.000	0.003
UBQLNL	-0.03	1.75	-1.82	0.006	0.040
CCDC9B	2.43	4.24	-1.83	0.000	0.003
PDK2	2.68	4.40	-1.83	0.001	0.015
NEK3	3.55	5.40	-1.84	0.000	0.002
ARL17B	2.24	4.09	-1.84	0.001	0.008
GLB1L	1.25	3.11	-1.84	0.001	0.013
SPRY3	1.16	2.85	-1.84	0.001	0.013
SCD5	1.44	3.38	-1.86	0.006	0.041
SERPINB9	4.28	6.22	-1.88	0.001	0.010
MUC1	0.90	2.90	-1.88	0.002	0.022
GCSAML	5.00	6.86	-1.89	0.001	0.013
IKZF4	1.48	3.36	-1.89	0.001	0.008
HDAC11	1.21	3.13	-1.89	0.003	0.025
TNRC6C	3.50	5.45	-1.89	0.001	0.008
SYNJ2	3.51	5.35	-1.89	0.001	0.012
PRDM8	3.82	5.53	-1.91	0.005	0.036
BICD1	3.76	5.60	-1.91	0.000	0.002
TRIM62	1.20	2.87	-1.91	0.005	0.036
PRKCH	4.41	6.30	-1.91	0.005	0.035
ZNF507	3.49	5.48	-1.92	0.005	0.037
SKI	3.03	4.89	-1.92	0.002	0.023
ZNF594	3.40	5.45	-1.93	0.004	0.031
TANC2	3.96	5.76	-1.93	0.004	0.030
FAM118A	4.06	6.04	-1.94	0.000	0.002
SEPTIN1	2.30	4.47	-1.94	0.004	0.031
ARMCX4	2.17	4.05	-1.94	0.000	0.002
C17orf67	1.14	2.99	-1.94	0.002	0.018
SMAGP	0.65	2.56	-1.94	0.002	0.022
ZNF563	0.43	2.56	-1.97	0.003	0.026
TMEM63A	5.26	7.22	-1.97	0.000	0.000
STON1	1.12	3.17	-1.98	0.003	0.026
GPR137B	0.47	2.29	-1.98	0.004	0.034
TREML2	1.92	3.81	-1.98	0.002	0.022
SLC4A8	3.46	5.50	-1.98	0.000	0.001

ABO	4.39	6.39	-1.99	0.001	0.015
PSTPIP1	2.59	4.50	-1.99	0.000	0.007
PARP3	2.53	4.45	-1.99	0.001	0.014
ZNF471	2.73	4.85	-1.99	0.002	0.018
VAMP5	1.34	3.34	-1.99	0.005	0.035
PABPC1L	4.21	6.15	-1.99	0.000	0.001
TMEM65	4.59	6.58	-2.00	0.000	0.007
FCHSD1	3.29	5.35	-2.00	0.001	0.016
GPRASP1	1.58	3.53	-2.00	0.001	0.011
F2R	3.98	6.05	-2.00	0.000	0.002
OXCT1	3.57	5.75	-2.01	0.005	0.039
GPR135	2.02	3.99	-2.01	0.000	0.003
PFKM	2.70	4.83	-2.01	0.000	0.000
DUSP18	2.72	4.77	-2.01	0.000	0.002
DNM3	1.85	3.85	-2.03	0.001	0.008
ITGA2B	4.09	5.92	-2.03	0.002	0.017
ACTR3C	2.72	4.72	-2.03	0.000	0.000
TBL1X	2.54	4.42	-2.03	0.004	0.033
RGS12	2.73	4.75	-2.04	0.001	0.016
MCTP1	4.88	6.77	-2.05	0.004	0.030
COL18A1	1.62	3.69	-2.05	0.002	0.023
NYNRIN	4.53	6.48	-2.06	0.006	0.044
POU2F2	2.21	4.32	-2.07	0.007	0.048
TRIP6	2.64	4.70	-2.08	0.004	0.029
DRAM1	3.73	5.74	-2.09	0.000	0.003
ACVR1	2.27	4.34	-2.09	0.002	0.022
CCDC24	0.69	2.76	-2.10	0.006	0.040
SAMD10	2.06	4.24	-2.10	0.000	0.001
ACOT11	4.20	6.23	-2.10	0.001	0.011
LRRC37A	1.87	3.72	-2.10	0.005	0.035
KLHL31	-0.39	1.75	-2.11	0.008	0.049
GUCY1B1	4.16	6.24	-2.12	0.000	0.006
RNF215	2.29	4.42	-2.12	0.000	0.006
ADHFE1	1.20	3.42	-2.13	0.001	0.015
SLC9A9	1.66	3.86	-2.13	0.000	0.002
FAM117A	5.82	7.97	-2.14	0.000	0.001
VSIG10	2.79	4.96	-2.15	0.000	0.001
TET1	3.05	5.11	-2.16	0.001	0.010
ZNF853	-0.15	2.13	-2.16	0.006	0.042
FOXO3B	1.68	3.72	-2.16	0.006	0.040
ZNF449	1.72	3.86	-2.16	0.004	0.034
NFATC2	4.35	6.49	-2.17	0.000	0.001

FAM13A	3.95	6.08	-2.17	0.000	0.000
ATP8B2	4.91	7.11	-2.17	0.000	0.000
KSR1	3.94	6.03	-2.17	0.000	0.005
TMEM140	3.06	5.16	-2.17	0.000	0.004
ME3	4.08	6.32	-2.18	0.005	0.038
FRMD4B	4.51	6.76	-2.19	0.000	0.002
GIMAP1	1.22	3.47	-2.19	0.000	0.006
NR1H3	3.80	5.95	-2.19	0.000	0.002
IGF2BP3	2.70	4.71	-2.20	0.001	0.008
E2F5	1.56	4.16	-2.20	0.007	0.049
L3HYPDH	3.61	5.87	-2.21	0.000	0.000
ZNF662	3.21	5.38	-2.21	0.001	0.012
NRIP1	8.08	10.30	-2.22	0.000	0.001
TAS2R31	1.07	3.25	-2.22	0.000	0.007
HSF5	1.71	3.98	-2.23	0.000	0.000
ANO8	1.02	3.27	-2.24	0.005	0.039
GFOD1	3.03	5.20	-2.25	0.001	0.015
GPR52	0.34	2.54	-2.25	0.008	0.049
MICAL2	2.66	4.92	-2.25	0.005	0.039
ACACB	3.22	5.60	-2.25	0.001	0.009
GDPD3	0.27	2.64	-2.25	0.004	0.030
PLEKHG2	3.47	5.60	-2.27	0.000	0.003
TAFA2	3.34	5.57	-2.27	0.000	0.000
SNX21	-0.51	1.65	-2.27	0.003	0.027
C10orf105	-0.25	2.13	-2.28	0.005	0.035
CLEC2D	3.74	6.06	-2.28	0.000	0.003
NHSL1	0.67	2.78	-2.29	0.003	0.027
KLHL3	2.89	5.22	-2.29	0.000	0.004
ATP6V0A1	3.50	5.82	-2.29	0.005	0.036
CHST13	1.10	3.21	-2.30	0.006	0.043
TJP2	1.62	3.86	-2.31	0.000	0.002
DYNLT5	4.12	6.31	-2.31	0.003	0.025
MYOZ3	1.55	3.88	-2.31	0.006	0.043
NEK10	0.50	2.82	-2.32	0.001	0.012
N6AMT1	2.21	4.72	-2.33	0.000	0.005
NFE2L3	2.54	4.88	-2.33	0.001	0.011
ARHGEF3	4.07	6.47	-2.33	0.000	0.000
ITGB8	2.52	4.57	-2.36	0.006	0.044
AKR7A3	-0.80	1.46	-2.37	0.003	0.023
STARD9	5.88	8.24	-2.37	0.000	0.002
SGIP1	-0.18	2.17	-2.39	0.001	0.016
SNX32	0.31	2.78	-2.41	0.001	0.009

NOTCH2NLA	-0.66	1.84	-2.43	0.002	0.021
H2AJ	2.07	4.73	-2.43	0.005	0.035
TAS2R46	-0.47	1.99	-2.45	0.001	0.013
DNAJC6	2.43	4.85	-2.45	0.000	0.001
LTBP3	3.19	5.54	-2.45	0.000	0.004
ZNF391	1.60	4.24	-2.45	0.002	0.017
GGT7	0.87	3.22	-2.45	0.001	0.009
BIN1	3.75	6.10	-2.46	0.001	0.010
C1R	-0.14	2.20	-2.46	0.001	0.009
ZFHX3	3.16	5.62	-2.47	0.006	0.043
SPINDOC	1.89	4.33	-2.47	0.003	0.028
TMOD2	3.85	6.43	-2.48	0.002	0.016
AMOT	2.16	4.54	-2.48	0.000	0.001
HSPB1	2.02	4.51	-2.48	0.000	0.005
C1orf56	-0.91	1.70	-2.49	0.002	0.020
CEP85L	3.34	5.84	-2.49	0.004	0.035
CUBN	3.05	5.55	-2.50	0.000	0.000
DYTN	2.22	4.68	-2.50	0.001	0.008
RAB3IP	2.24	4.97	-2.51	0.002	0.020
GCAT	1.10	3.45	-2.51	0.003	0.028
FSIP1	-0.45	2.03	-2.52	0.005	0.035
LRBA	7.76	10.28	-2.52	0.000	0.000
TIAM1	-0.22	2.28	-2.53	0.003	0.024
TAS2R19	0.29	2.72	-2.53	0.002	0.019
C11orf80	1.12	3.56	-2.54	0.000	0.006
SLC43A2	1.97	4.47	-2.54	0.000	0.002
CACNA1F	-0.32	2.34	-2.54	0.003	0.024
SLC18B1	0.27	2.89	-2.56	0.008	0.050
SLC6A16	0.01	2.53	-2.56	0.000	0.001
BCL11A	5.41	7.97	-2.57	0.000	0.000
C18orf54	2.64	5.21	-2.57	0.000	0.004
AGPAT4	4.00	6.71	-2.57	0.003	0.024
PPFIBP1	3.64	6.19	-2.57	0.000	0.001
TAS2R3	-0.91	1.79	-2.58	0.001	0.016
DAPK1	5.83	8.41	-2.58	0.001	0.013
DLG5	2.24	4.55	-2.58	0.003	0.029
SH3TC1	4.05	6.58	-2.58	0.001	0.008
MAP1A	4.43	7.08	-2.59	0.003	0.024
CYFIP1	4.52	7.08	-2.59	0.000	0.003
CRIM1	2.98	5.60	-2.59	0.006	0.043
XKR5	-0.90	1.66	-2.59	0.007	0.047
MAP7	4.45	7.04	-2.60	0.000	0.001

TMEM178A	-1.22	1.40	-2.61	0.001	0.015
TAS2R4	0.79	3.55	-2.61	0.000	0.005
TPM2	2.44	5.05	-2.61	0.000	0.002
MFAP3L	-1.12	1.43	-2.62	0.006	0.040
STRIP2	-0.41	2.07	-2.63	0.001	0.009
GRB10	4.40	7.12	-2.63	0.000	0.003
FAAH2	-0.36	2.14	-2.63	0.000	0.007
GRAMD1C	1.23	3.89	-2.63	0.000	0.002
TBC1D3L	-1.08	1.56	-2.64	0.007	0.045
CR1	2.07	4.65	-2.64	0.001	0.008
ARHGAP31	1.59	4.19	-2.65	0.000	0.001
TAS2R20	0.14	2.89	-2.65	0.001	0.009
ATP7B	2.22	5.11	-2.65	0.000	0.001
IQCH	0.28	2.88	-2.66	0.000	0.003
PAQR8	2.44	5.20	-2.66	0.001	0.015
GIPC3	1.02	3.68	-2.67	0.000	0.004
RAB11FIP4	1.12	3.95	-2.67	0.006	0.042
TRIB3	0.59	3.25	-2.67	0.000	0.004
DNAH12	-0.43	2.25	-2.68	0.002	0.023
GNA12	3.34	6.08	-2.68	0.000	0.000
GSTO2	-0.20	2.46	-2.69	0.000	0.002
ADAM28	5.28	7.90	-2.69	0.004	0.034
PCSK5	-0.73	1.74	-2.69	0.005	0.036
GVQW3	3.56	6.32	-2.71	0.000	0.000
FUT10	2.28	5.18	-2.72	0.000	0.001
SNX33	1.88	4.71	-2.72	0.000	0.002
USP27X	0.04	2.64	-2.72	0.005	0.037
FAM47E	-0.16	2.60	-2.74	0.004	0.034
HMGN5	-0.30	2.42	-2.74	0.001	0.011
PLD5P1	0.39	3.27	-2.74	0.000	0.002
PLCG1	1.17	3.96	-2.76	0.002	0.018
RTN2	-0.82	1.95	-2.76	0.006	0.040
REC8	3.24	5.90	-2.77	0.000	0.000
KLRG1	1.58	4.37	-2.77	0.000	0.001
EMILIN1	1.34	4.41	-2.77	0.001	0.013
PNPLA7	2.33	5.10	-2.77	0.000	0.000
PRKN	0.56	3.42	-2.78	0.000	0.001
ANKS6	1.68	4.32	-2.78	0.001	0.015
DUSP19	0.66	3.51	-2.78	0.002	0.020
HSPG2	5.34	8.17	-2.79	0.000	0.002
KLF5	-0.97	1.79	-2.80	0.003	0.026
MAP3K12	2.71	5.38	-2.80	0.000	0.001

BAG2	1.94	4.60	-2.80	0.001	0.011
IL17RC	1.20	4.07	-2.81	0.001	0.012
NEURL1B	3.19	5.76	-2.82	0.008	0.049
SLC45A3	3.66	6.37	-2.82	0.001	0.014
FIGNL2	-1.66	1.21	-2.83	0.001	0.014
TUBG2	0.21	3.10	-2.87	0.000	0.005
EPSTI1	3.06	5.68	-2.87	0.000	0.003
MYO1C	-0.61	2.34	-2.87	0.003	0.026
ARG2	0.00	2.86	-2.89	0.001	0.014
CNKSR1	0.10	2.88	-2.89	0.000	0.005
SETD7	2.03	5.02	-2.90	0.000	0.003
SCN8A	-1.95	1.04	-2.90	0.001	0.010
TMEM144	1.71	4.41	-2.91	0.000	0.003
SH3BGRL2	1.13	4.08	-2.91	0.001	0.008
SPOCK2	0.84	3.93	-2.91	0.003	0.023
DNAH6	1.11	4.01	-2.92	0.003	0.025
LDLR	3.69	6.41	-2.92	0.001	0.012
TGFB1I1	0.23	2.97	-2.93	0.001	0.012
PVR	1.71	4.40	-2.93	0.005	0.039
EML5	-2.11	0.78	-2.93	0.002	0.022
LAYN	-1.96	0.88	-2.93	0.004	0.031
ANKH	1.17	4.03	-2.93	0.000	0.003
RRAS	-1.34	1.51	-2.94	0.006	0.042
TTC28	2.54	5.49	-2.94	0.000	0.007
WDR49	4.51	7.35	-2.94	0.001	0.010
CARD11	1.53	4.85	-2.94	0.000	0.003
SLC35E4	-1.56	1.33	-2.94	0.006	0.040
OSBP2	-0.92	2.02	-2.95	0.002	0.021
PKN3	1.32	4.11	-2.95	0.004	0.034
SEMA4F	-0.12	2.75	-2.95	0.003	0.026
TXNRD3	1.98	4.96	-2.95	0.001	0.014
OR2AK2	-0.87	1.99	-2.96	0.000	0.006
GALNT12	0.50	3.43	-2.96	0.002	0.023
TUBB1	-2.13	0.75	-2.97	0.005	0.037
VANGL1	2.32	5.26	-2.97	0.001	0.012
KHDRBS2	1.05	3.98	-2.97	0.000	0.002
KIF7	0.89	3.93	-2.97	0.000	0.001
OR2L8	-1.28	1.62	-2.97	0.001	0.012
L3MBTL3	2.52	5.54	-2.99	0.001	0.009
TTLL6	-0.13	2.96	-3.00	0.003	0.028
ANKRD6	1.75	4.63	-3.00	0.000	0.001
JAG2	-2.90	0.15	-3.00	0.007	0.047

ASPHD2	-1.41	1.57	-3.00	0.004	0.030
RAB27B	4.29	7.27	-3.00	0.000	0.006
NPHP1	-1.25	1.79	-3.01	0.004	0.033
MALRD1	2.34	5.07	-3.01	0.002	0.016
RAB38	0.56	3.47	-3.01	0.000	0.001
NUDT12	0.72	4.05	-3.01	0.001	0.009
MPP7	1.80	4.98	-3.02	0.007	0.046
DIP2C	-2.63	0.25	-3.03	0.005	0.039
GIMAP8	0.63	3.47	-3.03	0.003	0.023
ARVCF	0.94	4.07	-3.03	0.000	0.007
ECHDC3	-0.25	2.87	-3.04	0.003	0.025
SLC2A10	-0.04	2.96	-3.05	0.005	0.038
CTNNA1	4.24	7.17	-3.05	0.000	0.005
TCP11	-2.38	0.60	-3.06	0.004	0.032
EGF	-1.24	1.91	-3.08	0.006	0.041
TSPAN2	3.51	6.79	-3.08	0.005	0.036
HPSE	-0.30	2.63	-3.09	0.001	0.011
IL4R	1.91	4.81	-3.09	0.000	0.002
PDZD7	-2.64	0.31	-3.09	0.008	0.050
MYCBPAP	1.26	4.20	-3.10	0.001	0.013
ABLIM1	4.47	7.69	-3.11	0.000	0.002
IQSEC2	-0.79	2.26	-3.11	0.001	0.012
EPN2	-3.28	-0.30	-3.11	0.006	0.042
TNFRSF8	-2.21	0.95	-3.11	0.004	0.033
SESN3	5.27	8.28	-3.11	0.004	0.032
ZNF415	-0.16	2.95	-3.12	0.007	0.046
ARL9	-2.12	1.01	-3.12	0.000	0.006
IGF2R	0.10	3.24	-3.12	0.008	0.050
TPM1	2.59	5.51	-3.12	0.000	0.000
TMEM86A	-1.46	1.51	-3.12	0.006	0.044
ADAM22	2.19	5.28	-3.13	0.000	0.000
LTB	-0.78	2.36	-3.14	0.006	0.043
MISP3	-2.03	1.03	-3.14	0.003	0.026
SMO	0.36	3.47	-3.14	0.002	0.017
TNFSF12	-1.43	1.47	-3.14	0.003	0.024
LMO4	2.19	5.65	-3.14	0.002	0.017
ALDOC	-0.06	2.98	-3.15	0.000	0.004
ABHD6	-0.64	2.38	-3.15	0.001	0.007
CFAP54	-1.18	1.89	-3.16	0.001	0.014
PRKAR2B	2.47	5.71	-3.16	0.000	0.007
TNIK	3.01	6.19	-3.16	0.000	0.003
FAXDC2	0.63	3.74	-3.17	0.000	0.000

ARHGEF28	-2.57	0.48	-3.17	0.006	0.043
DLG4	2.23	5.25	-3.17	0.000	0.000
SLC16A14	-1.00	2.05	-3.17	0.004	0.032
TPST1	-0.63	2.48	-3.17	0.003	0.024
MPL	2.99	5.88	-3.17	0.002	0.018
MDK	0.96	4.04	-3.18	0.000	0.001
TRIM2	-0.42	2.70	-3.18	0.007	0.047
GDPD5	-0.32	2.77	-3.19	0.001	0.014
C2orf50	-2.65	0.39	-3.19	0.003	0.027
TRIM46	1.12	4.19	-3.20	0.000	0.001
PPBP	0.11	3.10	-3.20	0.000	0.002
FAM86B1	-1.86	1.27	-3.20	0.002	0.022
ARL10	2.66	5.85	-3.21	0.000	0.001
PLCH2	-1.82	1.47	-3.21	0.001	0.008
SLC16A13	-1.64	1.61	-3.21	0.001	0.008
MAPRE3	-1.87	1.35	-3.22	0.001	0.008
ROBO3	1.85	4.83	-3.22	0.000	0.006
JAG1	0.48	3.54	-3.22	0.001	0.013
SLC49A3	-0.50	2.55	-3.22	0.001	0.012
CD4	1.00	4.01	-3.22	0.001	0.012
SLC2A5	3.51	6.55	-3.23	0.000	0.002
FCN1	1.66	4.30	-3.23	0.007	0.047
TCF4	4.48	8.04	-3.23	0.007	0.047
RAPGEF3	2.03	5.08	-3.23	0.000	0.000
PPP2R2B	-0.98	2.34	-3.24	0.000	0.005
PLEKHA6	-0.94	2.19	-3.24	0.002	0.021
ANKEF1	-1.37	2.04	-3.24	0.004	0.030
STARD4	3.22	6.10	-3.24	0.005	0.039
DNAH10	0.98	4.31	-3.25	0.000	0.000
TYRO3	-1.80	1.40	-3.25	0.002	0.020
CNTNAP1	-2.10	1.21	-3.25	0.000	0.006
SLC10A5	-0.36	3.04	-3.26	0.000	0.001
RADIL	-1.73	1.43	-3.26	0.007	0.045
PTPRF	-1.64	1.56	-3.26	0.002	0.020
SH3TC2	0.92	4.11	-3.27	0.001	0.012
NOTCH2NLR	-2.02	1.35	-3.27	0.001	0.013
FILIP1L	-0.48	2.65	-3.27	0.003	0.024
ADAM8	3.49	6.68	-3.27	0.000	0.000
ELOVL7	0.88	4.01	-3.28	0.003	0.027
STAT4	1.93	5.37	-3.29	0.002	0.019
KCNK5	1.45	4.75	-3.29	0.003	0.025
ALDH2	1.11	4.38	-3.29	0.000	0.000

TSKS	-3.43	-0.18	-3.29	0.002	0.021
GP1BA	-0.71	2.54	-3.30	0.000	0.002
MAF	-0.80	2.23	-3.30	0.005	0.038
ZFP3	0.59	4.10	-3.30	0.005	0.035
MARCHF9	0.06	3.35	-3.30	0.000	0.002
MAP1LC3B2	-0.99	2.19	-3.30	0.000	0.004
NOXA1	-0.15	3.11	-3.30	0.001	0.010
PERP	-3.47	-0.24	-3.30	0.004	0.033
GBP1	1.34	4.51	-3.30	0.001	0.015
SLC22A5	0.72	3.70	-3.31	0.002	0.020
ABHD1	-1.59	1.66	-3.31	0.001	0.012
ARHGEF17	3.50	6.66	-3.31	0.000	0.001
TNFSF8	0.62	3.77	-3.32	0.000	0.002
MAP7D2	-2.24	1.07	-3.32	0.001	0.016
TUBB4A	-3.50	-0.18	-3.33	0.004	0.035
KIAA1522	1.64	4.86	-3.33	0.000	0.000
RASAL2	1.41	4.52	-3.33	0.000	0.005
HTR1F	2.74	6.48	-3.33	0.001	0.008
CBLN3	-2.18	1.07	-3.34	0.001	0.015
AATK	-0.49	2.80	-3.34	0.001	0.013
TCF7L2	2.27	4.97	-3.35	0.003	0.026
PCBP4	-0.76	2.57	-3.35	0.000	0.002
ABCA10	-0.82	2.46	-3.36	0.000	0.006
CD9	0.96	4.53	-3.36	0.007	0.047
ABCB6	-2.61	0.88	-3.36	0.001	0.012
CHST15	-1.79	1.39	-3.37	0.007	0.045
LRRN1	-1.74	1.55	-3.38	0.005	0.037
PDZK1IP1	-3.06	0.29	-3.38	0.008	0.049
SEMA6C	-0.73	2.68	-3.38	0.000	0.002
MPP2	-2.68	0.55	-3.39	0.004	0.034
TNFRSF18	-1.69	1.83	-3.39	0.003	0.024
ABCA5	2.82	6.17	-3.40	0.000	0.001
SMIM38	-2.18	1.23	-3.40	0.002	0.020
GRK5	-0.38	2.81	-3.40	0.001	0.016
PHLPP2	1.17	4.59	-3.41	0.000	0.000
RXRA	1.73	5.31	-3.41	0.000	0.001
OPHN1	0.35	3.83	-3.42	0.000	0.006
FAM151B	-1.47	1.79	-3.44	0.001	0.013
SLC23A1	-1.58	2.04	-3.45	0.001	0.015
LAMA3	-1.03	2.37	-3.45	0.004	0.029
RAB13	-2.00	1.40	-3.45	0.003	0.026
CAPN2	3.11	6.40	-3.46	0.003	0.026

F5	-2.71	0.55	-3.46	0.006	0.043
PCED1B	-2.39	0.94	-3.47	0.004	0.030
DOCK9	-1.87	1.58	-3.47	0.001	0.014
CLIP3	-1.12	2.46	-3.48	0.000	0.005
PGAP1	1.58	4.85	-3.49	0.000	0.001
SERPINH1	1.07	4.45	-3.49	0.001	0.010
LRRC63	1.44	4.93	-3.49	0.000	0.001
MORC4	-2.58	0.86	-3.50	0.001	0.011
TMSB15B	-1.91	1.51	-3.50	0.007	0.045
OR2L5	-0.96	2.61	-3.51	0.000	0.001
NLGN2	-0.50	2.85	-3.52	0.003	0.024
CKAP4	-1.77	1.68	-3.53	0.006	0.041
ITPR3	0.82	4.37	-3.53	0.000	0.000
KRT8	0.15	3.60	-3.54	0.000	0.001
EFHC2	1.87	5.47	-3.54	0.000	0.000
MORN4	-2.17	1.54	-3.55	0.002	0.019
LGR4	-1.27	2.16	-3.55	0.002	0.023
CCDC187	-1.97	1.40	-3.55	0.005	0.038
KLHDC8B	-0.24	3.44	-3.57	0.000	0.001
MEI4	-1.95	1.64	-3.57	0.005	0.035
PLEKHB1	-2.66	0.86	-3.57	0.001	0.014
PACRG	-2.20	1.16	-3.57	0.001	0.008
RIMKLB	3.92	7.39	-3.58	0.005	0.039
NLRP1	3.19	6.60	-3.58	0.000	0.000
ECE1	1.24	4.79	-3.58	0.000	0.000
ANXA5	2.10	5.18	-3.58	0.007	0.048
GPR141	0.97	4.44	-3.59	0.000	0.000
CCDC144A	0.71	4.58	-3.59	0.006	0.042
RHOC	0.20	3.81	-3.60	0.000	0.005
SCD	2.23	5.75	-3.60	0.000	0.001
PRELID3A	-0.40	3.32	-3.61	0.003	0.025
SKIDA1	-1.04	2.64	-3.61	0.000	0.003
NEIL1	-2.18	1.49	-3.62	0.000	0.002
TIMP3	-0.22	3.38	-3.62	0.001	0.014
TMEM231	-0.89	2.91	-3.62	0.000	0.004
SMIM10	-0.49	3.28	-3.62	0.001	0.016
ATP6V0E2	0.67	3.92	-3.63	0.002	0.022
BRSK1	-2.19	1.18	-3.63	0.002	0.017
LYPD5	-2.82	0.75	-3.63	0.001	0.014
CC2D2A	-2.31	1.18	-3.64	0.007	0.046
SLC30A4	-2.11	1.66	-3.64	0.000	0.006
TMEM150B	-2.14	1.35	-3.66	0.001	0.011

CA3	-2.41	1.26	-3.67	0.001	0.011
HK3	-1.86	1.46	-3.67	0.005	0.037
LRATD2	1.14	4.71	-3.67	0.000	0.001
CD14	-1.60	1.79	-3.68	0.003	0.023
NFAM1	-0.18	3.38	-3.68	0.000	0.006
KCNJ12	-1.34	2.39	-3.68	0.002	0.022
TTC29	-3.19	0.48	-3.68	0.003	0.025
FBN1	2.67	6.45	-3.69	0.000	0.000
CAPN12	-1.00	2.88	-3.69	0.000	0.001
RAB9B	-0.52	3.11	-3.70	0.004	0.031
GPR21	0.65	4.39	-3.70	0.000	0.000
BACE2	-1.79	1.83	-3.70	0.008	0.050
FRMD6	0.02	3.62	-3.71	0.003	0.026
ZNF287	-0.99	2.88	-3.72	0.002	0.019
SLC25A23	-1.65	1.98	-3.73	0.001	0.012
SCN3A	-3.14	0.76	-3.73	0.004	0.032
GPHN	0.31	4.09	-3.73	0.005	0.036
C17orf100	-1.80	1.99	-3.74	0.000	0.007
TNFAIP2	3.24	6.75	-3.74	0.000	0.004
PLAAT3	-3.32	0.42	-3.74	0.002	0.019
TUSC1	-2.35	1.28	-3.74	0.003	0.027
GYPE	-1.75	2.19	-3.74	0.000	0.002
KLF9	0.93	4.62	-3.74	0.002	0.017
PERCC1	-2.44	1.17	-3.76	0.007	0.045
ACR	-2.64	1.03	-3.76	0.001	0.009
PXDC1	-2.55	1.09	-3.76	0.000	0.002
SFXN3	2.60	6.17	-3.76	0.000	0.002
IL15	0.37	4.04	-3.76	0.000	0.000
VANGL2	-1.86	1.83	-3.77	0.001	0.011
CA13	0.60	4.42	-3.77	0.000	0.000
FAM83G	0.35	4.29	-3.78	0.000	0.000
TTLL10	-0.86	3.02	-3.78	0.001	0.014
KCNIP3	-2.38	1.33	-3.78	0.001	0.011
WBP2NL	-1.50	2.42	-3.78	0.001	0.013
TRPM4	-3.32	0.41	-3.79	0.007	0.047
LRRC49	-2.43	1.27	-3.79	0.003	0.024
ARHGEF5	-1.78	2.03	-3.80	0.000	0.002
CES3	-2.18	1.65	-3.80	0.001	0.013
NCKAP1	-2.63	1.23	-3.80	0.002	0.019
TINAGL1	-3.40	0.35	-3.80	0.002	0.019
C11orf45	-1.11	2.36	-3.80	0.002	0.016
SHANK3	3.23	6.84	-3.81	0.006	0.040

GBP2	3.58	7.17	-3.82	0.001	0.011
GJC2	-1.99	1.80	-3.83	0.000	0.002
FAM171A2	-1.78	1.94	-3.83	0.000	0.003
SERPINE2	1.10	4.75	-3.84	0.002	0.020
ASTN2	-2.43	1.27	-3.84	0.005	0.039
MLLT3	4.12	7.86	-3.85	0.001	0.015
CDK18	-0.34	3.41	-3.86	0.001	0.009
MYO5C	2.77	6.73	-3.86	0.000	0.000
ULBP3	-2.52	1.28	-3.86	0.000	0.006
MYL9	-3.11	0.70	-3.86	0.000	0.003
KIFC3	0.34	4.10	-3.88	0.001	0.011
CAPN11	0.55	4.16	-3.88	0.000	0.002
ID1	-0.33	3.17	-3.88	0.002	0.021
MTARC1	-1.59	2.23	-3.89	0.003	0.026
ADAMTSL4	1.23	4.93	-3.89	0.002	0.017
TDRD9	-2.63	1.29	-3.89	0.000	0.002
CAPN5	-2.75	1.09	-3.89	0.001	0.015
NPR2	-0.74	3.29	-3.90	0.000	0.001
PLD2	-0.94	2.96	-3.90	0.000	0.000
LILRA5	-2.46	1.18	-3.91	0.002	0.021
ARMCX2	-0.07	4.02	-3.91	0.000	0.000
DOCK6	-1.67	2.25	-3.92	0.004	0.031
MMP2	0.61	4.44	-3.93	0.001	0.007
DUSP15	-2.69	1.03	-3.93	0.001	0.015
SERPINI2	0.87	4.74	-3.93	0.000	0.000
SARM1	1.29	5.51	-3.93	0.000	0.000
ADAM32	-1.93	1.96	-3.94	0.005	0.036
KHDC1	-1.13	2.68	-3.94	0.000	0.004
MPV17L	-0.96	2.85	-3.95	0.004	0.032
ELAPOR2	0.24	4.37	-3.95	0.006	0.044
RASSF8	-0.37	3.39	-3.95	0.000	0.006
HDGFL3	1.63	5.68	-3.95	0.004	0.033
HABP4	-1.87	1.99	-3.97	0.000	0.002
SRC	1.02	5.02	-3.97	0.000	0.000
FHL2	-0.50	3.42	-3.97	0.000	0.000
NOTCH3	-2.40	1.46	-3.99	0.001	0.010
MIXL1	-3.73	0.25	-4.01	0.001	0.010
AMIGO2	-1.85	1.95	-4.01	0.001	0.013
PDE1A	-3.55	0.49	-4.02	0.001	0.009
FOXO1	0.74	4.92	-4.02	0.000	0.005
CD300E	-2.20	1.59	-4.03	0.001	0.013
NME8	-0.51	3.37	-4.03	0.000	0.005

TNS1	2.47	6.14	-4.03	0.000	0.001
TMEM150C	-2.40	1.53	-4.05	0.000	0.005
NRBP2	0.49	4.59	-4.06	0.000	0.000
DZIP1	-1.85	2.06	-4.07	0.001	0.010
CPS1	-2.90	1.17	-4.08	0.000	0.001
DYNC2H1	1.82	5.60	-4.09	0.000	0.001
BMP6	-2.34	1.55	-4.10	0.003	0.029
SGMS2	-0.17	3.98	-4.10	0.005	0.037
RASGRP1	-0.79	3.16	-4.10	0.001	0.013
TMEM273	-1.72	2.28	-4.11	0.000	0.003
EBF4	-3.55	0.48	-4.11	0.000	0.006
FAM221A	-0.29	3.80	-4.11	0.000	0.000
ASGR1	-2.35	1.63	-4.11	0.000	0.005
ZNF229	-0.23	4.06	-4.12	0.000	0.004
CFI	-0.37	4.04	-4.12	0.002	0.022
CLEC20A	-3.81	0.29	-4.13	0.001	0.014
ZNF311	-2.06	1.93	-4.13	0.000	0.004
ELAVL4	-3.32	0.82	-4.13	0.006	0.041
TUBB6	1.70	5.96	-4.14	0.000	0.005
JAKMIP2	1.39	5.81	-4.15	0.000	0.001
SPATA6	0.73	5.10	-4.15	0.001	0.008
RAB11FIP5	-2.66	1.37	-4.15	0.000	0.004
ADAMTS1	-3.24	0.87	-4.16	0.000	0.004
PHLDB2	0.43	4.38	-4.16	0.000	0.000
TLCD2	-2.81	1.40	-4.17	0.000	0.001
GARNL3	-1.87	2.34	-4.17	0.003	0.026
KL	-3.17	0.95	-4.17	0.000	0.001
VCAN	1.49	5.29	-4.18	0.002	0.019
SLC7A8	-3.42	0.72	-4.19	0.001	0.008
EFNA1	-1.08	3.12	-4.19	0.000	0.007
ZCCHC14	-0.20	3.91	-4.19	0.000	0.005
HEMGN	2.03	6.40	-4.20	0.000	0.000
CAMK2D	-1.05	2.97	-4.21	0.001	0.008
TRIM47	-0.09	4.16	-4.21	0.000	0.001
SLC2A8	-2.18	2.05	-4.21	0.001	0.013
NDN	-1.28	3.28	-4.22	0.008	0.050
TTC39B	1.52	5.74	-4.23	0.000	0.000
PLPP7	-2.48	1.79	-4.23	0.001	0.013
ACE	-0.77	3.24	-4.23	0.000	0.002
KCTD17	-1.92	2.16	-4.24	0.000	0.005
CCDC40	-1.94	2.39	-4.24	0.000	0.002
OBSCN	3.54	7.95	-4.25	0.000	0.001

LAPTM4B	3.48	7.50	-4.26	0.000	0.000
AKT3	2.90	6.98	-4.26	0.001	0.012
CFAP20DC	-1.82	2.38	-4.27	0.002	0.020
PTMS	-0.29	4.06	-4.27	0.000	0.000
TCEAL9	-0.07	4.16	-4.27	0.002	0.023
ZDHHC11B	-2.20	1.91	-4.27	0.001	0.009
XKR6	-2.61	1.56	-4.28	0.000	0.007
PRSS2	-3.43	0.88	-4.28	0.000	0.000
ACVR2B	-0.98	3.27	-4.29	0.000	0.000
GRID2IP	-2.47	1.74	-4.29	0.000	0.001
ZNF578	-2.51	1.77	-4.29	0.005	0.039
OR2M3	-2.85	1.50	-4.30	0.000	0.003
OR2L13	-1.63	2.73	-4.30	0.000	0.001
PALLD	-0.33	3.97	-4.30	0.000	0.000
NLRP2	0.08	4.38	-4.31	0.002	0.022
TUB	-2.78	1.47	-4.31	0.000	0.006
SNX25	-2.11	2.07	-4.32	0.000	0.001
OCLN	-0.62	3.40	-4.32	0.001	0.016
AFAP1L2	-0.62	3.76	-4.32	0.000	0.002
CD52	2.33	6.78	-4.32	0.001	0.014
TGFBI	-1.98	1.84	-4.32	0.004	0.033
ACKR3	-0.42	3.99	-4.33	0.000	0.001
ETNK2	-3.02	1.14	-4.33	0.000	0.003
CCDC136	0.51	4.93	-4.33	0.000	0.003
CYYR1	0.13	4.63	-4.34	0.003	0.024
ANO5	-2.93	1.23	-4.34	0.001	0.009
ARHGEF10	-3.03	1.29	-4.34	0.000	0.001
KCNH3	-3.12	1.21	-4.34	0.000	0.003
C4orf50	-3.55	0.79	-4.34	0.000	0.000
JAML	1.38	5.80	-4.35	0.000	0.001
LRRN2	-3.63	0.70	-4.36	0.000	0.004
OR2L3	-1.70	2.55	-4.36	0.000	0.003
TRIP10	-1.02	3.38	-4.37	0.000	0.001
CES4A	-1.82	2.54	-4.38	0.000	0.004
MMP28	-0.76	3.66	-4.38	0.000	0.002
OR2L2	-0.65	3.73	-4.40	0.000	0.000
RIC3	-0.94	3.36	-4.40	0.000	0.000
ARHGEF11	0.62	5.23	-4.40	0.001	0.014
COBLL1	1.06	5.27	-4.41	0.000	0.006
NHSL2	2.40	6.71	-4.42	0.000	0.001
CCSER1	1.35	5.98	-4.42	0.000	0.001
CRHBP	2.40	6.76	-4.42	0.000	0.000

TTC12	0.20	4.40	-4.42	0.001	0.011
TMEM45A	-3.22	1.21	-4.43	0.000	0.001
ARHGAP20	-2.84	1.57	-4.43	0.000	0.002
APBB2	-2.48	1.57	-4.44	0.002	0.019
NR6A1	0.58	4.90	-4.44	0.000	0.000
PDE5A	-3.24	1.07	-4.45	0.000	0.001
F2RL1	1.06	5.33	-4.46	0.000	0.005
PMEPA1	-2.93	1.35	-4.46	0.003	0.025
MEAK7	-0.09	4.34	-4.46	0.000	0.001
C3orf80	-0.47	4.23	-4.46	0.000	0.000
DNAH5	-3.15	1.33	-4.47	0.000	0.001
BCAS4	0.81	5.11	-4.47	0.000	0.000
SEMA3A	-3.29	1.08	-4.47	0.001	0.008
CAMK1D	2.61	7.06	-4.47	0.000	0.000
MCUB	0.79	5.35	-4.47	0.000	0.001
GNA11	-0.93	3.62	-4.49	0.000	0.001
OSBPL1A	1.53	6.17	-4.49	0.003	0.026
TAL1	2.34	7.06	-4.49	0.000	0.004
ECHDC2	0.38	4.70	-4.51	0.000	0.006
TSTD3	-0.39	3.92	-4.51	0.000	0.001
JAM2	-3.15	1.32	-4.52	0.000	0.000
HOPX	1.38	6.05	-4.52	0.000	0.000
FAM89A	-2.03	2.62	-4.54	0.000	0.002
ZC3H12C	2.14	6.28	-4.55	0.006	0.040
TEK	-2.72	1.72	-4.57	0.000	0.002
SLC8A1	0.08	4.49	-4.57	0.000	0.000
SPRED2	-0.74	3.60	-4.58	0.000	0.005
CYP4F22	-3.06	1.40	-4.59	0.000	0.000
ETS1	1.41	5.96	-4.60	0.000	0.005
ADGRL1	0.17	4.84	-4.60	0.000	0.000
CEACAM19	-2.21	2.20	-4.60	0.000	0.002
GIMAP7	-0.72	3.99	-4.60	0.000	0.001
MEX3A	-2.19	2.45	-4.60	0.000	0.007
STXBP6	-2.94	1.58	-4.60	0.000	0.002
IFITM3	0.55	4.83	-4.61	0.006	0.042
SLC16A1	0.82	5.39	-4.61	0.000	0.002
FSTL1	-0.29	4.21	-4.61	0.000	0.001
PLAG1	-1.42	3.13	-4.61	0.000	0.004
LRRC4C	-3.73	0.82	-4.61	0.000	0.000
PHGDH	0.07	4.84	-4.62	0.001	0.014
CYSTM1	-2.16	2.32	-4.62	0.000	0.002
MTX3	-0.09	4.84	-4.62	0.006	0.041

RASSF9	-3.60	1.03	-4.62	0.000	0.000
EPB41L2	1.01	5.46	-4.64	0.001	0.009
SAMD4A	-1.30	3.35	-4.64	0.000	0.000
TMEM117	-2.63	1.90	-4.65	0.000	0.000
IL2RA	-0.82	3.76	-4.66	0.000	0.001
TUBA4A	-1.86	2.66	-4.66	0.000	0.003
ZNF135	0.56	5.36	-4.66	0.003	0.027
CAND2	-2.71	1.79	-4.66	0.000	0.003
SOCS2	2.60	7.32	-4.66	0.000	0.001
SUCLG2	-1.24	3.33	-4.66	0.001	0.012
CACNB1	-1.56	2.96	-4.66	0.000	0.000
ATN1	0.70	5.40	-4.66	0.000	0.000
BICC1	-3.11	1.36	-4.67	0.000	0.005
PDZD2	0.16	4.88	-4.67	0.000	0.000
ADRB1	-3.46	1.13	-4.67	0.000	0.003
KCTD19	-3.01	1.50	-4.68	0.000	0.001
LAMC1	0.29	4.82	-4.68	0.002	0.021
PHETA2	-1.86	2.79	-4.69	0.000	0.002
SLC41A1	-0.67	4.06	-4.69	0.000	0.001
ARPIN	-2.22	2.36	-4.70	0.000	0.001
KCNQ1	-2.17	2.44	-4.71	0.000	0.003
ZNF98	-2.92	1.70	-4.72	0.000	0.005
ESR1	-2.17	2.44	-4.72	0.000	0.001
BEND6	-2.24	2.39	-4.72	0.000	0.001
EVA1C	-2.11	2.67	-4.72	0.000	0.001
RBM11	-2.85	1.86	-4.73	0.000	0.000
SALL4	-1.20	3.17	-4.73	0.000	0.007
EXPH5	-1.34	3.47	-4.75	0.000	0.001
CASKIN2	-1.60	3.09	-4.75	0.000	0.001
ESAM	-1.85	2.67	-4.75	0.002	0.020
HOXA4	-2.89	1.67	-4.75	0.000	0.001
CDKL5	-0.48	4.16	-4.76	0.000	0.000
BEX3	1.13	5.55	-4.76	0.002	0.023
MARVELD1	0.56	5.30	-4.77	0.000	0.000
LRIG1	-1.23	3.52	-4.77	0.000	0.001
DEPP1	-1.40	3.37	-4.77	0.000	0.000
MAP3K20	1.11	5.83	-4.77	0.000	0.001
PTGER3	-3.46	1.26	-4.77	0.000	0.000
PAPLN	-2.43	2.34	-4.78	0.000	0.000
ZNF154	0.85	5.85	-4.79	0.001	0.013
PDE1C	-2.84	1.91	-4.81	0.000	0.002
DST	4.18	9.04	-4.81	0.000	0.002

HOXB5	-3.73	1.09	-4.81	0.000	0.000
ZNF214	-3.07	1.68	-4.81	0.000	0.000
USP45	0.56	5.10	-4.82	0.000	0.005
SCN2A	-2.64	2.16	-4.84	0.000	0.001
EML6	-1.75	3.07	-4.84	0.000	0.000
SLC25A27	-0.99	3.75	-4.85	0.000	0.000
VWF	1.08	5.80	-4.85	0.000	0.000
SORBS3	-0.80	4.04	-4.85	0.000	0.000
DGKH	-0.18	4.80	-4.86	0.000	0.000
PECR	-2.17	2.71	-4.86	0.000	0.000
HOOK1	-1.73	3.10	-4.87	0.000	0.000
NBEA	1.02	5.90	-4.87	0.000	0.000
ARHGAP6	-2.84	1.85	-4.87	0.000	0.004
ADCY6	0.97	5.82	-4.88	0.000	0.000
CHRNA5	-2.14	2.73	-4.88	0.000	0.000
MDGA2	-3.81	1.03	-4.88	0.000	0.000
DYNC1I1	-2.87	1.93	-4.90	0.000	0.000
DOCK3	-0.49	4.24	-4.90	0.000	0.001
THNSL2	-1.31	3.69	-4.90	0.000	0.001
H1-0	1.75	6.35	-4.91	0.000	0.003
ZNF835	-2.36	2.53	-4.91	0.000	0.003
GPAT3	0.04	4.94	-4.92	0.000	0.000
SCN4A	-2.64	2.20	-4.92	0.000	0.000
PLEKHG1	-2.32	2.41	-4.92	0.000	0.001
ALOX15B	-3.09	1.74	-4.93	0.000	0.000
NSUN7	-1.46	3.35	-4.93	0.000	0.000
SH3BP5	-0.68	4.16	-4.93	0.000	0.001
APBB1	-1.99	2.75	-4.94	0.000	0.001
RTL8B	-3.43	1.40	-4.95	0.000	0.000
PKP2	-2.89	1.80	-4.95	0.001	0.013
CCDC42	-2.43	2.45	-4.96	0.000	0.000
TP53I11	-0.99	3.78	-4.96	0.004	0.033
SLC18A2	-1.55	3.38	-4.96	0.002	0.020
TTC22	-3.38	1.55	-4.96	0.000	0.000
MAGEE1	-3.81	1.13	-4.96	0.000	0.000
PROS1	-3.06	1.74	-4.96	0.000	0.001
ABI2	1.76	6.71	-4.97	0.000	0.000
HEG1	-1.26	3.65	-4.98	0.000	0.001
COL6A2	-2.81	2.02	-4.98	0.000	0.005
TRPC6	-3.55	1.45	-4.99	0.000	0.000
SERTM2	-3.03	1.84	-4.99	0.000	0.000
ALOX12	-3.55	1.46	-4.99	0.006	0.040

ZNF483	-2.97	1.89	-5.00	0.000	0.004
JCAD	-2.56	2.42	-5.00	0.000	0.005
MPP3	-2.86	2.00	-5.00	0.001	0.007
LTBP1	-0.68	4.00	-5.01	0.000	0.001
CNNM1	-2.70	2.13	-5.02	0.000	0.002
IL7	-2.20	2.78	-5.02	0.000	0.000
ODAD2	-2.80	2.19	-5.02	0.000	0.000
RAI14	-3.38	1.56	-5.03	0.000	0.001
SCML4	-0.19	5.17	-5.03	0.000	0.000
ZNF474	-3.11	1.89	-5.04	0.000	0.000
ENO2	-0.73	4.39	-5.04	0.000	0.000
STYK1	-1.50	3.58	-5.04	0.000	0.000
ZNF99	-3.81	1.24	-5.04	0.001	0.009
SULT1C4	-0.60	4.41	-5.05	0.000	0.000
IQSEC3	-0.98	3.82	-5.06	0.006	0.042
KLHL32	-3.99	1.03	-5.07	0.000	0.000
STARD8	-0.23	4.57	-5.07	0.000	0.001
DOC2B	-3.63	1.36	-5.07	0.005	0.037
ICA1	0.83	6.05	-5.07	0.000	0.000
PRR15	-2.75	2.28	-5.08	0.000	0.001
LDOC1	-3.67	1.35	-5.08	0.000	0.000
TBC1D12	-2.23	2.65	-5.09	0.000	0.000
AFAP1L1	-1.78	3.29	-5.09	0.000	0.000
MANSC1	-1.30	3.98	-5.11	0.000	0.000
ALS2CL	-1.11	3.67	-5.12	0.000	0.004
ARHGAP32	0.56	4.84	-5.12	0.007	0.045
IQCA1	-3.47	1.65	-5.12	0.000	0.000
TRIM61	-3.44	1.65	-5.14	0.000	0.000
RIN2	-0.92	4.03	-5.15	0.000	0.000
CACNB3	-1.66	3.45	-5.16	0.000	0.000
SPATS2L	-0.31	4.54	-5.16	0.000	0.000
SLC35G2	-1.77	3.29	-5.17	0.000	0.001
GPR63	-3.01	2.04	-5.18	0.000	0.002
RTL8A	-2.51	2.61	-5.19	0.000	0.002
MAP9	-0.61	4.40	-5.19	0.000	0.001
NDFIP1	1.68	6.77	-5.19	0.000	0.000
PKIA	-1.56	3.53	-5.20	0.000	0.001
PF4	-3.22	1.84	-5.20	0.000	0.000
SLITRK5	-3.34	1.89	-5.20	0.000	0.000
DZIP1L	-2.26	2.67	-5.21	0.000	0.001
ENPP5	-3.40	1.68	-5.21	0.000	0.000
OLFML2A	-2.81	2.20	-5.21	0.003	0.026

BCL9	-1.36	3.72	-5.22	0.000	0.002
CA8	-1.56	3.61	-5.22	0.000	0.007
LIN7A	-2.35	2.64	-5.23	0.001	0.010
TLCD3A	-2.73	2.39	-5.24	0.000	0.003
GRAMD1B	-0.06	4.88	-5.25	0.000	0.001
FXYD6	-2.01	3.04	-5.26	0.000	0.000
LOXL1	-3.43	1.79	-5.27	0.000	0.000
ITGA3	-2.93	2.28	-5.27	0.000	0.001
PHKA1	-0.63	4.49	-5.28	0.000	0.000
SMARCD3	-2.79	2.28	-5.29	0.000	0.001
GPR161	-2.33	3.06	-5.29	0.000	0.000
BACH2	-0.72	4.76	-5.29	0.000	0.000
GASK1B	0.04	4.77	-5.29	0.000	0.004
SLC35G1	-2.34	2.79	-5.30	0.000	0.001
SLC44A5	-1.66	3.31	-5.31	0.001	0.009
CAVIN2	0.98	6.28	-5.31	0.000	0.000
AADAT	-1.68	3.54	-5.31	0.000	0.000
PPP2R3A	-2.37	2.87	-5.32	0.000	0.001
JHY	-1.22	4.28	-5.32	0.000	0.001
PRKCZ	-1.84	3.46	-5.34	0.000	0.000
NUP62CL	-3.02	2.16	-5.34	0.000	0.001
CEP112	-1.26	4.02	-5.34	0.000	0.000
SLC16A2	-3.63	1.67	-5.35	0.000	0.000
RPS6KA6	-3.81	1.51	-5.36	0.000	0.000
CHIC1	-0.70	4.79	-5.37	0.000	0.005
C2orf88	-1.10	4.21	-5.37	0.000	0.000
ACVR2A	-1.51	3.81	-5.38	0.000	0.000
PARD3B	-2.06	2.93	-5.38	0.003	0.024
HSPA4L	-2.11	3.15	-5.38	0.000	0.000
KIF5A	-3.63	1.71	-5.40	0.000	0.000
TSPAN6	-3.73	1.61	-5.40	0.000	0.000
WDR17	-0.70	4.45	-5.41	0.000	0.000
FKBP10	-3.07	2.30	-5.42	0.000	0.000
CACHD1	-1.90	3.28	-5.43	0.000	0.007
TRPC1	-1.97	3.33	-5.43	0.000	0.000
OBSL1	0.87	6.27	-5.44	0.000	0.000
OR2AG2	-3.81	1.61	-5.45	0.000	0.000
EREG	2.45	7.30	-5.45	0.002	0.019
MCF2L2	-0.28	5.17	-5.46	0.000	0.000
FKBP9	-2.02	3.28	-5.46	0.000	0.000
MBOAT2	0.86	6.06	-5.47	0.000	0.002
TRPS1	2.83	7.77	-5.49	0.000	0.003

SLC22A17	-3.20	2.19	-5.49	0.000	0.000
LILRB2	-1.04	4.16	-5.50	0.000	0.000
ACP6	-0.19	5.34	-5.51	0.000	0.000
SGCZ	-3.63	1.93	-5.51	0.000	0.000
NLRP12	-2.59	2.74	-5.52	0.000	0.000
PATJ	0.91	6.03	-5.52	0.000	0.001
VNN2	-1.53	3.96	-5.53	0.000	0.000
DCHS1	-0.84	4.52	-5.53	0.001	0.015
SLC22A15	0.04	5.15	-5.53	0.001	0.009
HOXB6	-3.99	1.47	-5.54	0.000	0.000
ITGAV	0.76	5.88	-5.55	0.002	0.021
TMEM204	-2.80	2.79	-5.55	0.000	0.000
GIPC2	-3.24	2.28	-5.56	0.000	0.000
MYO1E	-0.67	4.96	-5.56	0.000	0.000
BAG3	-2.51	2.89	-5.57	0.000	0.001
ARHGEF12	-0.44	5.05	-5.58	0.000	0.000
ANO9	-2.35	3.16	-5.59	0.000	0.000
RHBDF1	-2.03	3.48	-5.60	0.000	0.000
EPHX2	-3.07	2.52	-5.61	0.000	0.000
RHPN1	-0.42	5.24	-5.62	0.000	0.000
NEDD4L	-0.29	5.20	-5.62	0.000	0.000
CDH2	-3.81	1.85	-5.63	0.000	0.000
SLC1A6	-3.99	1.57	-5.64	0.000	0.000
RUSC2	-0.27	5.07	-5.65	0.000	0.001
OR2C3	-3.63	1.95	-5.67	0.000	0.003
SPIRE1	-0.43	5.09	-5.70	0.000	0.000
NUDT10	-3.60	2.03	-5.70	0.000	0.000
MIPOL1	-2.44	3.24	-5.71	0.000	0.000
LRP6	-0.51	5.18	-5.72	0.003	0.026
CDC14B	-1.40	4.22	-5.73	0.000	0.000
RTL8C	-2.07	3.54	-5.74	0.000	0.001
CYP2S1	-3.20	2.42	-5.74	0.002	0.020
STXBP1	-2.97	2.66	-5.75	0.000	0.000
ACOX2	-2.99	2.73	-5.75	0.000	0.000
C8orf88	-1.82	3.74	-5.76	0.000	0.000
PHLDB1	-2.71	2.97	-5.76	0.000	0.000
CLIC2	-0.19	5.48	-5.77	0.000	0.000
GCNT2	0.18	5.66	-5.77	0.000	0.000
MYH10	0.18	6.04	-5.77	0.000	0.000
TBC1D4	-0.37	5.35	-5.78	0.000	0.000
BMPR1B	-2.81	2.90	-5.78	0.000	0.000
ZC3H12B	-3.07	2.54	-5.78	0.000	0.000

ITGB3	-1.96	3.62	-5.79	0.000	0.000
BMERB1	-3.07	2.70	-5.79	0.000	0.000
AR	-2.48	3.15	-5.79	0.000	0.000
CHMP4C	-3.47	2.35	-5.81	0.000	0.000
EPPK1	-3.63	2.17	-5.82	0.000	0.000
DCLK2	-2.58	2.99	-5.84	0.001	0.010
ATP9A	-0.27	5.70	-5.87	0.000	0.000
PCYT1B	-1.78	4.09	-5.87	0.000	0.000
LRCH2	-3.81	2.05	-5.89	0.000	0.000
SERPING1	0.25	5.64	-5.89	0.000	0.004
GPR162	-1.44	4.23	-5.91	0.000	0.000
ZNF532	-1.66	4.12	-5.91	0.000	0.000
TBC1D8B	-2.39	3.44	-5.93	0.000	0.000
NLGN1	-3.81	2.15	-5.93	0.000	0.000
ZNF112	-2.46	3.56	-5.93	0.000	0.000
ZNF727	-2.16	3.85	-5.93	0.005	0.039
NECAB1	-3.81	2.17	-5.95	0.000	0.000
MPIG6B	-2.57	3.26	-5.97	0.000	0.000
VWA2	-3.81	2.08	-5.97	0.000	0.000
TRIM32	-1.45	4.34	-5.97	0.000	0.000
RADX	-2.71	3.21	-5.99	0.000	0.000
CFH	0.69	6.78	-6.00	0.000	0.002
ZDBF2	-2.24	3.67	-6.00	0.000	0.000
PRXL2A	-1.33	4.37	-6.01	0.000	0.001
NAP1L2	-3.99	2.02	-6.01	0.000	0.000
CARMIL1	-0.10	6.02	-6.01	0.000	0.000
SCRN1	1.56	7.16	-6.02	0.000	0.006
STAC	-2.78	3.12	-6.02	0.000	0.000
BEX2	-1.57	4.21	-6.02	0.000	0.001
HSPA12A	-3.20	2.85	-6.03	0.000	0.000
ASAP2	-1.45	4.34	-6.03	0.000	0.001
GALNT5	-3.50	2.52	-6.04	0.000	0.000
CTTNBP2NL	-2.07	3.77	-6.04	0.000	0.004
PPP1R9A	-2.07	3.95	-6.06	0.000	0.000
PALS2	-0.06	5.93	-6.06	0.000	0.001
PRTFDC1	-3.46	2.56	-6.07	0.000	0.000
OR6A2	-3.99	2.08	-6.07	0.000	0.000
NFIB	-3.81	2.23	-6.08	0.000	0.000
UNC13B	-1.21	4.70	-6.08	0.000	0.001
GCNT4	-2.48	3.26	-6.09	0.000	0.000
SEMA3C	-1.67	4.42	-6.11	0.000	0.000
LAG3	-3.38	2.58	-6.11	0.000	0.000

ZC2HC1A	-2.32	3.66	-6.11	0.000	0.000
TVP23A	-3.55	2.44	-6.12	0.000	0.000
INTU	-0.78	5.36	-6.12	0.000	0.001
ZNF300	-2.23	3.81	-6.12	0.000	0.000
ABCC6	-3.20	2.82	-6.12	0.000	0.000
PEG3	-3.63	2.49	-6.13	0.000	0.000
SLC37A3	-1.44	4.75	-6.16	0.000	0.000
BMPR2	0.07	6.18	-6.17	0.000	0.000
ANXA3	-2.91	3.06	-6.18	0.000	0.000
P3H3	-3.16	2.94	-6.19	0.000	0.000
KIF16B	-0.60	5.25	-6.19	0.000	0.000
SAMD12	-2.83	3.35	-6.20	0.000	0.000
MAGI2	-2.53	3.60	-6.20	0.000	0.000
EDARADD	-3.12	3.08	-6.21	0.000	0.000
LURAP1	-2.67	3.55	-6.21	0.000	0.000
GSTM5	-1.89	3.96	-6.21	0.000	0.000
CD109	1.54	7.90	-6.21	0.000	0.001
ESR2	-3.15	2.93	-6.21	0.000	0.000
SALL2	-3.38	2.83	-6.22	0.000	0.000
PCCA	-0.42	5.50	-6.22	0.000	0.006
SLC52A3	-3.99	2.17	-6.24	0.000	0.000
LIMCH1	-2.54	3.55	-6.24	0.000	0.000
TANC1	-0.56	5.68	-6.25	0.000	0.000
ZNF208	-3.10	3.11	-6.25	0.000	0.000
BASP1	-2.41	3.73	-6.25	0.000	0.000
GATA3	-3.50	2.69	-6.26	0.000	0.000
SPOCK3	-2.84	3.26	-6.26	0.000	0.000
RNF150	-2.11	4.09	-6.27	0.000	0.000
EGLN3	-2.84	3.51	-6.27	0.000	0.000
MYLK	-2.52	3.75	-6.27	0.000	0.000
PRDM16	-3.12	2.98	-6.28	0.000	0.000
ZFYVE9	-2.02	4.04	-6.28	0.000	0.001
MCOLN2	-2.64	3.42	-6.30	0.000	0.000
MPZL2	-3.09	3.21	-6.31	0.000	0.000
EXT1	-2.79	3.46	-6.31	0.000	0.000
ALDH1A1	0.26	6.65	-6.34	0.000	0.000
DLG3	-2.73	3.64	-6.34	0.000	0.000
PLEKHG4B	-3.20	3.13	-6.35	0.000	0.000
FHL1	1.10	7.45	-6.35	0.000	0.000
CLEC9A	-2.42	3.97	-6.37	0.000	0.000
AFDN	-1.06	5.13	-6.38	0.000	0.000
ROBO4	-0.56	5.52	-6.39	0.000	0.000

L3MBTL4	-0.68	5.66	-6.40	0.000	0.001
SPRED1	-2.24	3.87	-6.41	0.000	0.001
PRR16	-3.81	2.59	-6.41	0.000	0.000
GPC5	-3.63	2.73	-6.42	0.000	0.000
TOM1L1	-2.53	3.71	-6.42	0.000	0.001
HFM1	-2.59	3.79	-6.44	0.000	0.000
CLU	-0.49	5.87	-6.45	0.000	0.000
STK33	-1.83	4.49	-6.47	0.000	0.000
GPRIN3	-0.62	5.62	-6.48	0.000	0.000
CTDSPL	-0.72	5.54	-6.49	0.000	0.000
ZNF334	-1.32	5.14	-6.49	0.000	0.000
SPON1	-3.73	2.81	-6.49	0.000	0.000
SLC29A2	-2.28	4.18	-6.49	0.000	0.000
NUDT11	-3.73	2.73	-6.50	0.000	0.000
VNN1	-1.81	4.50	-6.50	0.000	0.001
ST6GAL2	-3.81	2.62	-6.50	0.000	0.000
PEAR1	-1.52	4.86	-6.52	0.000	0.000
PIEZO2	-2.46	3.86	-6.53	0.000	0.001
TSPYL5	-1.30	5.22	-6.55	0.000	0.000
ZSCAN23	-2.53	3.97	-6.55	0.000	0.000
SYDE2	-2.64	3.90	-6.56	0.000	0.000
FAM169A	-0.89	5.62	-6.56	0.000	0.000
JAM3	-2.34	4.25	-6.58	0.000	0.000
EPB41L3	-1.87	4.64	-6.59	0.000	0.000
ITGA2	-2.56	4.05	-6.59	0.000	0.000
CIBAR1	-2.22	4.28	-6.59	0.000	0.000
ARHGAP22	-0.53	5.99	-6.61	0.000	0.000
ANK3	-1.83	4.88	-6.62	0.000	0.000
PTK2	-2.02	4.60	-6.62	0.000	0.000
UST	-2.87	3.78	-6.62	0.000	0.000
NAV1	-0.39	6.26	-6.63	0.000	0.001
CFAP92	-2.18	4.40	-6.65	0.000	0.000
RAB34	-0.68	5.92	-6.65	0.000	0.000
PLS3	-2.35	4.24	-6.68	0.000	0.000
PCLO	-3.63	3.05	-6.69	0.000	0.000
SORT1	-1.09	5.45	-6.72	0.000	0.000
CLDN10	-2.66	3.86	-6.72	0.000	0.000
ST8SIA6	0.10	6.80	-6.72	0.000	0.000
ZNF595	-2.20	4.29	-6.77	0.000	0.004
PLSCR4	-2.11	4.57	-6.78	0.000	0.000
CCDC152	-2.71	3.87	-6.79	0.000	0.000
SMARCA1	-1.42	5.02	-6.81	0.000	0.000

UCHL1	-2.91	3.68	-6.82	0.000	0.000
ZNF462	-2.32	4.31	-6.82	0.000	0.000
HDX	-3.99	2.82	-6.84	0.000	0.000
PLCB4	-0.59	6.48	-6.85	0.000	0.000
HOXB4	-2.95	3.70	-6.86	0.000	0.000
OPTN	-1.01	5.60	-6.90	0.000	0.000
ZNF215	-3.33	3.47	-6.91	0.000	0.000
SYT1	-3.20	3.65	-6.92	0.000	0.000
ABI3BP	-3.29	3.54	-6.92	0.000	0.000
H2AW	-3.12	3.69	-6.93	0.000	0.000
GPR173	-3.55	3.29	-6.94	0.000	0.000
ADGRG1	0.29	7.25	-6.94	0.000	0.000
H2BU1	-2.99	3.91	-6.95	0.000	0.000
SHTN1	-2.98	3.95	-6.96	0.000	0.000
PGM5	-3.02	3.81	-6.98	0.000	0.000
ARHGAP21	-0.22	6.65	-7.01	0.000	0.000
CNN3	-3.46	3.49	-7.02	0.000	0.000
TNS3	1.08	7.65	-7.02	0.000	0.000
DTX3	-2.39	4.48	-7.04	0.000	0.000
PTPRD	-1.61	5.47	-7.06	0.000	0.000
TLCD5	-3.81	3.20	-7.07	0.000	0.000
EVC2	-2.42	4.42	-7.07	0.000	0.001
NKX2-3	-3.99	3.05	-7.09	0.000	0.000
SETBP1	-0.79	6.20	-7.09	0.000	0.000
EFCC1	-2.65	4.21	-7.11	0.000	0.000
TMEM163	-2.64	4.20	-7.12	0.000	0.000
PGAP4	-2.44	4.56	-7.12	0.000	0.000
MPDZ	-1.90	5.06	-7.13	0.000	0.000
PDZRN4	-3.50	3.71	-7.15	0.000	0.000
ZNF90	-3.05	4.01	-7.16	0.000	0.000
CP	-0.66	6.38	-7.19	0.000	0.000
TM4SF1	-2.73	4.18	-7.19	0.000	0.000
ZDHHC15	-3.60	3.55	-7.23	0.000	0.000
ZNF711	-0.39	6.68	-7.23	0.000	0.000
ELN	-3.04	4.07	-7.26	0.000	0.000
HOXB2	-3.99	3.24	-7.26	0.000	0.000
UGGT2	-1.22	5.91	-7.29	0.000	0.000
NPDC1	-1.62	5.74	-7.31	0.000	0.000
PLA2R1	-2.37	4.91	-7.36	0.000	0.000
TMEM200A	-3.99	3.31	-7.37	0.000	0.000
TTLL7	-1.90	5.44	-7.40	0.000	0.000
CPED1	-1.69	5.64	-7.40	0.000	0.000

SHROOM4	-3.46	3.85	-7.42	0.000	0.000
NAALADL1	-2.68	4.58	-7.44	0.000	0.000
CDH7	-3.99	3.44	-7.48	0.000	0.000
CALCRL	-0.96	6.38	-7.48	0.000	0.000
HOXA7	-3.55	3.88	-7.49	0.000	0.000
FERMT1	-2.81	4.68	-7.49	0.000	0.000
THRB	-2.77	4.66	-7.51	0.000	0.000
BEND4	-1.03	6.28	-7.54	0.000	0.000
EMCN	-3.81	3.66	-7.55	0.000	0.000
KRT18	-2.96	4.52	-7.57	0.000	0.000
MPPED2	-3.50	4.07	-7.58	0.000	0.000
SCHIP1	-2.29	5.25	-7.61	0.000	0.000
C6orf141	-3.99	3.59	-7.61	0.000	0.000
PRKG2	-0.95	6.43	-7.62	0.000	0.000
SKAP1	-3.15	4.34	-7.62	0.000	0.000
DPYSL3	-1.14	6.58	-7.63	0.000	0.000
SEL1L3	-1.19	6.35	-7.63	0.000	0.000
CAVIN1	-1.17	6.54	-7.65	0.000	0.000
LOX	-3.73	3.94	-7.67	0.000	0.000
SDR42E1	-3.24	4.41	-7.67	0.000	0.000
HOXA3	-3.63	3.97	-7.70	0.000	0.000
FREM1	-2.71	4.93	-7.71	0.000	0.000
SLITRK4	-3.36	4.18	-7.71	0.001	0.015
RBFOX2	-3.12	4.45	-7.71	0.000	0.000
NFIA	-0.10	7.54	-7.72	0.000	0.000
FAT4	-2.26	5.38	-7.80	0.000	0.000
HOXA10	-2.88	4.86	-7.83	0.000	0.000
CEP126	-3.22	4.50	-7.85	0.000	0.000
GABBR1	-1.76	6.10	-7.89	0.000	0.000
SH3BP4	-3.20	4.68	-7.91	0.000	0.000
PRKG1	-3.40	4.53	-7.91	0.000	0.000
BEND7	-3.63	4.29	-7.92	0.000	0.000
XIRP2	-3.50	4.40	-7.93	0.000	0.000
CALN1	-1.53	6.25	-7.95	0.000	0.000
RNF217	-1.54	6.25	-7.95	0.000	0.000
LAMB2	-1.83	6.05	-8.03	0.000	0.001
PLOD2	-2.67	5.35	-8.05	0.000	0.000
COL5A1	-2.43	5.50	-8.05	0.000	0.000
PTPRM	-1.69	6.18	-8.06	0.000	0.000
EHD2	-3.19	4.74	-8.08	0.000	0.000
CHRDL1	-3.47	4.56	-8.10	0.000	0.000
EVC	-3.09	4.85	-8.10	0.000	0.000

AASS	-2.34	5.60	-8.12	0.000	0.000
FAM171B	-2.79	5.14	-8.12	0.000	0.000
CDC42BPA	-1.07	6.96	-8.12	0.000	0.000
NAP1L3	-3.09	4.89	-8.13	0.000	0.000
CCDC175	-3.46	4.82	-8.23	0.000	0.000
CACNB2	-2.96	5.21	-8.23	0.000	0.000
HOXB3	-2.46	5.66	-8.25	0.000	0.000
TRO	-2.10	5.86	-8.27	0.000	0.000
DSG2	-2.03	6.15	-8.35	0.000	0.000
SLC8A3	-2.48	5.78	-8.41	0.000	0.000
HLF	-1.91	6.59	-8.53	0.000	0.000
HOXA6	-3.99	4.70	-8.71	0.000	0.000
PAWR	-2.22	6.42	-8.74	0.000	0.000
SPAG17	-3.55	5.09	-8.77	0.000	0.000
SYTL4	-3.20	5.62	-8.89	0.000	0.000
IL12RB2	-2.79	6.18	-8.99	0.000	0.000
HOXA5	-3.81	5.14	-9.00	0.000	0.000
CHRM3	-2.56	6.44	-9.08	0.000	0.000
VWDE	-2.25	6.88	-9.17	0.000	0.000
FGD5	-3.02	6.10	-9.18	0.000	0.001
MYCT1	-3.60	5.54	-9.21	0.000	0.000
PBX1	-2.84	6.40	-9.23	0.000	0.000
DPPA4	-2.49	6.61	-9.30	0.000	0.000
DACH1	-3.60	5.74	-9.41	0.000	0.000
HOXA9	-3.63	5.86	-9.57	0.000	0.000
CPNE8	-3.07	6.48	-9.59	0.000	0.000
HMGA2	-3.46	6.25	-9.76	0.000	0.000
NKAIN2	-3.99	5.86	-9.87	0.000	0.000
SCN9A	-1.70	8.15	-9.88	0.000	0.000
ADGRG6	-2.10	7.70	-9.92	0.000	0.000
RBPMS	-3.24	6.64	-10.04	0.000	0.000
PCDH9	-2.64	7.46	-10.15	0.000	0.000
ZNF521	-2.01	8.09	-10.32	0.000	0.000
DOCK1	-3.16	7.26	-10.49	0.000	0.000
MECOM	-3.73	7.42	-11.14	0.000	0.000
MEIS1	-2.93	8.31	-11.43	0.000	0.000

Supplementary table 2: DEG in *CEBPA*$^{N/C}$ compared to t(8;21) AMLs..

hgnc_symbol	CEBPAx2_log2CPM_avg	t821_log2CPM_avg	log2FC	P.Value	adj.P.Val
TSPAN32	6.54	-1.58	8.30	0.000	0.000
LAT2	8.60	0.62	7.97	0.000	0.000
SHD	4.58	-3.15	7.85	0.000	0.002
CYP7B1	5.83	-1.66	7.80	0.000	0.000
ABO	4.39	-3.15	7.60	0.000	0.001
ARHGAP5	7.90	1.16	6.99	0.000	0.000
CTSW	8.98	2.23	6.89	0.000	0.000
ADGRG5	5.74	-0.97	6.88	0.000	0.000
GFI1B	4.69	-1.70	6.63	0.000	0.000
ADAMTS10	3.96	-2.47	6.62	0.000	0.004
MGAT3	3.38	-2.70	6.61	0.002	0.020
SPINK2	4.01	-2.70	6.57	0.005	0.038
FUT7	3.57	-2.47	6.15	0.000	0.001
HTR1F	2.74	-2.93	6.15	0.002	0.024
ADD2	4.99	-0.80	6.14	0.001	0.011
LSP1	7.04	1.14	6.08	0.000	0.000
RFX8	4.73	-1.39	6.05	0.000	0.000
C11orf21	6.54	0.67	6.04	0.000	0.000
CAPG	7.16	1.25	5.80	0.000	0.000
PRF1	4.93	-0.71	5.76	0.001	0.010
B3GNT7	4.18	-1.10	5.57	0.002	0.019
SMAD7	5.16	-0.11	5.25	0.005	0.042
TESC	5.94	1.10	5.22	0.000	0.000
PLXNC1	7.35	2.31	5.20	0.000	0.000
RUNX3	5.66	0.91	5.17	0.000	0.000
NIPA1	4.55	-0.70	5.15	0.000	0.000
APBA2	4.43	-0.47	5.14	0.000	0.001
ILDR2	5.40	0.44	5.13	0.000	0.000
ST8SIA1	2.18	-2.75	5.12	0.004	0.032
CD7	4.80	-0.10	4.93	0.000	0.002
PCBP3	1.83	-2.93	4.84	0.000	0.001
LTC4S	3.28	-1.58	4.83	0.000	0.000
NECTIN1	5.79	1.12	4.80	0.000	0.000
AKAP6	2.00	-2.52	4.75	0.000	0.000
VOPP1	3.83	-0.82	4.73	0.000	0.000
PROM1	8.39	3.67	4.72	0.001	0.013
SPNS3	5.18	0.51	4.72	0.000	0.001
SLC44A1	7.93	3.81	4.57	0.000	0.000
APBA1	4.14	-0.23	4.55	0.000	0.004

CMTM4	4.53	0.54	4.53	0.000	0.001
CYTH4	7.16	2.94	4.44	0.000	0.000
KCNK17	2.67	-1.90	4.43	0.001	0.011
CRYGD	2.73	-1.66	4.42	0.000	0.001
MED12L	5.39	1.30	4.37	0.002	0.023
ADCY7	7.50	3.11	4.31	0.000	0.000
ANGPT1	7.43	3.85	4.28	0.000	0.006
SORCS1	2.99	-1.41	4.27	0.000	0.004
P2RY10	3.81	-0.34	4.23	0.001	0.015
SLC46A3	4.01	0.21	4.19	0.000	0.005
ACP5	3.15	-0.79	4.18	0.000	0.003
S100B	5.36	1.68	4.12	0.001	0.015
TRMT9B	4.22	-0.16	4.09	0.002	0.019
CEBPA	9.48	5.45	4.07	0.000	0.000
ABCA1	5.84	2.51	4.01	0.000	0.002
CRLF2	2.68	-0.91	4.00	0.001	0.014
LPAR4	3.92	-0.11	3.99	0.000	0.001
OGG1	4.48	0.63	3.97	0.000	0.000
BTBD11	5.91	1.96	3.94	0.000	0.000
ADAMTS14	3.52	-0.54	3.93	0.000	0.001
GNB5	5.20	1.18	3.90	0.000	0.004
TNNI2	1.10	-2.82	3.82	0.000	0.001
NKG7	5.63	1.64	3.75	0.000	0.005
PALD1	4.59	0.71	3.72	0.002	0.024
SH2D3C	5.07	1.52	3.70	0.000	0.001
ST6GALNAC3	1.59	-1.69	3.70	0.002	0.024
SERPINF2	2.35	-1.25	3.69	0.000	0.005
GUCY2D	0.62	-2.93	3.69	0.000	0.006
MYEF2	5.59	1.36	3.68	0.001	0.017
RIMBP3	1.63	-1.81	3.66	0.000	0.002
CAMK1	0.47	-2.93	3.62	0.000	0.004
NKD2	0.69	-2.93	3.60	0.001	0.016
CST7	4.99	1.35	3.60	0.003	0.024
TMPRSS9	1.03	-2.52	3.59	0.000	0.002
C15orf39	6.86	3.42	3.58	0.000	0.000
LST1	4.79	1.32	3.58	0.001	0.009
CCDC102A	2.77	-0.61	3.54	0.000	0.001
GCSAML	5.00	1.49	3.52	0.000	0.002
PRKN	0.56	-2.82	3.49	0.000	0.003
PTPN22	6.09	2.71	3.49	0.000	0.000
CDCP1	3.41	0.53	3.40	0.006	0.046
SPON2	4.19	0.72	3.37	0.000	0.002

CD300A	5.49	2.50	3.37	0.000	0.000
CHN2	2.47	-0.84	3.37	0.000	0.003
NRG4	2.20	-0.83	3.33	0.000	0.003
TMEM229B	2.96	-0.23	3.32	0.001	0.014
IL9R	2.04	-1.50	3.32	0.004	0.032
IGF2BP3	2.70	-0.50	3.31	0.000	0.007
KHDRBS2	1.05	-2.12	3.28	0.001	0.014
ABCA7	5.15	1.97	3.25	0.000	0.004
PRR5L	5.80	2.88	3.25	0.000	0.004
PURA	4.75	1.76	3.24	0.001	0.009
ATP1B1	5.77	2.75	3.22	0.000	0.000
MEGF10	1.48	-1.81	3.19	0.001	0.013
TVP23C	3.70	0.95	3.17	0.006	0.046
SLC14A1	4.79	1.86	3.17	0.000	0.001
UMODL1	5.82	2.60	3.16	0.004	0.034
SSPN	0.81	-1.91	3.11	0.004	0.031
SUSD3	3.07	-0.04	3.10	0.002	0.024
NINJ2	3.31	0.40	3.10	0.001	0.015
ALCAM	7.45	4.02	3.09	0.000	0.003
RHOH	6.93	3.37	3.07	0.000	0.001
SRGAP3	4.74	1.90	3.06	0.000	0.000
ABHD12B	2.29	-0.40	3.06	0.002	0.019
NYNRIN	4.53	1.63	3.04	0.003	0.030
PLD4	6.20	3.35	3.04	0.000	0.002
MFSD2B	3.71	0.77	3.03	0.000	0.001
BCL2L10	-0.24	-3.15	3.02	0.006	0.045
PLEKHF1	1.09	-1.92	3.01	0.000	0.001
IFFO2	5.54	2.70	2.98	0.000	0.001
C3orf80	-0.47	-3.15	2.97	0.002	0.024
LRRC28	6.94	3.96	2.96	0.000	0.001
CLDN9	0.06	-2.82	2.94	0.000	0.006
ADRB2	5.82	3.04	2.93	0.000	0.004
GCHFR	2.51	-0.78	2.92	0.001	0.011
PAIP2B	2.25	-0.05	2.91	0.004	0.037
HSH2D	9.12	6.27	2.90	0.000	0.000
MRC2	5.63	3.09	2.90	0.006	0.045
LMNTD2	0.37	-2.47	2.90	0.000	0.001
SNAI3	2.73	-0.11	2.88	0.000	0.004
MEX3B	6.08	3.18	2.86	0.000	0.001
SNX9	3.78	0.91	2.84	0.001	0.012
PRR33	-0.41	-3.15	2.84	0.001	0.014
TNNT3	3.21	0.62	2.82	0.004	0.033

SELPLG	5.81	2.86	2.82	0.002	0.023
DYTN	2.22	-0.30	2.81	0.003	0.031
SLFN5	3.16	0.72	2.81	0.002	0.021
BAHCC1	8.83	6.07	2.75	0.000	0.000
GPR146	0.82	-1.72	2.75	0.002	0.023
GSTM2	4.47	1.88	2.75	0.002	0.021
CLIP2	7.88	5.25	2.70	0.000	0.000
ST7	5.34	2.95	2.69	0.000	0.008
ZFYVE28	1.45	-1.02	2.69	0.002	0.024
NKD1	2.98	0.76	2.68	0.002	0.024
NLRC3	6.24	3.66	2.68	0.000	0.000
ARHGAP10	5.61	3.23	2.68	0.000	0.001
GPR132	3.58	1.08	2.66	0.000	0.001
CD48	6.73	3.98	2.66	0.000	0.000
PSD2	-0.04	-2.70	2.65	0.001	0.010
TNFRSF14	6.81	4.22	2.63	0.000	0.000
CYP2E1	3.09	0.60	2.62	0.000	0.007
TYROBP	7.27	4.53	2.62	0.000	0.000
AOAH	5.12	2.18	2.61	0.001	0.009
CD84	8.19	5.67	2.60	0.000	0.000
SLC16A3	5.19	2.51	2.59	0.000	0.001
IQCD	0.02	-2.47	2.58	0.005	0.040
LDLRAD4	7.27	4.50	2.57	0.000	0.004
RGS9BP	0.14	-2.43	2.57	0.001	0.013
C10orf105	-0.25	-2.59	2.56	0.003	0.028
MAFK	6.00	3.54	2.56	0.000	0.000
RMND5B	2.75	0.08	2.56	0.000	0.002
GPT2	5.01	2.53	2.55	0.000	0.001
ASRGL1	4.36	2.01	2.55	0.006	0.043
TDRKH	2.09	-0.23	2.54	0.001	0.014
LAPTM5	9.03	6.51	2.53	0.000	0.000
SASH3	7.63	5.04	2.49	0.000	0.000
BLVRB	4.84	2.54	2.47	0.001	0.010
SIGLEC10	4.81	2.13	2.47	0.000	0.002
RGL4	3.15	0.60	2.45	0.001	0.013
DACT1	0.48	-1.77	2.43	0.004	0.031
PPBP	0.11	-2.30	2.42	0.007	0.050
ABI3	0.50	-1.69	2.40	0.006	0.043
NFIL3	6.06	3.60	2.40	0.004	0.032
F12	0.49	-1.86	2.39	0.004	0.034
IGFBP7	8.06	5.70	2.39	0.000	0.000
TNFSF13	2.92	0.59	2.36	0.001	0.012

CD82	7.06	4.55	2.35	0.000	0.000
PLEKHA1	2.89	0.36	2.35	0.001	0.011
CCDC122	2.14	0.19	2.35	0.003	0.026
GPR174	6.94	4.64	2.34	0.000	0.000
CEL	1.52	-0.83	2.34	0.007	0.048
C20orf203	0.23	-1.85	2.33	0.001	0.016
MAP3K8	7.66	5.30	2.33	0.000	0.003
PABPN1L	-0.15	-2.37	2.33	0.002	0.024
CYP2C8	1.47	-0.82	2.32	0.005	0.040
SEPTIN1	2.30	0.07	2.31	0.007	0.049
GCLM	3.23	1.31	2.31	0.001	0.011
KPTN	3.33	1.03	2.31	0.000	0.001
SYNPO2	0.71	-1.41	2.30	0.003	0.026
TPCN1	5.31	2.94	2.30	0.000	0.000
CCL23	2.07	-0.08	2.29	0.002	0.019
AIF1	7.35	5.23	2.26	0.000	0.000
MITF	3.49	1.46	2.26	0.000	0.001
ITGA2B	4.09	1.81	2.22	0.005	0.038
CHST12	6.69	4.48	2.22	0.000	0.000
ADARB1	4.14	2.04	2.20	0.000	0.003
PKIB	0.82	-1.59	2.19	0.004	0.035
VSIR	6.70	4.50	2.18	0.000	0.001
RASSF5	6.75	4.31	2.18	0.000	0.001
ZCCHC24	2.11	-0.07	2.18	0.002	0.018
SSX2IP	5.14	3.07	2.18	0.000	0.002
CAPRIN2	3.96	1.61	2.16	0.000	0.006
GRAMD4	7.50	5.36	2.16	0.000	0.000
DERL3	3.76	1.61	2.15	0.000	0.005
CARD19	5.71	3.51	2.13	0.000	0.000
MGAT4A	5.99	3.94	2.11	0.001	0.009
ABCA2	6.21	4.26	2.11	0.000	0.000
HERC5	4.99	3.22	2.10	0.001	0.016
SPAG1	4.53	2.57	2.07	0.000	0.000
IGFBP6	0.43	-1.58	2.07	0.004	0.034
ZDHHC2	7.45	5.09	2.07	0.001	0.016
BST2	5.58	3.73	2.06	0.001	0.012
PGM3	4.16	2.16	2.06	0.000	0.002
FKBP1B	0.20	-1.74	2.04	0.002	0.020
DEGS2	0.92	-0.96	2.04	0.002	0.019
TMEM25	2.30	0.06	2.04	0.000	0.007
ITGB2	8.17	6.19	2.04	0.000	0.000
CTSD	6.12	4.12	2.04	0.000	0.000

CKLF	3.76	1.96	2.03	0.001	0.014
ST3GAL4	5.78	3.74	2.03	0.000	0.000
EVL	6.76	4.90	2.02	0.000	0.000
EFHC2	1.87	-0.20	2.02	0.003	0.025
PET117	1.20	-0.63	2.01	0.005	0.039
SLC45A4	2.75	0.63	2.01	0.002	0.021
KLHL13	5.38	3.33	2.00	0.001	0.013
SUCNR1	7.32	5.08	2.00	0.003	0.025
ARL6IP4	0.86	-1.16	1.99	0.003	0.030
GBGT1	3.59	1.97	1.97	0.000	0.007
SPOUT1	0.41	-1.40	1.95	0.004	0.032
SLC1A4	5.40	3.39	1.94	0.000	0.006
ITGAL	7.16	5.04	1.93	0.000	0.001
SKIL	5.49	3.55	1.93	0.001	0.009
PKIG	4.15	2.08	1.93	0.003	0.030
TLR1	5.51	3.91	1.91	0.001	0.010
LYSMD4	3.77	1.82	1.88	0.001	0.015
GPR160	4.13	2.28	1.88	0.003	0.024
STARD9	5.88	4.26	1.86	0.000	0.005
TRIM8	5.82	3.96	1.86	0.000	0.000
SYTL1	6.22	4.40	1.84	0.000	0.002
KCTD6	3.37	1.65	1.84	0.001	0.017
CASZ1	3.10	1.35	1.83	0.004	0.035
CROT	3.89	1.99	1.83	0.002	0.022
SIPA1	6.92	5.03	1.83	0.000	0.001
SMOX	4.30	2.41	1.83	0.004	0.034
PLAAT4	5.25	3.35	1.83	0.000	0.001
LCP1	10.45	8.62	1.83	0.000	0.000
ATP8A1	7.88	6.18	1.83	0.000	0.002
CLDN12	2.36	0.87	1.82	0.002	0.024
ITM2A	9.09	7.24	1.81	0.000	0.006
MAGEF1	3.98	2.24	1.81	0.005	0.041
RPS6KA1	7.13	5.27	1.80	0.000	0.000
LY86	5.07	3.19	1.80	0.002	0.024
WDFY4	7.12	5.35	1.80	0.000	0.000
FBXO21	3.94	2.40	1.79	0.001	0.009
PARVG	8.16	6.35	1.78	0.000	0.000
PDIK1L	5.81	4.20	1.78	0.000	0.000
LGALS1	6.70	4.72	1.76	0.002	0.020
ATP13A2	4.31	2.29	1.76	0.001	0.015
ITGA6	8.05	6.33	1.75	0.001	0.012
DRAP1	6.27	4.50	1.74	0.000	0.000

SH3BP1	3.86	2.12	1.73	0.000	0.001
SVOPL	3.14	1.13	1.73	0.001	0.017
WDR81	6.82	5.08	1.73	0.000	0.000
PLP2	6.99	5.14	1.72	0.000	0.000
BCL7A	5.68	4.06	1.72	0.000	0.003
XYLT1	7.57	5.82	1.70	0.000	0.000
RAP1GAP2	6.26	4.65	1.70	0.000	0.001
B3GNT2	8.24	6.58	1.69	0.000	0.000
RPS6KA2	4.67	2.80	1.69	0.000	0.004
TMEM38B	4.40	3.04	1.69	0.005	0.040
MGLL	6.93	5.08	1.68	0.000	0.008
TRABD	5.62	3.95	1.68	0.000	0.001
APOBR	4.76	3.11	1.67	0.001	0.010
MATK	6.01	4.48	1.66	0.000	0.004
DENND6B	4.65	2.92	1.66	0.001	0.013
DHRS11	3.72	2.08	1.66	0.002	0.024
CBFA2T3	4.83	3.24	1.65	0.000	0.006
SLA	5.81	3.84	1.65	0.002	0.023
SH3BP2	6.38	4.84	1.65	0.000	0.000
HCST	6.91	4.99	1.65	0.000	0.003
RASSF7	3.25	1.52	1.64	0.000	0.006
CYP51A1	2.35	0.73	1.63	0.002	0.020
DLC1	7.59	5.93	1.63	0.002	0.020
HSF5	1.71	0.18	1.63	0.001	0.016
NFE2	7.16	5.43	1.63	0.000	0.005
DNAH14	5.11	3.53	1.61	0.001	0.016
LHFPL2	7.41	5.68	1.61	0.002	0.021
IL18	6.38	4.49	1.60	0.001	0.018
PRKCD	4.86	3.15	1.60	0.000	0.001
CDKN2D	3.75	2.14	1.60	0.004	0.034
ZBTB18	5.60	4.14	1.59	0.000	0.006
NUCB2	9.09	7.50	1.59	0.000	0.000
TFRC	9.45	7.87	1.58	0.000	0.000
CSF2RB	7.24	5.67	1.58	0.004	0.033
SEC11C	4.14	2.75	1.58	0.000	0.002
ADA	6.35	4.77	1.56	0.000	0.003
SNX10	3.56	2.21	1.55	0.002	0.022
SH3GLB2	5.04	3.49	1.55	0.000	0.002
TSEN54	5.60	4.09	1.55	0.000	0.000
PPM1M	3.54	1.95	1.54	0.000	0.007
TEX9	3.53	2.39	1.54	0.001	0.013
RAB5IF	4.45	3.07	1.53	0.004	0.033

IL12A	2.34	0.92	1.53	0.002	0.023
ANKRD27	7.70	6.17	1.51	0.000	0.000
KATNAL2	2.48	0.99	1.51	0.001	0.017
GCNT1	5.98	4.57	1.51	0.002	0.020
CXXC5	6.19	4.66	1.51	0.000	0.001
RFLNB	7.25	5.81	1.50	0.000	0.003
EMID1	6.66	5.13	1.49	0.000	0.002
JDP2	5.03	3.62	1.48	0.002	0.019
MEST	8.55	7.05	1.46	0.001	0.014
EEPD1	4.38	3.00	1.46	0.001	0.014
FRMD4B	4.51	3.25	1.45	0.004	0.036
MSI2	8.01	6.58	1.45	0.000	0.001
FMNL3	4.76	3.43	1.45	0.003	0.028
PRKCE	4.95	3.17	1.45	0.003	0.025
PELO	3.86	2.47	1.44	0.004	0.034
DENND2D	4.77	3.34	1.44	0.006	0.048
PSMB10	5.61	4.10	1.44	0.000	0.002
FECH	6.57	5.16	1.43	0.000	0.003
DYNLT3	4.63	3.26	1.43	0.001	0.010
BCL2	7.18	5.77	1.43	0.000	0.007
FAM78A	7.02	5.60	1.43	0.000	0.001
CCDC112	4.57	2.92	1.43	0.002	0.020
MROH6	3.87	2.32	1.41	0.003	0.025
STAMBPL1	3.93	2.68	1.41	0.001	0.012
ARID5A	5.52	4.04	1.41	0.000	0.004
DPEP2	4.97	3.41	1.40	0.000	0.002
FOXRED2	3.62	2.39	1.40	0.003	0.028
ATP2B4	7.89	6.48	1.40	0.000	0.006
SMIM24	7.16	5.82	1.40	0.001	0.014
SLC43A3	4.89	3.51	1.37	0.000	0.000
BIRC3	5.56	4.25	1.37	0.003	0.025
RAVER2	6.54	5.28	1.37	0.000	0.002
NDUFC2	5.15	3.89	1.36	0.002	0.022
C12orf75	3.93	2.49	1.36	0.003	0.027
GLCE	4.40	3.20	1.35	0.004	0.032
ST6GALNAC4	3.19	1.86	1.35	0.001	0.013
SLC27A2	5.08	3.96	1.35	0.001	0.009
MPND	4.83	3.39	1.35	0.000	0.004
LSM4	6.06	4.68	1.34	0.000	0.000
CMPK2	5.33	3.97	1.34	0.000	0.005
YPEL1	4.84	3.48	1.34	0.000	0.000
CARHSP1	5.07	3.69	1.34	0.000	0.003

SNTB1	7.02	5.65	1.34	0.000	0.001
TFAP2E	1.45	0.12	1.34	0.003	0.028
NOTCH1	6.55	5.29	1.33	0.002	0.018
SLC7A5	6.21	4.93	1.33	0.000	0.006
CD33	6.67	5.23	1.33	0.003	0.028
HIC2	4.86	3.51	1.33	0.000	0.001
SELENOH	4.47	3.05	1.33	0.001	0.015
RASAL3	6.37	4.91	1.32	0.000	0.003
ATG4D	4.85	3.51	1.32	0.003	0.026
FAM53B	6.11	4.79	1.32	0.000	0.000
C1orf162	4.10	2.65	1.32	0.005	0.042
GKAP1	3.71	2.54	1.31	0.001	0.010
MPG	5.74	4.24	1.30	0.003	0.025
OSBPL3	6.13	4.90	1.30	0.001	0.017
ELF4	6.65	5.36	1.30	0.000	0.003
GNA15	7.86	6.55	1.29	0.000	0.002
JTB	5.62	4.41	1.29	0.000	0.002
ICAM3	7.42	6.09	1.28	0.000	0.001
PARP10	6.32	5.03	1.28	0.001	0.014
CLN3	2.87	1.67	1.27	0.002	0.022
GPD2	6.44	5.19	1.27	0.000	0.002
HHAT	4.66	3.49	1.27	0.000	0.004
GALC	7.18	5.92	1.26	0.001	0.011
MICAL1	6.71	5.17	1.26	0.004	0.036
REPIN1	7.16	5.82	1.25	0.000	0.002
MEGF6	6.94	5.78	1.25	0.001	0.014
SLC12A4	4.80	3.59	1.24	0.000	0.008
SFT2D1	5.29	4.06	1.24	0.000	0.000
PLXNB2	7.37	6.17	1.24	0.000	0.004
ERP29	7.81	6.58	1.24	0.000	0.001
PDE7A	8.26	7.02	1.24	0.000	0.001
TIMM13	5.77	4.49	1.23	0.000	0.005
CDK2AP1	6.63	5.42	1.23	0.000	0.000
BTBD6	4.01	3.00	1.23	0.000	0.004
NUP210	8.51	7.31	1.22	0.000	0.002
INPP4A	5.98	4.83	1.22	0.000	0.002
TBC1D10C	6.15	4.88	1.22	0.000	0.002
HYI	4.12	2.90	1.21	0.003	0.025
STAU2	6.30	5.10	1.21	0.000	0.000
CCS	5.57	4.26	1.21	0.004	0.031
CDK9	6.55	5.31	1.21	0.000	0.000
CYFIP2	7.44	6.21	1.21	0.003	0.024

RHOBTB1	5.24	4.05	1.20	0.002	0.024
AP1S2	6.36	5.07	1.20	0.000	0.000
PSMG3	4.98	3.78	1.20	0.000	0.002
CYBA	8.02	6.84	1.20	0.001	0.016
KRT10	2.28	1.17	1.20	0.003	0.027
DNMT3B	5.44	4.22	1.20	0.002	0.023
CCPG1	4.58	3.47	1.19	0.006	0.047
GSR	6.51	5.34	1.19	0.000	0.000
COL24A1	6.75	5.70	1.19	0.005	0.040
RNF144A	6.96	5.72	1.18	0.000	0.002
IER3IP1	5.14	4.17	1.18	0.002	0.023
CDKN1B	6.95	5.71	1.17	0.005	0.037
MBOAT1	6.61	5.33	1.17	0.004	0.031
ORAI1	5.35	4.10	1.16	0.000	0.003
P2RY1	6.16	5.11	1.16	0.000	0.004
ATP5MG	6.39	5.24	1.16	0.000	0.004
CFL2	5.08	4.01	1.16	0.003	0.029
CCDC88B	5.62	4.48	1.15	0.005	0.042
MTMR1	4.96	3.78	1.15	0.000	0.001
RGS14	4.84	3.74	1.14	0.003	0.027
SLC16A7	5.49	4.50	1.13	0.001	0.014
SEC61G	5.43	4.40	1.12	0.001	0.011
CYTL1	7.00	5.86	1.12	0.003	0.026
NDUFA11	4.35	3.21	1.11	0.002	0.024
SVIP	4.85	3.87	1.11	0.002	0.019
CCDC102B	3.08	1.99	1.11	0.001	0.012
GAB3	7.36	6.22	1.11	0.000	0.001
PLAC8	8.01	6.90	1.11	0.000	0.005
PAXX	4.15	3.06	1.11	0.002	0.020
C9orf72	5.73	4.66	1.10	0.003	0.029
TCAF1	5.03	3.96	1.10	0.000	0.002
CENPJ	6.62	5.49	1.10	0.000	0.001
TBKBP1	4.32	3.38	1.10	0.001	0.016
TENT5A	8.38	7.28	1.10	0.002	0.024
ZBTB24	5.45	4.38	1.10	0.000	0.001
MZT1	4.78	3.84	1.10	0.002	0.021
NQO2	4.39	3.34	1.10	0.004	0.036
DPP7	6.02	4.85	1.09	0.005	0.042
PISD	6.15	5.05	1.09	0.000	0.000
ZDHHC14	3.95	2.93	1.09	0.002	0.024
RANGRF	4.05	2.93	1.08	0.002	0.021
ETS2	7.69	6.60	1.08	0.002	0.024

MAP2K6	4.51	3.46	1.08	0.007	0.049
RPLP1	10.09	9.01	1.08	0.003	0.029
PEX6	5.72	4.70	1.07	0.001	0.015
LDHB	6.74	5.72	1.07	0.007	0.049
KIZ	6.13	5.09	1.07	0.003	0.027
ROMO1	5.06	4.00	1.07	0.005	0.041
FUT4	8.06	6.98	1.07	0.000	0.007
LCP2	7.41	6.33	1.07	0.000	0.001
VAV1	6.76	5.74	1.06	0.000	0.007
USP20	5.91	4.82	1.06	0.000	0.003
RHOBTB2	3.47	2.28	1.06	0.003	0.026
MBP	6.67	5.54	1.06	0.001	0.015
TP53RK	4.87	3.82	1.05	0.002	0.023
LAGE3	4.18	2.98	1.05	0.005	0.039
NUDT1	4.85	3.79	1.05	0.006	0.044
UNC13D	7.64	6.62	1.05	0.001	0.008
LNPK	5.63	4.62	1.05	0.003	0.028
TWF2	5.42	4.18	1.05	0.002	0.024
LIPT2	2.32	1.25	1.05	0.005	0.039
ANKRD44	7.12	6.02	1.05	0.000	0.003
GTF2A2	5.81	4.78	1.05	0.001	0.010
ADGRE2	6.60	5.47	1.04	0.003	0.026
RASSF2	7.41	6.33	1.04	0.000	0.001
REXO5	6.14	5.08	1.04	0.000	0.006
SLC48A1	3.63	2.72	1.04	0.002	0.018
PIP5K1B	4.76	3.82	1.03	0.005	0.040
SFXN5	5.35	4.22	1.03	0.001	0.014
DEAF1	5.43	4.46	1.03	0.000	0.003
STIM2	5.18	4.12	1.02	0.005	0.039
DUT	6.95	5.97	1.02	0.001	0.012
SPAG16	3.93	2.91	1.02	0.002	0.021
RNF166	5.30	4.20	1.02	0.002	0.019
MFSD9	4.50	3.45	1.02	0.001	0.015
PPCDC	4.29	3.25	1.01	0.000	0.003
ZYG11B	5.99	5.04	1.01	0.000	0.004
RAP2C	6.72	5.73	1.01	0.002	0.024
CD47	8.44	7.43	1.00	0.000	0.004
DIPK1B	5.82	6.79	-1.00	0.004	0.035
MKNK1	5.14	6.04	-1.00	0.000	0.005
WARS1	5.76	6.74	-1.01	0.001	0.012
CNST	7.36	8.37	-1.01	0.000	0.003
CBX5	7.23	8.23	-1.01	0.001	0.011

L2HGDH	2.84	3.91	-1.02	0.005	0.037
H2BC21	7.84	8.87	-1.02	0.001	0.017
PIGZ	1.62	2.55	-1.03	0.007	0.050
LMTK2	4.13	5.14	-1.03	0.001	0.017
PPP1R10	6.66	7.68	-1.03	0.000	0.004
SPATS2	3.84	4.76	-1.03	0.003	0.028
SDCCAG8	6.81	7.83	-1.04	0.001	0.012
LPCAT1	4.19	5.28	-1.04	0.006	0.044
THBS3	4.67	5.67	-1.04	0.001	0.017
ANTXR2	6.96	8.00	-1.04	0.002	0.024
NUMB	5.63	6.65	-1.05	0.000	0.002
KIAA1958	4.94	5.97	-1.05	0.001	0.012
SLC22A16	4.88	5.83	-1.05	0.001	0.010
CMTM7	4.90	5.81	-1.06	0.001	0.016
ANKRD42	3.92	4.91	-1.06	0.002	0.019
NPIPB4	2.47	3.47	-1.06	0.007	0.050
ZSWIM6	3.78	4.84	-1.06	0.005	0.038
SHC1	5.36	6.36	-1.07	0.001	0.014
CSRP1	4.95	6.00	-1.07	0.000	0.001
ITGB1	7.10	8.17	-1.08	0.001	0.010
ZNF608	4.92	5.90	-1.09	0.003	0.028
TERF2	4.46	5.47	-1.09	0.000	0.002
NCK2	4.60	5.67	-1.09	0.001	0.012
DHRS12	1.29	2.27	-1.10	0.005	0.041
SAMSN1	5.67	6.74	-1.10	0.000	0.001
CCDC86	3.59	4.55	-1.10	0.007	0.049
ITGA9	7.62	8.73	-1.11	0.002	0.020
RELL1	6.19	7.29	-1.11	0.002	0.020
MINDY1	4.36	5.40	-1.11	0.000	0.002
CD58	5.35	6.36	-1.11	0.002	0.021
ABCC1	7.16	8.28	-1.12	0.000	0.000
BTG1	6.88	7.98	-1.12	0.003	0.028
UHRF1BP1L	5.83	6.91	-1.12	0.001	0.009
SLC6A6	5.86	6.97	-1.13	0.000	0.004
SAP30	4.49	5.60	-1.13	0.001	0.012
B4GALT5	4.94	6.11	-1.13	0.000	0.006
COTL1	6.03	7.12	-1.14	0.002	0.023
TGFBR2	6.16	7.25	-1.14	0.003	0.028
ZFP69B	1.66	2.80	-1.16	0.001	0.017
CA5B	4.98	6.11	-1.17	0.003	0.028
DENND10	5.46	6.62	-1.17	0.000	0.002
FSTL3	1.55	2.65	-1.17	0.005	0.039

MXI1	4.68	5.83	-1.17	0.000	0.002
IL27RA	4.49	5.68	-1.18	0.002	0.023
VAV3	7.02	8.21	-1.19	0.000	0.000
PCK2	3.79	4.78	-1.19	0.002	0.023
ARHGEF3	4.07	5.37	-1.19	0.001	0.009
TMEM268	3.88	4.93	-1.19	0.001	0.014
ZHX2	3.84	4.82	-1.20	0.006	0.046
DISC1	5.40	6.57	-1.20	0.004	0.034
LRP10	4.18	5.31	-1.21	0.002	0.024
CTSK	2.05	3.23	-1.21	0.006	0.047
F11R	5.66	6.84	-1.21	0.000	0.001
FAM117A	5.82	7.03	-1.22	0.000	0.005
MAST4	5.24	6.44	-1.22	0.000	0.002
PDXK	3.96	5.26	-1.22	0.000	0.003
SEPTIN11	7.07	8.30	-1.22	0.000	0.008
TRIM14	5.03	6.26	-1.22	0.001	0.010
SLC35F6	2.19	3.38	-1.23	0.005	0.039
TRAF3	4.44	5.70	-1.23	0.000	0.001
CIAO3	4.47	5.67	-1.24	0.003	0.028
GNS	6.50	7.71	-1.24	0.000	0.003
TMEM102	2.26	3.55	-1.24	0.004	0.035
TNFAIP8L1	3.89	5.12	-1.24	0.000	0.000
SPRY3	1.16	2.28	-1.25	0.002	0.021
NPIPB5	2.97	3.93	-1.25	0.002	0.019
B4GALT2	3.15	4.39	-1.25	0.001	0.014
VSIG10	2.79	4.17	-1.26	0.001	0.013
SLC26A6	2.77	3.84	-1.26	0.000	0.004
SVIL	4.95	6.22	-1.27	0.000	0.001
LRRC8B	5.32	6.58	-1.27	0.000	0.004
ZNF107	5.46	6.71	-1.27	0.000	0.002
C3orf18	0.71	1.95	-1.27	0.002	0.023
ATG7	5.20	6.42	-1.27	0.000	0.000
UAP1L1	3.48	4.79	-1.28	0.000	0.003
TAS2R31	1.07	2.30	-1.28	0.006	0.044
ENTPD4	5.11	6.38	-1.29	0.000	0.006
AGO2	6.12	7.41	-1.29	0.000	0.000
SSH2	6.86	8.14	-1.30	0.000	0.001
IKZF2	7.13	8.45	-1.31	0.001	0.015
CPD	6.78	8.08	-1.31	0.002	0.019
TMEM44	4.61	5.89	-1.32	0.000	0.002
NAGA	3.90	5.05	-1.33	0.002	0.021
CAMKK1	2.46	3.91	-1.35	0.000	0.005

NFAT5	6.45	7.78	-1.35	0.001	0.010
C6orf163	1.67	3.13	-1.35	0.007	0.050
FNDC3B	7.90	9.27	-1.36	0.000	0.001
NAT14	2.24	3.49	-1.36	0.000	0.008
FUT10	2.28	3.90	-1.37	0.006	0.044
U2AF1	3.29	4.36	-1.37	0.005	0.042
SLC9A1	2.81	4.21	-1.37	0.000	0.005
CGAS	4.28	5.60	-1.37	0.000	0.003
CSTB	3.09	4.63	-1.38	0.000	0.002
PHACTR2	5.15	6.50	-1.38	0.004	0.034
HLA-DOA	5.87	7.22	-1.39	0.004	0.032
ITGA5	7.45	8.84	-1.39	0.000	0.000
DEF8	3.52	4.82	-1.40	0.000	0.005
GNA12	3.34	4.80	-1.40	0.000	0.001
NCOA7	6.75	8.13	-1.41	0.001	0.017
MAP3K1	7.17	8.58	-1.41	0.000	0.002
SIPA1L1	5.25	6.65	-1.42	0.001	0.010
GMPR	3.19	4.21	-1.42	0.003	0.029
ZNF433	0.85	2.08	-1.42	0.001	0.012
SRGAP2C	2.51	3.90	-1.42	0.000	0.005
PDK2	2.68	3.94	-1.44	0.001	0.010
TMEM140	3.06	4.41	-1.44	0.001	0.013
PEAK1	5.29	6.74	-1.45	0.000	0.002
RNF215	2.29	3.61	-1.47	0.001	0.014
PITPNM2	3.56	4.96	-1.48	0.000	0.008
PARP15	3.79	5.29	-1.48	0.001	0.011
SOCS3	4.47	5.98	-1.49	0.005	0.039
ACVR1B	4.01	5.35	-1.49	0.002	0.024
SMTN	2.10	3.44	-1.51	0.000	0.008
ST3GAL6	4.07	5.45	-1.52	0.002	0.019
DNAAF9	4.87	6.29	-1.52	0.001	0.011
CCDC24	0.69	2.23	-1.53	0.006	0.044
IGF2BP2	5.51	7.04	-1.53	0.000	0.001
PIK3IP1	5.04	6.51	-1.53	0.003	0.028
KLF11	4.94	6.52	-1.53	0.005	0.039
HOMER2	4.26	5.71	-1.54	0.000	0.006
MICAL3	4.05	5.66	-1.54	0.000	0.001
NRSN2	0.34	1.81	-1.56	0.004	0.033
SELENON	4.72	6.19	-1.56	0.000	0.000
SNX21	-0.51	0.84	-1.58	0.005	0.040
ZNF662	3.21	4.82	-1.58	0.001	0.017
NFKB2	3.91	5.39	-1.59	0.002	0.018

SIAE	3.79	5.37	-1.60	0.001	0.011
FCHSD1	3.29	4.91	-1.61	0.001	0.009
SRGAP2	4.10	5.57	-1.62	0.000	0.002
TOB1	2.90	4.57	-1.62	0.007	0.049
TXLNB	1.09	2.80	-1.63	0.000	0.004
MAP3K12	2.71	4.26	-1.63	0.001	0.012
VWCE	1.95	3.37	-1.64	0.005	0.043
ALS2	6.77	8.42	-1.64	0.000	0.004
GIPC3	1.02	2.69	-1.65	0.003	0.024
PER1	5.89	7.58	-1.65	0.002	0.020
TBC1D16	2.99	4.85	-1.65	0.003	0.029
TAS2R46	-0.47	1.28	-1.66	0.002	0.024
AP1B1	6.59	8.26	-1.66	0.000	0.001
USP50	-0.90	0.82	-1.67	0.004	0.031
ERVFRD-1	1.38	2.83	-1.67	0.005	0.040
TNFRSF10A	3.48	5.11	-1.68	0.000	0.002
KSR1	3.94	5.52	-1.68	0.000	0.003
EGLN1	2.17	4.10	-1.68	0.003	0.030
DAPK1	5.83	7.52	-1.69	0.001	0.015
RHOB	6.94	8.62	-1.69	0.002	0.019
NAMPT	6.61	8.27	-1.69	0.001	0.010
SUN1	4.15	5.91	-1.70	0.000	0.000
RUNX1	6.97	8.68	-1.71	0.000	0.000
PLCD1	1.44	2.94	-1.72	0.000	0.008
FLVCR2	0.66	2.56	-1.72	0.001	0.011
ATP8B2	4.91	6.68	-1.72	0.000	0.000
PLXNB1	3.03	4.57	-1.73	0.000	0.007
SERPINB9	4.28	6.05	-1.73	0.000	0.001
RTKN	2.13	3.67	-1.74	0.002	0.019
AP1S3	-0.72	1.12	-1.74	0.001	0.013
FGFRL1	1.35	3.26	-1.74	0.005	0.042
DNAJA4	1.91	3.81	-1.74	0.001	0.008
HIPK2	4.52	6.17	-1.74	0.000	0.000
LAPTM4B	3.48	5.09	-1.74	0.003	0.028
PLK3	4.54	6.27	-1.75	0.000	0.002
TRERF1	4.22	5.87	-1.76	0.000	0.001
PTCH2	2.05	4.00	-1.77	0.001	0.015
DUSP5	3.12	4.73	-1.78	0.003	0.027
SLC25A1	4.63	6.37	-1.78	0.000	0.002
PRELID2	3.76	5.41	-1.79	0.000	0.003
SMAGP	0.65	2.46	-1.79	0.000	0.004
ARL10	2.66	4.54	-1.79	0.001	0.015

SORBS1	1.95	3.36	-1.79	0.005	0.038
TTC7B	4.44	6.10	-1.81	0.000	0.002
TLR2	6.10	7.85	-1.81	0.000	0.002
SLC35F2	3.82	5.67	-1.81	0.002	0.020
NFE2L3	2.54	4.53	-1.81	0.001	0.009
POLR2J3	0.59	1.02	-1.82	0.000	0.004
KLF2	4.75	6.59	-1.82	0.003	0.026
ANO8	1.02	2.71	-1.83	0.003	0.026
GLMP	2.32	4.12	-1.84	0.000	0.001
RGS12	2.73	4.48	-1.86	0.000	0.004
KCNH8	1.28	3.24	-1.86	0.003	0.027
L3MBTL3	2.52	4.45	-1.86	0.006	0.044
HK1	4.50	6.29	-1.86	0.000	0.004
DGKG	3.79	5.54	-1.86	0.000	0.003
HYAL2	3.08	4.78	-1.87	0.000	0.000
PLCB3	3.64	5.52	-1.87	0.000	0.000
ADAM8	3.49	5.23	-1.87	0.000	0.003
IRAK3	7.10	8.98	-1.88	0.000	0.000
VAT1	5.71	7.57	-1.88	0.000	0.000
TOGARAM2	0.18	2.05	-1.89	0.000	0.006
KLHDC7B	0.00	1.87	-1.89	0.004	0.035
ANKRD6	1.75	3.52	-1.90	0.000	0.008
RAB3IP	2.24	4.41	-1.91	0.002	0.023
LDLR	3.69	5.26	-1.92	0.003	0.029
NT5DC3	4.97	6.82	-1.93	0.002	0.021
ABHD4	4.21	6.03	-1.93	0.000	0.004
B3GNT9	-0.50	1.54	-1.93	0.001	0.012
MELTF	1.45	3.17	-1.94	0.003	0.028
MICAL2	2.66	4.57	-1.96	0.002	0.018
DIXDC1	1.88	3.81	-1.97	0.000	0.006
KLHL35	-1.83	0.08	-1.97	0.006	0.043
NUDT14	-0.20	1.77	-1.97	0.002	0.024
SNX33	1.88	3.70	-1.97	0.000	0.005
TXNRD3	1.98	3.77	-1.98	0.007	0.049
GPR137B	0.47	2.36	-1.98	0.000	0.003
ARID5B	4.89	6.79	-1.98	0.000	0.000
BAALC	5.69	7.59	-2.00	0.002	0.018
C16orf74	1.32	3.15	-2.00	0.000	0.007
ZNF821	1.14	2.77	-2.00	0.006	0.045
RAC3	0.63	2.55	-2.01	0.002	0.018
IL6ST	5.15	7.05	-2.01	0.000	0.005
ARHGEF17	3.50	5.40	-2.02	0.000	0.007

EHD4	1.71	3.66	-2.03	0.001	0.015
WDR49	4.51	6.38	-2.03	0.001	0.012
RGS10	4.58	6.40	-2.03	0.003	0.029
GFI1	5.80	7.84	-2.03	0.000	0.000
HDAC4	4.18	6.19	-2.04	0.000	0.000
KIAA1522	1.64	3.56	-2.05	0.000	0.008
SH2B2	-0.60	1.25	-2.05	0.000	0.006
KIAA1549	3.57	5.66	-2.06	0.000	0.000
MCTP1	4.88	6.78	-2.06	0.000	0.002
HSBP1L1	1.26	3.36	-2.06	0.001	0.016
ZNF682	1.72	3.80	-2.06	0.001	0.011
AGPAT3	3.80	5.94	-2.06	0.002	0.019
B3GNT8	1.06	3.05	-2.06	0.002	0.024
MMP14	-0.90	0.95	-2.07	0.002	0.019
FLOT1	3.91	5.80	-2.07	0.000	0.002
GLB1L	1.25	3.26	-2.08	0.000	0.000
NRGN	0.40	2.35	-2.08	0.001	0.010
SAPCD2	1.20	3.36	-2.09	0.000	0.002
DNM1	3.60	5.35	-2.09	0.000	0.005
ECE1	1.24	3.55	-2.09	0.001	0.011
ARNTL2	2.91	5.15	-2.09	0.003	0.029
VAMP5	1.34	3.22	-2.10	0.000	0.003
IRS2	3.56	5.32	-2.10	0.004	0.032
PODXL2	2.99	4.74	-2.11	0.002	0.019
GALNT14	2.40	4.39	-2.12	0.004	0.033
SRGAP2B	0.76	2.69	-2.13	0.000	0.004
FSCN1	4.44	6.60	-2.13	0.002	0.021
SKI	3.03	5.08	-2.14	0.000	0.001
VANGL1	2.32	4.39	-2.14	0.002	0.024
SH3PXD2B	0.07	2.22	-2.14	0.006	0.043
SCD	2.23	4.20	-2.14	0.002	0.020
PRDM8	3.82	5.77	-2.15	0.000	0.001
TNFSF12	-1.43	0.33	-2.15	0.006	0.048
HOMER3	3.11	5.02	-2.16	0.000	0.002
H2AC17	0.07	2.25	-2.16	0.003	0.027
SH2D2A	-0.53	1.58	-2.16	0.001	0.014
VEGFA	4.13	6.10	-2.17	0.000	0.006
NHSL1	0.67	2.51	-2.18	0.000	0.005
IRAG1	-0.84	1.22	-2.18	0.007	0.048
TLR4	3.77	5.74	-2.19	0.003	0.026
MS4A14	0.18	2.31	-2.19	0.004	0.035
COL9A3	-0.71	1.29	-2.19	0.002	0.019

AGPAT4	4.00	6.33	-2.21	0.001	0.008
TBXA2R	1.18	3.38	-2.21	0.002	0.019
STAR	3.15	5.17	-2.21	0.000	0.000
LYST	6.04	8.14	-2.22	0.002	0.023
MLNR	-1.98	0.13	-2.22	0.007	0.049
MAPK7	1.67	3.66	-2.22	0.000	0.000
SH3PXD2A	3.98	6.03	-2.23	0.005	0.041
CAPN11	0.55	2.60	-2.23	0.004	0.036
CHRNE	0.16	2.32	-2.24	0.001	0.013
LRMDA	3.08	4.87	-2.24	0.001	0.014
MGAM	1.14	3.52	-2.24	0.000	0.008
OBSCN	3.54	6.04	-2.25	0.001	0.017
ROBO3	1.85	3.83	-2.25	0.002	0.020
ZHX3	3.27	5.55	-2.26	0.000	0.000
AATK	-0.49	1.74	-2.26	0.004	0.037
MCF2	-1.00	1.10	-2.26	0.003	0.029
H2BC14	3.49	5.82	-2.27	0.000	0.007
CCNB3	-1.92	0.12	-2.29	0.004	0.033
PAPLN	-2.43	-0.03	-2.29	0.005	0.040
TRAF3IP2	3.72	5.95	-2.29	0.000	0.000
GPR157	-0.91	1.42	-2.30	0.006	0.046
GRB10	4.40	6.76	-2.30	0.000	0.001
ENC1	2.51	4.52	-2.30	0.000	0.006
ADGRG3	1.12	3.11	-2.30	0.001	0.009
CARNS1	-0.95	1.67	-2.32	0.001	0.013
M1AP	0.97	3.18	-2.32	0.002	0.021
TPK1	3.49	5.56	-2.33	0.000	0.000
CD83	4.65	6.74	-2.33	0.005	0.038
EMP1	3.59	6.08	-2.34	0.001	0.016
ZNRF3	0.24	2.58	-2.34	0.002	0.023
SLC37A2	-0.95	1.66	-2.35	0.003	0.027
SLCO4A1	2.48	4.89	-2.36	0.000	0.001
C12orf42	0.98	3.19	-2.36	0.000	0.000
MYO1C	-0.61	1.71	-2.36	0.002	0.018
NBL1	2.05	4.44	-2.36	0.002	0.019
UNC5B	-1.66	0.78	-2.36	0.005	0.041
SPINDOC	1.89	4.14	-2.37	0.000	0.006
ULBP3	-2.52	-0.30	-2.38	0.004	0.034
TP53INP2	2.35	4.49	-2.39	0.000	0.001
PLAUR	2.55	4.64	-2.40	0.000	0.001
TMEM45A	-3.22	-0.94	-2.40	0.002	0.024
KCNK6	1.00	3.34	-2.40	0.003	0.029

SERPINH1	1.07	3.47	-2.40	0.004	0.033
SERPINI2	0.87	3.12	-2.40	0.001	0.009
PCDHGB5	-0.63	1.77	-2.41	0.002	0.020
ZNF474	-3.11	-0.75	-2.41	0.004	0.031
HSPG2	5.34	7.81	-2.42	0.000	0.000
FCGRT	3.30	5.45	-2.42	0.000	0.004
PAPSS2	0.02	2.47	-2.43	0.002	0.022
HRH1	-2.61	-0.49	-2.43	0.006	0.046
RAB36	-3.07	-0.75	-2.43	0.004	0.036
CYFIP1	4.52	6.92	-2.43	0.000	0.000
PDE1A	-3.55	-1.12	-2.44	0.006	0.047
KAZN	-2.48	0.00	-2.44	0.007	0.049
INKA2	1.44	3.71	-2.45	0.000	0.004
SFXN3	2.60	4.72	-2.45	0.001	0.012
EMILIN2	5.36	7.76	-2.45	0.000	0.003
BACE1	2.28	4.82	-2.46	0.002	0.023
UBTD1	-0.43	1.74	-2.46	0.001	0.017
KCTD7	1.42	4.22	-2.46	0.000	0.005
PTPRF	-1.64	0.81	-2.48	0.002	0.021
DYNC2H1	1.82	3.77	-2.48	0.002	0.020
MYO5C	2.77	5.43	-2.48	0.000	0.004
KCNH3	-3.12	-0.53	-2.49	0.004	0.034
MS4A4A	-0.83	1.45	-2.49	0.004	0.032
ABHD6	-0.64	1.70	-2.49	0.000	0.006
TUFT1	-1.35	0.98	-2.51	0.007	0.048
MPIG6B	-2.57	-0.17	-2.51	0.002	0.021
MMP15	-0.16	2.37	-2.52	0.001	0.014
SDC4	0.83	3.28	-2.53	0.000	0.007
TGFB1I1	0.23	2.41	-2.53	0.000	0.005
BAIAP2	1.22	3.56	-2.53	0.000	0.004
CROCC2	-3.81	-1.12	-2.53	0.003	0.030
TAS2R43	-1.48	1.26	-2.54	0.003	0.024
YBX3	6.27	8.91	-2.56	0.003	0.027
ANXA6	5.70	8.22	-2.56	0.001	0.016
PHLPP2	1.17	3.84	-2.56	0.000	0.000
SPOCK2	0.84	3.43	-2.58	0.001	0.013
ACVR2B	-0.98	1.67	-2.58	0.000	0.001
GAREM2	-1.85	0.79	-2.59	0.005	0.043
C1orf116	-2.66	-0.10	-2.59	0.001	0.009
TFEB	-0.05	2.22	-2.59	0.002	0.020
DLG4	2.23	4.67	-2.59	0.000	0.000
PLEKHG2	3.47	5.91	-2.61	0.000	0.000

MACROD2	-0.15	2.82	-2.61	0.003	0.031
CDHR4	-2.09	0.41	-2.62	0.001	0.014
ADCY6	0.97	3.66	-2.63	0.001	0.013
MUC12	-2.93	-0.57	-2.63	0.007	0.049
TCN2	1.20	3.69	-2.64	0.000	0.006
EDARADD	-3.12	-0.49	-2.65	0.000	0.007
TET1	3.05	5.57	-2.66	0.000	0.000
FBXL2	-1.06	1.52	-2.66	0.000	0.005
MPL	2.99	5.36	-2.67	0.001	0.011
MCF2L2	-0.28	2.23	-2.67	0.000	0.004
ACKR3	-0.42	2.45	-2.67	0.002	0.019
C2orf50	-2.65	-0.19	-2.68	0.001	0.013
RIMKLB	3.92	6.50	-2.68	0.004	0.035
SIGLEC9	-1.41	1.05	-2.68	0.002	0.019
LRP3	2.52	4.72	-2.69	0.003	0.026
NLRP1	3.19	5.70	-2.69	0.000	0.001
EGR2	-0.44	2.17	-2.69	0.002	0.019
BCAT1	4.72	7.80	-2.69	0.006	0.045
PTGR1	-0.11	2.86	-2.69	0.001	0.012
GCAT	1.10	3.51	-2.70	0.000	0.002
PTH1R	-3.37	-0.57	-2.70	0.006	0.043
MSLN	-2.47	0.22	-2.71	0.006	0.043
CLCF1	-1.25	1.45	-2.72	0.001	0.011
PLD2	-0.94	1.71	-2.72	0.000	0.002
PCDHGA12	-1.17	1.61	-2.72	0.001	0.013
CCDC40	-1.94	0.72	-2.74	0.001	0.015
ARG2	0.00	2.63	-2.74	0.000	0.003
CEBPE	-0.41	1.83	-2.74	0.002	0.019
MAP3K6	0.73	3.54	-2.74	0.000	0.000
TMEM200A	-3.99	-1.42	-2.74	0.001	0.013
IGFBP2	0.74	3.53	-2.75	0.003	0.031
DGKH	-0.18	2.79	-2.75	0.000	0.007
TYMP	0.98	3.42	-2.75	0.001	0.010
CEACAM19	-2.21	0.55	-2.76	0.003	0.027
MYLK	-2.52	0.36	-2.77	0.001	0.014
STXBP6	-2.94	-0.21	-2.78	0.002	0.022
DRAM1	3.73	6.42	-2.78	0.000	0.000
ATAD3C	-2.17	0.41	-2.78	0.000	0.004
LOXL1	-3.43	-0.62	-2.79	0.001	0.008
FOXP4	0.52	3.19	-2.79	0.000	0.001
NTRK1	0.78	3.65	-2.79	0.000	0.005
C3AR1	2.65	5.43	-2.79	0.000	0.008

SOCS2	2.60	5.38	-2.79	0.001	0.009
FKBP9	-2.02	1.00	-2.80	0.006	0.044
EGR1	5.44	8.23	-2.81	0.001	0.011
GDPD5	-0.32	2.41	-2.81	0.000	0.005
TCF7L2	2.27	4.49	-2.81	0.001	0.017
SORT1	-1.09	1.48	-2.81	0.005	0.042
SMCO2	-2.70	0.00	-2.82	0.001	0.012
SYNE3	5.41	8.19	-2.82	0.000	0.000
RGCC	3.97	6.56	-2.82	0.000	0.003
ARHGAP6	-2.84	-0.17	-2.82	0.006	0.047
SCGB2B2	-2.32	0.53	-2.82	0.000	0.005
PVR	1.71	4.46	-2.83	0.001	0.009
MYO10	-2.29	0.41	-2.83	0.002	0.024
C6orf132	-2.44	0.29	-2.83	0.001	0.014
ATG9B	-2.66	0.04	-2.83	0.001	0.017
MMP25	-2.06	0.36	-2.83	0.005	0.040
FGFR1	3.44	6.35	-2.84	0.000	0.002
COCH	1.21	4.07	-2.84	0.002	0.023
LAMB4	-2.13	0.40	-2.84	0.006	0.047
CORO6	0.18	2.88	-2.84	0.000	0.001
BLVRA	1.89	4.77	-2.85	0.002	0.024
RAB13	-2.00	0.76	-2.86	0.001	0.017
KCTD17	-1.92	0.91	-2.87	0.002	0.019
FCER1A	1.74	4.66	-2.87	0.002	0.024
CAMK1D	2.61	5.41	-2.88	0.000	0.002
EGR3	-0.82	1.87	-2.88	0.000	0.005
GAS2L1	-1.21	1.56	-2.89	0.003	0.026
BRSK1	-2.19	0.40	-2.90	0.001	0.013
FAM89A	-2.03	0.77	-2.91	0.002	0.019
ZNF697	-0.49	2.53	-2.91	0.000	0.005
ZNF311	-2.06	0.88	-2.92	0.001	0.012
ICAM5	-0.58	2.15	-2.92	0.000	0.007
DNAJB5	-2.73	0.31	-2.92	0.001	0.016
SLC2A9	0.32	2.82	-2.92	0.000	0.003
CD276	-3.06	-0.50	-2.93	0.001	0.016
CD4	1.00	3.74	-2.93	0.000	0.004
TRIM47	-0.09	2.77	-2.93	0.001	0.008
FCGR1B	-0.06	2.82	-2.93	0.001	0.014
GFOD1	3.03	5.85	-2.93	0.000	0.000
HSPB1	2.02	4.96	-2.93	0.000	0.000
SERPINB10	-0.40	2.07	-2.94	0.002	0.022
CD72	1.40	3.93	-2.94	0.000	0.001

PKN3	1.32	4.08	-2.95	0.000	0.006
UST	-2.87	0.08	-2.95	0.002	0.023
SLC35E4	-1.56	1.33	-2.95	0.000	0.005
ST6GALNAC2	-2.37	0.44	-2.96	0.001	0.014
PINLYP	-1.40	1.47	-2.96	0.002	0.024
MS4A4E	2.22	5.35	-2.97	0.000	0.007
PHYHD1	-1.54	1.64	-2.97	0.001	0.011
RHEX	4.06	7.01	-2.97	0.000	0.004
DBN1	2.43	5.40	-2.97	0.000	0.005
TUBA4A	-1.86	0.91	-2.98	0.003	0.028
P2RY2	0.61	3.43	-2.99	0.000	0.007
INA	-3.73	-0.52	-2.99	0.001	0.012
SLC2A5	3.51	6.33	-2.99	0.000	0.000
STX2	2.42	5.23	-3.00	0.000	0.000
NRCAM	-0.91	1.78	-3.00	0.003	0.030
AGAP1	-3.24	0.11	-3.00	0.001	0.017
KCNE1	-2.11	0.53	-3.01	0.001	0.016
LRG1	-0.72	2.15	-3.02	0.000	0.004
NR4A3	0.25	2.97	-3.05	0.002	0.019
SLC22A4	1.54	4.14	-3.06	0.000	0.001
RAB44	4.02	6.80	-3.06	0.001	0.012
CFAP20DC	-1.82	1.26	-3.06	0.006	0.044
PSCA	-3.32	-0.30	-3.07	0.002	0.023
CAPN2	3.11	6.09	-3.07	0.001	0.010
SEMA3F	-2.21	0.80	-3.08	0.002	0.019
CACNB4	0.67	3.84	-3.08	0.002	0.020
MTMR11	-2.81	0.14	-3.09	0.001	0.017
CHD7	1.84	4.81	-3.09	0.002	0.020
LRATD2	1.14	4.29	-3.09	0.000	0.001
IL1R1	-1.96	0.79	-3.10	0.001	0.013
FAM43A	-0.59	1.97	-3.10	0.002	0.023
SLC29A4	-3.00	0.08	-3.11	0.002	0.020
CASKIN2	-1.60	1.71	-3.12	0.001	0.012
ZNF112	-2.46	0.79	-3.12	0.001	0.010
TRIB3	0.59	3.71	-3.15	0.000	0.000
DTX1	-3.40	-0.41	-3.15	0.001	0.010
RASSF8	-0.37	2.64	-3.16	0.001	0.009
PTPRJ	1.68	4.55	-3.16	0.000	0.001
C17orf107	-0.38	2.55	-3.17	0.000	0.004
FAM221A	-0.29	3.02	-3.18	0.000	0.000
DDAH1	-0.76	2.04	-3.18	0.006	0.047
SEMA3D	-2.94	0.38	-3.18	0.001	0.009

EFCC1	-2.65	0.31	-3.18	0.000	0.006
PTGDR2	0.63	3.44	-3.18	0.000	0.002
SGPP1	0.97	4.39	-3.18	0.000	0.008
PLEKHB1	-2.66	0.42	-3.19	0.000	0.004
CRISPLD2	0.17	3.38	-3.19	0.002	0.020
SCN1B	-0.44	2.46	-3.19	0.000	0.001
RCOR2	-2.81	0.30	-3.19	0.001	0.015
ELN	-3.04	0.09	-3.20	0.003	0.026
STON2	4.49	7.63	-3.20	0.001	0.012
CYP46A1	-3.81	-0.53	-3.21	0.002	0.019
CCDC50	2.66	5.66	-3.21	0.000	0.006
MOXD1	-3.07	0.30	-3.21	0.000	0.004
SULT1C4	-0.60	2.64	-3.22	0.001	0.009
AEBP1	1.67	4.95	-3.22	0.001	0.015
ABI2	1.76	5.13	-3.23	0.000	0.003
CD8B	-2.83	0.26	-3.23	0.000	0.004
MIXL1	-3.73	-0.47	-3.25	0.000	0.007
MS4A3	1.90	5.08	-3.26	0.000	0.000
SLC2A6	0.42	3.73	-3.26	0.001	0.012
PTP4A3	0.37	3.42	-3.27	0.006	0.048
SLC35G1	-2.34	0.78	-3.28	0.002	0.023
PDGFC	3.72	6.68	-3.29	0.004	0.033
LRRC2	-3.18	-0.16	-3.29	0.001	0.010
ABCC6	-3.20	0.14	-3.30	0.000	0.002
NPDC1	-1.62	2.05	-3.30	0.004	0.031
ADGRB1	-1.60	1.99	-3.30	0.001	0.013
SAMD11	-2.75	0.82	-3.31	0.005	0.040
CORO2A	2.16	4.89	-3.31	0.000	0.005
FAM124B	2.44	5.41	-3.32	0.003	0.028
CKB	0.86	4.35	-3.32	0.001	0.011
SLC11A1	0.19	3.01	-3.33	0.001	0.010
ADPRHL1	-0.22	3.03	-3.33	0.000	0.001
GSTM3	-0.63	2.84	-3.34	0.001	0.009
MEIS2	-2.43	0.65	-3.34	0.001	0.011
RASL10A	-1.47	1.51	-3.35	0.000	0.006
GRIP1	-1.60	1.90	-3.35	0.000	0.004
MDK	0.96	4.24	-3.35	0.000	0.000
ATN1	0.70	4.21	-3.35	0.000	0.000
TRPV3	-2.82	0.77	-3.35	0.001	0.011
ANXA2	4.76	7.94	-3.36	0.000	0.007
ADGRD2	-3.15	0.22	-3.37	0.001	0.014
DENND2B	-2.90	0.27	-3.38	0.000	0.003

HMCN1	-2.78	0.83	-3.39	0.000	0.003
GBP2	3.58	6.71	-3.39	0.000	0.003
KRT1	-3.81	-0.56	-3.39	0.006	0.044
AQP6	-2.65	0.51	-3.40	0.000	0.004
SMARCD3	-2.79	0.48	-3.40	0.001	0.014
TM6SF1	0.46	3.59	-3.40	0.000	0.001
S100A16	-3.38	0.25	-3.40	0.005	0.039
DAGLA	-2.64	0.82	-3.41	0.001	0.016
AFAP1	0.04	3.19	-3.41	0.003	0.027
CTNNA1	4.24	7.53	-3.41	0.000	0.000
EPS8L1	-2.45	0.83	-3.41	0.000	0.004
SYNE2	1.21	4.72	-3.43	0.000	0.003
ABCB4	-2.31	1.00	-3.44	0.000	0.006
SLC7A8	-3.42	0.01	-3.44	0.000	0.005
TBL1X	2.54	5.78	-3.45	0.000	0.000
CACNB3	-1.66	1.79	-3.46	0.000	0.001
TTLL9	-2.13	1.19	-3.47	0.000	0.004
SLC5A5	-3.11	0.06	-3.47	0.000	0.003
NEURL1B	3.19	6.43	-3.47	0.000	0.002
HCAR3	-0.54	2.21	-3.48	0.002	0.021
PTPRN2	0.87	3.86	-3.48	0.000	0.001
ZNF536	-3.81	-0.46	-3.48	0.000	0.006
PROCR	-2.17	1.13	-3.48	0.000	0.004
EBF1	-2.29	1.05	-3.48	0.002	0.023
KRT18	-2.96	0.90	-3.49	0.005	0.042
IL17RB	-3.12	0.36	-3.49	0.002	0.023
AGXT	-3.99	-0.06	-3.50	0.004	0.032
MPP3	-2.86	0.93	-3.50	0.002	0.023
PHETA2	-1.86	1.37	-3.50	0.000	0.007
ZCCHC14	-0.20	3.22	-3.50	0.000	0.006
ISG20	1.39	4.94	-3.50	0.000	0.000
LONRF3	-0.92	2.45	-3.51	0.000	0.003
PRXL2A	-1.33	1.99	-3.51	0.006	0.044
BTBD19	0.44	3.64	-3.51	0.000	0.000
SIX5	-3.32	0.33	-3.51	0.000	0.001
CCDC8	-3.04	0.76	-3.51	0.006	0.043
WWC3	1.74	5.41	-3.52	0.000	0.006
NTNG2	3.04	6.43	-3.52	0.000	0.000
TEAD4	-3.46	0.28	-3.53	0.002	0.020
ADCYAP1	-3.81	-0.10	-3.53	0.002	0.020
PTPN14	1.28	5.20	-3.53	0.004	0.032
IL4R	1.91	5.16	-3.53	0.000	0.000

ZDHHC11B	-2.20	1.16	-3.53	0.000	0.007
RGS9	-2.38	1.19	-3.53	0.001	0.009
MEAK7	-0.09	3.18	-3.54	0.000	0.002
C5AR2	-0.61	2.59	-3.54	0.000	0.007
CCL3L3	-0.35	2.69	-3.55	0.006	0.044
KLRG2	-0.97	2.40	-3.55	0.000	0.002
VENTX	-1.49	1.69	-3.56	0.004	0.036
SIGLEC6	1.30	4.99	-3.58	0.000	0.000
GLIS3	0.59	3.80	-3.58	0.000	0.001
STYK1	-1.50	2.16	-3.58	0.000	0.003
COL27A1	-1.97	1.64	-3.59	0.003	0.024
S100A10	2.81	6.39	-3.59	0.001	0.014
ECM1	-0.58	2.95	-3.59	0.000	0.001
USP2	-2.69	0.79	-3.59	0.000	0.003
LHX6	-1.09	2.44	-3.60	0.000	0.004
C11orf45	-1.11	2.25	-3.60	0.000	0.004
AADAT	-1.68	1.99	-3.60	0.000	0.006
SLC45A3	3.66	7.13	-3.61	0.000	0.000
LOX	-3.73	0.07	-3.61	0.003	0.029
BMP6	-2.34	1.14	-3.62	0.001	0.013
FIBCD1	-3.73	0.00	-3.63	0.002	0.020
ABHD17C	0.55	4.40	-3.63	0.000	0.007
AR	-2.48	1.02	-3.64	0.001	0.013
SH3RF3	-1.13	2.27	-3.64	0.000	0.008
PBX4	-1.16	2.02	-3.66	0.000	0.003
MMP28	-0.76	2.92	-3.66	0.000	0.002
MCAM	-0.78	2.91	-3.66	0.000	0.002
F3	-3.73	-0.04	-3.66	0.000	0.005
VASN	-2.54	0.88	-3.68	0.000	0.001
SPINK4	-3.06	0.22	-3.68	0.003	0.029
PLCD3	-0.19	3.33	-3.68	0.000	0.000
TRIB1	4.02	7.27	-3.69	0.000	0.001
TDRD10	-3.81	0.25	-3.69	0.002	0.024
DNAH17	-3.29	0.56	-3.70	0.000	0.001
ATP9A	-0.27	3.50	-3.70	0.000	0.002
SLC2A3	4.81	8.30	-3.70	0.000	0.001
SLC2A8	-2.18	1.69	-3.70	0.000	0.006
EXT1	-2.79	0.87	-3.73	0.000	0.004
LPAR5	-0.04	3.61	-3.73	0.000	0.005
LAMA3	-1.03	2.79	-3.74	0.000	0.002
EHD2	-3.19	0.69	-3.76	0.001	0.017
VIPR1	-2.86	0.89	-3.76	0.000	0.001

SERPINE2	1.10	4.69	-3.78	0.000	0.006
TTC28	2.54	6.35	-3.79	0.000	0.000
DDR1	-1.88	2.12	-3.82	0.002	0.023
HCAR1	-2.46	1.14	-3.82	0.002	0.018
EBI3	-3.15	0.66	-3.83	0.000	0.005
LAMC3	-1.90	2.34	-3.83	0.001	0.008
GALNT18	-3.73	0.77	-3.83	0.006	0.046
DLG3	-2.73	1.08	-3.83	0.000	0.002
CPAMD8	-2.85	1.00	-3.88	0.000	0.007
B9D1	-2.39	1.57	-3.88	0.000	0.001
SOX15	-3.46	0.29	-3.90	0.000	0.000
SLC9A3R2	-0.53	3.26	-3.90	0.000	0.003
PLAAT3	-3.32	0.62	-3.91	0.000	0.001
COL6A3	-0.89	3.03	-3.93	0.000	0.007
CAV2	-1.60	2.36	-3.93	0.000	0.001
RHOC	0.20	4.04	-3.94	0.000	0.000
NCALD	0.60	4.84	-3.94	0.000	0.003
HCAR2	-0.86	2.58	-3.95	0.000	0.004
CD24	-1.19	2.47	-3.95	0.002	0.021
ZSCAN23	-2.53	1.36	-3.95	0.001	0.009
OSBPL1A	1.53	5.64	-3.96	0.002	0.020
PDE4A	-2.31	1.61	-3.97	0.000	0.001
RRAS	-1.34	2.47	-3.98	0.000	0.000
ACP6	-0.19	3.83	-3.99	0.000	0.002
IER3	0.67	4.03	-3.99	0.005	0.040
AFAP1L1	-1.78	2.28	-4.00	0.000	0.000
PGPEP1L	-3.29	0.69	-4.00	0.000	0.000
PALM	2.14	6.01	-4.00	0.000	0.000
FOXO1	0.74	5.03	-4.00	0.000	0.001
RD3	-2.86	0.95	-4.00	0.000	0.005
NR6A1	0.58	4.44	-4.01	0.000	0.000
F13A1	3.40	6.71	-4.01	0.004	0.031
LTBP4	0.05	3.93	-4.02	0.003	0.027
PMEPA1	-2.93	0.79	-4.02	0.001	0.011
PAX5	1.46	5.17	-4.03	0.000	0.004
GPR153	-1.38	2.73	-4.03	0.001	0.009
CCN2	-3.12	1.06	-4.06	0.000	0.006
SETD7	2.03	6.25	-4.06	0.000	0.000
COL6A2	-2.81	1.06	-4.07	0.000	0.006
SGMS2	-0.17	3.67	-4.07	0.001	0.014
NID1	-1.57	2.81	-4.08	0.002	0.024
TNS3	1.08	4.56	-4.08	0.001	0.011

AXL	-2.23	1.77	-4.08	0.000	0.005
ALPK3	-0.01	3.63	-4.09	0.000	0.007
CD52	2.33	6.57	-4.12	0.000	0.004
TNFSF9	-0.62	3.13	-4.12	0.000	0.005
VWDE	-2.25	1.81	-4.13	0.003	0.028
HS3ST4	-3.99	0.22	-4.13	0.007	0.048
RAB6B	-1.30	3.28	-4.13	0.005	0.040
PHLDB1	-2.71	1.50	-4.13	0.000	0.000
MNDA	2.35	5.98	-4.14	0.000	0.003
FHL1	1.10	5.27	-4.14	0.000	0.000
CERS4	0.00	4.28	-4.14	0.001	0.012
UBXN10	-2.25	1.84	-4.15	0.001	0.011
SSC5D	-2.32	1.81	-4.15	0.000	0.000
ACVRL1	-3.38	0.51	-4.16	0.000	0.002
PSD3	3.02	6.81	-4.16	0.000	0.000
VNN1	-1.81	2.27	-4.19	0.002	0.020
ICA1	0.83	5.20	-4.20	0.000	0.000
ITGA3	-2.93	1.61	-4.21	0.000	0.001
DLGAP3	-1.82	2.27	-4.22	0.000	0.000
TRIM32	-1.45	2.58	-4.22	0.000	0.005
CLC	-0.87	2.90	-4.22	0.001	0.016
CACNA1H	-1.78	2.47	-4.23	0.000	0.005
BEST1	-1.33	2.32	-4.23	0.000	0.001
PTPRG	-2.79	1.75	-4.24	0.000	0.006
CPA3	2.56	6.58	-4.24	0.000	0.006
TREM1	1.11	4.92	-4.24	0.000	0.000
KALRN	-2.55	1.57	-4.25	0.000	0.002
TP53I11	-0.99	2.68	-4.25	0.005	0.039
ROBO4	-0.56	3.47	-4.27	0.000	0.001
TKTL1	-3.81	0.36	-4.27	0.000	0.005
CTTNBP2NL	-2.07	2.01	-4.28	0.003	0.028
TSPAN9	-2.96	1.44	-4.28	0.000	0.002
SLC2A7	-3.81	0.44	-4.28	0.000	0.003
ASIC1	-3.63	0.51	-4.30	0.000	0.004
STARD8	-0.23	3.77	-4.32	0.000	0.001
CPNE7	0.38	4.89	-4.33	0.000	0.004
PTX3	2.01	5.98	-4.33	0.000	0.002
CDKN1A	2.33	6.15	-4.34	0.000	0.000
CTDSPL	-0.72	3.77	-4.34	0.000	0.003
PTK2	-2.02	2.14	-4.34	0.000	0.002
ITGB4	0.77	5.00	-4.36	0.000	0.000
EPCAM	0.00	4.60	-4.36	0.001	0.011

AIF1L	0.26	5.01	-4.37	0.000	0.005
LOXHD1	-1.70	2.62	-4.37	0.002	0.020
ALOX12	-3.55	1.08	-4.38	0.002	0.023
MYOF	-1.42	3.17	-4.38	0.005	0.038
S100P	-0.70	3.39	-4.39	0.000	0.000
GPC1	-3.81	0.77	-4.39	0.000	0.003
LDLRAD3	-1.65	2.61	-4.42	0.000	0.003
HIF3A	-3.73	0.67	-4.42	0.003	0.028
IRX1	-3.81	1.17	-4.43	0.002	0.024
LARGE2	-3.55	0.40	-4.43	0.000	0.003
SPRED2	-0.74	3.48	-4.43	0.000	0.001
MAB21L4	-3.99	0.51	-4.44	0.000	0.004
CLEC4D	-3.81	0.92	-4.45	0.001	0.017
ENTPD1	-0.16	4.03	-4.46	0.000	0.000
FUT1	-2.20	2.28	-4.48	0.000	0.005
GRAMD1B	-0.06	4.39	-4.48	0.000	0.001
SUCLG2	-1.24	3.36	-4.50	0.000	0.004
IL2RA	-0.82	3.45	-4.51	0.000	0.000
MYL9	-3.11	1.38	-4.53	0.000	0.000
HAL	2.03	5.99	-4.53	0.000	0.000
SAMD3	-3.32	0.68	-4.54	0.000	0.005
PEAR1	-1.52	3.07	-4.54	0.000	0.000
SIPA1L2	3.99	8.18	-4.54	0.000	0.000
CRIP2	-1.29	3.14	-4.55	0.001	0.008
CCN3	-1.16	3.21	-4.56	0.000	0.000
CYSLTR2	1.43	6.00	-4.57	0.000	0.000
CAV1	-0.01	4.55	-4.58	0.007	0.049
MBOAT2	0.86	5.26	-4.61	0.000	0.003
LPIN3	-3.99	0.70	-4.63	0.000	0.000
TMIE	-3.32	1.19	-4.63	0.000	0.001
SMAD6	-1.52	2.69	-4.64	0.000	0.001
ASAP2	-1.45	2.80	-4.64	0.000	0.006
BAIAP3	-0.17	4.38	-4.70	0.000	0.005
MTSS1	1.85	6.81	-4.73	0.000	0.002
EVPL	0.63	4.93	-4.73	0.000	0.001
DNTT	-1.24	3.75	-4.74	0.001	0.012
DLGAP2	-1.83	3.37	-4.76	0.003	0.025
CCND1	-2.70	2.57	-4.76	0.001	0.008
PRKCA	-0.95	3.76	-4.80	0.001	0.012
FAM166B	-2.94	1.56	-4.80	0.000	0.001
PTGIR	-0.86	3.79	-4.81	0.000	0.000
MARVELD1	0.56	5.39	-4.81	0.000	0.000

SLC28A3	-2.33	2.36	-4.82	0.002	0.019
SHANK1	-0.02	4.66	-4.84	0.000	0.001
ALOX5	-0.05	4.70	-4.86	0.000	0.000
SLC37A3	-1.44	3.46	-4.86	0.000	0.000
NDFIP1	1.68	6.48	-4.88	0.000	0.000
TSPAN15	-3.03	1.52	-4.89	0.000	0.000
FAM171A1	-2.74	2.16	-4.90	0.002	0.018
TRIM71	1.57	5.69	-4.91	0.001	0.012
KIF16B	-0.60	4.19	-4.91	0.000	0.002
ADRA2A	-2.87	1.91	-4.99	0.000	0.000
GPR162	-1.44	3.29	-4.99	0.000	0.000
IL5RA	1.92	6.75	-4.99	0.000	0.000
TPPP3	-0.49	4.47	-5.00	0.000	0.005
GRK5	-0.38	4.41	-5.00	0.000	0.000
ADAMTS7	-3.29	1.61	-5.01	0.000	0.000
KLF9	0.93	5.74	-5.02	0.000	0.000
MAP3K20	1.11	6.15	-5.03	0.000	0.000
ADAMTSL4	1.23	6.00	-5.04	0.000	0.000
PTPRH	-3.01	2.05	-5.04	0.000	0.000
INPP5J	-3.42	1.62	-5.06	0.000	0.003
OLFML2A	-2.81	2.48	-5.07	0.000	0.007
MFAP4	-1.06	3.68	-5.09	0.000	0.002
IL1RL1	-0.05	4.54	-5.10	0.000	0.005
TSKS	-3.43	1.58	-5.14	0.000	0.000
H1-0	1.75	6.59	-5.15	0.000	0.001
KRT17	-3.81	1.60	-5.19	0.000	0.000
TAMALIN	0.14	5.09	-5.20	0.000	0.000
PCSK6	-3.25	2.04	-5.20	0.000	0.005
IGSF10	1.50	6.26	-5.22	0.006	0.045
CD19	-0.26	4.66	-5.23	0.000	0.001
SLC16A1	0.82	6.05	-5.24	0.000	0.000
ITGAV	0.76	5.24	-5.24	0.001	0.014
GNPDA1	0.42	5.56	-5.27	0.000	0.000
NRP2	-1.05	3.79	-5.28	0.000	0.000
PLPPR3	-0.25	4.99	-5.28	0.000	0.000
CD40	-2.02	3.25	-5.30	0.000	0.000
ARAP3	-2.39	2.59	-5.30	0.000	0.001
EPB41L2	1.01	6.26	-5.31	0.000	0.001
CACNA2D2	-0.72	4.35	-5.32	0.000	0.004
DPEP1	-3.99	1.37	-5.33	0.000	0.002
SHE	-3.24	2.67	-5.35	0.001	0.009
CFD	1.93	6.82	-5.36	0.000	0.002

DCHS1	-0.84	4.53	-5.36	0.000	0.007
TUBB6	1.70	7.20	-5.37	0.000	0.000
CD226	-0.70	4.34	-5.38	0.000	0.000
TRO	-2.10	2.92	-5.39	0.000	0.001
PLCG1	1.17	6.60	-5.41	0.000	0.000
FLT4	-1.36	4.25	-5.43	0.000	0.000
RBFOX3	-3.81	1.64	-5.43	0.000	0.000
RUSC2	-0.27	4.85	-5.47	0.000	0.000
PLXNB3	-3.28	1.91	-5.47	0.000	0.001
DACH1	-3.60	2.20	-5.50	0.000	0.004
MEX3A	-2.19	3.55	-5.51	0.000	0.000
PDE2A	-2.85	2.72	-5.52	0.000	0.003
UNC13B	-1.21	4.43	-5.59	0.000	0.001
RBPMS	-3.24	2.77	-5.61	0.001	0.011
ADGRA2	-0.87	4.74	-5.61	0.001	0.011
FBN2	-0.01	5.25	-5.62	0.001	0.012
DLL3	-3.67	1.48	-5.63	0.000	0.001
CLEC4E	-3.22	2.49	-5.63	0.000	0.002
PPL	-3.46	2.59	-5.65	0.000	0.006
FBLN2	-2.07	3.65	-5.72	0.000	0.002
NAALADL1	-2.68	3.02	-5.77	0.000	0.000
C2orf66	-3.99	1.46	-5.81	0.000	0.001
AZU1	1.12	6.58	-5.82	0.000	0.001
DOCK6	-1.67	3.79	-5.87	0.000	0.000
MMP19	-2.41	3.07	-5.87	0.000	0.000
ARC	-2.49	3.06	-5.89	0.000	0.001
ZNF90	-3.05	2.69	-5.97	0.000	0.000
BCL6B	-2.20	3.26	-6.02	0.000	0.000
TPSD1	-1.97	3.64	-6.07	0.001	0.010
TCN1	-2.75	3.60	-6.29	0.000	0.000
MYRF	-1.35	4.93	-6.32	0.000	0.001
GPM6B	-2.88	2.99	-6.32	0.004	0.037
TLCD5	-3.81	2.43	-6.33	0.000	0.000
BCL9	-1.36	4.79	-6.33	0.000	0.000
SLC52A3	-3.99	2.52	-6.35	0.000	0.000
TPO	-3.99	2.60	-6.37	0.000	0.000
NAV1	-0.39	6.11	-6.38	0.000	0.000
THBS1	-0.64	4.76	-6.39	0.002	0.021
KIRREL1	-3.36	3.45	-6.41	0.000	0.000
RNF217	-1.54	4.76	-6.46	0.000	0.001
SLC18A2	-1.55	5.03	-6.57	0.000	0.000
SLCO5A1	-0.61	6.07	-6.59	0.000	0.001

ALS2CL	-1.11	5.26	-6.61	0.000	0.000
ZNF521	-2.01	4.15	-6.63	0.000	0.007
AFDN	-1.06	5.46	-6.67	0.000	0.000
RASAL1	-3.06	3.40	-6.77	0.000	0.000
TINAGL1	-3.40	3.29	-6.80	0.000	0.000
FAM171B	-2.79	3.48	-6.81	0.000	0.001
RAB34	-0.68	6.19	-6.95	0.000	0.000
HDX	-3.99	2.67	-6.96	0.000	0.000
DOC2B	-3.63	3.00	-6.98	0.000	0.000
EVC2	-2.42	4.23	-7.05	0.000	0.000
LAMB2	-1.83	5.28	-7.16	0.000	0.002
ESAM	-1.85	5.23	-7.31	0.000	0.000
EPN2	-3.28	3.86	-7.33	0.000	0.000
PRTN3	-1.55	6.10	-7.83	0.000	0.002
ARHGEF12	-0.44	7.32	-7.86	0.000	0.000
ELANE	-0.63	6.92	-7.89	0.000	0.001
EVC	-3.09	4.61	-7.93	0.000	0.000
DNAH8	-3.24	4.66	-8.15	0.000	0.001
SLC24A3	-1.77	6.08	-8.25	0.000	0.000
RUNX1T1	-2.93	8.12	-11.06	0.000	0.000

Supplementary table 3: DEG in t(8;21) AML compared to PBSCs.

hgnc_symbol	t821_log2CPM_avg	PBSC_log2CPM_avg	log2FC	P.Value	adj.P.Val
RUNX1T1	8.13	-0.16	8.23	0.000	0.000
S100P	3.39	-3.27	6.83	0.001	0.019
SIGLEC6	5.00	-0.71	5.80	0.000	0.005
SIPA1L2	8.19	2.36	5.78	0.002	0.030
C12orf42	3.20	-2.48	5.73	0.000	0.008
TPO	2.61	-3.27	5.62	0.001	0.018
PTPRN2	3.87	-1.32	5.26	0.003	0.034
RBFOX3	1.65	-3.27	4.84	0.001	0.011
IL5RA	6.75	2.11	4.75	0.003	0.033
SLC24A3	6.09	1.55	4.61	0.002	0.022
PDE3B	7.36	2.96	4.43	0.000	0.000
EPN2	3.87	-0.28	4.20	0.000	0.002
CD96	8.50	4.38	4.05	0.002	0.029
MPO	13.32	9.40	3.93	0.000	0.000
LPIN3	0.70	-3.27	3.88	0.002	0.030
STAR	5.17	1.32	3.77	0.003	0.036
PLIN2	8.32	4.68	3.64	0.000	0.009
BTBD19	3.65	0.27	3.52	0.003	0.033
RHOB	8.63	5.26	3.33	0.001	0.013
PLK3	6.28	2.96	3.29	0.002	0.024
TLR2	7.85	4.74	3.11	0.000	0.005
PER1	7.59	4.52	3.06	0.003	0.035
GNPDA1	5.57	2.53	3.02	0.003	0.035
TINAGL1	3.30	0.37	2.98	0.003	0.035
PALM2AKAP2	8.15	5.28	2.88	0.000	0.000
TSC22D3	9.58	6.69	2.87	0.000	0.004
HYAL2	4.79	2.15	2.75	0.002	0.028
FAM107B	6.65	4.08	2.63	0.000	0.000
PLCG1	6.60	3.98	2.62	0.000	0.009
CD69	10.18	7.56	2.62	0.005	0.048
SLC31A2	5.43	3.00	2.49	0.003	0.034
COTL1	7.13	4.69	2.46	0.001	0.014
ZG16B	3.71	1.42	2.30	0.004	0.043
ARHGEF12	7.32	5.07	2.27	0.001	0.019
PDK1	7.66	5.43	2.24	0.004	0.044
FNDC3B	9.28	7.05	2.23	0.000	0.001
FLT3	9.41	7.17	2.23	0.002	0.023
LILRA2	5.33	3.26	2.15	0.003	0.038
PTGER2	6.58	4.44	2.15	0.000	0.006

HAVCR2	6.17	4.17	2.01	0.003	0.036
SMAP2	7.79	5.82	1.98	0.001	0.019
RELL1	7.30	5.33	1.95	0.002	0.026
TUBA1A	9.07	7.11	1.95	0.000	0.005
SDE2	7.50	5.56	1.94	0.005	0.048
PDLIM1	7.43	5.49	1.94	0.001	0.014
SFMBT2	6.72	4.80	1.91	0.003	0.036
KLF6	10.14	8.23	1.91	0.003	0.032
GFI1	7.84	5.93	1.89	0.003	0.035
RRP12	7.42	5.53	1.88	0.003	0.032
TFB2M	5.76	3.89	1.81	0.001	0.016
DBI	6.75	4.96	1.81	0.001	0.017
CALR	10.54	8.74	1.80	0.000	0.001
PGAM1	6.48	4.73	1.77	0.000	0.001
HK2	7.43	5.70	1.75	0.000	0.002
DDX21	8.76	7.02	1.74	0.000	0.000
GAS7	7.65	5.92	1.73	0.001	0.011
KIAA1958	5.97	4.30	1.72	0.003	0.037
MED17	6.50	4.84	1.66	0.004	0.043
GLUL	10.05	8.40	1.64	0.001	0.021
CD99	9.24	7.60	1.63	0.001	0.022
LSM14B	6.49	4.86	1.63	0.000	0.003
EDEM1	8.18	6.56	1.62	0.000	0.004
MAPRE1	7.88	6.26	1.62	0.000	0.007
MXI1	5.83	4.22	1.62	0.002	0.026
PLD1	7.22	5.64	1.58	0.000	0.005
KPNA2	7.25	5.65	1.57	0.003	0.038
ARL4A	6.66	5.08	1.55	0.003	0.038
AKIRIN1	6.74	5.18	1.55	0.001	0.019
PDCL3	4.50	3.01	1.53	0.004	0.045
ETF1	8.17	6.64	1.53	0.002	0.025
APLP2	9.43	7.91	1.52	0.001	0.017
AGTPBP1	7.93	6.41	1.52	0.001	0.011
DNAJB11	6.44	4.89	1.51	0.002	0.028
FUT4	6.99	5.49	1.51	0.002	0.031
RNH1	6.75	5.25	1.49	0.002	0.028
HSP90B1	9.60	8.16	1.45	0.003	0.036
GPX1	7.99	6.54	1.44	0.003	0.037
GTPBP4	6.99	5.57	1.43	0.000	0.001
CMTM3	6.72	5.31	1.42	0.000	0.010
TUBA1B	9.60	8.19	1.41	0.000	0.007
PXK	7.68	6.28	1.41	0.003	0.034

ATP11A	6.64	5.23	1.40	0.002	0.027
DAD1	6.86	5.48	1.38	0.002	0.025
WARS1	6.74	5.38	1.38	0.005	0.050
SCCPDH	7.81	6.44	1.38	0.004	0.040
DNAJC14	5.83	4.50	1.38	0.001	0.021
MAP3K1	8.59	7.21	1.37	0.005	0.050
CMTM6	7.96	6.60	1.37	0.001	0.010
YBX1	9.55	8.20	1.36	0.000	0.001
POLE4	3.70	2.37	1.34	0.002	0.026
UBE2J1	8.08	6.74	1.34	0.005	0.047
GPI	8.12	6.80	1.32	0.001	0.020
UBE2G1	6.68	5.38	1.30	0.000	0.003
NIP7	5.27	3.96	1.30	0.001	0.019
ATP6V0B	6.72	5.41	1.30	0.001	0.020
EIF5	9.51	8.22	1.30	0.003	0.035
PTMA	10.64	9.36	1.29	0.000	0.001
ARHGAP19	5.11	3.79	1.27	0.004	0.040
HSPA8	10.98	9.71	1.27	0.002	0.029
ARF4	6.79	5.54	1.27	0.001	0.012
MAN2B1	7.18	5.92	1.26	0.001	0.018
VAT1	7.57	6.31	1.26	0.004	0.045
F11R	6.85	5.62	1.24	0.003	0.037
NDEL1	6.57	5.34	1.22	0.005	0.046
CDC42	9.59	8.37	1.22	0.001	0.017
SSH2	8.14	6.93	1.22	0.004	0.045
CTSA	7.42	6.21	1.22	0.002	0.023
BZW1	8.36	7.15	1.21	0.001	0.015
SLC38A2	9.50	8.29	1.21	0.003	0.038
PDIA3	8.33	7.14	1.20	0.003	0.034
DGKD	6.97	5.77	1.20	0.000	0.007
IQGAP1	9.05	7.86	1.19	0.005	0.048
DPH3	5.01	3.87	1.18	0.003	0.035
CDC123	6.69	5.51	1.17	0.000	0.001
P4HB	8.64	7.48	1.16	0.000	0.004
TBC1D1	7.89	6.73	1.16	0.002	0.028
ARF1	8.25	7.10	1.15	0.001	0.017
UBE2M	5.06	3.97	1.15	0.003	0.036
TUBA1C	6.82	5.67	1.15	0.001	0.019
UQCRFS1	6.59	5.43	1.14	0.004	0.042
SH3KBP1	6.89	5.75	1.13	0.001	0.010
RPL6	10.72	9.59	1.13	0.003	0.034
CTSC	7.96	6.84	1.12	0.002	0.023

PGD	8.23	7.13	1.10	0.003	0.037
EIF2A	8.03	6.94	1.09	0.001	0.021
C1QBP	7.34	6.25	1.09	0.002	0.028
GALNT1	8.15	7.07	1.08	0.000	0.003
CALU	6.76	5.69	1.08	0.001	0.016
DNTTIP2	6.98	5.90	1.07	0.002	0.027
TPM3	9.91	8.84	1.07	0.001	0.015
EIF5A	8.08	7.01	1.07	0.002	0.030
RAD23B	7.61	6.55	1.06	0.002	0.031
PSMB7	6.72	5.67	1.06	0.001	0.012
TARS1	7.82	6.77	1.06	0.000	0.006
HSPA9	8.63	7.58	1.06	0.001	0.011
LRRC59	7.06	5.99	1.05	0.000	0.006
VDAC2	7.36	6.32	1.05	0.001	0.011
NECAP2	6.43	5.40	1.04	0.002	0.024
ALAS1	5.90	4.88	1.04	0.005	0.049
GAPDH	11.50	10.46	1.04	0.000	0.007
GNPTAB	8.61	7.58	1.04	0.001	0.019
GM2A	6.57	5.53	1.03	0.001	0.015
C1orf43	7.37	6.35	1.03	0.001	0.012
CDV3	8.39	7.36	1.03	0.000	0.006
C16orf54	7.10	6.09	1.03	0.003	0.032
UBE2A	6.62	5.57	1.03	0.002	0.022
HYOU1	6.96	5.94	1.03	0.003	0.033
PYGB	6.35	5.34	1.03	0.005	0.048
ZCCHC7	6.77	5.75	1.02	0.001	0.016
CCT2	8.52	7.51	1.01	0.001	0.011
EIF3A	9.36	8.36	1.01	0.001	0.015
LAMP1	7.48	6.47	1.00	0.001	0.011
KIF5B	8.41	7.41	1.00	0.002	0.025
PARP14	7.49	8.49	-1.01	0.004	0.042
ARGLU1	8.16	9.16	-1.01	0.001	0.012
SFI1	5.04	6.06	-1.01	0.003	0.032
CDK9	5.32	6.38	-1.03	0.002	0.023
TIGD1	4.54	5.56	-1.03	0.002	0.029
ZNF785	3.99	5.02	-1.03	0.003	0.035
SLC43A3	3.52	4.59	-1.03	0.002	0.031
CEP57L1	4.58	5.58	-1.04	0.004	0.039
NBPF14	4.56	5.56	-1.04	0.003	0.036
BMP2K	6.91	7.94	-1.04	0.002	0.022
ICAM3	6.10	7.18	-1.05	0.005	0.049
NLK	5.21	6.26	-1.05	0.004	0.043

THAP6	3.99	4.94	-1.06	0.003	0.035
MAP4K1	4.81	5.93	-1.06	0.003	0.036
ZSCAN30	5.27	6.36	-1.07	0.003	0.035
ACAP1	6.56	7.66	-1.08	0.001	0.011
VPS8	6.78	7.87	-1.08	0.005	0.049
ZNF354B	4.26	5.21	-1.08	0.002	0.029
TAMM41	3.83	4.96	-1.09	0.002	0.031
RERE	6.09	7.20	-1.09	0.004	0.042
PARP11	4.68	5.74	-1.09	0.003	0.038
PRKCQ	5.27	6.42	-1.09	0.002	0.027
PINK1	4.03	5.21	-1.10	0.003	0.035
LANCL1	5.65	6.75	-1.10	0.001	0.014
OGT	9.59	10.70	-1.11	0.000	0.007
ZNF445	6.42	7.54	-1.11	0.001	0.013
CDC16	5.86	6.96	-1.12	0.000	0.005
PDCD6	3.31	4.45	-1.12	0.004	0.046
BCLAF3	3.97	5.13	-1.12	0.002	0.028
AGAP2	5.44	6.57	-1.12	0.003	0.036
DGKE	5.08	6.21	-1.13	0.005	0.050
STXBP4	4.57	5.67	-1.13	0.000	0.009
RFTN1	5.22	6.43	-1.13	0.004	0.043
LUC7L3	7.69	8.83	-1.13	0.002	0.031
CDK2AP1	5.42	6.54	-1.14	0.000	0.010
ZNF169	3.27	4.44	-1.15	0.003	0.037
CAMK2G	5.76	6.87	-1.15	0.000	0.004
ZNF891	4.62	5.68	-1.15	0.001	0.018
ARHGAP27	5.38	6.56	-1.16	0.001	0.013
RAD51B	4.39	5.50	-1.16	0.001	0.015
RAD52	4.21	5.36	-1.16	0.002	0.030
STK36	4.06	5.23	-1.16	0.003	0.036
FLVCR1	4.28	5.40	-1.17	0.000	0.010
AP1G2	6.41	7.61	-1.17	0.001	0.020
TFB1M	4.15	5.31	-1.17	0.005	0.049
HSD17B7	3.01	4.29	-1.18	0.005	0.048
KIAA0825	3.63	4.60	-1.18	0.004	0.045
ZNF514	4.99	6.18	-1.18	0.001	0.016
LENG8	7.62	8.80	-1.19	0.004	0.041
ZNF33B	5.84	7.04	-1.19	0.001	0.010
STX16	5.24	6.47	-1.21	0.001	0.018
SLC25A30	4.54	5.69	-1.21	0.002	0.028
SNX16	3.98	5.10	-1.21	0.003	0.034
ZNF83	6.21	7.44	-1.21	0.001	0.011

TMEM63A	6.05	7.25	-1.22	0.000	0.004
EXOG	3.70	4.87	-1.22	0.003	0.034
PABPC1L	4.93	6.17	-1.22	0.003	0.035
IQSEC1	3.85	5.03	-1.22	0.005	0.050
PTPN4	5.18	6.32	-1.22	0.002	0.024
ZNF518B	4.92	6.08	-1.22	0.003	0.038
C20orf96	3.59	4.77	-1.22	0.001	0.010
ZNF141	6.13	7.36	-1.23	0.004	0.042
TARBP1	7.93	9.18	-1.25	0.000	0.008
KRI1	4.77	6.05	-1.25	0.000	0.009
IQGAP2	7.96	9.21	-1.25	0.001	0.019
SLC23A2	5.10	6.26	-1.25	0.001	0.012
GPR89B	3.08	4.24	-1.25	0.001	0.012
TRPV1	2.45	3.66	-1.25	0.001	0.020
CLK4	5.36	6.63	-1.27	0.003	0.036
ZNF619	4.25	5.54	-1.27	0.000	0.003
DNHD1	5.17	6.47	-1.28	0.001	0.020
TIRAP	2.43	3.72	-1.28	0.002	0.026
GBP3	4.54	5.82	-1.28	0.003	0.035
FAM185A	2.89	4.10	-1.28	0.001	0.017
AGER	1.82	3.15	-1.28	0.004	0.044
ZNF397	4.79	6.02	-1.28	0.001	0.013
ZNF69	4.93	6.25	-1.28	0.000	0.002
L3MBTL1	3.43	4.67	-1.28	0.002	0.028
DNASE1	5.26	6.54	-1.28	0.000	0.002
PLCL2	5.14	6.38	-1.29	0.000	0.010
CARF	5.10	6.37	-1.29	0.000	0.001
GNA12	4.80	6.10	-1.29	0.000	0.010
ETAA1	4.31	5.60	-1.29	0.000	0.001
SNAPC3	5.11	6.41	-1.30	0.002	0.023
TRANK1	6.56	7.90	-1.30	0.002	0.031
RSRP1	7.68	8.99	-1.30	0.000	0.010
DZIP3	4.95	6.22	-1.31	0.000	0.010
CHD3	6.96	8.27	-1.31	0.000	0.001
SLC37A3	3.46	4.77	-1.31	0.001	0.015
MSMO1	3.25	4.59	-1.31	0.003	0.034
SLC38A6	2.66	3.85	-1.31	0.003	0.033
UNKL	3.62	4.99	-1.32	0.003	0.038
EFCAB7	3.14	4.37	-1.32	0.000	0.005
ICA1L	3.48	4.68	-1.32	0.004	0.045
DTNB	3.61	4.85	-1.32	0.005	0.048
RAVER2	5.29	6.51	-1.33	0.004	0.042

ZNF589	4.17	5.33	-1.34	0.003	0.037
FAM200B	2.34	3.68	-1.34	0.003	0.038
ZFP36L2	7.59	8.94	-1.35	0.001	0.016
RNPC3	5.59	6.94	-1.35	0.000	0.001
BBS2	4.59	5.97	-1.36	0.000	0.009
ANKAR	3.62	4.95	-1.36	0.001	0.013
DTWD2	3.44	4.82	-1.37	0.002	0.031
MFSD4B	5.51	6.87	-1.38	0.001	0.012
ZDHHC13	3.75	5.20	-1.39	0.002	0.028
MRTFB	4.37	5.66	-1.39	0.002	0.027
ANKRD26	4.87	6.13	-1.39	0.000	0.008
TCTN2	3.12	4.47	-1.39	0.002	0.022
ZNF620	2.91	4.25	-1.39	0.001	0.013
ZMAT1	5.50	6.87	-1.39	0.001	0.012
CLSTN3	4.45	5.84	-1.40	0.000	0.009
ALG10B	4.57	6.01	-1.40	0.000	0.006
USP6NL	5.25	6.66	-1.40	0.000	0.007
PRKD2	3.70	5.09	-1.41	0.002	0.031
MFGE8	4.06	5.35	-1.41	0.003	0.037
MBP	5.54	7.03	-1.41	0.003	0.033
LMF1	2.76	4.38	-1.42	0.001	0.011
SMAD3	4.68	6.09	-1.42	0.000	0.007
ANKRD36B	6.13	7.53	-1.42	0.000	0.005
AOPEP	4.11	5.54	-1.42	0.000	0.002
MTMR1	3.79	5.24	-1.42	0.000	0.005
FNBP1	7.08	8.51	-1.42	0.000	0.000
YPEL1	3.49	4.95	-1.43	0.000	0.004
RBM12B	5.66	7.17	-1.43	0.003	0.036
HEXD	4.14	5.61	-1.43	0.001	0.015
ARMC2	3.04	4.40	-1.44	0.000	0.007
GSE1	6.50	7.95	-1.44	0.000	0.001
SAMD10	2.73	4.26	-1.44	0.002	0.030
CRAT	3.16	4.65	-1.45	0.003	0.035
TRIM8	3.96	5.42	-1.45	0.001	0.014
IFT81	3.25	4.64	-1.46	0.000	0.005
MAPKBP1	5.07	6.43	-1.46	0.001	0.018
ERICH1	5.14	6.64	-1.46	0.000	0.005
SNTB1	5.66	7.14	-1.46	0.001	0.014
TMEM91	2.84	4.34	-1.47	0.001	0.018
PSMG4	3.80	5.18	-1.47	0.001	0.016
NIPAL2	4.76	6.23	-1.47	0.001	0.013
RABGAP1	5.82	7.30	-1.47	0.000	0.000

PLA2G6	4.83	6.37	-1.47	0.002	0.025
RPS6KA1	5.27	6.80	-1.48	0.001	0.013
IFT80	4.04	5.49	-1.48	0.001	0.016
ACP2	3.08	4.75	-1.48	0.001	0.012
SCAI	5.38	6.83	-1.50	0.000	0.003
FRA10AC1	3.90	5.29	-1.50	0.003	0.032
P4HTM	4.15	5.68	-1.50	0.000	0.002
TCEA2	2.71	4.18	-1.50	0.002	0.030
CLIP2	5.26	6.70	-1.52	0.000	0.006
CCDC102B	2.00	3.50	-1.52	0.001	0.016
ABR	4.66	6.22	-1.53	0.004	0.044
NPHP3	3.27	4.85	-1.54	0.000	0.004
GRK4	2.57	4.10	-1.54	0.000	0.003
ZNF780B	4.70	6.27	-1.55	0.001	0.021
INPP4A	4.84	6.32	-1.56	0.000	0.006
NEK3	3.65	5.42	-1.57	0.001	0.020
ZNF568	2.82	4.34	-1.57	0.004	0.045
SLC12A4	3.60	5.15	-1.57	0.001	0.020
ANKRD44	6.03	7.64	-1.57	0.000	0.004
STK32C	2.49	4.04	-1.58	0.004	0.044
TAFA2	3.89	5.59	-1.58	0.000	0.000
RASSF7	1.53	3.25	-1.59	0.005	0.049
TTC21A	1.69	3.27	-1.59	0.004	0.039
EXD3	2.79	4.51	-1.60	0.001	0.011
CCDC171	5.80	7.44	-1.62	0.002	0.022
TTC14	6.24	7.87	-1.62	0.000	0.004
LMO7	2.74	4.33	-1.63	0.000	0.003
APOL3	4.23	5.67	-1.64	0.005	0.050
ZNF133	3.31	4.96	-1.65	0.000	0.003
FAM13A	4.51	6.10	-1.65	0.000	0.009
GPR174	4.65	6.26	-1.65	0.004	0.039
ELK3	4.87	6.56	-1.67	0.003	0.035
SVIP	3.87	5.44	-1.69	0.001	0.013
NAALADL1	3.02	4.60	-1.69	0.000	0.006
USP20	4.82	6.57	-1.69	0.000	0.001
PIGM	4.11	5.75	-1.71	0.000	0.004
CXXC5	4.67	6.42	-1.71	0.000	0.005
GKAP1	2.55	4.08	-1.71	0.001	0.020
FMO4	1.71	3.48	-1.71	0.005	0.048
KANTR	4.25	5.89	-1.71	0.000	0.003
PDP2	2.60	4.15	-1.72	0.005	0.048
ACVR2B	1.67	3.29	-1.72	0.002	0.024

DPEP2	3.41	5.30	-1.73	0.000	0.005
SLC15A2	5.29	6.99	-1.74	0.004	0.040
PARVG	6.36	8.13	-1.75	0.000	0.001
C9orf43	3.53	5.27	-1.76	0.002	0.022
RAP1GAP2	4.65	6.34	-1.76	0.000	0.009
SC5D	3.57	5.14	-1.77	0.002	0.030
YAE1	2.11	3.90	-1.78	0.003	0.038
SLC16A7	4.50	6.15	-1.78	0.000	0.009
GPR135	2.47	4.01	-1.78	0.001	0.013
SLC6A16	0.69	2.55	-1.79	0.002	0.028
SFXN1	4.18	5.93	-1.81	0.003	0.035
KATNAL2	1.00	2.67	-1.81	0.003	0.038
SREBF2	5.33	7.17	-1.81	0.002	0.025
SLC12A7	4.29	6.25	-1.81	0.002	0.031
MAP2K6	3.47	5.25	-1.82	0.001	0.018
SYNE1	5.54	7.41	-1.82	0.000	0.000
DNM3	2.26	3.87	-1.82	0.002	0.031
TXK	3.88	5.50	-1.83	0.004	0.043
FAM118A	4.27	6.07	-1.83	0.000	0.008
ZNRF1	4.81	6.73	-1.83	0.000	0.001
PPFIBP1	4.51	6.21	-1.84	0.002	0.030
CCDC9B	2.30	4.26	-1.85	0.000	0.009
ATP2B4	6.48	8.35	-1.85	0.001	0.022
SLC4A8	3.44	5.52	-1.86	0.000	0.002
GLCE	3.21	4.94	-1.87	0.003	0.038
NFATC2	4.60	6.51	-1.88	0.000	0.005
RGS14	3.75	5.62	-1.90	0.000	0.005
GVQW3	4.48	6.34	-1.90	0.000	0.001
MUC1	0.88	2.92	-1.91	0.002	0.029
GUCY1B1	4.44	6.26	-1.92	0.002	0.026
SH3BP2	4.84	6.66	-1.92	0.000	0.001
PLA2G4A	3.53	5.67	-1.93	0.000	0.006
SLC43A2	2.39	4.49	-1.93	0.002	0.026
TAS2R4	1.78	3.57	-1.94	0.003	0.035
PARP3	2.40	4.47	-1.94	0.004	0.043
HSH2D	6.28	8.18	-1.95	0.001	0.022
SYTL1	4.41	6.35	-1.95	0.001	0.019
GAS8	1.89	3.82	-1.95	0.000	0.007
LAPTM5	6.51	8.47	-1.96	0.000	0.010
AMPD3	3.85	6.04	-1.97	0.001	0.014
C1QTNF6	1.34	3.31	-1.97	0.000	0.010
ERMP1	5.72	7.67	-1.98	0.000	0.001

PPM1M	1.96	4.00	-1.98	0.000	0.009
SLC1A4	3.40	5.42	-1.98	0.003	0.037
LRBA	8.31	10.31	-1.99	0.000	0.001
ADHFE1	1.37	3.44	-2.00	0.004	0.044
ACTR3C	2.72	4.74	-2.01	0.000	0.000
MACC1	4.38	6.51	-2.01	0.001	0.018
PEAR1	3.08	4.88	-2.02	0.001	0.021
SPAG8	0.42	2.44	-2.02	0.002	0.025
NUMBL	1.54	3.60	-2.02	0.001	0.011
GPR132	1.09	3.11	-2.03	0.004	0.045
TMEM65	4.50	6.60	-2.04	0.001	0.019
PDLIM2	1.95	3.96	-2.04	0.003	0.035
SH3GLB2	3.49	5.57	-2.05	0.000	0.002
TEX9	2.40	4.09	-2.05	0.001	0.021
TPCN1	2.94	5.10	-2.06	0.001	0.010
CROCC	2.97	5.09	-2.06	0.002	0.023
AGBL3	1.39	3.31	-2.06	0.001	0.011
RAPGEF3	3.26	5.10	-2.07	0.000	0.005
NAPEPLD	3.08	5.04	-2.08	0.000	0.002
SSBP2	6.49	8.59	-2.08	0.000	0.002
ATP8A1	6.19	8.16	-2.09	0.001	0.017
SNX32	0.70	2.80	-2.10	0.003	0.036
LPIN1	5.75	7.86	-2.11	0.000	0.000
BCL11A	5.91	7.99	-2.11	0.000	0.000
DGKH	2.80	4.82	-2.12	0.001	0.013
ZNF563	0.55	2.58	-2.13	0.002	0.026
ROBO4	3.48	5.55	-2.14	0.001	0.012
WDFY4	5.36	7.47	-2.15	0.000	0.001
FAM83G	2.07	4.31	-2.16	0.001	0.017
TNS1	4.18	6.16	-2.16	0.004	0.045
RAB38	1.35	3.49	-2.17	0.002	0.022
CFAP70	1.95	3.81	-2.17	0.002	0.022
CTDSPL	3.78	5.56	-2.17	0.004	0.039
PRR5	2.07	4.24	-2.18	0.000	0.001
FAXDC2	1.54	3.76	-2.18	0.000	0.007
ATP9A	3.50	5.72	-2.18	0.001	0.015
CROT	2.00	4.42	-2.18	0.003	0.032
ZNF862	3.59	5.91	-2.19	0.000	0.002
VSIR	4.51	6.69	-2.19	0.001	0.017
NAALADL2	1.73	4.14	-2.19	0.003	0.037
SLC48A1	2.72	4.79	-2.20	0.000	0.000
GCNT1	4.58	6.71	-2.21	0.001	0.018

ST6GALNAC4	1.86	4.07	-2.22	0.000	0.002
SERAC1	2.90	5.29	-2.22	0.000	0.001
NOTCH1	5.30	7.45	-2.22	0.000	0.009
RXRA	3.13	5.33	-2.23	0.002	0.028
FHL1	5.28	7.47	-2.23	0.001	0.015
C17orf67	0.69	3.02	-2.25	0.001	0.019
GPRASP1	1.58	3.56	-2.27	0.001	0.012
N6AMT1	2.45	4.74	-2.27	0.000	0.007
ADCY6	3.67	5.84	-2.27	0.002	0.022
PTK2	2.14	4.62	-2.28	0.003	0.032
PFKM	2.63	4.85	-2.28	0.000	0.000
NRIP1	8.04	10.32	-2.28	0.000	0.002
TMEM144	2.00	4.43	-2.29	0.003	0.035
TMEM38B	3.05	5.14	-2.29	0.004	0.042
ADAM22	3.28	5.30	-2.30	0.000	0.005
KLRG1	1.85	4.40	-2.30	0.001	0.015
SCD5	1.28	3.40	-2.30	0.002	0.026
CARD19	3.51	5.88	-2.30	0.000	0.000
GCNA	0.61	2.86	-2.32	0.001	0.021
GPR141	2.22	4.46	-2.33	0.000	0.004
DNMT3B	4.23	6.57	-2.33	0.000	0.002
GSTO2	0.15	2.48	-2.34	0.001	0.013
CAPS2	1.47	4.16	-2.34	0.003	0.033
CAPN12	0.40	2.90	-2.34	0.003	0.034
KLHL31	-0.52	1.77	-2.34	0.005	0.047
KIF7	1.74	3.95	-2.35	0.000	0.010
C18orf54	2.88	5.23	-2.35	0.001	0.017
NFE2	5.44	7.92	-2.37	0.000	0.008
KANSL1L	3.54	6.35	-2.38	0.005	0.048
PDE4DIP	3.87	6.00	-2.38	0.001	0.013
XRRA1	3.59	5.98	-2.39	0.001	0.015
EVL	4.90	7.14	-2.39	0.000	0.002
PTPN12	3.96	6.24	-2.40	0.001	0.017
FMNL3	3.44	5.67	-2.40	0.000	0.010
EFEMP2	0.03	2.59	-2.40	0.004	0.040
COL24A1	5.71	8.01	-2.42	0.000	0.009
ZNF572	1.25	3.81	-2.42	0.000	0.003
IL12A	0.92	3.14	-2.42	0.000	0.007
SGIP1	-0.28	2.19	-2.42	0.003	0.032
ATP7B	2.60	5.13	-2.42	0.000	0.004
RAB27B	4.71	7.29	-2.43	0.003	0.038
PGAP1	2.73	4.87	-2.43	0.001	0.016

GDPD3	0.54	2.66	-2.43	0.003	0.035
NOTCH2NLA	-0.44	1.86	-2.44	0.004	0.040
L3HYPDH	3.44	5.90	-2.44	0.000	0.000
STAMBPL1	2.69	4.98	-2.44	0.000	0.001
MARCHF9	0.72	3.37	-2.45	0.002	0.025
GBGT1	1.97	4.23	-2.45	0.000	0.006
PAQR8	2.81	5.22	-2.45	0.004	0.040
TPM2	2.78	5.07	-2.45	0.000	0.009
NEK10	0.55	2.85	-2.46	0.001	0.017
GIMAP1	1.03	3.49	-2.46	0.000	0.007
IFFO2	2.71	5.02	-2.46	0.002	0.023
KLHL3	2.81	5.24	-2.47	0.000	0.008
IFIT1	1.31	3.47	-2.47	0.002	0.022
CD82	4.56	7.19	-2.48	0.000	0.000
FBXO21	2.41	4.68	-2.48	0.000	0.007
ARHGAP31	1.61	4.21	-2.48	0.000	0.008
TRIM58	3.51	5.99	-2.49	0.001	0.017
ZNF471	2.71	4.87	-2.50	0.001	0.012
LOXL1	-0.62	1.82	-2.50	0.002	0.028
HIP1	4.48	6.75	-2.50	0.003	0.035
ARMCX4	1.78	4.07	-2.50	0.000	0.001
PAPLN	-0.02	2.37	-2.52	0.003	0.035
REC8	3.52	5.92	-2.52	0.000	0.001
DLG3	1.09	3.66	-2.52	0.001	0.013
LAPTM4B	5.10	7.52	-2.53	0.001	0.010
RASAL2	2.02	4.55	-2.53	0.004	0.043
NEIL1	-1.05	1.51	-2.54	0.004	0.039
IQCH	0.35	2.90	-2.56	0.000	0.009
SSX2IP	3.08	5.58	-2.58	0.000	0.004
EXT1	0.88	3.48	-2.60	0.001	0.017
DNAH14	3.54	6.09	-2.60	0.000	0.004
CNKSR3	1.08	3.65	-2.60	0.002	0.031
SEMA6C	0.00	2.71	-2.61	0.002	0.024
OR2AK2	-0.54	2.01	-2.61	0.001	0.012
ZSCAN23	1.37	3.99	-2.61	0.003	0.034
PLEKHF1	-1.92	0.73	-2.61	0.003	0.037
CACNB1	0.55	2.98	-2.61	0.003	0.033
OR2T8	-0.79	1.76	-2.62	0.001	0.018
ZNF474	-0.75	1.91	-2.65	0.003	0.033
PTMS	1.35	4.08	-2.65	0.001	0.015
TIAM1	-0.35	2.31	-2.66	0.004	0.040
SRGAP3	1.91	4.30	-2.67	0.000	0.008

HMGN5	-0.24	2.44	-2.67	0.002	0.028
CBFA2T3	3.25	5.84	-2.68	0.000	0.001
PGM3	2.17	4.86	-2.72	0.000	0.001
CR1	1.93	4.67	-2.72	0.002	0.025
CHST12	4.49	7.21	-2.72	0.000	0.000
FKBP9	1.00	3.30	-2.73	0.004	0.044
NRBP2	1.86	4.62	-2.76	0.000	0.002
SYNJ2	2.66	5.38	-2.76	0.000	0.004
HEMGN	3.14	6.42	-2.76	0.001	0.013
PTPN22	2.72	5.36	-2.76	0.000	0.008
ELOVL6	2.13	4.63	-2.76	0.000	0.007
TLCD2	-1.39	1.42	-2.77	0.001	0.017
FAM171A2	-0.73	1.96	-2.77	0.003	0.038
KLHDC8B	0.67	3.46	-2.77	0.001	0.012
AOAH	2.19	5.15	-2.77	0.002	0.030
TJP2	1.19	3.88	-2.78	0.000	0.002
ATP13A2	2.30	5.40	-2.78	0.000	0.002
LRRC63	2.21	4.95	-2.79	0.001	0.015
MCF2L2	2.23	5.19	-2.79	0.000	0.001
RHPN1	2.64	5.26	-2.80	0.002	0.023
PNPLA7	2.30	5.12	-2.80	0.000	0.000
MCUB	2.91	5.37	-2.82	0.001	0.019
SLA	3.85	7.02	-2.83	0.000	0.004
SNX25	-0.85	2.10	-2.83	0.002	0.030
ZNF112	0.79	3.58	-2.83	0.000	0.009
NLGN2	-0.02	2.87	-2.84	0.004	0.040
DZIP1L	-0.04	2.70	-2.86	0.003	0.033
ABCC6	0.14	2.84	-2.86	0.000	0.003
LMO4	2.97	5.67	-2.86	0.003	0.036
BIVM	2.67	5.65	-2.87	0.003	0.036
EVA1C	0.02	2.69	-2.87	0.002	0.024
SORBS3	1.37	4.06	-2.88	0.001	0.017
ABLIM1	4.61	7.71	-2.88	0.000	0.007
DOCK3	1.51	4.26	-2.88	0.004	0.045
ATP1B1	2.75	5.43	-2.89	0.000	0.000
TRO	2.93	5.88	-2.89	0.000	0.002
C17orf100	-0.92	2.01	-2.91	0.005	0.047
SLC49A3	-0.30	2.58	-2.93	0.004	0.044
ADARB1	2.05	4.98	-2.93	0.000	0.001
MSI2	6.59	9.52	-2.95	0.000	0.000
AUTS2	3.10	6.23	-2.95	0.003	0.037
SNX10	2.22	5.06	-2.95	0.000	0.001

SH3TC1	3.42	6.60	-2.95	0.001	0.014
TNS3	4.57	7.67	-2.98	0.003	0.036
SYNPO2	-1.40	1.40	-2.98	0.004	0.042
ITPR3	1.40	4.39	-2.98	0.000	0.001
TDRKH	-0.22	2.45	-2.99	0.003	0.038
CUBN	2.72	5.58	-3.00	0.000	0.000
CYSTM1	-0.35	2.34	-3.01	0.002	0.023
TTC39B	2.54	5.77	-3.02	0.000	0.001
MAP1A	4.08	7.10	-3.03	0.002	0.025
ZFHX3	3.05	5.64	-3.03	0.004	0.039
SKIDA1	-0.23	2.66	-3.04	0.001	0.018
SLC44A1	3.82	6.39	-3.04	0.005	0.048
CHST13	0.17	3.24	-3.04	0.003	0.032
LTC4S	-1.57	1.53	-3.05	0.001	0.011
KHDC1	-0.18	2.71	-3.06	0.003	0.034
TRIP10	0.33	3.40	-3.06	0.001	0.011
ABCA2	4.26	7.17	-3.06	0.000	0.000
SDSL	-0.22	2.79	-3.07	0.002	0.026
SCN4A	-0.74	2.22	-3.07	0.000	0.005
TMEM150B	-1.57	1.38	-3.07	0.004	0.046
ZNF853	-1.13	2.15	-3.08	0.001	0.017
TNFRSF8	-1.92	0.97	-3.09	0.004	0.039
GRID2IP	-1.25	1.76	-3.10	0.002	0.025
OR2W3	0.44	3.59	-3.10	0.000	0.004
GCLM	1.31	4.18	-3.11	0.000	0.005
SLC18B1	-0.24	2.91	-3.12	0.003	0.036
DEPP1	0.51	3.39	-3.12	0.000	0.005
PROS1	-1.22	1.76	-3.13	0.002	0.029
SARM1	2.64	5.53	-3.14	0.000	0.001
GRAMD1C	1.05	3.91	-3.14	0.000	0.002
NME8	0.32	3.39	-3.15	0.004	0.040
AFAP1L2	0.57	3.78	-3.15	0.001	0.022
DNAJC6	1.76	4.87	-3.15	0.000	0.001
BTBD11	1.96	5.14	-3.16	0.000	0.005
CYP2C8	-0.81	2.34	-3.16	0.002	0.025
CPEB2	1.10	4.63	-3.16	0.002	0.030
CHRNA5	-0.40	2.75	-3.17	0.000	0.007
CHN2	-0.84	2.22	-3.18	0.004	0.043
SLC9A9	0.69	3.88	-3.18	0.000	0.000
TMEM273	-0.68	2.30	-3.19	0.002	0.028
OR2L2	0.70	3.75	-3.19	0.000	0.001
ATP6V0A1	2.78	5.84	-3.19	0.002	0.027

THNSL2	0.38	3.71	-3.20	0.002	0.023
OR2L13	-0.40	2.75	-3.22	0.001	0.013
CLU	2.69	5.89	-3.22	0.001	0.018
GNA11	0.17	3.64	-3.22	0.001	0.015
MAP7	3.88	7.06	-3.23	0.000	0.001
SLC41A1	0.94	4.08	-3.23	0.002	0.025
SELPLG	2.86	6.24	-3.25	0.003	0.037
CCSER1	3.09	6.00	-3.26	0.000	0.008
TBC1D4	1.91	5.37	-3.27	0.000	0.004
GPR21	1.07	4.42	-3.28	0.000	0.000
CCDC92	1.01	4.66	-3.29	0.004	0.045
GOLGA6L9	-0.82	2.37	-3.29	0.003	0.035
OR2L8	-1.57	1.64	-3.29	0.000	0.009
C15orf39	3.43	6.60	-3.31	0.000	0.000
PSTPIP1	1.23	4.52	-3.31	0.000	0.001
TNNI2	-2.81	0.44	-3.32	0.002	0.031
RAI14	-1.28	1.58	-3.32	0.003	0.035
CFH	3.17	6.80	-3.32	0.005	0.048
SAMD4A	0.04	3.38	-3.33	0.000	0.006
PRKAR2B	2.96	5.73	-3.33	0.001	0.014
CNTNAP1	-2.13	1.23	-3.34	0.001	0.011
CA3	-2.03	1.28	-3.34	0.003	0.035
MAPRE3	-1.80	1.37	-3.34	0.001	0.016
CCDC122	0.19	3.33	-3.34	0.001	0.011
GPR155	-0.76	2.32	-3.35	0.002	0.030
RIN2	0.61	4.06	-3.36	0.001	0.014
BAG2	1.00	4.62	-3.38	0.001	0.020
PCSK5	-1.59	1.76	-3.39	0.002	0.026
ZFYVE9	0.72	4.06	-3.45	0.002	0.027
NLRC3	3.67	7.05	-3.45	0.000	0.000
CLIP3	-0.90	2.49	-3.45	0.001	0.013
ABCA7	1.97	5.43	-3.46	0.000	0.007
PRR15	-0.83	2.31	-3.46	0.002	0.023
SNCA	2.08	4.97	-3.46	0.003	0.034
MPIG6B	-0.16	3.28	-3.47	0.000	0.001
PDZD2	1.12	4.90	-3.47	0.000	0.000
TNFSF10	1.97	5.57	-3.47	0.001	0.016
GIMAP7	0.67	4.02	-3.48	0.001	0.015
GLIPR2	1.47	5.07	-3.51	0.002	0.029
SNX9	0.92	4.50	-3.51	0.000	0.010
BAG3	-0.39	2.91	-3.51	0.001	0.019
MYLK	0.36	3.77	-3.52	0.000	0.000

CPS1	-2.19	1.19	-3.53	0.000	0.009
DACT1	-1.76	1.57	-3.53	0.002	0.022
GP1BA	-1.05	2.56	-3.53	0.000	0.002
CD300A	2.51	5.65	-3.55	0.000	0.001
NPHP1	-1.63	1.82	-3.55	0.002	0.031
ABCA10	-0.83	2.49	-3.55	0.001	0.011
PRR5L	2.89	6.12	-3.56	0.001	0.012
LTBP1	0.81	4.03	-3.56	0.001	0.012
TMEM178A	-2.13	1.42	-3.56	0.000	0.005
JAG1	0.06	3.57	-3.56	0.002	0.022
OR2L5	-0.98	2.64	-3.57	0.000	0.004
CNKSR1	-0.64	2.90	-3.57	0.000	0.003
EDARADD	-0.48	3.10	-3.57	0.000	0.000
DNAH5	-2.06	1.35	-3.57	0.000	0.009
EFNA1	-0.05	3.14	-3.58	0.002	0.026
TTLL6	-0.61	2.98	-3.59	0.002	0.030
PURA	1.77	5.11	-3.60	0.001	0.019
NPR2	-0.25	3.31	-3.60	0.000	0.004
LFNG	0.80	4.13	-3.60	0.000	0.008
ABCB6	-2.59	0.90	-3.61	0.001	0.017
JAM3	0.83	4.27	-3.61	0.002	0.022
CLEC2D	2.60	6.08	-3.61	0.000	0.000
SPATA6	1.77	5.12	-3.62	0.002	0.025
RIMBP3	-1.80	1.80	-3.63	0.001	0.019
RTL8A	-0.77	2.64	-3.63	0.002	0.027
ADAMTS14	-0.54	3.17	-3.63	0.000	0.010
GASK1B	1.48	4.79	-3.64	0.005	0.048
CRHBP	2.92	6.78	-3.64	0.000	0.000
ZNF98	-1.70	1.72	-3.64	0.003	0.032
LTBP3	2.03	5.56	-3.64	0.000	0.002
FRMD4B	3.25	6.78	-3.66	0.000	0.000
MAP7D2	-2.62	1.09	-3.66	0.001	0.014
COL18A1	0.03	3.71	-3.68	0.000	0.002
ALOX15B	-1.96	1.76	-3.68	0.001	0.011
UST	0.08	3.80	-3.69	0.000	0.001
EGF	-1.52	1.93	-3.69	0.003	0.038
ZNF521	4.15	8.11	-3.71	0.001	0.011
CX3CR1	-2.09	1.58	-3.71	0.002	0.029
GUCY2D	-2.92	0.70	-3.71	0.004	0.045
ANXA3	-0.39	3.08	-3.72	0.001	0.012
SERPING1	2.47	5.67	-3.72	0.004	0.043
PLD5P1	-0.39	3.29	-3.74	0.000	0.000

LGR4	-1.56	2.18	-3.75	0.003	0.034
ANKS6	0.83	4.35	-3.75	0.001	0.011
ANO5	-2.29	1.25	-3.76	0.003	0.033
SMO	0.03	3.50	-3.77	0.001	0.017
NOXA1	-0.71	3.13	-3.77	0.001	0.015
OSBP2	-1.49	2.04	-3.77	0.001	0.013
SCN2A	-1.50	2.18	-3.78	0.001	0.017
CLGN	-1.08	2.94	-3.78	0.001	0.022
PHKA1	0.77	4.52	-3.78	0.000	0.000
PLEKHA1	0.37	4.13	-3.79	0.000	0.001
CAPRIN2	1.61	5.62	-3.80	0.000	0.000
GNB5	1.18	5.14	-3.81	0.001	0.017
GSTM5	-0.11	3.99	-3.81	0.001	0.015
NOTCH3	-2.29	1.49	-3.81	0.002	0.027
MYEF2	1.37	5.74	-3.81	0.004	0.042
FSTL1	0.75	4.24	-3.82	0.000	0.005
RBM11	-2.03	1.88	-3.82	0.000	0.007
TSTD3	-0.01	3.94	-3.82	0.000	0.009
TUB	-2.09	1.49	-3.82	0.002	0.025
ZEB1	3.30	6.73	-3.82	0.003	0.037
PRUNE2	-1.47	2.23	-3.83	0.001	0.015
TBC1D12	-1.10	2.68	-3.83	0.001	0.011
JAZF1	-1.84	1.69	-3.85	0.002	0.023
TMEM25	0.06	4.10	-3.86	0.000	0.000
ARHGAP20	-2.02	1.60	-3.87	0.001	0.013
CCDC136	0.95	4.95	-3.87	0.001	0.015
CDRT4	-1.96	1.67	-3.88	0.003	0.034
HSF5	0.19	4.00	-3.88	0.000	0.000
SH3BGRL2	0.07	4.10	-3.89	0.000	0.007
LRRC49	-2.36	1.29	-3.89	0.003	0.038
HEG1	-0.01	3.67	-3.89	0.000	0.007
PTGER3	-2.65	1.28	-3.89	0.000	0.001
TNFAIP2	3.26	6.77	-3.90	0.000	0.010
KCNQ1	-1.26	2.46	-3.91	0.001	0.015
PDE5A	-2.69	1.09	-3.91	0.000	0.006
SORT1	1.48	5.47	-3.91	0.000	0.001
DNAH10	0.42	4.33	-3.92	0.000	0.000
CYTH4	2.94	6.63	-3.92	0.000	0.000
EFCC1	0.31	4.23	-3.94	0.000	0.000
TNNT3	0.63	4.32	-3.94	0.001	0.015
CAMK1	-2.92	0.94	-3.95	0.001	0.016
DACH1	2.21	5.76	-3.95	0.000	0.001

ZDHHC15	-0.11	3.57	-3.95	0.001	0.018
PLEKHG1	-1.26	2.43	-3.95	0.001	0.014
LTB	-1.44	2.38	-3.95	0.003	0.034
STRIP2	-1.73	2.10	-3.96	0.000	0.002
TMEM150C	-2.26	1.56	-3.96	0.001	0.017
PHLDB2	0.47	4.40	-3.98	0.000	0.000
TSPYL5	0.74	5.25	-3.98	0.001	0.011
TNFRSF4	-2.36	1.49	-3.99	0.005	0.048
CTSW	2.23	6.07	-4.00	0.000	0.002
RAB11FIP4	0.06	3.98	-4.01	0.001	0.013
MAP1LC3B2	-1.75	2.21	-4.02	0.000	0.003
ECHDC2	1.06	4.72	-4.02	0.002	0.028
BICC1	-2.41	1.39	-4.02	0.002	0.022
HABP4	-2.01	2.01	-4.03	0.000	0.006
JAM2	-2.65	1.34	-4.04	0.000	0.004
TSPAN6	-2.19	1.63	-4.04	0.000	0.001
EPSTI1	1.69	5.70	-4.05	0.000	0.002
MICU3	0.15	4.20	-4.05	0.002	0.023
TTC22	-2.28	1.57	-4.06	0.000	0.004
NPDC1	2.05	5.76	-4.06	0.000	0.001
CA13	0.24	4.44	-4.06	0.000	0.000
XKR5	-2.42	1.68	-4.07	0.001	0.013
ELN	0.10	4.09	-4.08	0.000	0.001
LOX	0.08	3.96	-4.09	0.000	0.003
TVP23C	0.96	4.82	-4.09	0.003	0.038
C20orf203	-1.84	2.06	-4.09	0.000	0.001
TUSC1	-2.69	1.30	-4.10	0.003	0.037
HOXB5	-2.92	1.11	-4.11	0.000	0.000
NOTCH2NLR	-2.69	1.38	-4.12	0.000	0.006
XKR6	-2.42	1.58	-4.12	0.001	0.022
SLC16A14	-2.09	2.07	-4.13	0.002	0.022
PAIP2B	-0.05	3.65	-4.14	0.001	0.016
KRT18	0.90	4.54	-4.15	0.000	0.002
GOLGA8A	3.36	7.34	-4.15	0.004	0.040
CNNM1	-1.72	2.15	-4.16	0.000	0.009
TOM1L1	0.07	3.73	-4.16	0.001	0.014
KL	-3.15	0.97	-4.16	0.000	0.001
TMEM72	-3.15	1.01	-4.16	0.002	0.022
KRT8	-0.43	3.62	-4.17	0.000	0.001
CCDC187	-2.69	1.42	-4.17	0.004	0.041
LMNTD2	-2.47	1.73	-4.18	0.000	0.000
CAND2	-2.11	1.81	-4.18	0.000	0.010

EML6	-1.16	3.09	-4.19	0.000	0.001
KCNA6	-3.15	0.94	-4.19	0.002	0.031
NSUN7	-0.68	3.37	-4.19	0.000	0.002
WBP2NL	-1.52	2.45	-4.20	0.001	0.017
ARHGEF10	-2.81	1.31	-4.22	0.000	0.003
PDE1C	-1.97	1.93	-4.22	0.000	0.010
TRIM2	-1.10	2.72	-4.23	0.002	0.027
MDGA2	-3.15	1.05	-4.24	0.000	0.000
STARD9	4.26	8.26	-4.25	0.000	0.000
SEPTIN1	0.08	4.49	-4.25	0.000	0.002
ABCA1	2.51	6.00	-4.26	0.000	0.010
OR2L3	-1.50	2.58	-4.26	0.000	0.010
ITGA2B	1.82	5.94	-4.26	0.000	0.001
GYPE	-2.16	2.21	-4.27	0.000	0.001
HOXA4	-2.41	1.69	-4.28	0.000	0.004
CCDC102A	-0.60	3.60	-4.29	0.000	0.000
RMND5B	0.08	4.54	-4.29	0.000	0.000
ARHGEF5	-2.19	2.05	-4.30	0.000	0.002
CA8	-0.17	3.63	-4.30	0.003	0.034
SLITRK5	-2.36	1.91	-4.30	0.000	0.001
UACA	-0.27	3.49	-4.30	0.004	0.045
PALLD	-0.28	3.99	-4.30	0.000	0.000
GPR63	-2.11	2.06	-4.30	0.001	0.015
ABHD1	-2.47	1.68	-4.31	0.000	0.006
CMTM4	0.55	4.24	-4.31	0.000	0.006
TMEM204	-1.57	2.82	-4.31	0.000	0.000
SH2D3C	1.52	5.73	-4.31	0.000	0.000
LURAP1	-0.67	3.57	-4.32	0.000	0.003
SLC29A2	-0.39	4.20	-4.33	0.000	0.002
GPR161	-1.28	3.09	-4.36	0.000	0.000
PLCH2	-2.81	1.49	-4.36	0.000	0.002
EHD2	0.69	4.76	-4.36	0.000	0.000
SPIRE1	0.62	5.12	-4.37	0.000	0.007
FGD5	2.50	6.12	-4.37	0.000	0.009
FKBP10	-1.92	2.32	-4.38	0.000	0.001
OPTN	1.41	5.62	-4.38	0.000	0.000
CARD11	0.54	4.87	-4.39	0.000	0.000
RHAG	-2.39	1.76	-4.39	0.003	0.035
VNN2	-0.25	3.98	-4.39	0.000	0.004
CDKL5	-0.44	4.18	-4.40	0.000	0.003
ITGB8	0.32	4.59	-4.41	0.001	0.014
EPPK1	-2.09	2.19	-4.41	0.000	0.000

GOLGA8B	2.63	7.17	-4.41	0.001	0.016
CAPG	1.26	5.78	-4.42	0.000	0.000
FIGNL2	-3.15	1.23	-4.43	0.000	0.001
RYR3	-1.53	2.98	-4.43	0.001	0.019
TMPRSS9	-2.52	1.87	-4.43	0.000	0.003
MANSC1	-0.25	4.00	-4.44	0.000	0.000
SLC16A2	-2.59	1.69	-4.45	0.000	0.000
GCNT2	1.35	5.68	-4.46	0.000	0.000
HOOK1	-1.26	3.12	-4.46	0.000	0.001
APBB1	-1.55	2.77	-4.46	0.000	0.004
RBPMS	2.78	6.67	-4.48	0.000	0.001
SLC30A4	-2.69	1.68	-4.49	0.000	0.002
ADCY7	3.11	7.68	-4.49	0.000	0.000
ENPP5	-2.69	1.70	-4.49	0.000	0.000
OGG1	0.64	5.03	-4.49	0.000	0.000
TDRD9	-3.15	1.31	-4.50	0.000	0.002
SLC22A15	1.11	5.17	-4.50	0.004	0.045
TPM1	1.18	5.53	-4.51	0.000	0.000
ADGRL1	0.20	4.86	-4.53	0.000	0.002
RUNX3	0.92	4.99	-4.53	0.000	0.002
MPZL2	-1.08	3.23	-4.54	0.000	0.001
LDOC1	-3.15	1.37	-4.56	0.000	0.000
RIC3	-1.28	3.38	-4.57	0.000	0.001
SSPN	-1.91	2.51	-4.59	0.001	0.012
ANKH	-0.42	4.06	-4.60	0.000	0.001
SALL2	-1.69	2.85	-4.60	0.000	0.001
VWA2	-2.45	2.11	-4.60	0.000	0.000
EPHX2	-1.93	2.54	-4.61	0.000	0.000
IQCA1	-2.92	1.67	-4.62	0.000	0.000
CYP4F22	-3.15	1.42	-4.62	0.000	0.000
RTL8B	-3.15	1.42	-4.62	0.000	0.000
TMEM200A	-1.41	3.33	-4.63	0.000	0.000
MALRD1	0.25	5.09	-4.64	0.000	0.009
TRPC6	-3.15	1.47	-4.64	0.000	0.000
PF4	-2.69	1.86	-4.65	0.000	0.000
SAMD12	-0.78	3.37	-4.65	0.000	0.001
F2RL1	1.24	5.35	-4.65	0.001	0.012
ETS1	2.08	5.98	-4.66	0.001	0.013
CLIC2	0.97	5.51	-4.66	0.000	0.000
CCDC152	-0.44	3.89	-4.66	0.000	0.002
USP45	0.08	5.12	-4.67	0.002	0.030
TVP23A	-2.15	2.46	-4.67	0.000	0.000

SPRED1	-0.12	3.89	-4.67	0.001	0.014
SLC2A10	-1.45	2.98	-4.68	0.001	0.015
IL15	-0.42	4.07	-4.68	0.000	0.000
NLRP2	0.09	4.40	-4.69	0.004	0.039
PLS1	-1.19	3.35	-4.69	0.003	0.038
SERTM2	-2.69	1.86	-4.69	0.000	0.002
PLAG1	-1.52	3.15	-4.69	0.001	0.013
RTL8C	-0.98	3.56	-4.70	0.000	0.006
TNFRSF11A	-1.45	3.02	-4.70	0.001	0.020
SLC46A3	0.22	4.52	-4.71	0.000	0.007
SPON1	-1.80	2.83	-4.71	0.000	0.000
ANKRD20A4P	-3.15	1.45	-4.72	0.002	0.030
RPS6KA6	-3.15	1.54	-4.72	0.000	0.000
CP	1.37	6.40	-4.72	0.000	0.002
RBFOX2	0.28	4.47	-4.72	0.000	0.001
TNFRSF18	-2.81	1.85	-4.73	0.000	0.005
TMEM229B	-0.23	4.52	-4.73	0.000	0.003
PECR	-1.92	2.73	-4.74	0.000	0.002
TTC12	0.11	4.42	-4.74	0.002	0.023
ENO2	-0.11	4.41	-4.74	0.000	0.000
GPR146	-1.72	3.01	-4.75	0.000	0.001
HSPA4L	-1.40	3.17	-4.75	0.000	0.004
ARHGAP22	1.36	6.01	-4.76	0.000	0.000
NFIB	-2.36	2.25	-4.76	0.000	0.000
TRPS1	2.55	7.80	-4.78	0.003	0.035
TMEM117	-2.81	1.92	-4.78	0.000	0.000
ZNF300	-1.28	3.83	-4.79	0.000	0.000
CBR3	-3.15	1.64	-4.79	0.002	0.025
CD109	3.25	7.92	-4.80	0.000	0.010
OR2AG2	-3.15	1.63	-4.80	0.000	0.000
SPNS3	0.52	5.27	-4.82	0.000	0.003
HBD	0.21	5.06	-4.82	0.005	0.048
SLC40A1	3.09	7.87	-4.83	0.003	0.034
SPATS2L	-0.15	4.57	-4.84	0.000	0.003
TRIM61	-3.15	1.67	-4.84	0.000	0.000
MAP9	-0.36	4.42	-4.85	0.000	0.006
SALL4	-1.45	3.19	-4.86	0.001	0.013
C10orf105	-2.59	2.15	-4.86	0.000	0.001
C2orf88	-0.85	4.23	-4.87	0.000	0.000
CALCRL	1.43	6.40	-4.87	0.000	0.003
TPD52	0.22	4.55	-4.87	0.002	0.023
ZC3H12B	-2.11	2.56	-4.88	0.000	0.001

GCNT4	-1.35	3.28	-4.89	0.000	0.001
LAMC1	0.27	4.85	-4.90	0.005	0.048
KIF5A	-3.15	1.73	-4.91	0.000	0.000
ESR2	-1.80	2.95	-4.91	0.000	0.000
ESR1	-2.22	2.46	-4.91	0.000	0.004
BEND6	-2.59	2.42	-4.92	0.000	0.003
ZNF214	-3.15	1.70	-4.92	0.000	0.001
JAKMIP2	0.81	5.84	-4.92	0.000	0.001
SRC	0.12	5.04	-4.94	0.000	0.000
PPP2R2B	-2.36	2.36	-4.94	0.000	0.000
NUDT10	-2.81	2.05	-4.95	0.000	0.000
EXPH5	-1.09	3.50	-4.95	0.000	0.002
CCDC42	-2.36	2.47	-4.95	0.000	0.000
STK33	-0.19	4.51	-4.97	0.000	0.003
RHBDF1	-1.24	3.50	-4.97	0.000	0.000
VOPP1	-0.81	4.04	-4.98	0.000	0.000
NUP62CL	-2.69	2.18	-4.99	0.000	0.002
VWF	0.97	5.82	-5.00	0.000	0.000
NEDD4L	0.23	5.22	-5.00	0.000	0.000
CFAP92	-0.54	4.42	-5.01	0.000	0.000
STAC	-1.54	3.14	-5.01	0.000	0.001
NAP1L2	-2.92	2.04	-5.01	0.000	0.000
SLC22A17	-2.69	2.21	-5.02	0.000	0.000
DYNLT5	1.59	6.34	-5.03	0.000	0.003
DZIP1	-2.81	2.08	-5.03	0.000	0.007
NDN	-1.58	3.30	-5.04	0.005	0.047
BMERB1	-2.32	2.72	-5.05	0.000	0.000
TRPC1	-1.60	3.35	-5.05	0.000	0.002
VWDE	1.81	6.90	-5.06	0.000	0.000
GALNT12	-1.43	3.45	-5.06	0.000	0.005
LST1	1.33	6.08	-5.08	0.000	0.002
ACE	-1.39	3.26	-5.09	0.000	0.002
MAGI2	-1.27	3.62	-5.09	0.000	0.000
GATA3	-2.26	2.71	-5.09	0.000	0.000
LAG3	-2.24	2.60	-5.10	0.000	0.000
SGCZ	-3.15	1.95	-5.12	0.000	0.000
DYNC1I1	-3.15	1.95	-5.12	0.000	0.001
SH3BP5	-0.75	4.19	-5.12	0.000	0.004
AKAP6	-2.52	2.46	-5.12	0.000	0.001
BMPR1B	-1.96	2.92	-5.13	0.000	0.000
P3H3	-1.80	2.97	-5.13	0.000	0.000
LILRB2	-0.77	4.18	-5.14	0.000	0.002

FXYD6	-1.75	3.06	-5.14	0.000	0.001
OBSL1	1.65	6.29	-5.14	0.000	0.001
NUDT11	-2.47	2.75	-5.14	0.000	0.000
NYNRIN	1.63	6.51	-5.15	0.000	0.002
SEL1L3	1.80	6.38	-5.16	0.000	0.001
ARHGEF11	0.52	5.25	-5.16	0.001	0.020
ANGPT1	3.85	8.34	-5.18	0.001	0.014
PRR16	-2.48	2.61	-5.19	0.000	0.000
ALDH2	-0.68	4.40	-5.20	0.000	0.000
FBN1	1.25	6.47	-5.20	0.000	0.000
ABCA5	1.32	6.19	-5.21	0.000	0.001
EMILIN1	-0.84	4.43	-5.21	0.000	0.001
PPP2R3A	-2.15	2.90	-5.24	0.000	0.003
ANKEF1	-3.15	2.06	-5.26	0.000	0.004
SHROOM4	-0.97	3.87	-5.26	0.000	0.004
OR6A2	-3.15	2.10	-5.27	0.000	0.000
ACVR2A	-1.30	3.83	-5.28	0.000	0.000
LRCH2	-3.15	2.07	-5.29	0.000	0.000
GPRIN3	0.78	5.64	-5.30	0.000	0.004
PLEKHG4B	-1.96	3.16	-5.30	0.000	0.000
AKT3	1.73	7.00	-5.30	0.002	0.030
TANC1	0.41	5.70	-5.30	0.000	0.000
SLC25A27	-1.31	3.77	-5.30	0.000	0.001
PROM1	3.67	8.99	-5.31	0.004	0.041
NLGN1	-3.15	2.17	-5.32	0.000	0.000
BASP1	-1.28	3.75	-5.32	0.000	0.000
ZNF208	-2.05	3.13	-5.33	0.000	0.000
CALN1	1.95	6.27	-5.33	0.000	0.001
NECAB1	-3.15	2.19	-5.34	0.000	0.000
TTLL10	-2.13	3.04	-5.35	0.000	0.006
PEG3	-2.74	2.51	-5.35	0.000	0.000
DYTN	-0.29	4.70	-5.35	0.000	0.000
PRKCZ	-1.78	3.48	-5.38	0.000	0.000
ANO9	-2.06	3.18	-5.38	0.000	0.000
ODAD2	-3.15	2.22	-5.39	0.000	0.000
PCLO	-2.36	3.07	-5.41	0.000	0.000
GCSAML	1.50	6.88	-5.42	0.000	0.000
PLXNC1	2.31	7.57	-5.43	0.000	0.000
NLRP12	-2.65	2.76	-5.46	0.000	0.000
GALNT5	-2.81	2.54	-5.47	0.000	0.000
CLDN10	-1.26	3.88	-5.48	0.000	0.003
GIPC2	-3.15	2.30	-5.49	0.000	0.000

CDCP1	0.54	5.62	-5.50	0.000	0.005
GPR173	-1.88	3.31	-5.52	0.000	0.000
ARHGAP21	1.19	6.67	-5.52	0.000	0.000
NIPA1	-0.70	5.01	-5.54	0.000	0.000
IGF2BP3	-0.49	4.73	-5.54	0.000	0.000
EFHC2	-0.19	5.50	-5.56	0.000	0.000
SLC35G2	-1.99	3.31	-5.56	0.000	0.002
CHMP4C	-3.15	2.37	-5.57	0.000	0.000
PRTFDC1	-2.92	2.59	-5.58	0.000	0.000
RFX8	-1.39	4.27	-5.60	0.000	0.002
PKIA	-2.06	3.55	-5.62	0.000	0.005
PCBP3	-2.92	2.63	-5.62	0.000	0.001
ARMCX2	-1.42	4.04	-5.62	0.000	0.000
SLC8A1	-0.77	4.51	-5.63	0.000	0.001
IL7	-2.69	2.81	-5.64	0.000	0.000
PPBP	-2.29	3.12	-5.64	0.000	0.000
ITGA2	-1.09	4.07	-5.65	0.000	0.000
LSP1	1.14	6.60	-5.66	0.000	0.000
ST6GAL2	-2.92	2.64	-5.67	0.000	0.000
CPVL	-0.36	4.87	-5.68	0.001	0.019
H2BU1	-1.68	3.93	-5.69	0.000	0.000
CNN3	-1.89	3.51	-5.69	0.000	0.000
HSPA12A	-2.81	2.88	-5.71	0.000	0.000
JAML	0.00	5.82	-5.72	0.000	0.000
LIMCH1	-1.92	3.57	-5.74	0.000	0.000
CFI	-1.29	4.06	-5.75	0.001	0.013
EMCN	-2.06	3.68	-5.76	0.000	0.000
H2AW	-2.02	3.71	-5.77	0.000	0.000
CAVIN1	1.33	6.56	-5.79	0.000	0.000
TSPAN2	0.91	6.82	-5.81	0.001	0.018
FHL2	-2.36	3.44	-5.82	0.000	0.000
SCML4	-0.60	5.20	-5.84	0.000	0.000
ZNF334	-0.27	5.16	-5.84	0.000	0.000
XIRP2	-1.60	4.42	-5.85	0.000	0.000
STXBP1	-3.15	2.68	-5.86	0.000	0.000
FRMD6	-1.97	3.64	-5.86	0.001	0.014
LRIG1	-2.19	3.55	-5.87	0.000	0.001
MPP7	-0.74	5.00	-5.90	0.001	0.015
PIEZO2	-1.46	3.88	-5.91	0.000	0.003
ABI3BP	-2.29	3.56	-5.92	0.000	0.000
ACOX2	-3.15	2.75	-5.92	0.000	0.000
GPC5	-3.15	2.75	-5.93	0.000	0.000

PCYT1B	-1.88	4.11	-5.94	0.000	0.000
SKAP1	-1.31	4.36	-5.95	0.000	0.000
FZD3	-2.03	3.85	-5.95	0.003	0.034
CYYR1	-1.03	4.65	-5.96	0.001	0.019
TCEAL9	-1.43	4.18	-5.98	0.002	0.025
COBLL1	-0.62	5.29	-6.00	0.001	0.012
CDC14B	-1.82	4.24	-6.01	0.000	0.000
SLC44A5	-2.62	3.33	-6.01	0.001	0.021
RADX	-2.74	3.23	-6.02	0.000	0.000
SPOCK3	-2.59	3.28	-6.04	0.000	0.000
GABBR1	0.66	6.12	-6.05	0.000	0.001
PTPRM	1.19	6.20	-6.07	0.000	0.001
MCOLN2	-2.47	3.44	-6.09	0.000	0.000
ZNF532	-1.85	4.15	-6.10	0.000	0.000
DST	2.79	9.06	-6.11	0.000	0.004
SHTN1	-1.85	3.98	-6.12	0.000	0.000
PLA2R1	-0.88	4.93	-6.14	0.000	0.000
ZDBF2	-2.34	3.69	-6.14	0.000	0.000
CIBAR1	-1.68	4.30	-6.16	0.000	0.001
ADGRG1	1.23	7.27	-6.16	0.000	0.000
PRKG2	0.33	6.45	-6.18	0.000	0.000
BMPR2	0.17	6.20	-6.18	0.000	0.000
GPAT3	-1.02	4.96	-6.20	0.000	0.000
MYO1E	-0.99	4.98	-6.20	0.000	0.000
PRDM16	-3.15	3.00	-6.20	0.000	0.000
JHY	-1.49	4.30	-6.24	0.000	0.001
HOXB2	-2.92	3.26	-6.24	0.000	0.000
SDR42E1	-1.68	4.43	-6.25	0.000	0.000
NBEA	-0.53	5.93	-6.26	0.000	0.000
CLNK	-2.81	3.25	-6.26	0.000	0.005
BEX3	-0.35	5.57	-6.27	0.005	0.047
KHDRBS2	-2.12	4.00	-6.27	0.000	0.000
PRKN	-2.81	3.44	-6.28	0.000	0.000
NKX2-3	-3.15	3.07	-6.28	0.000	0.000
ZNF215	-2.69	3.50	-6.29	0.000	0.000
BCAS4	-0.97	5.13	-6.29	0.000	0.000
BACH2	-1.39	4.78	-6.30	0.000	0.000
PLSCR4	-1.41	4.59	-6.31	0.000	0.000
PGAP4	-1.73	4.59	-6.31	0.000	0.000
CHIC1	-1.23	4.81	-6.33	0.000	0.009
TM4SF1	-1.85	4.20	-6.35	0.000	0.000
SYT1	-2.52	3.68	-6.37	0.000	0.000

ANK3	-1.44	4.90	-6.40	0.000	0.000
LAT2	0.62	7.08	-6.45	0.000	0.000
CEP112	-2.29	4.05	-6.45	0.000	0.000
TBC1D8B	-2.92	3.46	-6.46	0.000	0.000
PLCB4	0.01	6.50	-6.46	0.000	0.000
SETBP1	0.11	6.22	-6.47	0.000	0.000
MIPOL1	-3.15	3.26	-6.47	0.000	0.000
FERMT1	-1.43	4.70	-6.50	0.000	0.000
HOPX	-0.08	6.07	-6.50	0.000	0.000
DTX3	-2.06	4.50	-6.50	0.000	0.000
C8orf88	-2.69	3.76	-6.52	0.000	0.001
EPB41L3	-1.73	4.66	-6.59	0.000	0.000
ATXN1	0.51	6.60	-6.59	0.004	0.041
ARHGAP5	1.17	7.47	-6.60	0.000	0.000
TMEM163	-2.13	4.22	-6.63	0.000	0.000
PGM5	-2.59	3.83	-6.63	0.000	0.000
ADGRG5	-0.97	5.44	-6.64	0.000	0.000
PPP1R9A	-2.59	3.97	-6.65	0.000	0.000
ZNF462	-2.02	4.33	-6.67	0.000	0.000
CDH7	-3.15	3.46	-6.68	0.000	0.000
ZC2HC1A	-2.92	3.68	-6.68	0.000	0.000
CAVIN2	-0.29	6.30	-6.71	0.000	0.000
EGLN3	-3.15	3.53	-6.73	0.000	0.000
C11orf21	0.68	7.22	-6.74	0.000	0.000
HOXA3	-2.69	3.99	-6.75	0.000	0.000
MED12L	1.31	7.73	-6.75	0.000	0.003
CLEC9A	-2.69	3.99	-6.80	0.000	0.000
C6orf141	-3.15	3.61	-6.81	0.000	0.000
FAT4	-1.09	5.40	-6.84	0.000	0.000
ITGB3	-3.15	3.64	-6.86	0.000	0.000
PDZRN4	-3.15	3.73	-6.86	0.000	0.000
CEP126	-2.13	4.52	-6.87	0.000	0.000
COL5A1	-1.05	5.52	-6.89	0.000	0.000
PTPRD	-1.51	5.49	-6.90	0.000	0.001
MPPED2	-2.81	4.09	-6.91	0.000	0.000
BEND4	-0.55	6.30	-6.92	0.000	0.004
SYDE2	-2.92	3.92	-6.92	0.000	0.000
RNF150	-2.69	4.11	-6.94	0.000	0.000
HOXB4	-3.15	3.72	-6.94	0.000	0.000
MYH10	-0.93	6.06	-6.96	0.000	0.000
PLS3	-2.59	4.27	-6.97	0.000	0.000
HFM1	-3.15	3.81	-6.98	0.000	0.000

UCHL1	-3.15	3.71	-6.98	0.000	0.000
WDR17	-2.36	4.47	-6.99	0.000	0.001
BEX2	-2.74	4.24	-7.01	0.000	0.002
HOXA7	-3.15	3.90	-7.07	0.000	0.000
PATJ	-1.03	6.05	-7.12	0.000	0.006
GFI1B	-1.70	5.29	-7.12	0.000	0.000
CARMIL1	-0.65	6.04	-7.18	0.000	0.000
SEMA3C	-2.62	4.44	-7.19	0.000	0.000
UGGT2	-1.19	5.94	-7.20	0.000	0.000
SMARCA1	-2.19	5.05	-7.21	0.000	0.001
FAM169A	-1.26	5.65	-7.21	0.000	0.001
CHRDL1	-2.47	4.58	-7.22	0.000	0.000
ADAMTS10	-2.47	4.66	-7.25	0.000	0.002
PRKG1	-2.59	4.55	-7.28	0.000	0.000
ZNF385D	-2.92	4.34	-7.31	0.004	0.044
SH3BP4	-2.48	4.70	-7.32	0.000	0.000
ELAPOR2	-2.81	4.39	-7.33	0.001	0.020
KLF12	-0.97	6.28	-7.44	0.003	0.036
C3orf80	-3.15	4.25	-7.44	0.000	0.000
THRB	-2.69	4.69	-7.50	0.000	0.000
L3MBTL4	-1.64	5.68	-7.51	0.000	0.002
BEND7	-3.15	4.31	-7.52	0.000	0.000
DPYSL3	-0.95	6.60	-7.53	0.000	0.000
CYP7B1	-1.66	5.51	-7.54	0.000	0.001
FREM1	-2.47	4.95	-7.57	0.000	0.000
HOXA5	-2.29	5.17	-7.62	0.000	0.000
CCDC144A	-2.92	4.60	-7.63	0.000	0.010
INTU	-2.10	5.38	-7.67	0.000	0.003
CHRM3	-1.31	6.47	-7.78	0.000	0.000
CACNB2	-2.47	5.23	-7.82	0.000	0.000
MYCT1	-2.12	5.56	-7.88	0.000	0.000
SPAG17	-2.59	5.11	-7.89	0.000	0.000
HOXA6	-3.15	4.72	-7.91	0.000	0.000
SCHIP1	-2.52	5.28	-7.96	0.000	0.000
SYTL4	-2.20	5.64	-7.96	0.000	0.000
CCDC175	-3.15	4.84	-7.99	0.000	0.000
IL12RB2	-1.36	6.20	-8.01	0.000	0.000
TTLL7	-2.47	5.47	-8.02	0.000	0.000
ZNF711	-1.23	6.71	-8.06	0.000	0.002
HOXA10	-3.15	4.88	-8.08	0.000	0.000
MPDZ	-2.92	5.08	-8.09	0.000	0.000
NAP1L3	-3.15	4.91	-8.11	0.000	0.000

HLF	-1.24	6.61	-8.15	0.000	0.000
CPED1	-2.36	5.66	-8.17	0.000	0.000
PLOD2	-2.69	5.37	-8.18	0.000	0.000
ST8SIA6	-1.19	6.82	-8.24	0.000	0.000
DSG2	-1.85	6.17	-8.26	0.000	0.000
AASS	-2.59	5.62	-8.28	0.000	0.000
TSPAN32	-1.58	6.54	-8.31	0.000	0.000
ALDH1A1	-1.46	6.67	-8.32	0.000	0.000
SLC8A3	-2.59	5.80	-8.36	0.000	0.000
PAWR	-1.96	6.44	-8.56	0.000	0.000
HOXB3	-2.81	5.68	-8.60	0.000	0.000
PBX1	-1.98	6.43	-8.63	0.000	0.000
NFIA	-1.02	7.56	-8.76	0.000	0.000
NKAIN2	-2.92	5.88	-8.87	0.000	0.000
CPNE8	-2.36	6.50	-9.00	0.000	0.000
HOXA9	-3.15	5.88	-9.07	0.000	0.000
PCDH9	-1.59	7.48	-9.13	0.000	0.000
SPINK2	-2.69	6.33	-9.14	0.001	0.012
HMGA2	-2.92	6.27	-9.27	0.000	0.000
DPPA4	-2.69	6.63	-9.36	0.000	0.000
DOCK1	-1.86	7.28	-9.36	0.000	0.000
HTR1F	-2.92	6.50	-9.50	0.000	0.002
CDC42BPA	-2.36	6.98	-9.51	0.000	0.000
ABO	-3.15	6.41	-9.60	0.000	0.000
ADGRG6	-1.61	7.72	-9.63	0.000	0.000
MECOM	-2.06	7.44	-9.70	0.000	0.000
SCN9A	-1.39	8.17	-9.81	0.000	0.000
MEIS1	-2.01	8.33	-10.58	0.000	0.000

Supplementary table 3: AP-1, C/EBP, RUNX and TGIF1 GRN modules.

AP-1 targets		C/EBP targets		RUNX targets		TGIF1 targets	
geneName	AP-1 motif	geneName	C/EBP motif	geneName	RUNX motif	geneName	TGIF1 motif
NCOR2	4	FAM200B	3	HNRNPD	3	UBL5	1
RPTOR	3	PDE3B	2	TRAP1	3	ZDHHC14	1
FPR3	3	ZFAT	2	IRX1	3	UBL3	1
RPLP1	2	TP53BP2	2	BCL2	2	SUMO3	1
HNRNPD	2	HMGB2	2	PDE3B	2	AGA	1
EIF3C	2	TRAF3	2	RPS3A	2	PCSK5	1
PIGY	2	TEX2	2	STEAP3	2	LAPTM5	1
CEP78	2	FCN1	2	CXCR4	2	VPS8	1
PMFBP1	2	FPR3	2	BCL7A	2	UBE2V1	1
PLEKHO2	2	YES1	2	ACSF3	2	LEMD2	1
EBF1	2	DHCR24	2	UCK1	2	TRAF3	1
SLC38A7	2	SLCO4A1	2	CRACR2A	2	RBPJ	1
PPP1CB	2	MAP10	2	UBAP1	2	MFGE8	1
VDAC1	2	UBASH3B	2	IGLL5	2	ZSWIM4	1
WARS	2	CYBA	1	PARD3	2	SPN	1
HS6ST1	2	GALT	1	PLEKHO2	2	IRAK2	1
YES1	2	GLA	1	ZFP36L1	2	ZC3H18	1
TOM1L1	2	LYZ	1	NRN1	2	THY1	1
NAMPT	2	MPO	1	TMEM57	2	IRX1	3
ELL	2	MSH2	1	LYSMD4	2	PIK3R2	1
TMEM104	2	NCF1	1	TEX2	2	CBLB	1
CDCA4	2	PTEN	1	HTRA3	2	SLC38A7	1
WIPI1	2	TCN2	1	LPAR1	2	TCOF1	1
ELAC1	2	TPMT	1	ITGA9	2	DIAPH1	1
MAP10	2	ABCC2	1	NAPG	2	SP2	1
PREX1	2	CYBB	1	TNFRSF10A	2	WIPI1	1
ADPGK	2	CYB5R3	1	TRIM24	2	PPP2R2A	1
GLT1D1	2	PECAM1	1	HS6ST1	2	SCCPDH	1
RNF175	2	TEK	1	TOM1L1	2	DHX29	1
SFXN4	2	PMS1	1	SRSF6	2	TEK	1
ACADM	1	ORM1	1	B3GNT2	2	GYPC	2
F13A1	1	NOS2	1	UBL3	2	CNDP2	1
FTL	1	PTGIR	1	FAM53B	2	OSBPL5	1
LYZ	1	ZNF425	1	LPGAT1	2	HNRNPDL	1
SLC4A1	1	MGLL	1	ZNF292	2	TTI1	2
CTSK	1	GTF2IRD2B	1	VPS13D	2	DDX43	1
CYBB	1	YPEL2	1	TMEM38B	2	PARP12	1
NCF2	1	CXCR4	1	FAM105A	2	ARHGAP17	1

TEK	1	SPDYC	1	TPCN2	2	SNRNP27	1
FCGR3A	1	CLSTN1	1	AGA	1	SPPL2A	1
NCAM1	1	VPS8	1	ERCC8	1	TUBE1	1
GLRB	1	SYTL3	1	EPHX1	1	ZNF771	1
PDE3B	1	AFMID	1	FUT1	1	ITGA9	1
PLAT	1	MSL1	1	GALT	1	RPS6KC1	1
POMC	1	LSP1	1	GBE1	1	HMGN3	1
PTGS1	1	SLTM	1	KCNQ1	1	NFU1	1
ZNF425	1	OCIAD2	1	NCF1	1	ATP2A3	1
UQCR10	1	DNAJC25	1	PHKA2	1	CELF2	1
OR2T8	1	KIAA2026	1	GPD2	1	UBE2D1	1
NUMB	1	PODXL	1	EYA1	1	MYO18A	1
ARHGAP17	1	TNRC6B	1	FBP1	1	MYO18B	1
ZSCAN2	1	ARPP21	1	RAG2	1	RC3H2	1
COA5	1	TAF5L	1	VHL	1	ACTR3C	1
PICALM	1	RPS28	1	FCGR3A	1	IQSEC1	1
SH3D19	1	VSTM4	1	NCAM1	1	PHLDA1	1
KIAA2018	1	SERPINB8	1	NOS2	1	PMFBP1	2
CASC10	1	STK24	1	RFX2	1	ZG16B	1
LSP1	1	REV1	1	CACNA1D	1	WDR41	1
RFFL	1	TRIM71	1	GSTM2	1	PANK2	1
ERMAP	1	THEMIS2	1	POMC	1	CETN3	1
SFMBT2	1	AKR1E2	1	PPIC	1	PEPD	1
VLDLR	1	CD83	1	PRRG1	1	LTC4S	1
PODXL	1	MAPK8IP3	1	PTGER4	1	FBXL13	1
NRP1	1	ZBTB8A	1	RPL23	1	GMDS	1
RUNX3	1	LINS	1	RPL31	1	TIPRL	1
TP53BP2	1	DPH3	1	ZNF425	1	UBXN2B	1
VSTM4	1	MUTYH	1	DENND6B	1	SNX33	1
MAF	1	UBL5	1	FCRLB	1	ZNF516	1
RABGAP1L	1	SREK1	1	RPLP1	1	OCIAD2	1
ARL5A	1	SEC31A	1	OGDH	1	SDK2	1
AGPAT3	1	UBXN2B	1	QSOX1	1	MAU2	1
MDH1B	1	IKZF2	1	OR2T8	1	PDLIM1	2
FKRP	1	GXYLT2	1	GTDC1	1	TSPYL2	1
LINS	1	SLC45A4	1	SFI1	1	CCDC57	1
ABCE1	1	DGKG	1	COA5	1	UCK1	1
GSDMB	1	RGS9	1	MXRA7	1	MAP3K8	1
MAP4K1	1	MYSM1	1	TPST2	1	HCK	2
FAM159A	1	IRF5	1	PICALM	1	ARL5A	1
SREK1	1	PHF21A	1	DSP	1	FTL	1
SLC38A1	1	SYCE2	1	SYTL3	1	TYRO3	1

UBN1	1	FBXL13	1	SSBP4	1	ARL5B	1
IKZF2	1	FANCL	1	SHE	1	PAFAH2	1
DIAPH1	1	ACSF3	1	PIK3R6	1	SNRPB2	1
PACRG	1	LACC1	1	C1GALT1C1	1	ZNRF1	1
CACTIN	1	MYO9B	1	HAUS8	1	VASH2	3
SCARB1	1	CLDN5	1	SERPINI2	1	ZNF24	1
CADM1	1	INPP4A	1	CTNNBIP1	1	DNAJC3	1
SIGLEC14	1	GBP5	1	RTKN	1	TADA3	1
TLE3	1	PDHX	1	TNRC6B	1	WDR37	1
ARMC5	1	FNDC3B	1	ARPP21	1	ZNF425	1
ZFYVE16	1	TPRA1	1	TAF5L	1	HS3ST3B1	2
UBE2K	1	IFFO2	1	SCMH1	1	WDFY1	1
PABPC4L	1	VASH2	1	TRMT11	1	TTC39C	1
WDR26	1	NEDD9	1	SGK3	1	FBXO38	1
PTGER3	1	AIMP1	1	NRCAM	1	ITGAE	1
CASK	1	CTF1	1	EIF3C	1	HES6	1
ACSF3	1	KNSTRN	1	TRIM71	1	ZNF292	1
LRRC8A	1	SGK1	1	ELMO1	1	LRPAP1	1
HIVEP3	1	DIS3L	1	ACTR3B	1	GABRR2	1
REPS1	1	LEMD2	1	AKR1E2	1	GRTP1	1
SLC44A5	1	OSBPL5	1	AGTRAP	1	OTUD1	1
GAS7	1	PHLDB1	1	SYCP2L	1	SMAD3	1
TMEM194A	1	DOK3	1	ZCWPW2	1	LTB4R	1
C3orf58	1	SNX20	1	GDAP1	1	POLB	1
VASH2	1	TPM4	1	CYLD	1	ZNF837	1
ZNF771	1	MPZL1	1	SLC16A3	1	STT3B	2
AIMP1	1	MGAT4A	1	TGFB1I1	1	PLP2	1
HMMR	1	PMFBP1	1	FILIP1L	1	TSC2	1
PIK3R5	1	ZBP1	1	MAP4K1	1	LHFPL2	1
SMCO2	1	TMEM189	1	RERE	1	HTRA3	1
FAM200B	1	SMIM6	1	FAM159A	1	STRIP1	1
ZNF880	1	GTF2I	1	ZNF557	1	TMEM11	1
SCRN1	1	DLC1	1	SEC31A	1	PELI3	1
SLCO5A1	1	SKA3	1	MS4A14	1	PRAME	1
GSK3B	1	CD244	1	DBI	1	SKIDA1	1
KDM4C	1	XIAP	1	DGKG	1	SLC7A8	1
ZBP1	1	FUS	1	RGS9	1	SLCO4A1	2
TMEM189	1	SRGAP2	1	TCTN1	1	CTF1	1
PLXNB3	1	MIB2	1	SCARB1	1	TCFL5	1
TBCK	1	SLC25A21	1	PRF1	1	EHD1	1
GTF2I	1	TBP	1	RB1CC1	1	CEP41	1
PLIN3	1	HCK	1	MYSM1	1	SH2B2	1

DLC1	1	ZNF408	1	CADM1	1	MCAT	1
MTF2	1	PHF8	1	LRRC43	1	SAR1A	1
ANKRD33B	1	FBXL20	1	MRVI1	1	UBE2V2	1
NFKB1	1	FAM219A	1	TOX2	1	AIMP1	1
SKA3	1	PCSK5	1	CEP78	1	NFRKB	1
SHMT2	1	COQ7	1	NUTM2A	1	TRIOBP	1
TESC	1	SIRT5	1	ZFAND5	1	LSP1	1
TJP2	1	PPP2R4	1	PAQR5	1	CCDC115	1
UBAP1	1	REST	1	TLE3	1	ABCA7	1
GOLGA3	1	TTC27	1	TMEM177	1	ABCA1	1
PPP1R16B	1	TMEM126B	1	ZFYVE16	1	RFT1	2
SH2D4A	1	TEX22	1	DGKZ	1	ABTB1	2
ASNS	1	PDZD7	1	FAM160A1	1	PRKD2	1
IGLL5	1	MICU1	1	ARHGEF7	1	TOX	1
UHMK1	1	AIFM2	1	ZNF276	1	TMEM254	2
KLHDC4	1	YY1AP1	1	ZBTB37	1	ALOX5AP	1
TMEM127	1	POC1B	1	CASK	1	KIAA2026	1
PPP2R4	1	NDUFS1	1	ZNF469	1	SGMS1	1
REST	1	NETO1	1	SPON2	1	ZMYND8	1
MR1	1	NETO2	1	SLC14A1	1	RB1CC1	1
ARL14EPL	1	SLC25A27	1	KCTD15	1	RPTOR	3
TUBB3	1	TBC1D10A	1	ACAA1	1	EPS15	1
CNOT2	1	TAX1BP3	1	MEF2A	1	DDX10	2
POC1B	1	DNAH8	1	SUN1	1	CCNA1	1
EZH2	1	HIF1A	1	INPP4A	1	TMEM41B	1
SLC25A27	1	ZFP36L1	1	AP3M2	1	CLIP2	1
ABHD12B	1	SEL1L	1	IQSEC1	1	CNOT8	1
PITRM1	1	NT5C	1	ZDHHC4	1	SPTBN1	1
RNF146	1	RHNO1	1	RPS6KC1	1	CXCR4	2
AKT2	1	CDC5L	1	RCOR3	1	N4BP1	2
INPP5F	1	GMDS	1	GPR107	1	DHRS7B	1
TIGD6	1	WDR92	1	ARFGAP3	1	TTLL4	1
HLA-DRB1	1	P2RX4	1	LMO2	1	ALDH3B1	1
MAP3K8	1	POLD1	1	NEDD9	1	MCM10	1
CERS6	1	LOC339862	1	SLMO1	1	ITGB4	1
LRRC39	1	SRP72	1	FCMR	1	LTBP1	1
MEGF10	1	LTBR	1	HMMR	1	UXS1	1
GYPC	1	SRGAP2C	1	FBRSL1	1	QRICH2	1
FAM49B	1	ZNF518A	1	HNRNPLL	1	TTLL9	1
P2RX4	1	PDK1	1	TCTN2	1	SFSWAP	1
TMEM265	1	PTPN1	1	CDYL	1	CREB1	1
DCSTAMP	1	NRN1	1	SDK2	1	SARDH	1

LMNA	1	TAGAP	1	SNX20	1	PLEKHO2	1
TSKU	1	WDR86	1	SLCO3A1	1	PDE12	1
OASL	1	ANLN	1	ZNF619	1	PLA2G4A	1
TUBA1A	1	ADAP1	1	TANC1	1	ST6GALNAC3	1
MED4	1	LYSMD4	1	ANGPT1	1	SNX20	2
CHST15	1	IQGAP2	1	SLCO5A1	1	NIPAL2	1
SQRDL	1	RPA2	1	PTGR2	1	SLC35F6	1
DYNC1I2	1	C2CD5	1	EPS15	1	E2F3	1
TRAP1	1	NME4	1	SSH1	1	C3AR1	1
USP10	1	CRISPLD1	1	TMEM189	1	RPL32	1
STIM1	1	PTTG1IP	1	RPTOR	1	CERK	1
ARL6	1	GAK	1	ZBTB24	1	FN3KRP	1
PHYKPL	1	AMD1	1	ACTR3C	1	NCL	1
ZNF518A	1	TRAF3IP3	1	NFKB1	1	FUT1	1
UBE2E3	1	CSF1R	1	FHIT	1	KDM7A	1
ZNF316	1	HSH2D	1	TMEM178A	1	EWSR1	1
PTPN1	1	TSNARE1	1	FAM21C	1	LIN7B	1
RFXANK	1	MAP3K4	1	TJP2	1	EPHX1	1
PCED1B	1	CLNS1A	1	SRPX	1	IKBKB	1
PIK3CG	1	SIN3B	1	SIGLEC10	1	SFMBT1	1
PTGES3	1	CETN3	1	SLC25A21	1	SFMBT2	2
FAM107B	1	ZNF333	1	HCK	1	C5AR1	1
RASGEF1A	1	SLC17A9	1	HAVCR1	1	TNRC6B	1
WDYHV1	1	C20orf197	1	SPEG	1	TMEM177	1
LYSMD4	1	WDR61	1	TXNRD3	1	USP21	1
RPA2	1	RPRD1A	1	TRPV4	1	B3GNT7	2
AGTPBP1	1	TTI1	1	PPP2R2A	1	VPS9D1	1
TRMT10B	1	VPREB1	1	ALDH7A1	1	SLCO5A1	2
DNAJC16	1	UBE3D	1	PCSK5	1	POPDC2	1
DAPK1	1	PGD	1	ORC4	1	EIF3C	2
TEX2	1	NMT2	1	PPP2R4	1	ADRA2C	1
ST6GALNAC1	1	CYSLTR2	1	TUBA8	1	PCF11	1
MAP3K4	1	DECR1	1	TTC27	1	NEO1	1
HTRA3	1	DNASE2	1	MLLT10	1	GMPR	1
C11orf24	1	LPAR1	1	TUBB3	1	TEX22	1
PPCDC	1	DNAJA1	1	ADCY4	1	NDUFA13	1
TPM2	1	ADRBK1	1	AIFM2	1	RELB	1
CCR7	1	C5AR1	1	USP19	1	PIP4K2A	1
TCFL5	1	COX7C	1	GLRX3	1	PRX	1
TMEM159	1	ETV6	1	UQCRB	1	NABP1	2
ZNF202	1	GABRR2	1	NDUFS1	1	DAZAP2	1
RPRD1A	1	FOXN2	1	CTDP1	1	CRISPLD1	1

UBE3D	1	ICAM3	1	EZH2	1	MRPL35	1
ZKSCAN4	1	IRF8	1	ABHD12B	1	TSNAX	1
HDHD3	1	ITGA9	1	NSFL1C	1	RAB5B	1
ATP9B	1	TACSTD2	1	RHOBTB1	1	RFFL	1
TM2D3	1	MARCKS	1	ALCAM	1	LPP	1
ZNF24	1	PABPC1	1	LOC388849	1	TNFRSF21	2
CYSLTR2	1	PPP1CB	1	RAD23B	1	NMT2	1
CTSW	1	SRGN	1	ASAP1	1	EDEM1	1
DNASE2	1	PSMA3	1	GALNT14	1	NTPCR	1
EXTL3	1	PSMB1	1	YME1L1	1	RFX8	1
C5AR1	1	PTPRG	1	GYPC	1	PTGES3	1
CCND2	1	SAT1	1	USP3	1	EFR3A	2
CDR2	1	SECTM1	1	USP39	1	SCARB1	2
DEFA6	1	SKI	1	FAM49B	1	ZNF280D	1
STX2	1	SLC18A2	1	DCSTAMP	1	RFX2	1
ITGAE	1	SNAPC4	1	TSKU	1	ABHD12B	1
KPNA1	1	SP2	1	HPCAL1	1	NETO2	1
NUDT1	1	SPG7	1	EPS15L1	1	SPTY2D1	1
NPTX1	1	SYN2	1	JARID2	1	ELMO1	1
NTSR1	1	TRPM2	1	TUBA1A	1	KIF11	1
PFDN4	1	XPO1	1	CDC42EP3	1	NFATC3	1
PLCG1	1	VAPA	1	CHST15	1	VLDLR	1
PSMA3	1	DDO	1	STRIP1	1	MSL2	1
PTPRG	1	HSD17B6	1	LTBR	1	PCED1B	1
RGS12	1	EIF3G	1	SQRDL	1	SNX8	1
SECTM1	1	MBTPS1	1	DENND2D	1	SERINC1	2
SLC18A2	1	TRIM24	1	RSRC1	1	NDUFC2	1
SNAPC4	1	USP13	1	SHISA5	1	COPS4	1
SPTBN1	1	PTK2B	1	PHF20L1	1	ZNF696	1
TIMP4	1	GTF2F2	1	TADA3	1	YTHDF2	1
UNG	1	DUSP1	1	PDK1	1	MED4	1
WNT10B	1	RABGGTB	1	MYBL2	1	BTF3L4	1
PTP4A1	1	HS6ST1	1	RFXANK	1	HSBP1	1
PAX8	1	CDH6	1	SIGMAR1	1	YPEL4	1
AXIN1	1	TRIM25	1	ADAMTS10	1	ADORA2B	2
VAPA	1	ABCA1	1	NRBF2	1	YPEL1	1
CUL1	1	SRSF4	1	ZNF343	1	PTEN	1
STX11	1	NAMPT	1	FAM107B	1	ZNF608	1
MBTPS1	1	LHFPL2	1	PDIA6	1	ZBTB8A	1
TMEM11	1	OLIG2	1	TRPS1	1	DERL1	1
GTF2F2	1	SPRY2	1	ZNF341	1	IFT52	1
CHST2	1	AKAP8	1	RTFDC1	1	ARHGAP15	1

CDH1	1	MAN1A1	1	ASCC3	1	CD44	1
RABGGTB	1	SMYD5	1	TBC1D22A	1	TRAF3IP3	1
TRAF6	1	LUC7L3	1	RCAN1	1	GPR160	2
WNT11	1	POU4F1	1	IQGAP2	1	ANGPT1	1
CLIC3	1	FBLN5	1	RPA2	1	PLXDC2	1
DHRS3	1	PARP4	1	DYNC1LI2	1	TCF4	1
ROCK2	1	B3GNT2	1	ZNF79	1	RASGEF1A	2
SLC27A4	1	TMED2	1	RCL1	1	DPYSL2	1
RBPJ	1	TMED10	1	TRMT10B	1	BST2	1
SLC20A1	1	UQCR11	1	AMD1	1	RPP25	1
KRTAP5-9	1	SNRNP27	1	ZNF92	1	ASNS	1
LHFPL2	1	POLR3A	1	FDFT1	1	MLLT10	1
SMYD5	1	UBL3	1	TRAF3IP3	1	SMYD4	1
POLE	1	ZNF175	1	ST6GALNAC1	1	SMYD5	2
PPP1R3D	1	CD2AP	1	SMARCA2	1	RAB8A	1
THY1	1	QPCT	1	XKR5	1	SHE	1
KHDRBS3	1	PPARGC1A	1	PPP2R2D	1	GALNT6	1
ZBTB6	1	UBE2T	1	TSNARE1	1	GALNT7	1
SRCAP	1	OPN3	1	ZNF330	1	CSRNP1	1
COPS8	1	MCAT	1	TSSC4	1	ABTB2	1
SPIN1	1	TTLL4	1	CETN3	1	HACD2	1
LAPTM5	1	ZNF516	1	MDFI	1	FAM78A	1
PNRC1	1	TOMM20	1	IBTK	1	MEF2A	2
CD160	1	DENND3	1	GMFG	1	BBS12	1
DUSP10	1	TBC1D9B	1	PPCDC	1	HS6ST1	3
GALNT6	1	MYCBP2	1	SGSM3	1	VPS51	1
PHLDA1	1	HIC2	1	RASA2	1	ARPP21	1
RBM15B	1	GRAMD4	1	TXNDC11	1	VPS54	1
CELSR1	1	SMCHD1	1	TTI1	1	ZNF337	1
CAPN7	1	TNS2	1	FGD4	1	TMEM131	2
TNFRSF21	1	TMEM131	1	TRIM68	1	ANKRD13A	1
DOCK4	1	TECPR1	1	AGRN	1	TEX14	1
VASH1	1	TRIM33	1	TM2D3	1	RPLP1	2
SPAST	1	SCCPDH	1	PLEKHG3	1	NFATC2IP	1
STK38L	1	ZNF589	1	DNAH6	1	TEX10	1
HIC2	1	CPQ	1	DPAGT1	1	SPRY2	1
ATP11A	1	WBP11	1	GATM	1	TREM1	1
MAU2	1	WAC	1	CD2	1	CD300LB	1
RIMBP3	1	SEPSECS	1	COX7C	1	SH3BP2	1
SCCPDH	1	CHRAC1	1	CTSD	1	TRIP11	1
TFB1M	1	AGO4	1	FCN1	1	DUSP16	1
DHRS7	1	FAM46A	1	FGF7	1	TMEM14C	1

RAB14	1	TMEM104	1	GLP1R	1	AKNA	1
SEPSECS	1	RPP25	1	IRF8	1	CSF1R	1
GALNT7	1	KIAA1551	1	INHBA	1	DNAJB6	1
UHRF1BP1	1	UTP6	1	KPNA1	1	TPM1	1
SLC25A38	1	SLC35E3	1	LRPAP1	1	WDR26	1
VAC14	1	DHX29	1	MARCKS	1	ZNF341	1
IMP3	1	TWSG1	1	MAFK	1	RANBP9	1
PGM2	1	PREX1	1	MEIS1	1	FANCL	1
PAG1	1	TMEM181	1	MN1	1	SUGP2	1
PDLIM1	1	WDFY1	1	NUDT1	1	TTC22	1
PELI2	1	LRRN1	1	MX2	1	DPAGT1	1
PCIF1	1	UVSSA	1	PLCG1	1	FGD2	1
YTHDC2	1	PDLIM1	1	PPP1CB	1	TET1	1
PAPOLG	1	SLC30A1	1	PRKCB	1	SEPHS1	1
UBE2Z	1	PELI2	1	MAPK7	1	TPMT	1
CAMKV	1	TMBIM1	1	PSMB1	1	CELSR1	1
OGFRL1	1	XPO4	1	PYGB	1	LAMP5	1
SH3TC2	1	PLEKHF2	1	RFNG	1	PARD3	1
FN3KRP	1	RNF122	1	SNAPC4	1	SND1	1
PRKRIP1	1	ATP8B4	1	SORL1	1	PACRG	1
CLMN	1	USP36	1	TAF2	1	TSPO	1
RNF122	1	CXorf21	1	TIMP4	1	TJP2	1
NUP210	1	RAI1	1	TSSC1	1	NPTX2	1
CXorf21	1	FAM49A	1	WNT10B	1	DOT1L	1
PDCD1LG2	1	TMEM163	1	XPNPEP2	1	DLC1	1
PBX4	1	RPS6KL1	1	YY1	1	SFXN4	1
TTYH3	1	TMEM120A	1	ZFP36	1	MGST1	1
SH3BP5L	1	CEP192	1	PTP4A1	1	RPS3A	2
AKNA	1	PRAM1	1	AXIN1	1	FAM32A	1
ZNRF1	1	ACAD11	1	VAPA	1	RNF146	1
C15orf48	1	ZNRF1	1	CUL1	1	ERCC8	1
PARD6G	1	CYSTM1	1	DCHS1	1	TGFB3	1
MICALCL	1	DNAJC5B	1	USP13	1	STAB1	1
COL27A1	1	RBM18	1	FCER1G	1	UVSSA	1
ADAM19	1	ESCO1	1	CCR6	1	ST6GAL1	1
TMEM261	1	TMEM203	1	ETV5	1	UQCR11	1
RFT1	1	GLT1D1	1	RPS6KA3	1	MSH2	1
FAM167A	1	ZBTB47	1	SREBF2	1	PCBD1	1
MYO18A	1	TRMT61A	1	WNT11	1	SF3B1	1
ABCA6	1	TMTC2	1	RAB7A	1	TRAP1	2
ADAMTS14	1	PROSER2	1	C21orf33	1	MSH6	1
CNTNAP5	1	SNX33	1	ROCK2	1	RPRD1A	1

ZNF837	1	CACUL1	1	PRCP	1	RPRD1B	1
ZBTB47	1	SLC41A1	1	GPR12	1	F13A1	1
DDIT4L	1	IQGAP3	1	RAB8A	1	SMARCA2	1
SLC15A4	1	TMEM105	1	YES1	1	MYBL2	2
PIWIL4	1	STT3B	1	MAFB	1	RABL3	1
MFSD6L	1	MRPL21	1	RANBP9	1	ACCS	1
UBE2E2	1	POLN	1	KRTAP5-9	1	IQGAP3	1
COL24A1	1	NAIF1	1	CTDSP2	1	RERE	1
RBM45	1	ZC3H12D	1	NAMPT	1	FBXL20	1
CBLB	1			SLC23A1	1	CEBPD	2
SIK1	1			STAG1	1	RGL4	1
TTBK2	1			EIF1B	1	SUPT3H	1
RABL3	1			MCM4	1	CDYL	1
CCDC71L	1			ARID1A	1	PFKL	1
RASSF3	1			HS3ST3B1	1	TNNI2	1
ZNF428	1			SMYD5	1	MED16	1
CCDC57	1			LUC7L3	1	CRACR2A	1
CCZ1B	1			POU4F1	1	MFSD9	1
RBM43	1			PRKAA1	1	CDC5L	1
NHLRC1	1			STK4	1	LIAS	1
UAP1L1	1			TYRO3	1	ATAD3A	1